COMPLETE THERMODYNAMIC PHENOMENOLOGIES FOR LEAD ZINC NIOBATE: LEAD TITANATE (PZN:PT) AND THE LEAD MAGNESIUM NIOBATE: LEAD TITANATE (PMN:PT) SINGLE CRYSTAL SYSTEM

Period May 1, 1999 To June 30, 2001

Final Report

OFFICE OF NAVAL RESEARCH
Contract No: N00014-99-1-0530

APPROVED FOR PUBLIC RELEASE-
DISTRIBUTION UNLIMITED

L. Eric Cross

THE MATERIALS RESEARCH LABORATORY
UNIVERSITY PARK, PA

PENNSTATE

1855

REPORT DOCUMENTATION PAGE

Form Approved
OMB No. 0704-0188

1. AGENCY USE ONLY *(Leave blank)*	2. REPORT DATE	3. REPORT TYPE AND DATES COVERED
	13 November 2001	FINAL REPORT 05/01/1999--06/30/2001

4. TITLE AND SUBTITLE COMPLETE THERMODYNAMIC PHENOMENOLOGIES FOR LEAD ZINC NIOBATE: LEAD TITANATE (PZN:PT) AND THE LEAD MAGNESIUM NIOBATE: LEAD TITANATE (PMN:PT) SINGLE CRYSTAL SYSTEM

5. FUNDING NUMBERS
ONR CONTRACT NO.
N00014-99-1-0530

6. AUTHORS
The Pennsylvania State University
Materials Research Institute
University Park, Pa 16802

7. PERFORMING ORGANIZATION NAME(S) AND ADDRESS(ES)

8. PERFORMING ORGANIZATION REPORT NUMBER

9. SPONSORING/MONITORING AGENCY NAME(S) AND ADDRESS(ES)
Office of Naval Research
ONR 321SS
Ballston Centre Tower One
800 N. Quincy Street
Arlington, VA 22217-5660

Office of Naval Research
Regional Office Chicago
536 S. Clark Str. RM 208
Chicago, IL 60605-1588

10. SPONSORING/MONITORING AGENCY REPORT NUMBER

11. SUPPLEMENTARY NOTES

12a. DISTRIBUTION/AVAILABILITY STATEMENT
Approved for Public Release; distribution is Unlimited

12b. DISTRIBUTION CODE

13. ABSTRACT *(Maximum 200 words)*

SEE FOLLOWING PAGE

14. SUBJECT TERMS

15. NUMBER OF PAGES

16. PRICE CODE

17. SECURITY CLASSIFICATION OF REPORT	18. SECURITY CLASSIFICATION OF THIS PAGE	19. SECURITY CLASSIFICATION OF ABSTRACT	20. LIMITATION OF ABSTRACT
UNCLASSIFIED	UNCLASSIFIED	UNCLASSIFIED	

INSTRUCTIONS FOR COMPLETING SF 298

The Report Documentation (RDP) is used in announcing and cataloging reports. It is important that this information be consistent with the rest of the report, particularly the cover and title page. Instructions for filling each block of the form follow. It is important to ***stay within the lines to meet optical scanning requirements.***

Block 1. Agency Use Only *(Leave blank)*.

Block 2. Report Date. Full publication date including day, month, and year, if available (e.g., 1 Jan 88). Must cite at least the year.

Block 3. Type of Report and Dates Covered. State whether report is interim, final, etc. If applicable, enter inclusive report dates (e.g., 10 Jul 87 - 30 Jun 88).

Block 4. Title and Subtitle. A title is taken from the part of the report that provides the most meaningful and complete information. When a report is prepared in more than one volume, repeat the primary title, add volume number, and include subtitle for the specific volume. On classified documents enter the title classification in parentheses.

Block 5. Funding Numbers. To include contract and grant numbers; may include program element number(s), project number(s), task number(s), and work unit number(s). Use the following labels:

C -	Contract	**PR -**	Project
G -	Grant	**TA -**	Task
PE -	Program Element	**WU -**	Work Unit Accession No.

Block 6. Author(s). Name(s) of person(s) responsible for writing the report, performing the research, or credited with the content of the report. If editor or compiler, this should follow the name(s).

Block 7. Performing Organization Name(s) and Address(es). Self-explanatory.

Block 8. Performing Organization Report Number. Enter the unique alphanumeric report number(s) assigned by the organization performing the report.

Block 9. Sponsoring/Monitoring Agency Name(s) and Address(es). Self-explanatory.

Block 10. Sponsoring/Monitoring Agency Report Number. *(If known)*

Block 11. Supplementary Notes. Enter information not included elsewhere such as: Prepared in cooperation with . . . ; Trans. of . . . ; To be published in . . . . When a report is revised, include a statement whether the new report supersedes or supplements the older report.

Block 12a. Distribution/Availability Statement. Denotes public availability or limitations. Cite any availability to the public. Enter additional limitations or special markings in all capitals (e.g., NOFORN, REL, ITAR).

DOD -	See DoDD 5230, "Distribution Statements on Technical Documents"
DOE –	See authorities.
NASA –	See Handbook NHB 2200.2.
NTIS –	Leave blank.

Block 12b. Distribution Code.

DOD -	Leave blank.
DOE –	Enter DOE distribution categories from the Standard Distribution for Unclassified Scientific and Technical Reports.
NASA –	Leave blank.
NTIS –	Leave blank.

Block 13. Abstract. Include a brief *(Maximum 200 words)* factual summary of the most significant information contained in the report.

Block 14. Subject Terms. Keywords or phrases identifying major subjects in the report.

Block 15. Number of Pages. Enter the total number of pages.

Block 16. Price Code. Enter appropriate price code *(NTIS only)*.

Blocks 17. - 19. Security Classifications. Self-explanatory. Enter U.S. Security Classification in accordance with U.S. Security Regulations (i.e., UNCLASSIFIED). If form contains classified information, stamp classification on the top and bottom of the page.

Block 20. Limitation of Abstract. This block must be completed to assign a limitation to the abstract. Enter either UL (unlimited) or SAR (same as report). An entry in this block is necessary if the abstract is to be limited. If blank, the abstract is assumed to be unlimited.

Complete Thermodynamic Phenomenologies for Lead Zinc Niobate: Lead Titanate (PZN:PT) and the Lead Magnesium Niobate: Lead Titanate (PMN:PT) Single Crystal System

L. Eric Cross
The Pennsylvania State University
Materials Research Laboratory
University Park, PA 16802
Phone: 814-865-1181
Fax: 814-863-7846
E-mails lec3@psu.edu

Grant Number No. N00014-99-1-0530

ONR Program Officer Wallace A. Smith

TABLE OF CONTENTS

ABSTRACT

This final report covers the work carried out under ONR Grant N00014-99-0530 developing the Thermodynamic Phenomenology to describe the properties of Lead zinc niobate: Lead titanate (PZN:PT) and Lead magnesium niobate: Lead titanate (PMN:PT) single crystals, over the period May 1, 1999 to June 30, 2001. Early into these studies it became apparent that the solution grown PZN:PT crystals at compositions close to the morphotropic phase boundary were more homogeneous with lower concentration gradients than the then available Bridgeman grown PMN:PT so the major effort was focused upon the PZN:PT family.

Early success for the program was the demonstration that E field induced monoclinic tilting of the P vector in the rhombohedral domain of the 001 field poled PZN 96.5:PT 4.5% was more than adequate to account for the crystal change of shape. The surprisingly large predicted intrinsic tilting of P in the dodecahedral prototypic mirror plane was later confirmed by Z. Ye (1) from optical measurements on single domain crystals. *

Fitting of the full elasto-dielectric behavior even using 8^{th} power expansion of the polarization order parameter proved surprisingly difficult. Realistic values of the coefficients required to model the dielectric behavior over estimated the fields required to produce phase switching and gave an orthorhombic phase of nearly identical free energy at the MPB composition.* It was tempting to believe the difficulty to be associated with the relaxor character. Recently however, the inverse experiment switching tetragonal to rhombohedral phase in $BaTiO_3$ single crystal have been analyzed using the well authenticated Devonshire function and again grossly overestimates switching fields.

Clearly both in PZN:PT and in $BaTiO_3$ we are calculating the E field required to switch between single domain end states; however, in both experiments the original poling induces a polydomain state with charged domain walls and an imposed different macro symmetry. For PZN 95.5: PT 4.5% we have used the phenomenology to calculate S_4,S_5,S_6 as a function of 001 oriented field imposed on the rhombohedral single domain. Experimental measurements of domain strain by x-ray methods should permit the evaluation of the polydomain constraints. Demonstration of the induced monoclinic state in PZN:PT has catalyzed a more systematic search for the low symmetry phases in other MPB systems, and the role played by this program

* Stabilization of an orthorhombic state in 110 field poled 0.95 PZB:008 PT crystals has been recently confirmed.

in the discovery of a stable monoclinic phase in the lead zirconate titanate (PZT) system is delineated in attached appendices.

1. INTRODUCTION

Following earlier established precedent the report will make use of earlier published papers as technical appendices so as to avoid repetition wherever possible. The early background of experimental information upon which first calculations of field induced strain in 001 poled PZN:PT crystals was based are given in appendices 1,2,3. In situ observations of domains in 0.9 Pb $(Zn_{1/3}\ Nb_{2/3})\ O_3$-0.1 $PbTiO_3$ Single crystals (Appendix 1) confirm that after field treatments the crystals of this compositions are in a mixed phase state which persists and are therefore unsuitable for our analysis. Evidence for the superior stability of the Engineered domain configuration in the 001 E field poled 0.92 PMN: 0.08 PT is given in appendix 2. Clearly the domain motion is inadequate to describe the shape change leading to the need for an intrinsic model. Measurements on 0.955 PZN:0.045 PT given in appendix 3 confirm the elegant anhysteretic quasi-linear strain, the very small volume change for fields up to 30 Kv/cm and the ability to phase switch into the tetragonal state at fields above 40 kV/cm. It is the dielectric and elastic data of appendix 3 which formed the basis for the simple application of the phenomenology given in appendix 4.

2. PHENOMENOLOGICAL ANALYSIS OF ACTUATION STRAIN

First application of the phenomenology was to ascertain whether the intuitive monoclinic tilting of the polarization vector in the 001 poled rhombohedral domain as proposed for example in Fig. 7 of appendix 3 is adequate to explain the exceptional quasi linear anhysteretic strain for E field levels up to 35 Kv/cm in the 95.5 PZN:4.5 PT single crystal. The simple analysis is given in appendix 4. Two basic simplifying assumption are made:

(a) That the magnitude of the polarization vector does not change significantly, as is evidenced by the volume strain in appendix 3 fig. 6.

(b) That the electrostriction coefficients Q_{11}, Q_{12} may be derived from the slope of the saturation arm of the induced tetragonal state at high fields.

Under these assumptions it is clear that if the polarization vector tilts through ~ 25° under 001 E field of 40 Kv/cm the electrostrictive strain associated with the rotation is more than adequate to explain the observed shape change. That just through prototypic electrostriction, intrinsic tilting of the polarization vector in the rhombohedral domain under 001 oriented field is sufficient to describe the anhysteretic piezoelectric strain of up to 0.4% is a most important result. Since the induced monoclinic phase is unstable without field the model nicely describes also the unusual absence of hysteresis.

Possible reasons why the simple model gives over estimates of the S_3 strain include:

(1) In relaxor ferroelectrics the Q_{ij} are not true constants due to the complex interplay of micro-polar regions. In pure PMN the magnitude of Q_{11} varies from 0.018 near Tm to 0.094 above T_d the Burns temperature. It is true that in the PZN: PT the crystal is field poled into a ferroelectric state but some inhomogeneity may persist so that the very high field gives spuriously high values of the Q_{ij}.

If instead of using the saturation arm, Q_{11} and Q_{12} are calculated from the total induced strain in the field forced tetragonal state, values of $Q_{11} = 0.0535$ and $Q_{12} = 0.0276$ (Appendix 5) are deduced and the calculated strain in the field forced monoclinic phase now fits almost perfectly with the measured data.

(2) A second possible explanation involves the nature of the end state in the experimental situation and will be taken up in section 4.

Without independent corroboration the theory would still be fragile. More recent optical measurements by Z-G. Ye (1) on single domain rhombohedral flakes of PZN 95.5: PT 4.5 under 001 oriented driving fields have confirmed substantial rotation of the optical indicatrix (fig. 1) confirming the field induced monoclinic tilt. It is interesting to note that the single domain tilt of the polarization is larger than that deduced in the 001 poled multidomain sample. A second confirmation of the monoclinic tilt comes from synchotron x-ray measurements at Brookhaven National Labs (Appendix 6). Here however, the measurements were made on a PZN 0.82:PT 0.08 sample where the polarization vector appears to leave the Dodecahedral Mirror at higher field levels. Again one must stress that field switching to the orthorhombic state is surprisingly easy in this composition and once switched the sample does not revert to single phase at zero field. The complexity of polarization change in the 8 Mole % PT composition is further demonstrated in the optical

studies of Z-G Ye, (1) which show mixtures of tetragonal and rhombohedral phases with very complex domain and phase boundary structures.

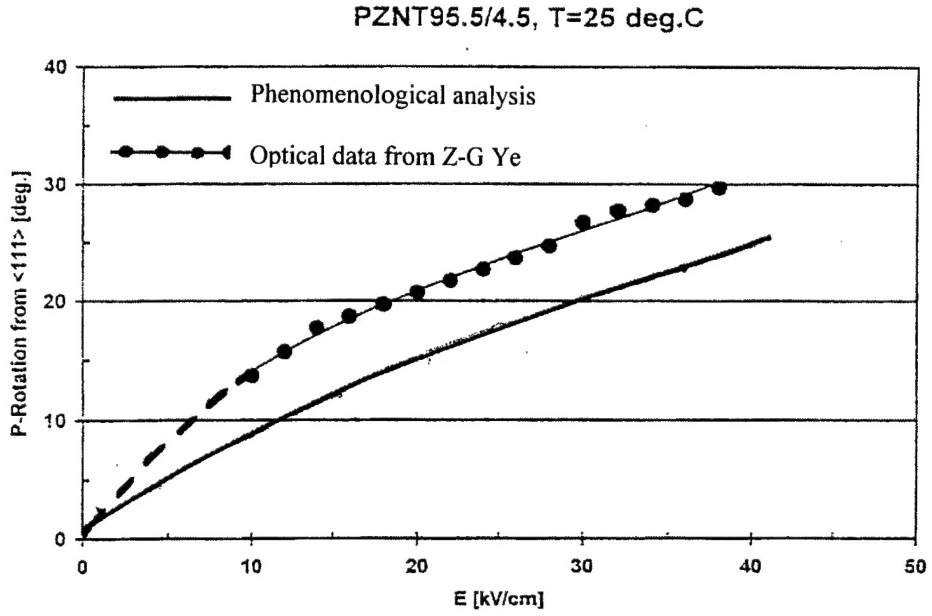

Fig. 1 Rotation of the rhombohedral polarization **P**(R3m) from $<111>_{cub}$ toward $<001>_{cub}$ in a (110)/(100) crystal of PZNT (95.5/4.5).

3. DETAILED FITTING FOR 0.955 PZN: 0.045PT

The equation describing the change of Gibbs Free Energy associated with changing polarization in the cubic m3m symmetry Perovskite may be written in the form:

$$\begin{aligned}
\Delta G = {} & \tfrac{1}{2}\alpha_1(P_1^2+P_2^2+P_3^2)+\tfrac{1}{4}\alpha_{11}(P_1^4+P_2^4+P_3^4)+\tfrac{1}{2}\alpha_{12}(P_1^2P_2^2+P_2^2P_3^2+ \\
& +P_3^2P_1^2)+\tfrac{1}{6}\alpha_{111}(P_1^6+P_2^6+P_3^6)+\tfrac{1}{4}\alpha_{112}[P_1^4(P_2^2+P_3^2)+P_2^4(P_1^2+P_3^2)+ \\
& +P_3^4(P_1^2+P_2^2)]+\tfrac{1}{2}\alpha_{123}P_1^2P_2^2P_3^2+\tfrac{1}{8}\alpha_{1111}(P_1^8+P_2^8+P_3^8)+\tfrac{1}{4}\alpha_{1112}\cdot \\
& \cdot[P_1^6(P_2^2+P_3^2)+P_2^6(P_1^2+P_3^2)+P_3^6(P_1^2+P_2^2)]+\tfrac{1}{4}\alpha_{1122}(P_1^4P_2^4+P_2^4P_3^4+ \\
& +P_3^4P_1^4)+\tfrac{1}{2}\alpha_{1123}P_1^2P_2^2P_3^2(P_1^2+P_2^2+P_3^2)-\tfrac{1}{2}s_{11}[X_1^2+X_2^2+X_3^2]- \\
& -s_{12}[X_1X_2+X_2X_3+X_3X_1]-\tfrac{1}{2}s_{44}[X_4^2+X_5^2+X_6^2]-Q_{11}[X_1P_1^2 \\
& +X_2P_2^2+X_3P_3^2]-Q_{12}[X_1(P_2^2+P_3^2)+X_2(P_1^2+P_3^2)+X_3(P_1^2+P_2^2)] \\
& -Q_{44}[X_4P_2P_3+X_4P_1P_3+X_6P_1P_2]-E_i\cdot P_i
\end{aligned} \tag{1}$$

Where P_i are the components of P along the axial direction (i = 1,2,3,) X_i the components of elastic stress, s_{ij} the elastic constants, Q_{ij} the components of the electrostriction tensor. Solution of the Energy function of interest are:

Parelectric Cubic Phase

$$P_1^2 = P_2^2 = P_3^2 = 0 \tag{2}$$

Tetragonal Phase

$$P_3^2 \neq 0,\ P_1^2 = P_2^2 = 0 \tag{3}$$

Monoclinic Phase

$$P_3^2 \neq P_1^2 = P_2^2 \neq 0 \tag{4}$$

Rhombohedral Phase

$$P_1^2 = P_2^2 = P_3^2 \neq 0, \tag{5}$$

In the tetragonal phase

$$\Delta G_T = \tfrac{1}{2}\alpha_1 P_3^2 + \tfrac{1}{4}\alpha_{11} P_3^4 + \tfrac{1}{6}\alpha_{111} P_3^6 + \tfrac{1}{8}\alpha_{1111} P_3^8 - Q_{11} X_3 P_3^2 - \tag{6}$$

$$- Q_{12}[X_1 P_3^2 + X_2 P_3^2] - E_3 \cdot P_3$$

Electric Field

$$\frac{\partial \Delta G}{\partial P_i} = E_i \tag{7}$$

Dielectric stiffness coefficients

$$\frac{\partial \Delta G}{\partial P_i \partial P_j} = \chi_{ij} \tag{8}$$

From symmetry

$$\chi_T = \begin{vmatrix} \chi_{11} & 0 & 0 \\ 0 & \chi_{11} & 0 \\ 0 & 0 & \chi_{33} \end{vmatrix} \tag{9}$$

In the monoclinic phase

$$\Delta G_M = \tfrac{1}{2}\alpha_1(2P_1^2 + P_3^2) + \tfrac{1}{4}\alpha_{11}(2P_1^4 + P_3^4) + \tfrac{1}{2}\alpha_{12}(P_1^4 + 2P_1^2P_3^2)$$
$$+ \tfrac{1}{6}\alpha_{111}(2P_1^6 + P_3^6) + \tfrac{1}{2}\alpha_{112}[P_1^6 + P_1^4P_3^2 + P_1^2P_3^4] + \tfrac{1}{2}\alpha_{123}P_1^4P_3^2$$
$$+ \tfrac{1}{8}\alpha_{1111}(2P_1^8 + P_3^8) + \tfrac{1}{3}\alpha_{1112}[P_1^8 + P_1^6P_3^2 + P_1^2P_3^6)] + \tfrac{1}{4}\alpha_{1122}[P_1^8 +$$
$$+ 2P_1^4P_3^4] + \tfrac{1}{2}\alpha_{1232}[2P_1^6P_3^2 + P_1^4P_3^4] - Q_{11}[P_1^2(X_1 + X_2) +$$
$$+ X_3P_3^2] - Q_{12}[(X_1 + X_2)(P_1^2 + P_3^2) + 2X_3P_1^2] -$$
$$- Q_{44}[X_4P_1P_3 + X_5P_2P_3 + X_6P_1^2] - 2E_1 \cdot P_1 - E_3 \cdot P_3 \qquad (10)$$

Electric field for zero Stress

$$E_3^M = \frac{\partial \Delta G}{\partial P_3} = \alpha_1 P_3 + \alpha_{11}P_3^3 + 2\alpha_{12}P_1^2P_3 + \alpha_{111}P_3^5 + \alpha_{112}[P_1^4P_3 +$$
$$+ P_1^2P_3^3] + \alpha_{123}P_1^4P_3 + \alpha_{1111}P_3^7 + \alpha_{1112}P_1^6P_3 + 2\alpha_{1122}P_1^4P_3^3 + 2\alpha_{1123}[P_1^6P_3 + P_1^4P_3^3] \qquad (11)$$

$$E_1^M = \frac{\partial \Delta G}{\partial P_1} = \alpha_1 P_1 + \alpha_{11}P_1^3 + \alpha_{12}[P_3^3 + P_1P_3^2] + \alpha_{111}P_1^5 + \alpha_{112}\left[\frac{3}{2}P_1^5 + P_1^3P_3^2 + \frac{1}{2}P_1P_3^4\right]$$
$$+ \alpha_{123}P_1^3P_3^4 + \alpha_{1111}P_1^7 + \alpha_{1112}\left[2P_1^7 + \frac{3}{2}P_1^5P_3^2 + \frac{1}{2}P_1P_3^6\right] + \alpha_{1122}[P_1^7 + P_1^3P_3^4] + \alpha_{1123}[3P_1^5P_3^2 + P_1^3P_3^4] \qquad (12)$$

Dielectric stiffness coefficients χ_{ij}

$$\chi_{11} = \alpha_1 + 3\alpha_{11}P_1^2 + \alpha_{12}(P_1^2 + P_3^2) + 5\alpha_{111}P_1^4 + \tfrac{1}{2}\alpha_{112}[7P_1^4 + 6P_1^2P_3^2 + P_3^4] +$$
$$+ \alpha_{123}P_1^2P_3^2 + 7\alpha_{1111}P_3^6 + \tfrac{1}{3}\alpha_{1112}[16P_1^6 + 15P_1^4P_3^2 + P_3^6] + 6\alpha_{1122}P_1^4P_3^2 +$$
$$+ \alpha_{1123}[7P_1^4P_3^2 + P_1^2P_3^4] \qquad (13)$$

$$\chi_{33} = \alpha_1 + 3\alpha_{11}P_3^2 + 2\alpha_{12}P_1^2 + 5\alpha_{111}P_3^4 + \alpha_{112}[5P_3^4 + P_1^4 + 6P_1^2P_3^2] + \alpha_{123}P_1^4 +$$
$$+ 7\alpha_{1111}P_3^6 + \tfrac{2}{3}\alpha_{1112}[P_1^6 + 15P_3^4P_1^2] + 6\alpha_{1122}P_1^4P_3^2 + 2\alpha_{1123}[P_1^6 + 3P_1^4P_3^2] \qquad (14)$$

$$\chi_{12} = 2\alpha_{12}P_1^2 + 4\alpha_{112}P_1^4 + 2\alpha_{123}P_1^2P_3^2 + 4\alpha_{1112}P_1^6 + 4\alpha_{1122}P_1^6 +$$
$$+ 2\alpha_{1123}[4P_1^4P_3^2 + P_1^2P_3^4] \qquad (15)$$

$$\chi_{13} = 2\alpha_{12}P_1P_3 + 2\alpha_{112}(P_1^3P_3 + P_3^3P_1) + 2\alpha_{123}P_1^3P_3 + 2\alpha_{1112}(P_1^5P_3 + P_3^5P_1) +$$
$$+ 4\alpha_{1122}P_1^3P_3^3 + 2\alpha_{1123}[3P_1^5P_3 + 2P_1^3P_3^3] \qquad (16)$$

and in the rhombohedral phase

$$\Delta G_R = \tfrac{3}{2}\alpha_1 P_3^2 + \tfrac{3}{4}(\alpha_{11} + 2\alpha_{12})P_3^4 + \tfrac{1}{2}(\alpha_{111} + 3\alpha_{112} + \alpha_{123})P_3^6 + \tfrac{3}{8}(\alpha_{1111} + \\ + 8\alpha_{1112} + 2\alpha_{1122} + 4\alpha_{1123})P_3^8 - \tfrac{1}{2}s_{44}[2X_4^2 + X_6^2] - Q_{11}[X_1 + X_2 + X_3]P_3^2 - \\ - 2Q_{12}[X_1 + X_2 + X_3]P_3^2 - Q_{44}[X_4 + X_5 + X_6]P_3^2 - (E_1 + E_2 + E_3)\cdot P_3 \qquad (17)$$

with dielectric stiffness coefficients

$$\chi = \begin{vmatrix} \chi_{11} & \chi_{12} & \chi_{12} \\ \chi_{12} & \chi_{11} & \chi_{12} \\ \chi_{12} & \chi_{12} & \chi_{11} \end{vmatrix} \qquad (18)$$

$$\chi_{11} = \alpha_1 + (3\alpha_{11} + 2\alpha_{12})P_3^2 + (5\alpha_{111} + 3\alpha_{112} + \alpha_{123})P_3^4 + (7\alpha_{1111} + \tfrac{32}{3}\alpha_{1112} + \\ + 6\alpha_{1122} + 8\alpha_{1123})P_3^6 \qquad (19)$$

$$\chi_{12} = 2\alpha_{12}P_3^2 + (4\alpha_{112} + 2\alpha_{123})P_3^4 + (4\alpha_{1112} + 4\alpha_{1122} + 10\alpha_{1123})P_3^6 \qquad (20)$$

To develop coefficients in the Energy Function electric polarization and dielectric permittivity for a 111 poled single domain sample was measured over the range from –180°C to +200°C. Least squares fitting yielded for the constants values.

Tc	= 150.6C
C	= 390,000
x_{11}	= $5.4.10^7$
x_{12}	= $1.61\ 10^8$
x_{111}	= $1.65\ 10^9$
x_{112}	= $1.65\ 10^9$
x_{123}	= $4.28\ 10^9$
x_{1111}	= $6.4\ 10^9$

The fitting achieved is shown in fig 2

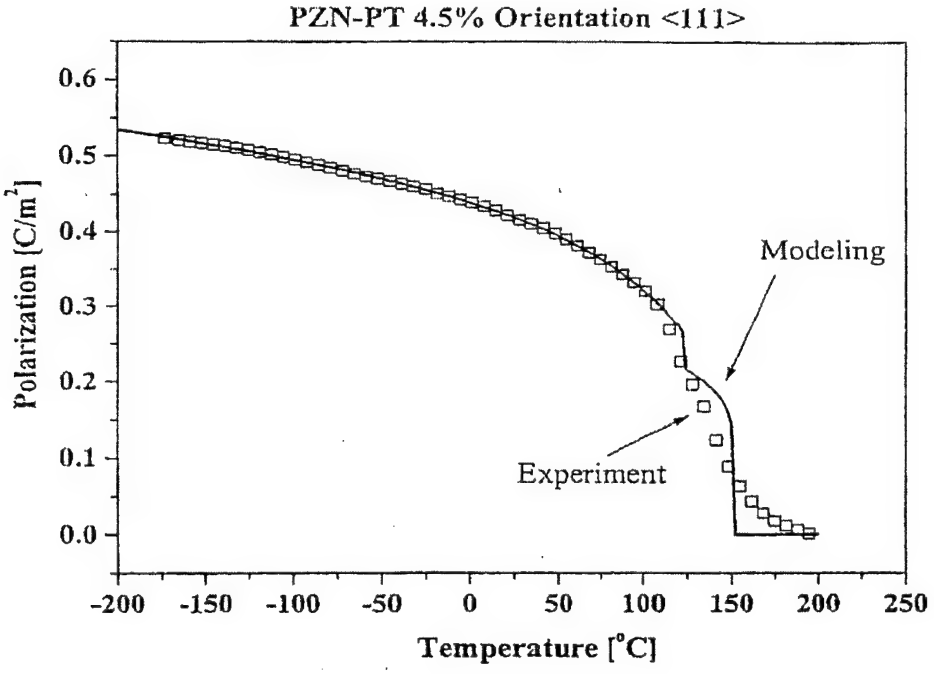

Fig 2 Best fitting of the Phenomenological Polarization to experimental data covering the range from –200°C to +200°C

From the polarization-derived constants, the calculated dielectric response is compared with values measured at 100 Hz under weak field (100 V/cm) in fig. 3

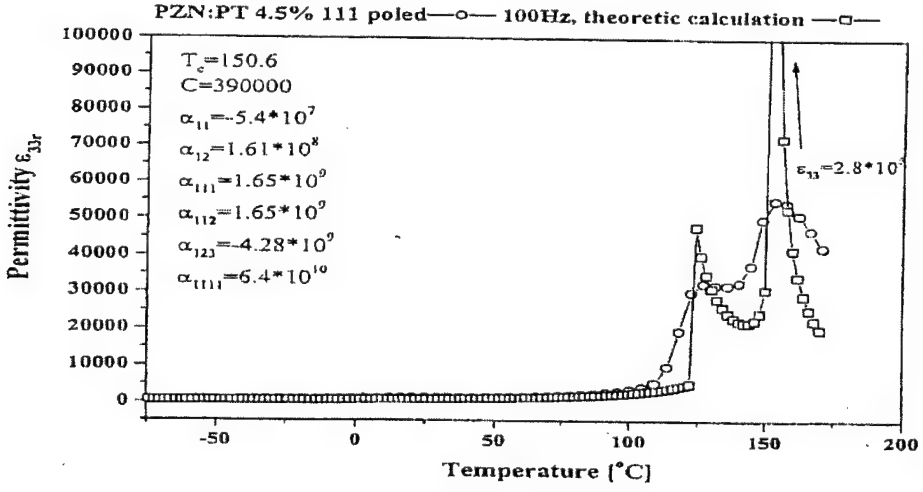

Fig. 3 Dielectric permittivity E_{33} measured at 100 Hz 100 V/cm compared with weak field permittivity derived from the thermodynamic function. Note that above 130°C the sample is in a relaxor state and not expected to fit with the phenomenology.

Dielectric saturation measured under DC bias fields at fixed temperature from 240K to 320 K shown in fig 4 is not fitted at all well with the chosen parameters.

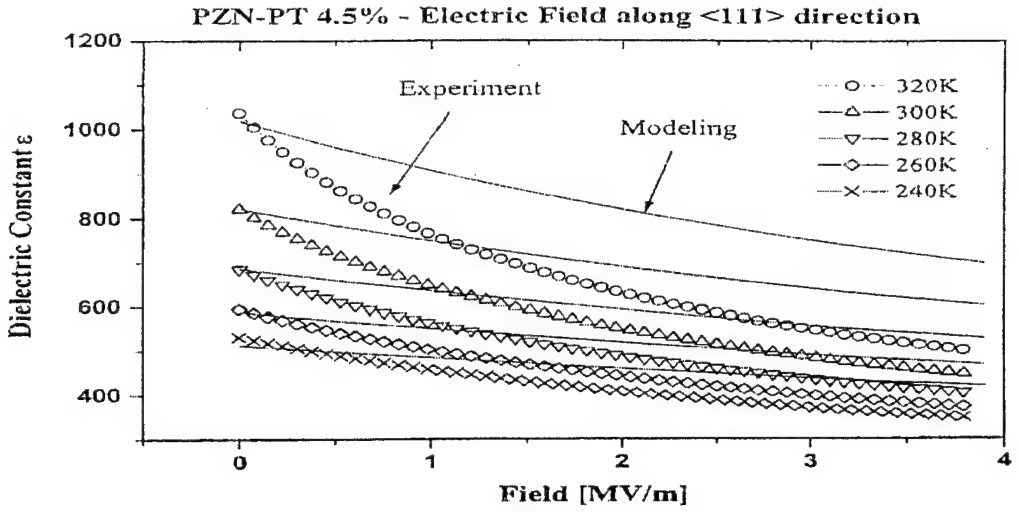

Fig. 4. Saturation of the relative weak field dielectric permittivity E_{33} as a function of applied DC field at fixed temperature between 240Kand 320K. Measured curves at 100 Hz compared to calculation from the phenomenology.

Clearly also the high <111> permittivity persisting to high fields contrary to the experimental finding limits the tilting of the polarization vector so that the calculated tilt as a function of 001 oriented E field (fig 5) is much less than the observed behavior.

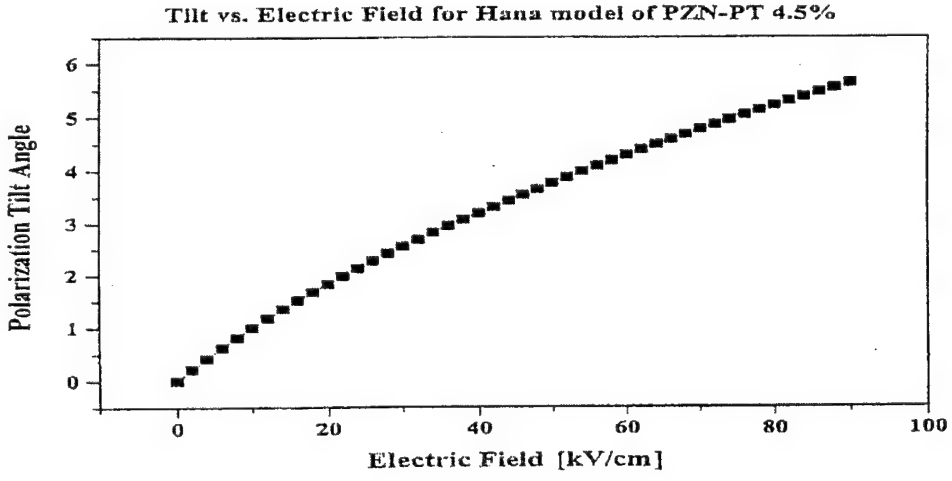

Fig. 5 Tilting of the Polarization Vector as a function of E field applied along 001 direction as derived from the phenomenology.

A simple Devonshire function, expanded to include all 6th order terms has been used by Abe et al (2) to describe the PZN:PT. The function models quite well the morphotropic phase boundary but uses constants which develop strong first order phase changes. Taking slightly modified constants to suit the 4.5 mole% PT composition of the form

$\theta = 155^{\circ}C$
$C = 6.84\ 10^{5}$
$x_{11} = 2.39\ 10^{8}$
$x_{12} = 1.26\ 10^{8}$
$x_{111} = 3.026\ 10^{9}$
$x_{112} = 3.65\ 10^{9}$
$x_{123} = 1.75\ 10^{9}$

Shows the following characteristics

A strong first order phase change at 177° C into the tetragonal phase, followed at 152° with a change to rhombohedral form (fig 6)

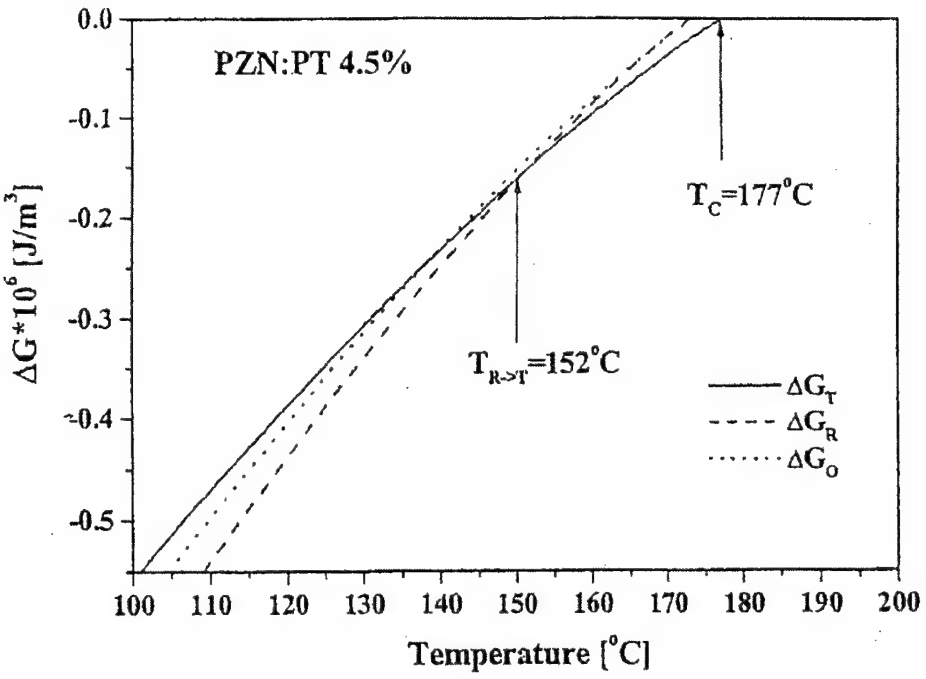

Fig. 6. Free Energy as a function of Temperature derives from the modified Abe Function

It is interesting however to note that a metastable orthorhombic phase is tracking very close to the stable phase, and crosses below the tetragonal phase at 130°C. Polarization behavior (fig 7) is much more abrupt and does not model well the experimental response,

however the significantly stiffer 111 polarization tilts under 001 applied field in reasonable agreement with the observed behavior. (Fig 8)

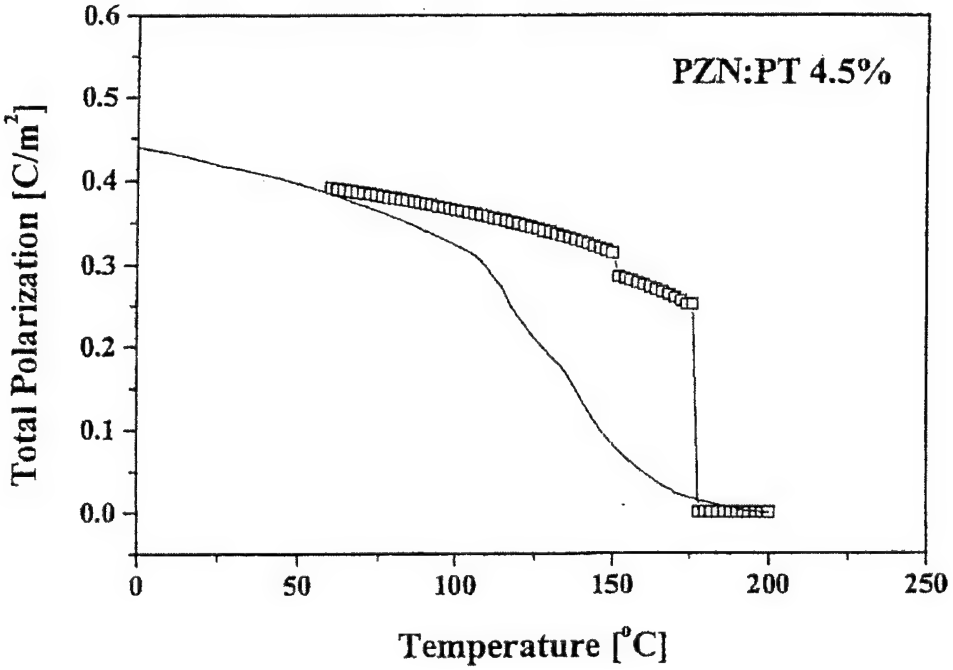

Fig. 7 Polarization vs Temperature calculated from the modified Abe function

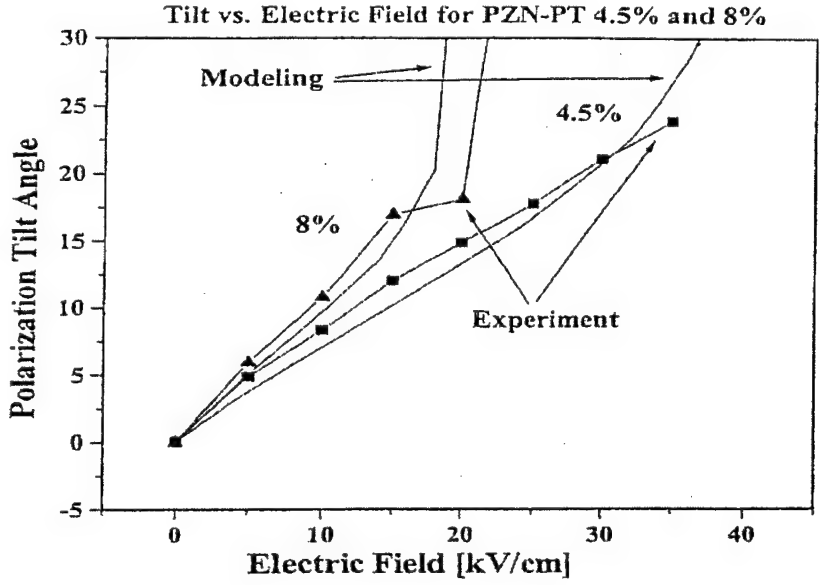

Fig. 8 Polarization tilting vs applied 001 oriented E field derived from the modified Abe function for 4.5% and 8% PT modified PZN:PT

4. DOMAIN ENGINEERED CRYSTALS of $BaTiO_3$

In view of the problems encountered with the PZN:PT system, it is important to explore the possible induced piezoelectric effects in single crystals of $BaTiO_3$ where there is already much experience with quantitative thermodynamic phenomenology (3) (4) (5) and a well authenticated modified Devonshire function (6) fitting the properties in all phases. Two types of experiments are possible:

(i) With 001 oriented E fields, developing domain engineered domain states in the orthorhombic and rhombohedral phases at low temperature and exploring the piezoelectric field induced strain as a function of temperature (Appendix 7).

(ii) Experiments with 111 oriented E fields applied to single crystal $BaTiO_3$ at room temperature to induce a domain engineered state of rhombohedral macro-symmetry and to explore the induced piezoelectric strain in the 111 direction (Appendix 8).

It is clear from the data presented in Appendix 7 (Fig 6) that the phenomenology accounts very well for the enhanced d_{33} values in the domain engineered states. Unfortunately the experimental set-up was such that it was not possible to explore phase switching at higher field levels.

For the experimental situation discussed in Appendix 8, A. Bell has carried out a detailed analysis using the modified Devonshire function (6). The function models the sequence of states observed perfectly in a qualitative manner, however, field magnitude required for switching in the phenomenology is some 3 time too large. A second feature of the 111 poled $BaTiO_3$ data in appendix 8 which was initially puzzling concerns the strain behavior. Clearly from tetragonal to rhombohedral states one is switching from high to low spontaneous strain yet from appendix 8 the switched strain is clearly positive. Exploring the situation further it is clear that the 111 direction intersects the tetragonal strain ellipsoid of revolution in a very low strain direction ($S_{111}(T) = 0.00025$) so that even though the rhombohedral strain is small ($S_4 = S_{111}(R) = 0.0023$), there is a positive step in spontaneous strain S_{111} (R) $-S_{111}(T)=$ 0.002 which is reasonably comparable to the measured strain $S_{111(M)} =0.0015$. These considerations however then lead directly to the second possible origin of disagreement between calculated and observed switching behavior, i.e. the fact that the initial state from which switching is accomplished in both PZN:PT and $BaTiO_3$ is a domain engineered

polydomain state where the engineered state has a higher macro-symmetry then the single domain thus involving both internal stress and internal electric fields.

For PZN:PT the rhombohedral form is of low spontaneous strain so that the stress which would be required to force pseudo-tetragonal symmetry is a modest $92MN/m^2$. In $BaTiO_3$ the tetragonal is the high strain form so it is not surprising that the system seeks an intermediate orthorhombic state by a strongly hysteretic path and only then appears to switch reversibly between metastable orthorhombic and final rhombohedral states. Unfortunately, neither in $BaTiO_3$ nor in PZN:PT has there been any effort to explore the difference in strain between poled domain engineered states and equilibrium domain configurations. In the 0.955 PZN:0.045PT it is possible to calculate directly the expected departure from rhombohedral strain (fig 9) for the single domain under 001 oriented E field. Precise X-ray measurement on a single domain flake would enable verification of the correct electrostriction constants and also analysis of the effects of the boundary conditions of the domain engineered crystal on performance.

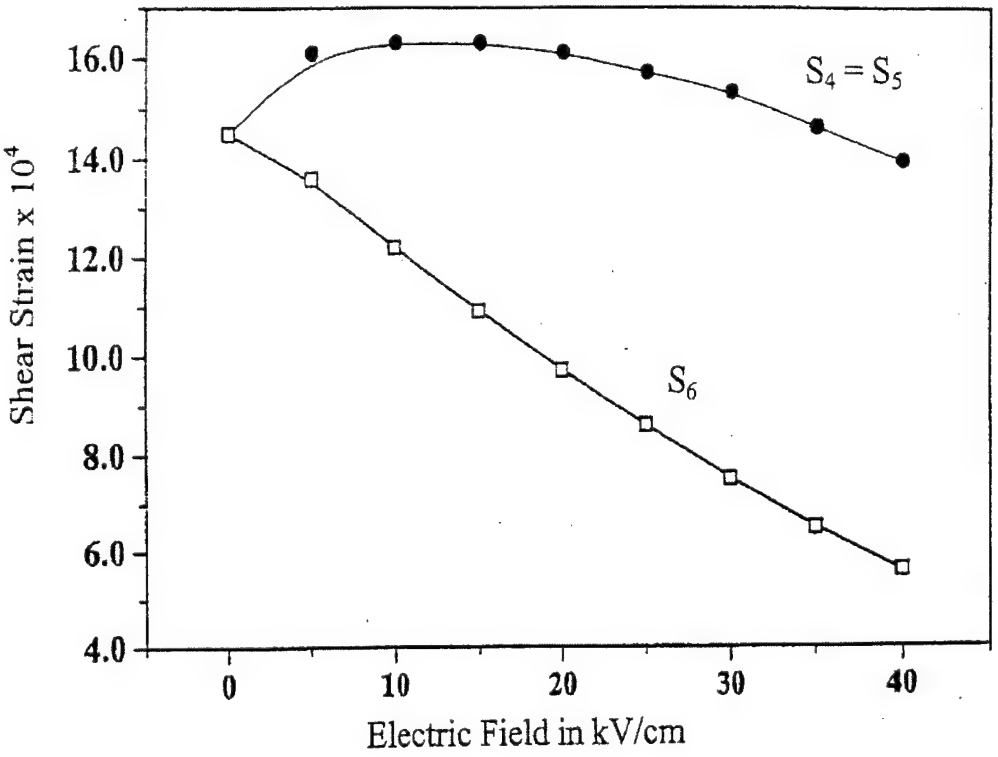

Fig. 9 Elastic Shear Strain as a function of applied 001 oriented E field calculated for a free single domain single crystal of 0.955 PZN:0.045PT

In $BaTiO_3$ the situation is more difficult due to the initial hysteretic response which clearly involves significant domain wall motion. For the stabilized anhysteretic response it will be interesting to compute the orthorhombic to rhombohedral shape change under 111 oriented field and to compare with optical and X-ray analysis.

5. MONOCLINIC TILTING OF P IN OTHER MPB SYSTEMS

Early in the contract period we were alerted to unusual behavior in the conventional Lead zirconate titanate (PZT) family which was being explored at Brookhaven National Laboratory in cooperation with the group of J.A. Gonzalo in Madrid. By supplying highly homogeneous PZT samples at the critical 52:48 Zr/Ti ratio and the early symmetry papers of L.A. Shuvalov we were able to help with the identification of a new monoclinic phase in the very well known, but here-to-fore inadequate phase diagram for PZT (Appendices 9, 10,11, 12).

The area is clearly of major relevance to current studies in that it re-affirms the propensity for easy tilting of the polarization vector in perovskite ferroelectrics at compositions close to the rhombohedral: tetragonal MPB. For the ceramics we have been long accustomed to looking for a maximum number of domain states to aid in poling, and clearly monoclinic symmetry with 24 vector states offers significant advantage. It may be noted also that intrinsic tilting of P in the domain and possible phase boundary motion under field are new polarization mechanisms (Appendix 11, 12) for this system.

The occurrence of the stable monoclinic phase now requires a re-examination of the original phenomenology by Haun et al (7, 8, 9, 10, 11). Rather than moving to 8^{th} order equations which are essential for a single order parameter system Andrew Bell, working with Eugene Furman on this program has suggested a two polarization order parameter model which more naturally explains the monoclinic phase. (12)

6. DISCUSSION

A clear strength of the phenomenology has been the ability to rapidly highlight the importance of tilting of the polarization vector in the rhombohedral domain of the 001 oriented and poled PZN:PT rhombohedral phase. Taken together with the optical evidence of tilting in a rhombohedral single domain flake under 001 field the intrinsic origin of the exciting quasi

linear piezoelectric strain was confirmed. Regarding the magnitude of the elastic strain clearly the Q_{11} and Q_{12} deduced from the very high field saturation arm of the field induced tetragonal state over estimates the induced strain. If however, the Q values are taken from total tetragonal strain induced after switchover there is close agreement between calculated and measured strain. It can be argued that the residual inhomogeneity of polarization in the induced ferroelectric phases leads to field and temperature dependence of the Q "constants" (13). Alternatively however, it can also be noted that in the Haun et al phenomenology for PZT (9) it is necessary to take $Q_{11} \sim 0.05$ and $Q_{12} \sim 0.015$ in the rhombohedral state to obtain agreement with experiment and in that treatment the Qs are taken as continuous function of composition. Another area of concern regards the crass assumption that we may treat the polarization processes in domain engineered and domain averaged crystals (Appendix 14, 15) as if the switching was between single domain states. The exciting possibilities for domain average engineering are highlighted in the appendices but the problem of compatibility conditions is not discussed. For PZN:PT at the 4.5% PT composition the spontaneous strains in the rhombohedral phase are low and the elastic compliance is high so that even to force the domain back to zero S_6 the required stress is tolerable. From the observed domain structures it is also clear that there must be charged domain walls which no doubt over time could accumulate compensation charges to stabilize the poled state.

Currently we are looking at the dimensions of carefully annealed samples and 001 field poled samples to begin exploring the state of internal stress. For $BaTiO_3$ tetragonal symmetry is the high strain state and 111 is a low strain direction which means that in the 111 poled crystal internal stresses must be very large, and may even force out the tetragonal state. Again unfortunately there is no experimental information.

It is disappointing that we were unable to obtain coefficients for the energy function which would describe the full family of elasto-dielectric properties. It may be argued that this is due to the residual relaxor character in the ferroelectric induced states. (Appendix 13) An alternative approach which must be explored concerns the possibility of a model involving two polarization order parameters, as has been proposed by Bell and Furman (11). If the order parameters are mutually coupled it is possible with just 6^{th} order equations to describe the full possible family of symmetry permitted phases for the ferroelectrics derived from prototypic m3m point symmetry. Similarly, if the components couple differently to the lattice, as might

be expected, a continuous mutation of the effective electrostriction constants with composition in the ferroelectric phases could be expected.

7. REFERENCES

1. Zou-Guang Ye, ONR Workshop on Piezoelectric Crystals, Washington DC, July 24-27 2001
2. K. Abe, O. Furukawa, H. Imagawa, Ferroelectrics 87 55 1988
3. A.F. Devonshire, Phil Mag 40 1040 1947
4. A.F. Devonshire, Advances in Physics Phil Mag. Suppl. 3.85 1954
5. W.R. Buessem, L.E. Cross, A.K. Goswami, J. Am Ceram. Soc 49
6. A.J. Bell, L.E. Cross, Ferroelectrics 59 197 1984
7. M.J. Haun, E. Furman, S.J. Jang, L.E. Cross, Ferroelectrics 99 13 1989
8. M.J. Haun, E. Furman, H.A. McKinstry, L.E. Cross, Ferroelectrics 99 27 1989
9. M.J. Haun, Z.Q. Zhang, E. Furman, S.J. Jang, L.E. Cross, Ferroelectrics 99 45 1989
10. M.J. Haun, E. Furman, T.R. Halemane, L.E. Cross, Ferroelecrics 99 55 1984
11. M.J. Haun, E. Furman, S. J. Jang, L.E. Cross, Ferroelectrics 99 1989
12. A.J. Bell, E. Furman, Private Communication
13. Shi-Fang Liu, S.E. Park, L.E. Cross, T.R. Shrout, to be Published

8. GRADUATE STUDENTS

None

9. HONORS AND AWARDS

L. Eric Cross	IEEE Ultrasonic Ferroelectric and Frequency Control: 3rd Millennium Medal 2000
L. Eric Cross	American Ceramic Society Honorary Life Member 2001
	IEEE Honorary Life Member 2001

10. PAPERS PUBLISHED IN REFEREED JOURNALS

1. Belegundu, Uma, X. H. Du, L.E. Cross and Kenji Uchino, "In Situ Observation of Domains in $0.9PB(Zn_{1/3}Nb_{2/3})O_3$-$0.1PbTiO_3$ Single Crystals", Ferroelectrics, Vol. 221, pp 67-71 (1999)

2. Wada, Satohsi, S.E. Park, L. E. Cross, and T. R. Shrout, "Engineered Domain Configuration in Rhombohedral PZN:PT Single Crystals and their Ferroelectric Related Properties", Ferroelectrics, Vol. 221, pp 147-155 (1999)
3. Liu, Shi-Fang, S.E. Park, T. R. Shrout, and L.E. Cross, "Electric field dependence of piezoelectric properties for rhombohedral 0.955 $Pb(Zn_{1/3}Nb_{2/3})O_3$-0.045$PbTiO_3$ single crystals", Journal of Applied Physics, Vol. 85, No. 5, pp 2810-2814 (March 1999)
4. Noheda, B., D.E. Cox, G. Shirane, S.E. Park, L.E. Cross, and Z. Zhong, " Polarization Rotation via a Monoclinic Phase in the Piezoelectric 92% $PbZn_{1/3}Nb_{2/3}O_3$-8%$PbTiO_3$", Physical Review Letters, Vol 86 No 17, pp 3891-3894, (April 2001)
5. Park, Seung-Eek, S. Wada, L.E. Cross, and T.R. Shrout, "Crystallographically engineered $BaTiO_3$ single crystals for high performance piezoelectrics", Journal of Applied Physics, Vol. 86 No. 5, pp 2746-2750 (September 1999)
6. Wada, Satoshi, S. Suzuki, T. Noma, T. Suzuki, M. Osada, M. Karmana, S.E. Park, L. E. Cross and T. R. Shrout, "Enhanced Piezoelectric Property of Barium Titanate Single Crystals with Engineered Domain Configurations", Jpn. J. Appl. Phys., Vol 38 Pt. 1 No. 9B, pp 5505-5511 (1999)
7. B. Noheda, J.A. Gonzalo, L.E. Cross, R. Guo, and S.E. Park, D. E. Cox, and G. Shirane, "Tetragonal –to monoclinic phase transition in a Ferroelectric perovskite: The structure of $PbZr_{0.52}$ $Ti_{0.48}O_3$", Physical Review B Vol 61 No. 13, pp 8687-8695 (April 2000)
8. Noheda, B., D. E. Cox, G. Shirane, R. Guo, B. Jones, and L.E. Cross, "Stability of the monoclinic phase in the ferroelectric perovskite $PBZ_{r1-x}Ti_xO_3$", Physical Review B, Vol 63, 014103, pp 014103-1-014103-8, (2000)
9. Noheada, B., J.A. Gonzalo, R. Guo, S.E. Park, L.E. Cross, D. E. Cox and G. Shirane, "The monoclinic phase in PZT: new light on morphotropic phase boundaries", American Institute of Physics, AIP Conference Proceedings Aspen Center for Physics Winter Workshop, pp 1-15, (2000)
10. Guo, R., L.E. Cross, S.E. Park, B, Noheda, D.E. Cox, and G. Shirane, "Origin of the high piezoelectric response in $PBZr_{1-x}Ti_xO_3$", Physical Review Letters, Vol 84, No. 23, pp 1-4, (June 2000)

11. Vieland, D., J. Powers, L.E. Cross, J. F. Li, "Importance of random fields on the properties and ferroelectric phase stability of <001> oriented 0.7 $PB(Mg_{1/3}Nb_{2/3})O_3$ –0.3 $PbTiO_3$ crystals", Applied Physics Letters, Vol 78, No. 18 (30 April 2001)

12. Fousek, J., D. B. Litvin, and L.E. Cross, "Domain geometry engineering and domain average engineering of Ferroics", Journal of Physics Condensed Matter, 13, L33-L38, (2001)

13. Fousek, J., L.E. Cross, "Engineering Multidomain Ferroic Samples" Ferroelectrics, Vol 252, pp. 171-180 (2001)

11. PAPERS APPEARING IN NON REFEREED PUBLICATIONS

1. Cross, L. Eric, P. Hana, "Phenomenology of the Elasto-dielectric Response in the Field Forced Ferroelectric Phase of Leas Zinc Niobate: Lead Titanate (PZN:PT) Relaxor Ferroelectric", The 9th US-Japan Seminar on Dielectric & Piezoelectric Ceramics, Summary and Extended Abstract, pp 15-18 (November 1999)

2. Cross, L. Eric, "Domain and Phase Change Contributions to Response in High strain Piezoelectric Actuators", Fundamental Physics of Ferroelectrics 2000: Aspen Center for Physics Winter Wkshp, pp 1-15 (2000)

12. INVITED PAPERS AT NATIONAL AND INTERNATIONAL MEETINGS

1. Cross, L.E., S. Park, and S. Liu, "Simple Phenomenological Analysis of the Strain Behavior in Relaxor Ferroelectric Lead Zinc Niobate: Lead Titanate Single Crystals", SPIE 6th Annual International Symposium on Smart Structures and Materials, Newport Beach, California (3-5 March 1999)

2. Cross, L.E., "High Strain Actuator Materials Current Status and Future Prospects," U.S. Navy Workshop on Acoustic Transduction Materials and Devices, State College, Pennsylvania (13-15 April 1999)

3 Cross, L.E. "Phenomenology of the Elasto-Dielectric Response in the Field Forced Ferroelectric Phases of Lead Zinc Niobate: Lead Titanate (PZN:PT) Relaxor Ferroelectrics Single Crystals", Ferroelectric Workshop in Puerto Rico, Guanica, Puerto Rico (12-14 May 1999)

4. Cross, L.E., "Electronic Ceramics: Current Progress and Prospects for the 21st Century", IUMRS-ICAM 99, Beijing China (13-19 June 1999)
5. Cross, L.E., "Piezoelectricity in Single Crystal Relaxor Ferroelectrics with Morphotropic Phase Boundaries Properties: Processing and Future Prospects", 1999 Annual Conference of British Association for Crystal Growth, Cambridge, England (16-17 September 1999)
6. Cross, L.E. "New Materials for Smart Applications in Progress in the USA", US: Japan 2nd collaboration Meeting, Penn State, University Park, Pennsylvania (23 September 1999)
7. Cross, L.E., "New Relaxor Ferroelectric Piezoelectric and Electrostrictive Actuators and Sensors for Smart Materials", Euromat 99, Munich, Germany, (27-30 September 1999)
8. Cross, L.E., "Current and Potential Future Developments in Electrostrictive Actuators Materials", ICAST 99, Paris, France (11-13 October)
9. Cross, L.E, "Phase switching perovskites for actuator applications", SPIE 7th Annual International Symposium on Smart Structures and Materials, Newport Beach, CA (March 2000)
10. Cross, L.E, P. Hana, "Progress in the Thermodynamic Phenomenology for the Lead Zinc Niobate: Lead Titanate Solid Solution System", (VII. 3), 2000 US Naval Workshop on Acoustic Transduction Materials and Devices, State College, (April 2000)
11. Cross, L.E., "Domain and phase change contributions to response in high strain ferroelectric materials", the 6th International Symp. On Ferroic Domains and Mesoscopic Structures (ISFD-6), May Nanjing University
12. Cross, L.E., "Overview of Active Materials", Aero Smart 2000, Texas A&M University, College Station, TX, (September 2000)
13. Cross, L.E., "Domain and Phase Change Contributions to Response in High Strain Piezoelectric Actuators",3rd Asia Meeting on Ferroelectric AMF3, Hong Kong, (December 2000)

14. Cross, L. E., "High Strain High Coupling Piezoelectric Ferroelectric Single Crystals: Current Status and Future Prospects", IEEE International Ultrasonics Meeting, Lake Tahoe, Nevada, (October 1999)
15. Cross, L.E., and P. Hanna, "Phenomenology of the Elasto-Dielectric Response in the Field-Forced Ferroelectric", 9th US: Japan Meeting on Dielectric and Piezoelectric Ceramics, Okinawa, Japan (2-5 November 1999)

13. CONTRIBUTED PAPERS

None

14. PERSONNEL

L.E. Cross	Evan Pugh Professor Emeritus of Electrical Engineering
Eugene Furman	Research Associate
Petr Hanna	Post Doctoral Fellow

Appendix 1

Ferroelectrics, 1999, Vol. 221, pp. 67-71
Reprints available directly from the publisher
Photocopying permitted by license only

In Situ Observation of Domains In $0.9Pb(Zn_{1/3}\ Nb_{2/3})O_3$ - $0.1PbTiO_3$ Single Crystals

UMA BELEGUNDU, X. H. DU, L. E. CROSS and KENJI UCHINO

International Center for Actuators and Transducers, Materials Research Laboratories, The Pennsylvania State University, University Park, PA 16802

Domains in $0.9Pb(\ Zn_{1/3}\ Nb_{2/3}\ )O_3 - 0.1PbTiO_3$ or "PZN-PT" single crystals under the application of electric field were investigated with an optical microscope. The dynamic response of the domains was studied under an electric field on PZNPT crystals is reported. In this study, electric field applied along [001]. The domain formation with the changing temperature showed the successive phase transitions from cubic to tetragonal and then to rhombohedral with decreasing temperature. The room temperature configuration showed the co-existence of both rhombohedral and tetragonal domains. Under the given experimental conditions we found that a single domain state could be induced only in the tetragonal state. Even though the temperature was lowered to - 100°C, complete transformation to the rhombohedral state was not observed.

Keywords: Relaxor Ferroelectric; Domain studies; Single crystals

INTRODUCTION

Relaxor materials such as $Pb(\ Zn_{1/3}\ Nb_{2/3}\ )O_3$ (PZN) and their solid solutions with $PbTiO_3$ (PT) have come into prominence due to their very high electromechanical coupling factors k[1,2]. In 1982, Kuwata, Uchino and Nomura discovered that poling along the [001] direction for rhombohedral crystals led to a very high value of k_{33} of 92%. Since the spontaneous polarization direction for the rhombohedral symmetry is along [111] direction, some hierarchial domain configuration is expected in the [001] poled sample. In general, the properties such as permittivity and piezoelectric properties are significantly affected by the domain motion. It is well known that the relative volume of domain orientation can be changed by the application of electric field in ferroelectrics and that these relative volumes affect the properties. In the present experiment, we have tried to understand and identify the various domains formed in the crystal under the influence of electric field.

PZN, is a relaxor ferroelectric[3] with a broad and frequency dependent phase transition near 140 °C and PT is a regular ferroelectric with a sharp phase transition at 490 °C. PZN has rhombohedral symmetry and PT has tetragonal symmetry. The composition chosen lies at the morphotropic phase boundary of the solid solution of these two systems.

For the present studies, single crystals 0.9PZN-0.1PT composition were grown in the laboratory. The different domains formed, their switching behaviour due to temperature variation with field applied along [001] direction, is reported herein.

PREPARATION OF THE SINGLE CRYSTAL SAMPLE

Single crystals of 0.9PZN- 0.1PT composition were grown by the conventional flux method. The crystallographic direction [011], [001] and [111] were determined by Laue Back Reflection method. The plate of the crystal lies in (110) plane so as to apply the field along [001] direction. The sample was then ground to a thickness of 100 μm using SiC powder and polished to mirror finish using diamond paste. Sputtered gold electrodes were deposited and silver lead wires were connected to the sample using air dry silver paste. The surface electrode gap was 400 μm.

The domain observation was carried out using Nikon Transmission Microscope under crossed polarizers. A temperature controlled sample stage (Linkam) was used to observe the domains as a function of the temperature. A VCR with the monitor connected to the microscope allowed the data to be recorded dynamically. A function generator was used to apply a triangular wave type with a frequency of 0.05 Hz (20 sec period) and the maximum value of 7 kV/cm to the sample. The temperature of the crystal was changed from –100° C to + 250° C at the rate of 10° C/min. In the figures given, the electrodes are located at top and bottom of the pictures. The plane of the picture (plane of the crystal) is perpendicular to [110] and [001] lies along top to bottom of the picture.

RESULTS

The 0.9PZN-0.1PT crystal showed the co-existence of both the rhombohedral and tetragonal domains at room temperature. "Needle shaped" domains are associated with rhombohedral symmetry and the "stripe pattern" with the tetragonal domains. As the temperature was lowered to -37°C, the needle shaped domains associated with rhombohedral symmetry emerged more clearly. Some tetragonal distortion remained at -100°C and complete transformation to rhombohedral state was not observed probably due to spatial

composition variation in the crystal. As the sample was heated, the transition from rhombohedral to tetragonal occurred over a wide temperature range and complete tetragonal state was observed at 90° C. With increasing temperature, these tetragonal domains increased in width to 40 μm finally disappearing at 228°C. On cooling, these domains appeared around 225°C, finally having a mixture of both tetragonal and rhombohedral domains at room temperature. The domain patterns at different temperatures, while heating are shown in Fig. 1a, 1b, 1c.

On application of the field ± 7kV/cm, the color changes associated with the birefringence occurred at 220°C. As the temperature was reduced, no clear stripe pattern associated with tetragonal domains was observed. Rather, the whole region between the electrodes switched in uniform manner. A small number of stripes were observed near the electrodes possibly due to electrode effect. Figure 1f shows the domain pattern at 148°C with the application of the field. Figure 1c shows the clear tetragonal pattern obtained at the same temperature without field. This temperature corresponds to stable tetragonal state with the polarization direction along [001]. Since in our experiment, the field is along [001] almost monodomain tetragonal phase was achieved, providing a few number of domain walls.

On further cooling near 135° C, some interesting results were observed. As mentioned above, complete tetragonal state was observed above 90° C without the electric field. Figure 2 shows the domain formation at zero field and maximum applied field at 125° C and 85° C. Figures a and c correspond to zero field, where a domain resembling a "needle" needle shape was induced. These disappeared for the maximum value of the field (Fig 2. b and d). The switching of these speculated rhombohedral domains took place in wave like motion. It appears that the rhombohedral phase is being induced at this temperature. Also the reduction in tetragonal domain width and the increase in their number began at this temperature. As the temperature was reduced further, these rhombohedral domains split into smaller needle shape microdomains[4]. This is shown in Fig. 1d. The switching of the domains continues till -25°C and freezes thereafter. Below this temperature, the rhombohedral domains increase in number.

ACKNOWLEDGEMENTS:

The support provided by Office of Naval Research, fund N00014-91-J-4145 is greatfully acknowledged

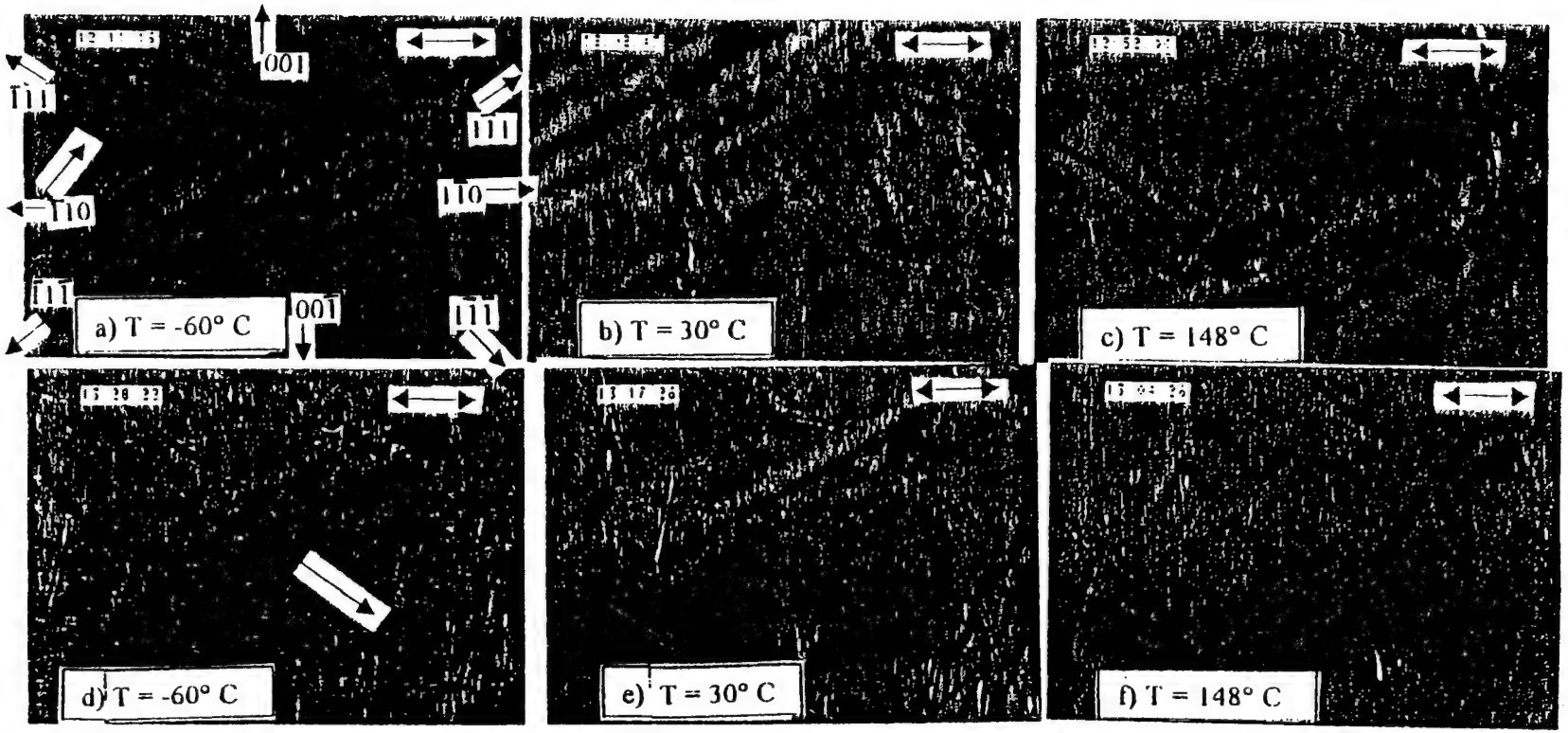

Fig. 1 Domain patterns formed with varying temperature and applied electric field. The electrodes are located at the top and bottom of the figures. The plane of the photograph is perpendicular to [110] and the relavent crystal directions are shown in the first figure.Figures a), b) and c) show the domains at different temperatures without the application of the field. The rhombohedral domains are indicated by the arrow. Figures d), e) and f) show the effect of field + 7kV/cm Monodomain state obtained by the application of field is clear in f). The bar on right top corner represents 20 μm length (⟷)

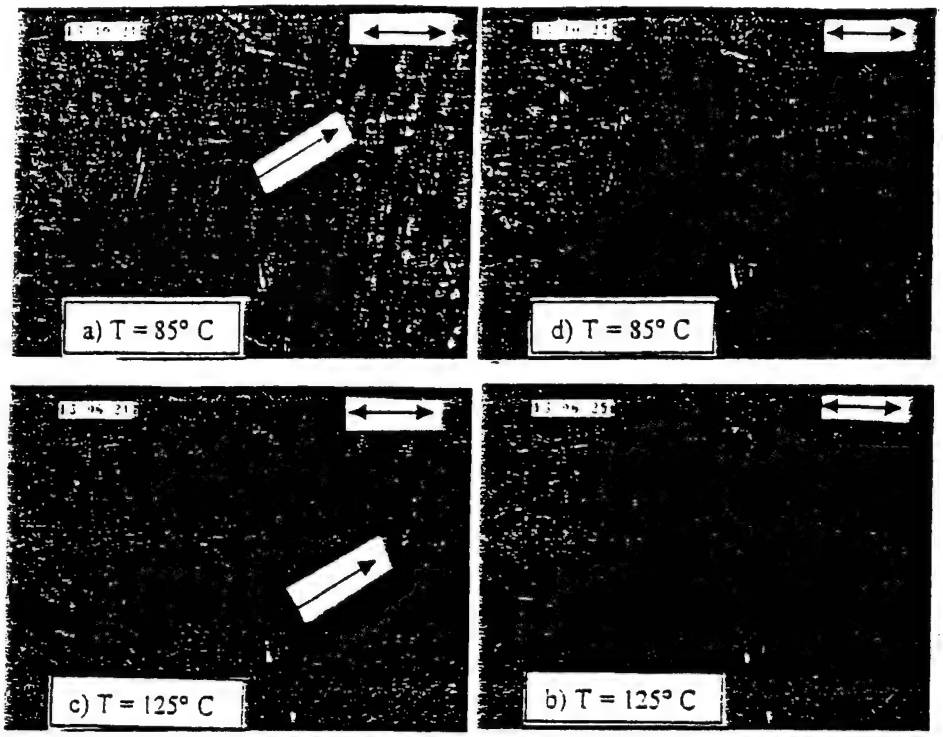

Fig. 2 Domain formation at zero field and maximum applied field of 7 kV/cm at 125° C and 85° C. Figures a) and c) correspond to zero field, where a domain resembling a "needle" (needle shape) was induced. (indicated by the arrow). The plane of the photograph is perpendicular to [110], the relavent crystal directions are shown in the Fig. 1 a).

References

[1] J. Kuwata, K. Uchino and S. Nomura. *Ferroelectrics.*, **37**. 579 (1981)
[2] S. E. Park and T. R. Shrout. *IEEE Transactions on Ultrasonics Ferroelectrics and Frequency Control*, (1997)
[3] G. A. Smolenski and A. I. Agranovskya. *Sov. Phys. Sol.-State.*, **1**, 1429.(1959)
[4] M. L. Mulvihill, L. E. Cross and K. Uchino. *J. Am Ceram. Soc.*, **78**. 3345. (1995)

Appendix 2

Ferroelectrics, 1999, Vol. 221, pp. 147-155
Reprints available directly from the publisher
Photocopying permitted by license only

Engineered Domain Configuration in Rhombohedral PZN-PT Single Crystals and their Ferroelectric Related Properties

SATOSHI WADA[a], SEUNG-EEK PARK[b], LESLIE ERIC CROSS[b] and THOMAS RICHARD SHROUT[b]

[a]*Tokyo University of Agriculture & Technology, 24–16 Nakamachi 2-chome, Koganei, Tokyo 184–8588, JAPAN; and* [b]*Materials Research Laboratory, The Pennsylvania State University, University Park, PA 16802, USA*

The domain configuration of rhombohedral PZN-8%PT single crystals has been observed as a function of electric-field and crystallographic orientation using polarizing microscope. Although a single domain state could be achieved by applying an E-field along the rhombohedral polar direction [111], a multidomain state was observed with the removal of the E-field. This domain instability was associated with large hysteresis of the strain vs. E-field behavior. In contrast, an engineered domain configuration of [001] oriented rhombohedral crystals was found to be stable with no domain motion detectable under DC-bias, resulting in hysteresis minimized strain vs. E-field behavior. The stable engineered domain configuration under bias in multidomain [001] oriented crystals was suggested as an evidence of macroscopic symmetry 4mm out of 3m rhombohedral crystals.

Keywords: PZN-PT; single crystal; domain; hysteresis; macroscopic symmetry

INTRODUCTION

In compositional engineering of conventional PZT ceramics, enhanced piezoelectric activity is achieved by adjusting Tc downward, resulting in "soft" PZT's (d_{33} > 500 pC/N) with low coercivity (Ec ~ 5 kV/cm). These soft PZT's are accompanied by large hysteresis in their strain vs. E-field behavior due to domain wall motion under bias, limiting applications to low frequencies. "Hard" PZTs with minimized strain vs. E-field hysteresis behavior are a consequence of acceptor dopants, constraining domain wall mobility. This non-hysteretic strain vs. E-field behavior, however, comes

with the expense of decreased piezoelectric activity (d_{33} ~ 200 pC/N). Hysteresis free strain vs. E-field behavior is also expected from single domain ferroelectric crystals. Ferroelectric single crystals such as $LiNbO_3$, however, have not been intensively investigated for actuators because of their inherently inferior piezoelectric activity (d_{33} < 50 pC/N).

Recently, ultrahigh piezoelectric properties (d_{33} ~ 2500 pC/N) and large strain (1.7 %) were achieved from [001] oriented rhombohedral crystals of relaxor based ferroelectric $Pb(A_{1/3}Nb_{2/3})O_3$ (A = Zn^{2+}, Mg^{2+}) and its solid solution with the normal ferroelectric $PbTiO_3$ (PT).[1-4] Fig. 1 presents the typical strain vs. E-field behavior observed in rhombohedral PZN-8%PT crystals. As [001] is not the polar direction, [001] poled crystals must be comprised of a multidomain state. Furthermore, these crystals are "softer" (Ec ~ 3 kV/cm) than soft PZT's (Ec > 5 kV/cm). However, strain values as high as 0.4 % were realized with minimized hysteresis, suggesting little domain motion under bias, a phenomenon not expected for multidomain "soft" ferroelectric crystals. In contrast, crystals oriented along [111], the polar direction of rhombohedral crystals, exhibited inferior properties such as d_{33} ~ 82 pC/N. The E-field induced strain was also accompanied by large hysteresis.

In this study, the domain configuration of rhombohedral PZN-8%PT crystals was observed as a function of E-field and crystallographic orientation using a polarizing microscope. The behavior of domain wall motion will be discussed in relation to the observed hysteretic strain vs. E-field behavior.

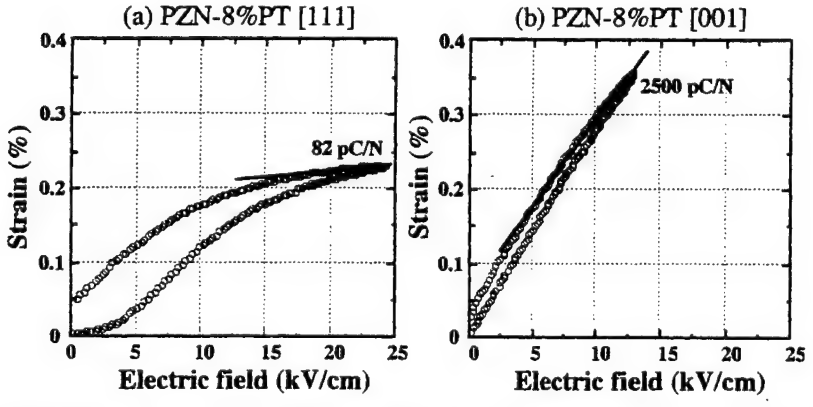

FIGURE 1 Strain vs. E-field behavior for PZN-8%PT crystals oriented along [111] and [001].

Moreover, the change of macroscopic symmetry induced by the engineered domain configuration will also be discussed.

EXPERIMENTAL

PZN-8%PT single crystals were grown by a flux method. Further details on the crystal growth were reported elsewhere.[2,5] Flux grown crystals were oriented along [111] or [001] direction using a back reflection Laue camera. Crystals were heat-treated at 250 °C for 16 hr in air prior to domain observation, to remove residual stress that might result in the formation of ferroelastic domains. For in-situ domain observation under DC-bias, the sample surface was mirror-polished with the sample thickness approximately 200-300 μm along the transmittance direction of polarized light. Gold electrodes were sputtered on both sides parallel to the polarized light. Sample width between sputtered Au electrodes was approximately 500-600 μm. Thin samples (~50 μm) with mirror-finished (111) or (001) surfaces were also prepared to observe detailed domain configurations more clearly before and after E-field exposure for crystallographic interpretation. The domain configuration was observed under crossed-nicols using a Polarizing microscope (Carl Zeiss, D-7082). The application of an E-field was along the [001] or [111] direction, being normal to the polarized light, using a Trek 610A HV Amplifier.

RESULTS AND DISCUSSION

Domain configuration - Zero-bias state before and after E-field exposure

PZN-8%PT is compositionally located near the morphotropic phase boundary (~ 9 mol%PT) between rhombohedral phase (R3m) and tetragonal phase (P4mm) at room temperature.[1] PZN-8%PT undergoes two phase transitions as a function of temperature, i.e., (1) rhombohedral <-> tetragonal phase transition around 90 °C ($PT_{R\text{-}T}$), and (2) tetragonal <-> cubic (Pm3m) phase transition around 170 °C ($PT_{T\text{-}C}$). Thus, the domain configuration observed at 25 °C before E-field exposure contains domain walls originating from $PT_{T\text{-}C}$ and $PT_{R\text{-}T}$. Figs. 2(a) and 3(a) show domain configurations of [111] and [001] oriented PZN-8%PT crystals before E-field exposure, respectively. Although ferroelectric domain-like pattern was obvious, crystallographic interpretation

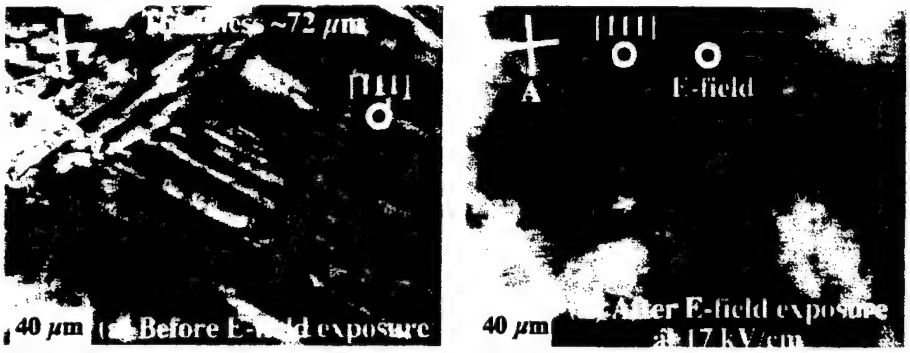

FIGURE 2 Domain configuration of [111] oriented PZN-8%PT crystals before and after poling.

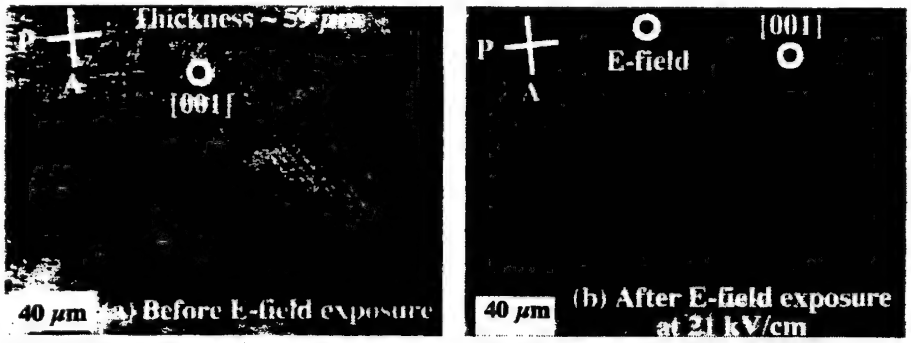

FIGURE 3 Domain configuration of [001] oriented PZN-8%PT crystals before and after poling.

was difficult due to vague domain boundaries.

Figs. 2(b) and 3(b) present the domain configurations of [111] and [001] oriented PZN-8%PT crystals after E-field (~ 20 kV/cm) exposure, respectively. In contrast to Figs. 2(a) and 3(a), E-field induced domain configuration was observed. The [111] oriented PZN-8%PT crystals (Fig. 2(b)) consisted of three kinds of the band-shaped domains with equivalent polar vectors ($[\bar{1}11]$, $[1\bar{1}1]$ and $[11\bar{1}]$) in the domain with polar direction of [111]. Therefore, all domain boundaries could be interpreted as 71° domain walls of {110} planes between [111] domain and three domains with polar directions ($[\bar{1}11]$, $[1\bar{1}1]$ and $[11\bar{1}]$) and 109° domain walls of {100} planes between three domains with polar directions ($[\bar{1}11]$, $[1\bar{1}1]$ and $[11\bar{1}]$), consistent with crystallographic domain wall relationships.[6-7] As shown in Fig. 3(b), fiber-like domains with sharp edges on both ends were observed for [001] oriented PZN-8%PT crystals. Although crystallographic interpretation

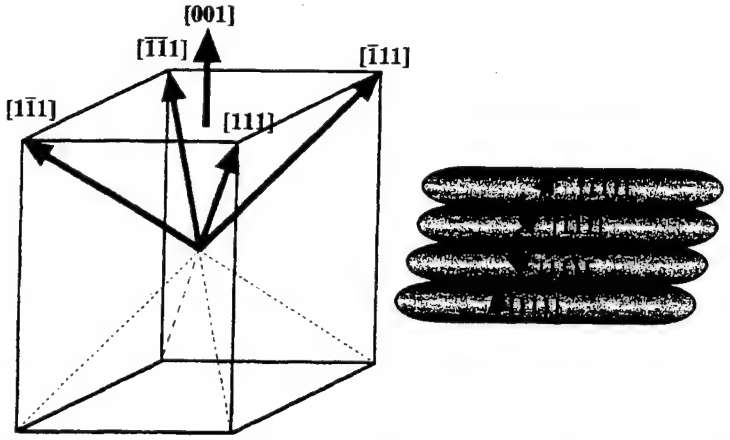

FIGURE 4. Schematic domain configuration of [001] oriented PZN-8%PT crystal.

was limited by the depth of focus of optical microscopy, each domain must have one of four possible polar vectors, [111], [$\bar{1}$11], [1$\bar{1}$1] and [11$\bar{1}$] in [001] poled PZN-8%PT crystals. This configuration is schematically presented in Fig. 4. Thus, all domain boundaries could be interpreted as 71° domain walls of {110} planes and 109° domain walls of {100} planes. Similar domain configuration was also reported for pure rhombohedral PZN.[8-9]

In-situ domain observations

For [111] oriented PZN-8%PT crystals, the domain configuration at 25 °C before an applied E-field is presented in Fig. 5(a). Figs. 5(b) and 5(c) exemplify the domain configuration at 25 °C as a function of E-field, increased incrementally to 13 kV/cm. The result shown in Fig. 5 was obtained at the second measurement in the repeated cycles (1 cycle: 0 kV/cm -> 13 kV/cm -> 0 kV/cm). The domain wall density in the crystals was found to decrease with increased E-field, implying increased domain size with domain reorientation. At approximately 13 kV/cm, the PZN-8%PT crystals became nearly single domain (Fig. 5(d)), with some domain walls observed near the electrode due to crystal-electrode interfacial stresses. However, upon removal of the E-field, a multidomain state was observed as presented in Figs. 5(e) and 5(f). Domain reorientation was found to occur at 4.5 kV/cm (Fig. 5(e)), starting near the electrode. The initial multidomain state of Fig. 5(b) was completely recovered as shown in Fig. 5(f). It should be noted, however, that the domain configuration exhibited hysteresis. The domain

wall density was observed to be reduced for an equivalent E-field upon removing the E-field, the origin of hysteresis in strain vs. E-field curve shown in Fig. 1(a).

In contrast to the domain instability observed with [111] oriented PZN-8%PT crystals, [001] oriented crystals exhibited stable domain configurations as shown in Fig. 6. The result shown in Fig. 6 was obtained at the second measurement in the repeated cycles (1 cycle: 0 kV/cm -> 15 kV/cm -> 0

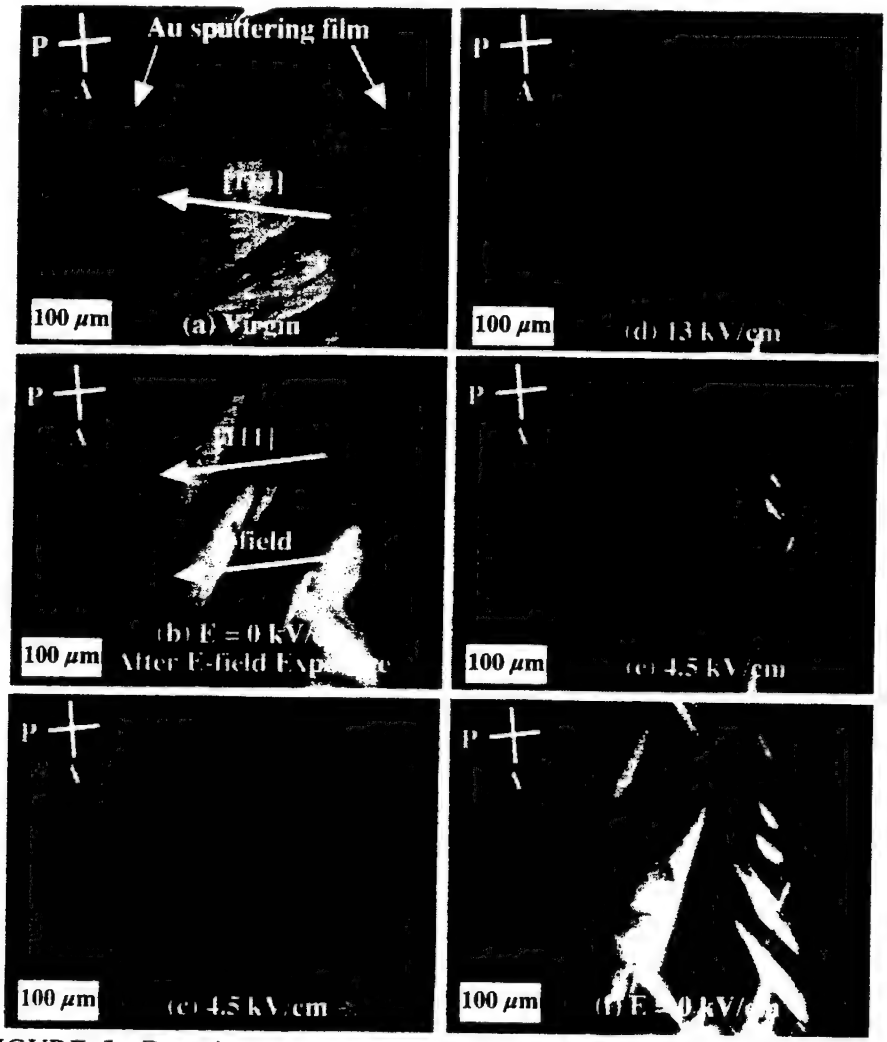

FIGURE 5 Domain configuration of [111] oriented PZN-8%PT crystal under DC-bias.

kV/cm). At the first cycle measurement, when very weak E-field below 0.2 kV/cm was applied along [001] direction of virgin crystal (Fig. 6(a)), the same domain configuration as shown in Fig. 6(b) was formed immediately. Moreover, this domain configuration did not change, although applied E-field increased under 15 kV/cm. Therefore, domain configuration did not change under DC-bias, being further evidenced by hysteresis minimized strain vs. E-field behavior in Fig. 1(b). However, if the E-field over 20

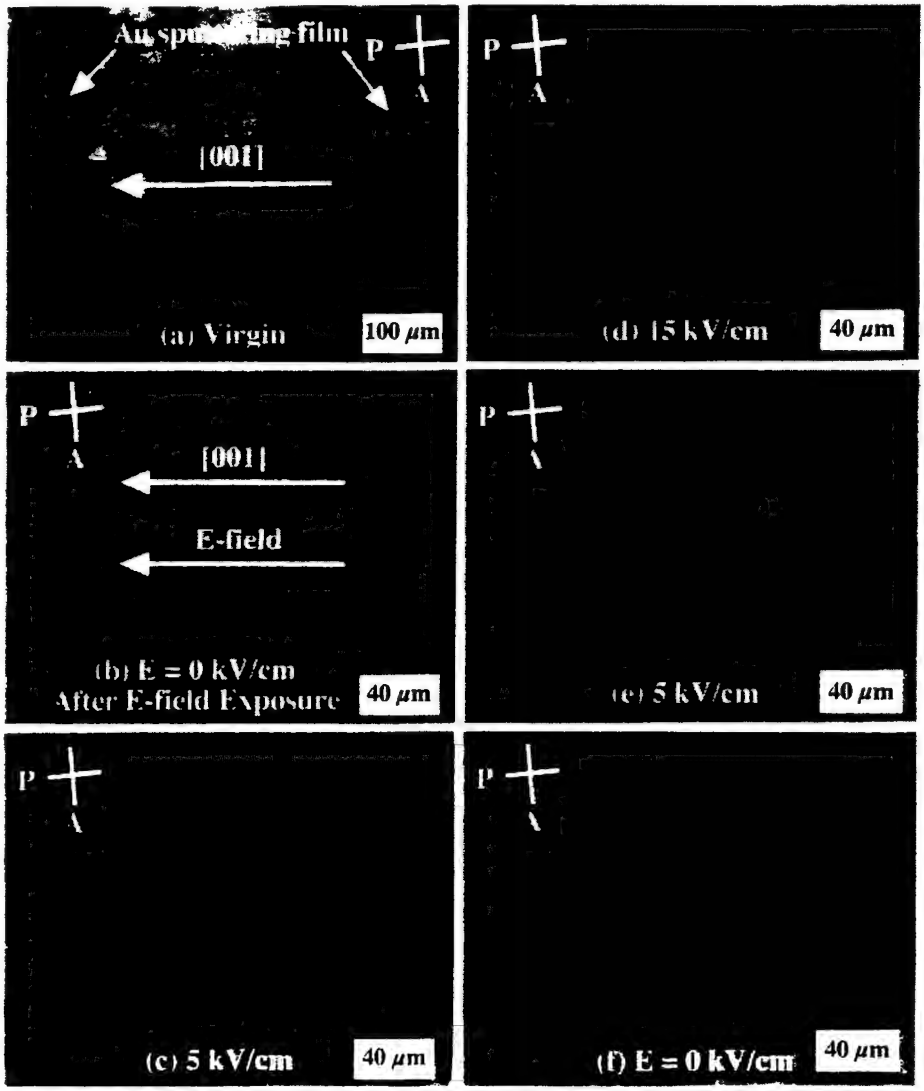

FIGURE 6 Domain configuration of [001] oriented PZN-8%PT crystal under DC-bias.

kV/cm was applied along [001] direction, the E-field induced phase transition from rhombohedral to tetragonal phase was observed and confirmed by both Polarization and strain vs. E-field curve and in-situ domain observation.

Domain engineering and macroscopic symmetry

Based on the domain observations presented in previous sections, the ability to engineer a macroscopic symmetry different from the local symmetry (lattice symmetry) is suggested, as can be found for the case of poled piezoelectric ceramics, i.e., the macroscopic symmetry being m regardless of the lattice symmetry resulting from randomly orientated grains. For ferroelectric single crystals, only single domain crystals possess macroscopic symmetry identical to the lattice symmetry. For example, unpoled tetragonal ferroelectric crystals are macroscopically m3m, if the number of each domain is equivalently distributed. As shown in Fig. 4, each domain in [001] poled crystals must have four possible polarization directions, [111], [$\bar{1}$11], [1$\bar{1}$1] and [$\bar{1}\bar{1}$1]. For [001] oriented crystals to exhibit a static domain configuration under DC-bias, each domain must be distributed equivalently. As a result, each domain experiences the same driving force for reorientation with respect to an applied E-field, otherwise domain reorientation under DC-bias would occur resulting in hysteresis in strain vs. E-field behavior. Therefore, the coexistence of domains with four equivalent polar vectors results in a 4-fold axis along [001], consequently resulting in the macroscopic symmetry 4mm arising from the local 3m symmetry.

SUMMARY

Domain configuration and ferroelectric related properties of rhombohedral PZN-8%PT crystals were investigated as a function of E-field and crystallographic orientation. In-situ domain observations revealed the domain instability for [111] oriented rhombohedral crystals, corresponding to large hysteresis of the strain vs. E-field behavior. In contrast, an engineered domain configuration of [001] oriented rhombohedral crystals was found to be stable. Domain motion was undetectable under DC-bias, resulting in hysteresis minimized strain vs. E-field behavior. Crystallographically, the macroscopic tetragonal symmetry (4mm) arising from local rhombohedral 3m symmetry resulting from the four equivalent domain state was suggested. Further detailed studies such as TEM observations are required to understand

the engineered domain observed in [001] poled PZN-8%PT crystals.

Acknowledgments

The authors thank Mrs. Lei for her great help with sample preparation, and also thank Dr. Fousek, Dr. Newnham, Dr. Randall and Dr. Cao for their helpful discussions and suggestions. This work has been supported by Office of Naval Research.

References

[1] J. Kuwata, K. Uchino and S. Nomura, *Jpn. J. Appl. Phys.*, **21**, 1298 (1982).
[2] S.-E. Park, M. L. Mulvihill, P. D. Lopath, M. Zipparo and T. R. Shrout, *Proceedings of the 10th IEEE International Symposium on Applications of Ferroelectrics,* Vol. **I**, 79 (1996).
[3] S.-E. Park and T. R. Shrout, *J. Appl. Phys.*, **82**, 1804 (1997).
[4] S.-E. Park and T. R. Shrout, *IEEE Trans. on Ultrasonics, Ferroelectric and Frequency Control Special Issue on Ultrasonic Transducers,* **44**, 1140 (1997).
[5] S.-E. Park, M. L. Mulvihill, G. Risch and T. R. Shrout, *Jpn. J. Appl. Phys.*, **36,** 1154 (1997).
[6] J. Fousek, Czech. *J. Phys.*, **B21,** 955 (1971).
[7] E. I. Eknadiosiants, V. Z. Borodin, V. G. Smotrakov, V. V. Eremkin and A.N. Pinskaya, *Ferroelectrics,* **111**, 283 (1990).
[8] S. Nomura, M. Endo and F. Kojima, *Jpn. J. Appl. Phys.*, **13** 2004 (1974).
[9] S. Wada, S.-E. Park, L. E. Cross and T. R. Shrout, *J. Korean Phys. Soc.*, **32,** S1290 (1998).

Appendix 3

Electric field dependence of piezoelectric properties for rhombohedral $0.955Pb(Zn_{1/3}Nb_{2/3})O_3-0.045PbTiO_3$ single crystals

Shi-Fang Liu,[a] Seung-Eek Park, Thomas R. Shrout, and L. Eric Cross
Materials Research Laboratory, The Pennsylvania State University, University Park, Pennsylvania 16802

(Received 24 August 1998; accepted for publication 3 December 1998)

The electric field dependence of the piezoelectric properties of rhombohedral $0.955Pb(Zn_{1/3}Nb_{2/3})O_3-0.045PbTiO_3$ crystals were investigated as a function of orientation with respect to the prototypic (cubic) axes. For ⟨111⟩ oriented fields, depolarization and subsequent domain reorientation resulted in an apparent maximum in the piezoelectric coefficients occurring at ~5 kV/cm, followed by nonhysteretic d_{ij} saturation, indicating a single domain state under bias. By extrapolation, single domain values for the piezoelectric coefficients d_{33} and d_{31} were determined to be 125 and −35 pC/N, respectively. The hydrostatic piezoelectric coefficient d_h for single domain crystals was calculated to be ~55 pC/N, coincident with the experimentally determined values under hydrostatic pressure. For ⟨001⟩ oriented fields, piezoelectric coefficients $d_{33\langle 001\rangle}$ and $d_{31\langle 001\rangle}$ as high as 2250 and −1000 pC/N were determined, respectively. Although a high value of $d_{h\langle 001\rangle}$ (~250 pC/N) was expected, the experimentally determined value was only ~50 pC/N. A change of polar vector within the crystal lattice was discussed in relation to the volume strain associated with an *E*-field induced phase transition and the possible origin of the discrepancy in hydrostatic d_h values. © *1999 American Institute of Physics.* [S0021-8979(99)05705-9]

I. INTRODUCTION

High levels of piezoelectric activity have been reported for single crystals in the rhombohedral ferroelectric $Pb(Zn_{1/3}Nb_{2/3})O_3$(PZN):$PbTiO_3$(PT) solid solution system.[1–4] It must be remembered that even in ferroelectric single crystals, the pizeoelectric response depends critically on its domain structure, and it is only in the single domain state, or in a carefully engineered domain state, that the properties are reproducible and age free.

In earlier studies of rhombohedral PZN–PT crystals poled along their polar axis, pseudocubic ⟨111⟩, Park[3] and Wada[5] presented evidence that a single domain state was not stable, indicating that previous reported piezoelectric coefficients were probably determined on partially depolarized samples. However, a stable domain state and correspondingly high level of piezoelectric activity could be achieved in nonpolar ⟨001⟩ oriented crystals; for such crystals, a single domain state cannot be achieved.

In this article, the piezoelectric behavior as a function of field direction was investigated for rhombohedral PZN–PT, specifically, PZN–4.5%PT crystals, located at the center of the rhombohedral compositional range (0%–9% PT). Longitudinal, transverse, and hydrostatic piezoelectricity were investigated as a function of crystallographic direction and related domain configuration. Piezoelectric–domain interrelationships were established in order to obtain single domain properties for ⟨111⟩ oriented crystals and to elucidate the induced phase transition behavior associated with these materials.

[a]Electronic mail: sxl43@psu.edu

II. EXPERIMENT

A. Crystal growth

Crystals of $(1-x)$PZN–xPT were grown using the high temperature flux technique. High purity (>99.9%) powders of Pb_3O_4, ZnO, Nb_2O_5, and TiO_2 (Aldrich, WI) were used. Excess Pb_3O_4 was added as flux. The powders were dry mixed using a tumbling mill. The mixed powders were loaded into a platinum crucible, which was placed in an alumina crucible sealed with an alumina lid and alumina cement to minimize PbO volatilization. The alumina crucible was placed in a tube furnace and held at soak temperature (1100–1200 °C), followed by slow cooling to 900 °C at a rate of 1–5 °C/h. The crucible was then furnace cooled to room temperature. Hot HNO_3 was used to separate the crystals from the melt. Typically, crystal sizes were 8–20 mm. Crystal samples, oriented along the ⟨001⟩ and ⟨111⟩ directions using a Laue Camera, were prepared by polishing with silicon carbide and alumina polishing powders to achieve flat and parallel surfaces onto which good electrodes were deposited by sputtering.

B. Electrical characterization

Dielectric and piezoelectric properties were measured using direct observations of strain as a function of electric field and low-field properties using the IEEE resonance technique.[6] The hydrostatic piezoelectric coefficient d_h was obtained by measuring the charge response under hydrostatic pressure. High-field measurements included polarization and strain hysteresis incorporated a modified Sawyer–Tower circuit and a linear variable displacement transducer (LVDT) driven by a lock-in amplifier (Stanford Research system, model SR830). Plate-shaped samples with thicknesses rang-

TABLE I. Dielectric and piezoelectric rhombohedral properties of PZN–4.5%PT crystal as a function of crystallographic orientation.

Crystal orientation	k_{33}	k_{31}	d_{33} (pC/N)	d_{31} (pC/N)	d_h (pC/N)	S_{11}^E (10^{-12} m^2/N)	S_{33}^E (10^{-12} m^2/N)	Dielectric constant	Loss
⟨111⟩	0.41	0.17	92	−47	55	13.6	8.32	640	0.002
⟨001⟩	0.92	0.57	2280	−1015	50	71.7	120.1	5000	0.003

ing from 0.2 to 0.5 mm were employed for measurements. Electric fields as high as ~80 kV/cm were applied using an amplified triangle or unipolar wave form at 0.2 Hz, from a Trek 609c-6 high voltage dc amplifier. During testing the samples were submerged in Fluorinert (FC-40, 3 m, St. Paul, MN), an insulating liquid, to prevent arcing.

III. RESULTS AND DISCUSSION

A. Low field measurements

Table I presents dielectric and piezoelectric properties of PZN–4.5%PT crystals as a function of crystallographic orientation, measured using the IEEE standard method.[6] As reported by Park *et al.*,[3] PZN–4.5%PT crystals oriented along ⟨001⟩ exhibited electromechanical coupling ($k_{33\langle001\rangle}$) and longitudinal piezoelectric coefficients ($d_{33\langle001\rangle}$) as high as 92% and 2280 pC/N, respectively. A transverse piezoelectric ($d_{31\langle001\rangle}$) value of −1020 pC/N was also determined, as presented in Table I. Crystals oriented along their polar direction ⟨111⟩, however, exhibited values of k_{33}~41% and d_{33} ~92 pC/N, significantly inferior to those oriented along ⟨001⟩, also reported by Kuwata *et al.*[1,2] and Park *et al.*[3]

For single domain rhombohedral crystals of symmetry $3m$, the hydrostatic piezoelectric coefficient d_h can be written as $d_{33}+2d_{31}$, as in the case of polycrystalline piezoelectric ceramics. From Table I, the piezoelectric coefficient d_h for ⟨111⟩ oriented crystals results in an abnormally low and negative value of −2 pC/N. Using axis transformation for ⟨001⟩ oriented rhombohedral crystals, the equation $d_{h\langle001\rangle} = 1/\sqrt{3}(d_{33}+2d_{31})$ is not applicable since a single domain state does not exist. Wada *et al.*[5] proposed that ⟨001⟩ polarized rhombohedral PZN–PT crystals possess a tetragonal macro symmetry ($4mm$) with the fourfold axis along the poling direction, a consequence of an engineered domain state. Therefore, taking ⟨001⟩ as the new symmetric axis, $d_{h\langle001\rangle}$ can be calculated using the relation $d_{h\langle001\rangle}=d_{33\langle001\rangle}+2d_{31\langle001\rangle}$, resulting in $d_{h\langle001\rangle}$~250 pC/N. However, as presented in Table I, d_h values directly measured were only 55 pC/N (⟨⟨111⟩⟩) and 50 pC/N (⟨⟨001⟩⟩). In Sec. III B, this discrepancy is discussed in relation to domain configuration and domain (in)stability.

B. Strain versus *E*-field behavior for (⟨111⟩) oriented PZN–4.5%PT crystals

As the pseudocubic ⟨111⟩ is the polar direction for rhombohedral ferroelectric crystals, this is also the direction in which an electric field must be applied to obtain a single domain state. Figure 1 shows longitudinal/transverse strain versus unipolar *E*-field behavior for a ⟨111⟩ poled crystal. As presented, hysteresis in the strain versus *E*-field curves at low fields is the result of domain instability and subsequent domain reorientation under bias.[3] Nearly linear and hysteresis free behavior at fields greater than 30 kV/cm indicates a single domain state. Wada *et al.*[5] also observed single domain behavior of ⟨111⟩ oriented PZN–PT rhombohedral crystals at *E* fields >30 kV/cm. This domain instability and subsequent difficulty in obtaining single domain crystals may be related to residual elastic strain upon poling.[7] As for the case of $BaTiO_3$ crystals, single domain PZN–PT crystals may require a specific elastic treatment during the poling process. The d_{ij}s of ⟨111⟩ oriented crystals given in Table I, therefore, are coefficients measured from partially depoled crystals, and not single domain crystals. Fundamentally, this inherent domain instability is believed to be the origin of the

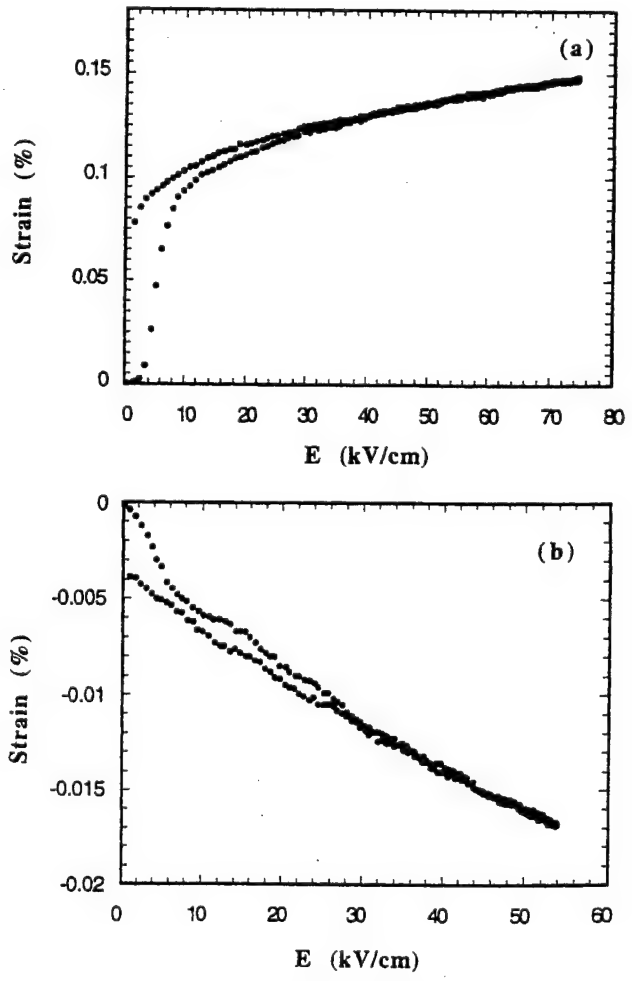

FIG. 1. Strain vs unipolar *E*-field behavior for ⟨111⟩ poled crystals: (a) longitudinal strain, (b) transverse strain.

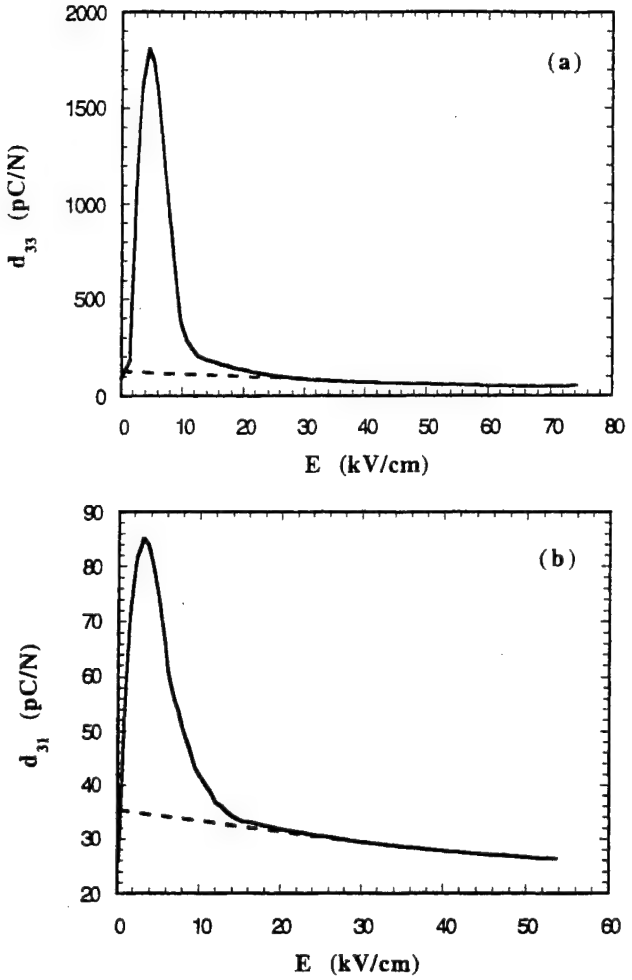

FIG. 2. Piezoelectric coefficients (d_{33} and d_{31}) obtained from the slope of strain vs E-field curves in Fig. 1(a) d_{33}; (b) d_{31}.

calculated negative hydrostatic d_h coefficients, since depolarization results in the longitudinal (transverse) piezoelectric coefficient to decrease (increase).

Figure 2 presents longitudinal and transverse piezoelectric coefficients (d_{33} and d_{31}) obtained from the slope of the strain versus E-field curves in Fig. 1. The maxima in d_{ij}s at 5 kV/cm are believed to be the result of domain reorientation under bias. Since the strain versus E-field curve in Fig. 1 was hysteresis free at $E>30$ kV/cm, d_{ij}s at $E>30$ kV/cm in Fig. 2 correspond to single domain values. The piezoelectric coefficients of single domain crystals at low fields, therefore, may be extrapolated as indicated by the dashed line, resulting in d_{33} and d_{31} values of 125 and -35 pC/N, respectively, being significantly different than the low field values given in Table I. It is also important to note that these values result in a $d_h \sim 55$ pC/N, coinciding well with the experimentally determined d_h value.

C. Strain versus *E*-field behavior for (⟨001⟩) oriented crystals

Polarization hysteresis behavior and subsequent strain versus E-field (bipolar) curves of ⟨001⟩ oriented PZN–4.5%PT crystals are shown in Fig. 3. Remanent polarization (P_r) values of ~ 25 μC/cm^2 for ⟨001⟩ oriented crystals are

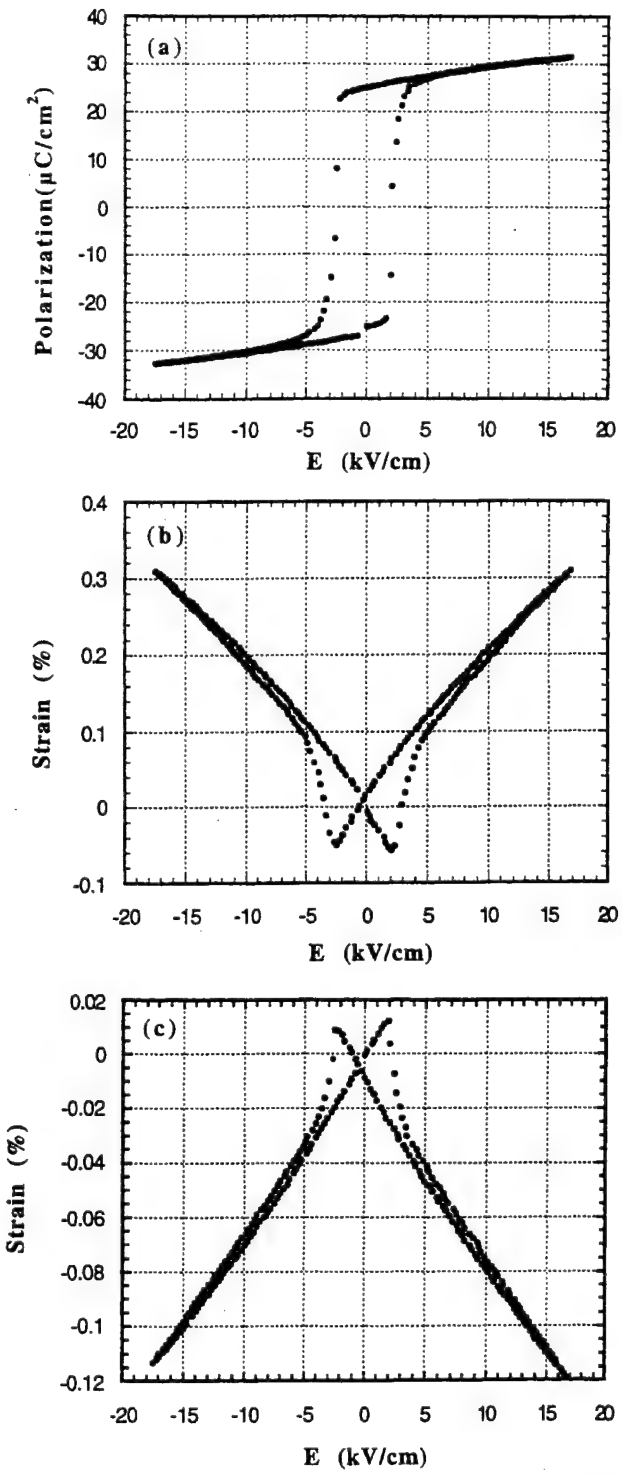

FIG. 3. Polarization and strain vs E-field (bipolar) curves for ⟨001⟩ oriented PZN–4.5%PT crystals: (a) polarization; (b) longitudinal strain; (c) transverse strain.

reported corresponding to $1/\sqrt{3}P_{r\langle 111\rangle}$. The abrupt change in polarization at E_c is a characteristic of domain switching, as found in general for all ferroelectrics, i.e., ⟨001⟩ nonpolar orientation. However, a consequence of the engineered domain state is the hysteresis minimized longitudinal/transverse strain behavior (unipolar) above E_c shown in Fig. 4. The longitudinal and transverse piezoelectric coefficients d_{33} and d_{31} calculated by the slope of the strain versus

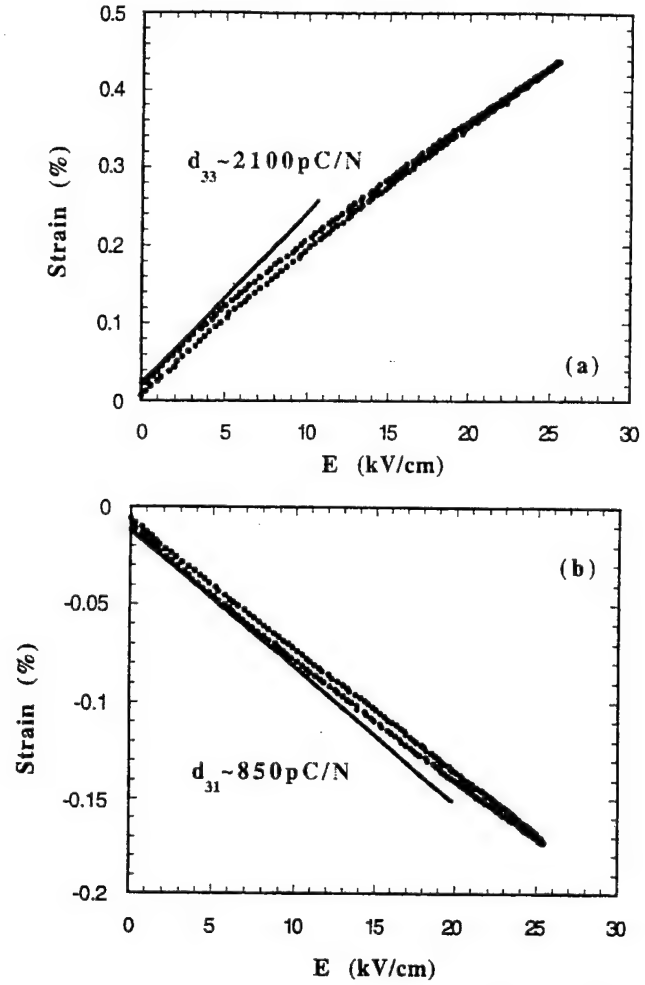

FIG. 4. Strain vs unipolar E-field behavior for ⟨001⟩ crystals: (a) longitudinal strain; (b) transverse strain.

E-field curve were ~2100 and −850 pC/N, respectively, slightly lower than that measured by the IEEE resonance technique. In regard to hydrostatic d_h, using the $d_{33\langle 001\rangle}$ and $d_{31\langle 001\rangle}$ values from Fig. 4 resulted in a calculated $d_{h\langle 001\rangle}$ of ~400 pC/N, still significantly larger than that experimentally determined. Unlike ⟨111⟩ oriented crystals, this inconsistency could not be explained by domain instability because the engineered domain configuration was stable with no or minimal domain motion under bias. It seems that the change in domain wall configuration under bias may be the underlying cause of this discrepancy. Further investigation of the domain wall state as a function of the E field is required.

D. *E*-field induced phase transition

High field strain versus E-field behavior for ⟨001⟩ oriented crystals is presented in Fig. 5. As suggested by Park[3] and supported using *in situ* domain observations,[8] the high-field phase induced at E fields >~36 kV/cm is believed to be a tetragonal phase. The volumetric strain associated with the induced phase transition is presented in Fig. 6. Although a volume expansion of ~0.3% was associated with the induced phase transition, a decrease in volume was detected starting at 20 kV/cm. The volumetric strain may be written as follows:

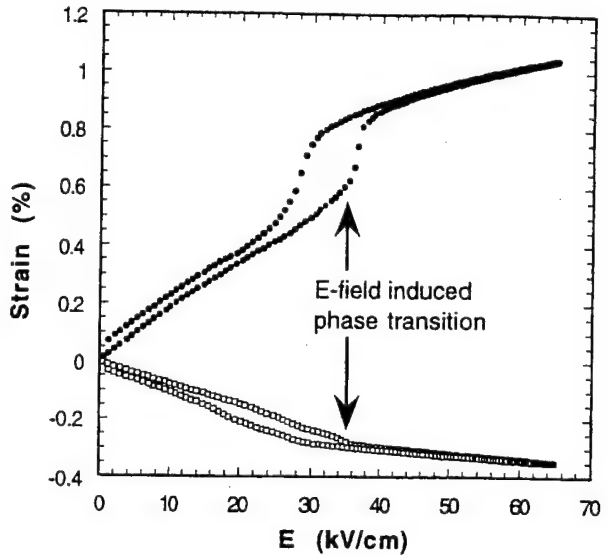

FIG. 5. High field strain vs unipolar E-field behavior for ⟨001⟩ crystals.

$$dV/V_0 = Q_h(P_E^2 - P_L^2), \tag{1}$$

where V_0 is the initial volume of the crystal, Q_h is the hydrostatic electrostrictive coefficient ($=Q_{11}+2Q_{12}$), P_L is the magnitude of zero-field spontaneous lattice polarization, and P_E is the magnitude of total lattice polarization under dc bias. Since Q_h is a material constant,[9] the volumetric strain is, therefore, dependent only upon the polarization change by the lattice response under bias or phase switching. It should be noted that P_L and P_E are not the apparent polarization, but the magnitude of the polar vector in the crystal lattice. For example, the apparent spontaneous polarization is a function of crystallographic direction (43 μ and 25 μC/cm^2 for ⟨111⟩ and ⟨001⟩ oriented crystals, respectively), but P_L is 43 μC/cm^2, independent of the orientation. In Eq. (1), P_E is equal to P_L ($=P_{\langle 111\rangle}$) under zero bias and to $P_{\langle 001\rangle}$ only if the entire crystal is occupied by the induced phase. The volume decrease, as shown in Fig. 6, indicates that the magnitude of the polar vector in the crystal lattice decreases during the induced phase transition. This is schematized in Fig. 7,

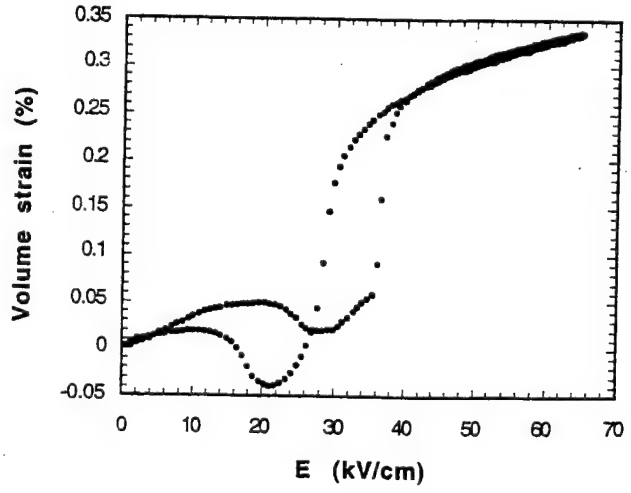

FIG. 6. Volume strain vs unipolar E-field behavior for ⟨001⟩ crystals.

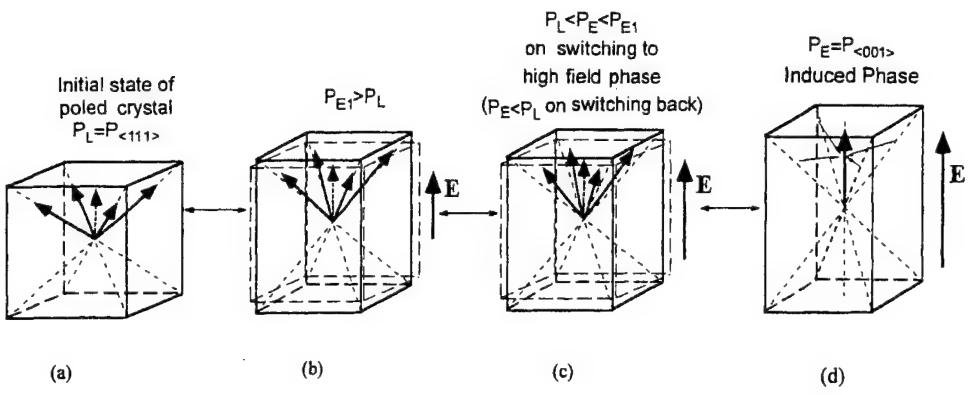

FIG. 7. Schematic of changes in polar vectors and unit cell volume for ⟨001⟩ oriented rhombohedral crystals under bias. Note that polar vectors are no longer along the body-diagonal direction of pseudocubic unit cell, under bias, for the engineered domain state (b) and (c).

adding an intermediate stage between Figs. 7(b) and 7(d).[3] The magnitude of the polar ionic shift in the crystal lattice may have to be reduced with the change of its shift direction, i.e., from ⟨111⟩ to ⟨001⟩, implying the crystal symmetry becomes closer to its prototype symmetry $m3m$ during the induced phase transition. It is noted that the volumetric strain becomes negative on switching back to the low field phase, indicating that P_E becomes smaller than P_L. As the induced phase transition gradually occurs with nucleation and growth processes,[8] volumetric strain can be positive or negative depending on the nucleation and/or growth speed with respect to the E-field change rate. It is noted that under high electric field, the polar vectors no longer lie in the body-diagonal direction of the pseudocubic unit cell within the engineered domain state, as shown in Figs. 7(b) and 7(c). Further discussion associated with the changes in polarization values for domain engineered crystals will be reported elsewhere.[10]

IV. CONCLUSION

The ferroelectric related properties of rhombohedral PZN–4.5%PT crystals were investigated as a function of crystallographic direction and subsequent domain configuration. For crystals oriented along the polar ⟨111⟩ direction, inconsistency among low field piezoelectric properties was believed to be the result of domain instability and subsequent partial depolarization. At high fields >30 kV/cm, strain versus E-field curves were hysteresis free and single domain rhombohedral crystals could be ascertained. Piezoelectric coefficients $d_{33}\sim 125$ pC/N, $d_{31}\sim -35$ pC/N, and $d_h\sim 55$ pC/N for single domain crystals were determined by extrapolating high field d_{ij} values. In contrast, low field strain versus E-field curves were hysteresis minimized as a result of the stable engineered domain state for ⟨001⟩oriented PZN–PT rhombohedral crystals. Although $d_{h\langle 001\rangle}$ values of >200 pC/N were expected from measured piezoelectric coefficients ($d_{33}\sim 2280$ pC/N and $d_{31}\sim -1020$ pC/N), the experimentally determined d_h value was only ~50 pC/N. Further investigation of the engineered domain state(s) and domain wall modulation under bias is required to answer the origin of this inconsistency. High field strain versus E-field behavior was characterized by an induced phase transition rhombo–tetragonal, resulting in volume strain as high as 0.35%. Volume strain versus E-field curves indicated that the magnitude of polarization in the crystal lattice decreases transiently in order for the direction of ionic shift to change from ⟨111⟩ to four-fold symmetric ⟨001⟩ axis.

ACKNOWLEDGMENTS

This research has been supported by the Office of Naval Research and DARPA. The authors would like to thank Hua Lei for her help with crystal growth and sample preparation.

[1] J. Kuwata, K. Uchino, and S. Nomura, Ferroelectrics **37**, 579 (1981).
[2] J. Kuwata, K. Uchino, and S. Nomura, Jpn. J. Appl. Phys., Part 1 **21**, 12989 (1982).
[3] S.-E. Park and T. R. Shrout, J. Appl. Phys. **82**, 1804 (1997).
[4] S.-E. Park, M. L. Mulvihill, P. D. Lopath, M. Zipparo, and T. R. Shrout, Proc. IEEE **1**, 79 (1996).
[5] S. Wada, S.-E. Park, L. E. Cross, and T. R. Shrout, The 8th US/Japan Seminar on Dielectric and Piezoelectric Ceramics, October 1997, pp. 11–15.
[6] *IEEE Standard on Piezoelectricity* (American National Standards Institute, Washington, D.C. 1976).
[7] O. Nakano, K. Tomomatusu, S. Ajimura, A. Kurosaka, and H. Tominaga, Jpn. J. Appl. Phys., Part 1 **31**, 3117 (1992).
[8] S. Wada, S.-E. Park, L. E. Cross, and T. R. Shrout, Proceedings of the Fifth International Symposium on Ferroic Domain and Mesoscopic Structure (ISFD-5), April 6–10, 1998.
[9] A. E. Glazounov, J. Zhao, and Q. M. Zhang, Proceedings of the Fifth Williamsburg Workshop of First-Principles Calculations for Ferroelectrics, February 1–4, 1998.
[10] L. E. Cross (unpublished).

Appendix 4

Phenomenology of the Elasto-Dielectric Response in the Field Forced Ferroelectric Phases of Lead Zinc Niobate : Lead Titanate (PZN:PT) Relaxor Ferroelectrics

L. Eric Cross and Petr Hana
Materials Research Laboratory, The Pennsylvania State University, University Park, PA 16802
Fax: (814) 863-7846, email: lec3@psu.edu

In the relaxor ferroelectric phases of the perovskite structure dielectrics it is clearly not possible to apply simple Landau:Ginsburg:Devonshire phenomenology as below the Vogel:Fulcher freezing temperature the system is in a metastable frozen state. In single crystals of PZN:PT solid solution at compositions close to the morphotropic boundary (MPB) however, the most interesting and useful properties occur in the field forced ferroelectric phase, where the dielectric response is not dispersive at low frequency. For the 001 oriented electric field poled rhombohedral state which exhibits the most exciting piezoelectric properties it is shown that the high field deformation can be described by a field forced monoclinic phase and that the intrinsic shape change calculated for the single domain states is more than adequate to account for the exceptionally high strain behavior. The capability to field force a strongly monoclinic phase was unexpected, however very recent precise x-ray studies using the synchrotron source at Brookhaven appear to confirm a stable monoclinic phase in PZT at compositions close to the morphotropic phase boundary.

From the induced spontaneous electric polarization as a function of temperature in the 111 field poled single crystal it appears that the PZN:4.5% PT composition in the rhombohedral ferroelectric phase is very close to tricritical behavior, as may be expected from the close approach in free energy of rhombohedral and tetragonal states. These and aspects of the proposed phenomenology will be briefly discussed.

1. INTRODUCTION

Earlier studies[1,2] have suggested that the high initial anhysteritic strain of 001 oriented electric fields in rhombohedral phase PZN:PT with compositions which are not too close to the morphotropic phase boundary (MPB) may be associated with a field driven phase change from rhombohedral to monoclinic ($3m \Rightarrow m$) symmetry. Since the $3m \Rightarrow m$ ferroelectric phase change in the perovskite can be second order (continuous) even large intrinsic domain shape changes could be reversible and anhysteritic. For field forced phase changes in the relaxor, dispersion is very largely lost and the properties are stabel with time, so that it is not outrageous to expect that reversible thermodynamics may be applied to derive estimates of the elasto-dielectric responses. In this brief report Landau:Ginsburgh:Devonshire phenomenology is applied to demonstrate for 95.5 PZN:4.5 PT:

(a) That the intrinsic shape change of the rhombohedral domain induced in the $3m \Rightarrow m$ phase change which is consistent with the observed polarization change is more than adequate to account for the observed quasi-linear strain induced by the 001 oriented field.

(b) The observed P^4 vs T dependence of the polarization in the ferroelectric rhombohedral phase suggests a tricritical behavior which may be expected in a system derived from the m3m prototype where the orthorhombohic phase is suppressed.

(c) The dielectric behavior below, and well above the relaxation range is consistent with the proposed simple phenomenology.

2. THERMODYNAMIC PHENOMENOLOGY

For the perovskite ferroelectrics stemming from the prototype m3m symmetry the Gibbs Free Frequence AG takes the form.

The coefficienta α_i, α_{ij}, α_{ikj} are the dielectric stiffness and higher order stiffness at constant and zero stress, s_{ij} the elastic compliances at constant polarization and Q_{ij} the electrostrictive coupling constants in polarization notation. The function contains all permitted stiffness coefficients up to sixth order, but only first order elastic and electrostrictive constants.

$$
\begin{aligned}
\Delta G \quad &= \alpha_1\left[P_1^2+P_2^2+P_3^2\right]+\alpha_{11}\left[P_1^4+P_2^4+P_3^4\right] \\
&+\alpha_{12}\left[P_1^2P_2^2+P_2^2P_3^2+P_3^2P_1^2\right] \\
&+\alpha_{111}\left[P_1^6+P_2^6+P_3^6\right] \\
&+\alpha_{112}\left[P_1^4\left(P_2^2+P_3^2\right)+P_2^4\left(P_1^2+P_3^2\right)+P_3^4\left(P_1^2+P_2^2\right)\right] \\
&+\alpha_{123}P_1^2P_2^2P_3^2 \\
&-\frac{1}{2}S_{11}\left[X_1^2+X_2^2+X_3^2\right] \\
&-S_{12}\left[X_1X_2+X_2X_3+X_3X_1\right] \\
&-\frac{1}{2}S_{44}\left[X_4^2+X_5^2+X_6^2\right] \\
&-Q_{11}\left[X_1P_1^2+X_2P_2^2+X_3P_3^2\right] \\
&-Q_{12}\left[X_1\left(P_2^2+P_3^2\right)+X_2\left(P_1^2+P_3^2\right)+X_3\left(P_1^2+P_2^2\right)\right] \\
&-Q_{44}\left[X_4P_2P_3+X_5P_1P_3+X_6P_1P_2\right] \qquad (1)
\end{aligned}
$$

From equation (1) relations may be simply derived for the polarization states, the relative free energies and the dielectric stiffness from which the susceptibility (permittivity) may also be derived.

Since the deformation of the prototype is purely electrostrictive the shape change for any ferroelectric phase including monoclinic and triclinic can be derived from equation (1). These relations are given in Table I. It is also interesting to note that the volume change s_v into each phase is of the same form, Table II and depends only on the total polarization.

3. APPLICATION TO 95.5 PZN:4/5 PT

For 001 poling field rhombohedral PZN:PT may be driven to single domain tetragonal state where measurements of longitudinal strain change Δs_3 and transverse strain change Δs_1, between 50 kV/cm and 65 kV/cm compared to total polarization P_3 yield values of $Q_n = +0.094\ m^4/c^2$ and $Q_{12} = -0.047\ m^4/c^2$. Measurements of ΔV_s over the field range up to 40 kV/cm suggest ΔV_s is small and that P_T does not change much. Assuming P_T is constant P_1 and P_2 can be calculated over the field range 0 to 40 kV/cm and the tilt angle from 001 direction evaluated from the induced monoclinic phase (Table III)

Table I
Possible Electrostrictive Spontaneous Deformation in Perovskite Ferroelectrics

Cubic	$P_1=P_2=P_3=0$
Prototype	$s_1=s_2=s_3=0 \quad s_4=s_5=s_6=0$
Tetragonal	$P_1=P_2=0 \quad P_3^2=0$
	$s_1=s_2=Q_{12}P_3^2 \quad s_3=Q_{11}P_3^2$
	$s_4=s_5=s_6=0$
Orthorhombic	$P_1=0 \quad P_2^2=P_3^2=0$
	$s_1=2Q_{12}P_3^2$
	$s_2=s_3=\left(Q_{11}+Q_{12}\right)P_3^2 \quad s_4=Q_{44}P_3^2$
	$s_5=s_6=0$
Rhombohedral	$P_1^2=P_2^2=P_3^2=0$
	$s_1=s_2=s_3=\left(Q_{11}+2Q_{12}\right)P_3^2$
	$s_4=s_5=s_6=Q_{44}P_3^2$
Monoclinic (1)	$P_1^2=P_2^2\neq 0 \quad P_3^2\neq 0 \quad P_1^2\neq P_3^2$
	$s_1\left(Q_{11}+Q_{12}\right)P_1^2+Q_{12}P_3^2$
	$s_2=\left(Q_{11}+Q_{12}\right)P_1^2+Q_{12}P_3^2$
	$s_3=Q_{11}P_3^2+\left(Q_{11}+Q_{12}\right)P_1^2$
	$s_4=Q_{44}P_1P_3$
	$s_5=Q_{44}P_1P_3$
	$s_6=Q_{44}P_1^2$
Monoclinic (2)	$P_1^2\neq 0 \quad P_2^2\neq 0 \quad P_1^2\neq P_2^2 \quad P_3^2=0$
	$s_1=Q_{11}\left(P_1^2+Q_{12}P_1^2\right)$
	$s_2=Q_{12}P_1^2+Q_{11}P_1^2$
	$s_3=Q_{12}\left(P_1^2+P_2^2\right)$
	$s_4=0 \quad s_5=0 \quad s_6=Q_{44}P_1P_2$
Triclinic	$P_1^2=0 \quad P_2^2=0 \quad P_3^2=0$
	$P_1^2=P_2^2=P_3^2$
	$s_1=Q_{11}P_1^2+Q_{12}\left(P_2^2+P_3^2\right)$
	$s_2=Q_{11}P_2^2+Q_{12}\left(P_1^2+P_3^2\right)$
	$s_3=Q_{11}P_3^2+Q_{12}\left(P_1^2+P_2^2\right)$
	$s_4=Q_{44}P_2P_3 \quad s_5=Q_{44}P_1P_3$
	$s_6=Q_{44}P_1P_2$

Table II
Volume Strain s_v as a Function of
Total Polarization PT in All Possible Phases

	Volume Change
Cubic	$s_v = 0$
Tetragonal	$s_v = (Q_{11} + 2Q_{12})P_3^2$
Orthorhombic	$s_v = 2(Q_{11} + 2Q_{12})P_3^2$ $= (Q_{11} + 2Q_{12})P_{Total}^2$
Rhombohedral	$s_v = 3(Q_{11} + 2Q_{12})P_3^2$ $= (Q_{11} + 2Q_{12})P_{Total}^2$
Monoclinic (1)	$s_v = 2(Q_{11} + 2Q_{12})P_1^2 + (Q_{11} + 2Q_{12})P_3^2$ $= (Q_{11} + 2Q_{12})P_{Total}^2$
Monoclinic (2)	$s_v = (Q_{11} + 2Q_{12})P_1^2 + (Q_{11} + 2Q_{12})P_2^2$ $= (Q_{11} + 2Q_{12})P_{Total}^2$
Triclinic	$s_v = (Q_{11} + 2Q_{12})(P_1^2 + P_2^2 + P_3^2)$ $= (Q_{11} + 2Q_{12})P_{Total}^2$

Table III
Calculated Polarization and Tilt Angle for PZN:PT
95.5/4.5 Under High DC E_3 Field

Field kV/cm	Polarization P_3 $\mu c/cm^2$	Angle θ	Polarization P_1 $\mu c/cm^2$
5	27.8	50.1	23.47
10	29.8	46.5	22.21
15	31.4	43.4	21.04
20	33	40.34	19.82
25	34.3	37.5	18.64
30	35.6	34.6	17.42
35	36.75	31.9	16.19
40	37.85	29.1	14.87

From P_3 and P_1 in Table III, s_1 and s_3 can be determined and shown to be larger than the measured values (figure 1). Thus the calculated intrinsic change is more than adequate to describe the total shape change in this field region.

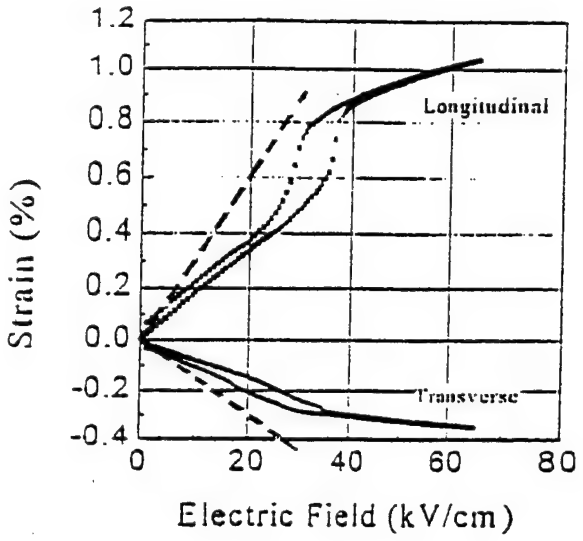

Fig. 1 Field Induced Strain s_3 and s_1 for 001 E-field on 95.5 PZN:4.5PT.
— Measured Values.
---- Intrinsic Calculated Strains.

Examination of P_3 vs T shows a behavior close to P^4 α T suggesting tricritical behavior and very small values of α_{11} and α_{12}. In this case the sixth order terms will dictate phase stability and it is easy to see why the orthorhombic phase may be suppressed.

Measurements of the dielectric permittivity for the <111> poled single domain state give linear relations for $1/\varepsilon$ vs T with Curie constant $C \sim 3.10^5$ similar to the value measured in the paraelectric phase above 220°C where $C \sim 2.8.10^5$.

In connection with the proposed monoclinic phase in PZN:PT it is interesting to note that recent studies at Brookhaven[3] have confirmed a stable monoclinic phase in PZT at lower temperature in compositions close to the MPB, and the induction of a monoclinic phase at room temperature on poling the ceramics.[4]

4. FUTURE DEVELOPMENTS

Work is in progress to determine the magnitude and temperature dependence of the α_{ij} for a sequence of composition in the PZN:PT family including both rhombohedral 3m and tegragonal 4mm ferroelectric phases.

5. REFERENCES

1. Park, S.E. and T. R. Shrout, "Relaxor Based Ferroelectric Single Crystals for Electro Mechanical Actuators," Mat. Res. Innov. **1**, 20-25 (1997).

2. Park, S.E. and T.R. Shrout, "Characteristics of Relaxor Based Piezoelectric Single Crystals for Ultrasonic Transducers, IEEE Trans. UFFC **44** (5), 1140-1147 (1997).

3. Noheda, B., D.E. Cox, G. Shirane, J. Gonzalo, L.E. Cross, and S.E. Park, "A Monoclinic Ferroelectric Phase in the $Pb(Zr_{1-x}Ti_x)O_3$ Solid Solution," Applied Physics Letters **74**(14), 2059-2061 (1999).

4. G. Shirane, Private Communication (1999).

Appendix 5

Domain and Phase Change Contributions to Response in High Strain Piezoelectric Actuators

L. Eric Cross

Evan Pugh Professor Emeritus of Electrical Engineering
Materials Research Laboratory
The Pennsylvania State University
University Park, PA 16802 USA

Abstract. Current solid state actuators are briefly compared to traditional actuator technologies to highlight the major need for enhanced strain capability. For the ferroelectric piezoelectric polycrystal ceramics, the balance of evidence suggests a large entrinsic contribution to the field induced strain from ferroelectric-ferroelastic domain wall motion. Here-to-fore the intrinsic single domain contribution has been derived indirectly from phenomenological analysis. Now, new evidence of a stable monoclinic phase at compositions very close to the MPB suggest that the previous assessment will need to be revised.

Actuator behavior in the new lead zinc niobate-lead titanate (PZN:PT) single crystal shows most unusual anisotropic behavior. For 111 oriented field poled crystals in the rhombohedral phase normal low induced strain is observed. For 001 field poled crystals however massive (0.6%) quasi-linear anhysteritic strain can be induced. Since the 001 oriented field in the rhombohedral phase can not drive ferroelastic domain walls it is suggested that the strain must be intrinsic. The suggestion is that it is due to an induced monoclinic phase in which the Ps vector tilts under increasing field up to more than 20° from 111, before the vector switches to the tetragonal 001 direction. Such a polarization rotation mechanism has also been suggested by Fu and Cohen [1]. Calculations of induced single domain strain using measured electrostriction constants agree well with observed behavior.

Recent measurements by Park et al [2] and Wada et al [3] on single crystal $BaTiO_3$ show strongly enhanced piezoelectricity at temperatures near the ferroelectric phase transitions. Of particular relevance is the inverse experiment forcing the tetragonal over to the rhombohedral phase with high 111 oriented field. From this result it is suggested that both cubic and dodecahedral mirrors participate in the reorientation through orthorhombic to the rhombohedral state giving rise to different value of the induced d_{33} at different field levels.

CP535, *Fundamental Physics of Ferroelectrics 2000: Aspen Center for Physics Winter Wkshp.*, edited by R. E. Cohen

INTRODUCTION

Characteristics of stress levels, strain capability and efficiency for a number of actuator systems are summarized in Table 1. Traditional electromagnetic, pneumatic and hydraulic systems have high efficiency good stroke (strain levels) and adequate force. They are however bulky, rather slow, and require extensive backup generator equipment. Solid state electrical piezoelectric, electrostrictive and phase switching actuators clearly have adequate force, tolerable efficiency, however the stroke permitted by induced strain levels is miniscule. These materials are still important as the actuation can be very fast, inertia is low and compact systems can be engineered, however there is still a major need for enhanced strain capability.

In this paper, the mechanisms responsible for strain in the polycrystal ferroelectric ceramics will be discussed. Currently the balance of evidence points to a major contribution from ferroelastic domain wall motion particularly in the soft PZTs, but the discovery of a new monoclinic phase, just at the critical morphotropic phase boundary composition requires a re-assessment of the intrinsic contribution to response. Evidence from the new lead zinc niobate:lead titnate (PZN:PT) single crystals suggests that the ultra high strain in 001 field poled crystals may be dominantly intrinsic involving the field induction of a monoclinic phase in which P_s is strongly tilted in the dodecahedral mirror plane before finally switching to the 001 polar tetragonal form. Recent experiments on $BaTiO_3$ where the inverse experiment, forcing the tetragonal over to rhombohedral symmetry by high (111) oriented E-field at room temperature lends further support for a monoclinic mechanism for the switching, but now involving both cubic and dodecahedral mirrors.

Polarization and Strain Mechanisms

For the simple linear nonferroelectric insulator the induced deformation under electric field may be described by

$$x_{ij} = s_{ijkl}X_{ij} + d_{mij}E_m + M_{mnij}E_mE_n \qquad (1)$$

where x_{ij} are components of induced strain, X_{ij} components of applied stress E_m, E_n components of electric field s_{ijkl} the elastic compliance, d_{mij} the piezoelectric tensor and

M_{mnij} the electrostriction coefficients. Obviously if the d_{mij} are non zero, in the absence of stress

$$x_{ij} = d_{mij}E_m \qquad (2)$$

TABLE 1. Salient Features of Traditional and Solid State Actuators

TRADITIONAL TECHNOLOGIES

	Stress (MPa)	Strain	Efficiency
Electromagnetic	0.02	0.5	90%
Hydraulic	20	0.5	80%
Pneumatic	0.7	0.5	90%

SOLID STATE ACTUATORS

	Stress (MPa)	Strain	Efficiency
Shape Memory Alloys	200	01	3%
Piezoelectric	35	0.002	50%
Electrostrictive	50	0.002	50%
Phase Switching Electroceramic	50	0.004	?
Electrostrictive Polyurethane	0.1	0.10	20%
Contractile Polymer	0.3	0.5	30%
Muscle	0.35	0.2	30%

which is the piezoelectric actuation function and if the d_{mij} are zero by symmetry

$$x_{ij} = M_{mnij}E_mE_n \tag{3}$$

and the system will be electrostrictive.

In a polycrystal ensemble, as for the randomly axed ceramic, the system is much more complex. With any symmetry in the crystallites (fig. 1a) the random axial arrangement will introduce two infinite fold rotation axes ($\infty\infty$) in the macro-ensemble symmetry wiping out all piezoelectricity. One of the few way out of this dilema is to consider a ferroelectric crystallite where in the ferroelectric state spontaneous electric polarization is distributed in domains with different equivalent orientation states that can be reoriented by an external poling field (fig. 1b). The remanent polar vector drops the macro-symmetry to conical (∞m) which is piezoelectric with non zero $d_{31} = d_{32}$, d_{33}, $d_{15} = d_{24}$.

All practical polycrystal ceramic actuators use compositions in the lead zirconate:lead titanate (PZT) solid solution system (fig. 1c). The reason for the infatuation with PZT is the near vertical (morphotropic) phase boundary close to the 52:48 Zr/Ti cation ratio, separating tetragonal and rhombohedral ferroelectric phases. Qualitatively two clear advantages stem from working with compositions near this boundary, and this is where most practical systems are pitched.

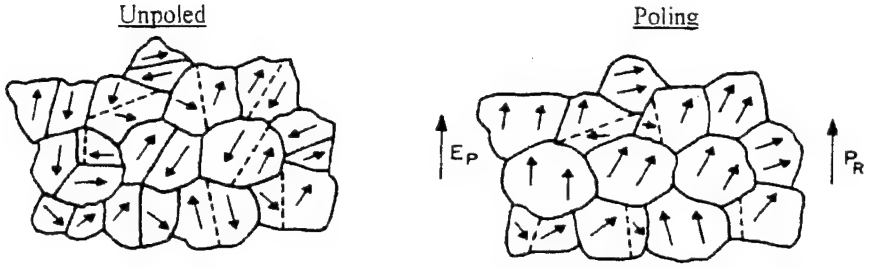

(a) the symmetry is ∞∞m which is centric and forbids piezoelectricity

(b) the symmetry is ∞m which is non centric (polar) and permits piezoelectricity.

Macro Symmetry and the importance of poling of a ferroelectric species.

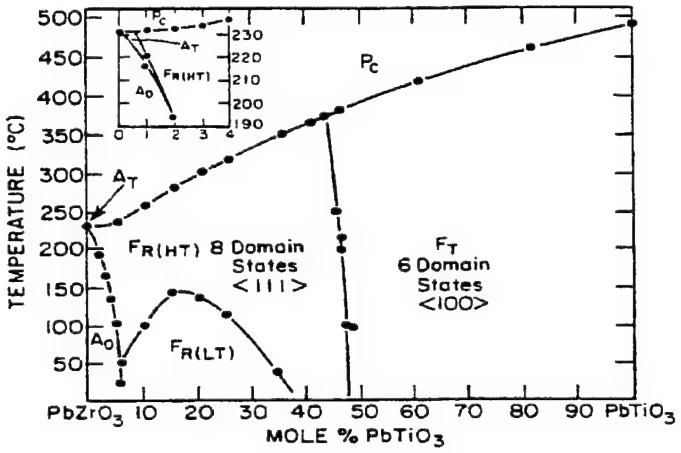

(c) Lead zirconate titanate phase diagram.

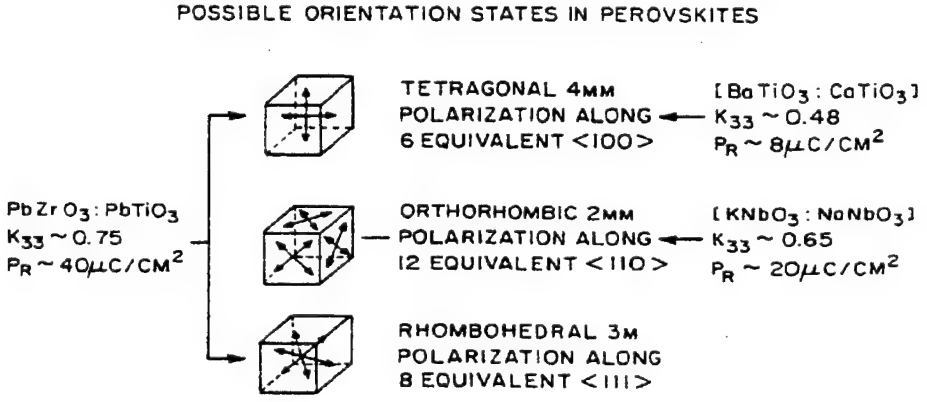

(d) Importance of many orientation states for polycrystal polability and performance.

FIGURE 1. Important features in piezoelectric polycrystal ceramic materials.

Firstly, the MPB is a first order phase change, so that in the co-existence region for the two phases it is possible in the poling process to make use of 14 domain orientation states (fig. 1d) leading to more complete poling. Secondly, for properly chosen compositions one can stay close to the phase boundary over a wide temperature range and use its destabilizing influence to enhance the intrinsic polarizability of the single domain states.

From these basic advantages stem two fundamental problems in understanding the behavior. Firstly, what is the balance between intrinsic single domain and extrinsic contributors to response; and secondly, what exactly is the nature of the dominant extrinsic contributor.

In the randomly axed polycrystal ceramic, ferroelectric domain wall motion is essential to permit the induction of strong remanent polarization essential for piezoelectricity. For the quasi-reversible behavior working about this induced remanent polar state the question is to what extent are ferroelastic:ferroelectric wall motions the primary extrinsic contributor to both dielectric and piezoelectric response.

No practical PZTs are in fact pure lead zirconate titanate solid solutions, all are modified by aleovalent cation additions (fig. 2). We speak of excess charge cation added or donor doped soft PZTs, and of charge deficient cation or Acceptor doped hard PZTs. The terminology "hard" versus "soft" is derived from magnetism and clearly implying difficult or easy domain wall motion as in the magnetic counterparts. For the hard PZTs however, there is compelling evidence [4,5], that stabilization by weakly mobile oxygen vacancy:defect dipole pairs is of the whole domain not just the wall. A mechanism that has no counterpart in magnetism but does however indirectly make the walls more difficult to move.

In soft donor doped PZTs, there is very strong evidence for enhanced extrinsic response in both dielectric and piezoelectric behavior, however evidence that it is associated with domain wall motion is indirect. It is clear that at fields well below the coercivity, the response is hysteritic [6] and can be well described by the Rayleigh law [7] suggesting a domain wall origin. There is however also evidence from transmission electron microscopy that the donor dopants tend to break-up the normal domain structure leading to tweed like and micro-polar relaxor like structures [8].

Earlier a rather complete phenomenology has been presented for the whole PZT family [9-13] from which single domain intrinsic values can be dervied for both tetragonal and rhombohedral phases adjacent to the MPB and averaged values for permittivity and piezoelectric response derived. It was on this basis that some 80% of dielectric response in hard PZTs, but only of order 30% of response in soft PZTs was predicted to be intrinsic (fig. 3).

Very recently the whole basis for evaluating both contribution to response has been changed by the discovery using very precise x-ray analysis [14,15] of a new monoclinic phase just on the rhombohedral side of the MPB (fig. 4). In this phase, the axial components of spontaneous polarization Ps are

$$P_1^2 = P_2^2 \neq 0 \qquad P_3^2 \neq 0 \quad but \quad P_1^2 \neq P_3^2 \tag{4}$$

(a)

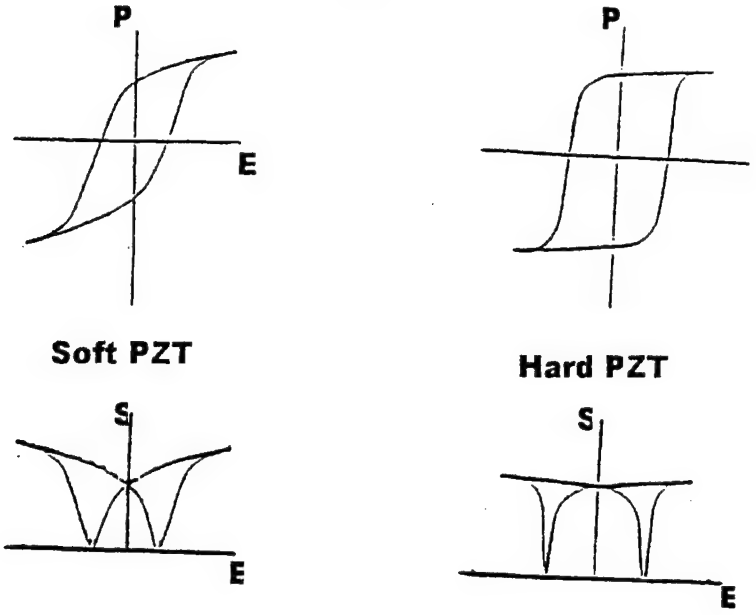

(b)

DONOR ADDITIVES		ACCEPTOR ADDITIVES
Nb_2O_5	$PbNb_2O_6$	Fe_2O_3
Ta_2O_5	$PbTa_2O_6$	Al_2O_3
WO_3		Cr_2O_3
Bi_2O_3		MnO_2
Sb_2O_3		MgO
La_2O_3		NiO

(c)

	Wall Motion Promoters	Wall Motion Inhibitors
d_{33}	593 pC/N	150 pC/N
d_{31}	273 pC/N	60 pC/N
Tc	195°C	350°C
ε3	3,450	1,000
Kp	0.69	0.52
Tan δ	0.02	0.004
E_c	6 Kv/cm	15 Kv/cm

FIGURE 2. (a) Typical polarization and strain curves. (b) Donor and Acceptor Dopants. (c) Dielectric and Piezoelectric Parameters

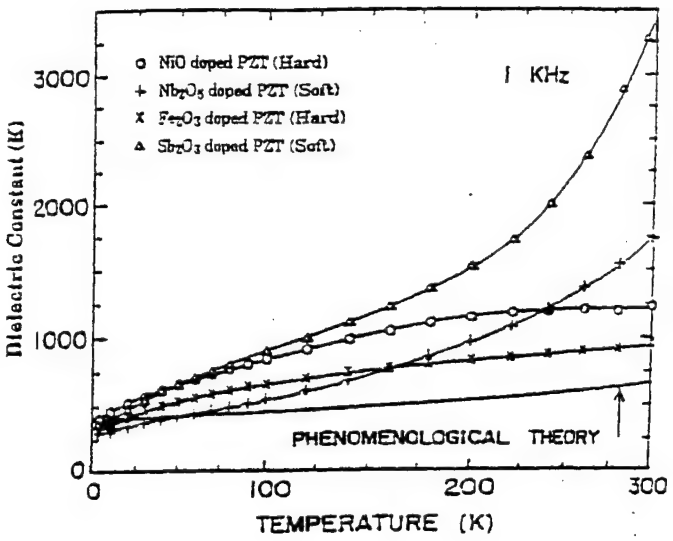

FIGURE 3. Dielectric response for Soft and Hard PZTs vs Temperature (4.2K to 300K) intrinsic response derived from Phenomenological Theory.

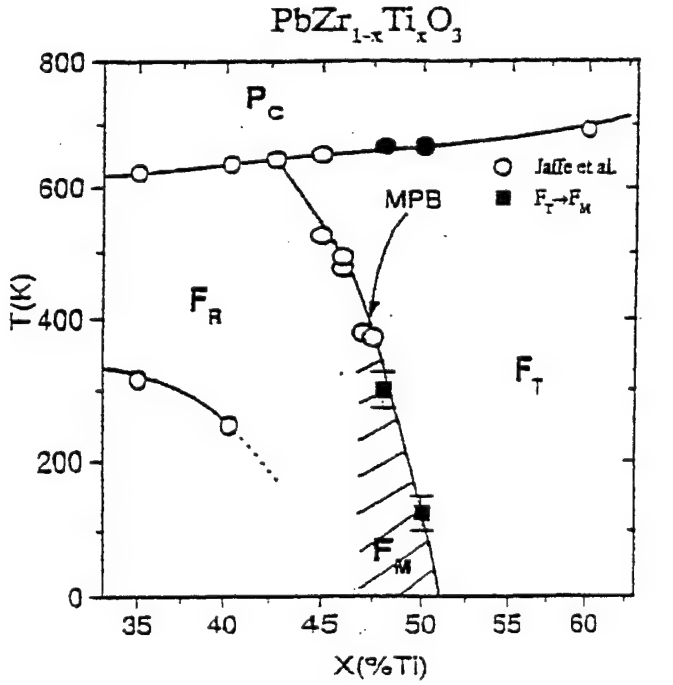

FIGURE 4. Modified PZT phase diagram after Noheda [2].
The open symbols represent the PZT phase diagram after Jaffee et al.
Note: The temperature axis is in degrees K not celcius as in the original studies.

The polar vector lies within the dodecahedral mirror plane of the prototype m3m and there are 24 orientation states for this species. From symmetry, the transitions rhombohedral 3m ↔ monoclinic m and tetragonal mm 2 ↔ monoclinic m may be either first or second order.

The presence of this newly discovered phase does require a revision of the phenomenology, as in the earlier treatment all phases other than tetragonal and rhombohedral were chosen to be metastable in the composition range of the MPB. Similarly the possible extrinsic contributions to response now need further consideration. The possibility for the E-field to drive phase boundary motion of a weakly hysteritic first order 3m ↔ m or 4mm ↔ m phase change could contribute here-to-fore unimagined extrinsic response that could mimic domain wall motion but contribute very strongly to elastic strain and piezoelectricity. Either intrinsic or extrinsic contributions from this very narrow insert of monoclinic phase could explain the very sharp peaking of k_{33} near the MPB that is evident in pure PZTs and has been most difficult to explain on earlier theories.

Alternative Single Crystal Systems

The complexity of the elasto-dielectric behavior of the polycrystal PZTs highlight the need for single crystal and single domain studies to properly explore the phenomena in lead based perovskite structures. PZT has proven markedly intractable for crystal growth, but more recent studies of the lead zinc niobate:lead titanate PZN:PT, and lead magnesium niobate:lead titanate (PMN:PT) have yielded "respectable" crystals for compositions close to the pseudo-morphotropic boundaries between rhombohedral and tetragonal phases in both systems [16,17,18].

Dielectric and piezoelectric properties have been well characterized [19,20] and the massive anisotropy in response between 111 and 001 E-field poled crystals in the rhombohedral phase underscored. The piezoelectric $d_{33} > 2000$ pC/N, $k_{33} > 92\%$, $\varepsilon_{33}^{T} > 5{,}000$ for 001 E-field rhombohedral phase crystal at composition close to the MPB are of strong practical interest. Of major concern here is the actuator performance where it has been shown that in 001 field poled PZN:PT strains up to 1.7% can be induced at high fields (fig. 5a).

There is good evidence that at the highest field levels the crystal is switched over into the tetragonal phase through a field induced first order phase change that is necessarily hysteritic. Of special interest is the long quasi-linear anhysteritic strain, up to 0.6% (fig. 5b) and polarization change 10 $\mu c/cm^2$ (fig. 5c) that can be induced by fields up to 60 Kv/cm.

It is suggested that the sequence of phase changes induced by the 001 high E-field is as in fig. 6. In the virgin state, the crystal is a relaxor with presumable a largely frozen rhombohedral nano/micro domain structure (fig. 6a). On first poling with 001 oriented field the P_r which is almost exactly $1/\sqrt{3}$ of the rhombohedral states, i.e. *111, $\bar{1}11$, $1\bar{1}1$, and $11\bar{1}$* oriented polarizations have been induced (fig. 6b). Note that this

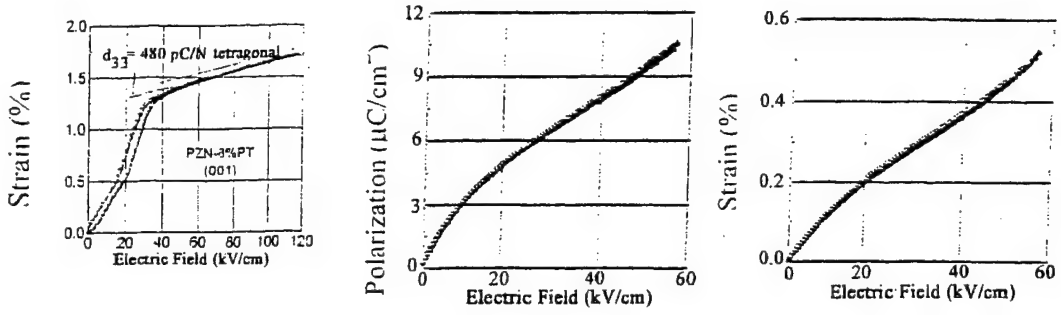

(a) E_3 field induced longitudinal strain in 001 Poled PZN 92:PT8.

(b) Electric Field induced polarization under 001 field in poled rhombohedral PZN 95.5 PT 4.5.

(c) Electric Field Induced Strain in 001 field Poled PZN 95.5 PT 4.5 anhysteritic for repeated field application.

FIGURE 5. Actuator behavior of 001 electric field poled rhombohedral PZN:PT single crystal.

structure requires a high concentration of charged walls, and gives rise to a domain averaged tetragonal 4mm macro symmetry. Since the high 001 field will change the energy of each of the 4 symmetry equivalent domains in the same way, there is no driving force to move the ferroelastic walls between the remaining domain states. Obviously the high field will induce a tilting of the Ps vector of the domain into the appropriate dodecahedral mirror plane givng rise to monoclinic domain states (fig. 6c) in which

$$P_1^2 = P_2^2 \neq 0 \qquad P_3^2 \neq 0 \qquad P_3^2 > P_1^2 \tag{5}$$

Again the monoclinic domains will average to macro 4mm symmetry. Eventually one expects the field to induce a true tetragonal monodomain state in which macro and micro symmetries coincide (fig. 6d).

An interesting question is whether the proposed sequence of changes can account for the observed large strain changes without extrinsic domain wall contribution.

Since intrinsic shape changes are electrostrictive it is only necessary to know the total polarization and the electrostrictive coefficients Q_{11}, Q_{12}, and Q_{44}. For m3m, it is simple to show that the volume strain s_v in all possible ferroelectric phases is given by

$$s_v = (Q_{11} + 2Q_{12})P_{Total}^2 \tag{6}$$

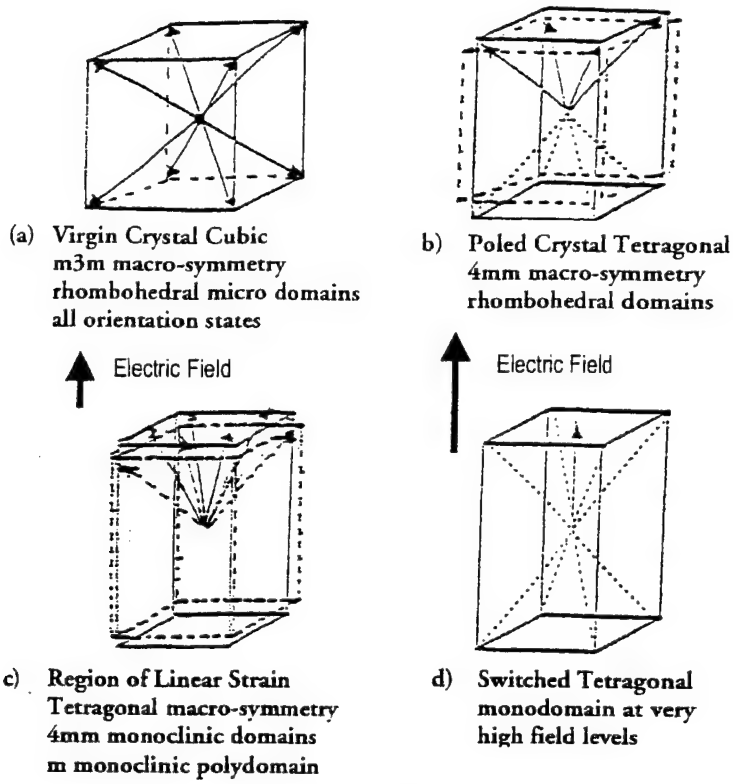

FIGURE 6.

Sequence of states in high 001 field poled rhombohedral PZN 95.5 PT 4.5 under increasing 001 E-field.

Measurements by Park [20] show that over the linear strain range up to 35 Kv/cm the volume change in PZN 0.95.5 PT 0.045 is less than 0.05%. Taking as a first aproximation $s_v = 0$, the polarization vector is just rotating under field and from fig. 5c the tilt angle in the induced monoclinic phase can be deduced and is presented in Table 2.

Taking Q_{11} from the total strain and total polarization in the induced tetragonal monodomain state

$$\begin{aligned} Q_{11} &= 0.0535 \\ \text{taking } Q_h &= 0 \quad \text{then yields} \\ Q_{12} &= 0.0267. \end{aligned}$$

In the field induced monoclinic phase

$$\begin{aligned} s_1 &= (Q_{11} + Q_{12})P_1^2 + Q_{12}P_3^2 \\ s_2 &= (Q_{11} + Q_{12})P_1^2 + Q_{12}P_3^2 \\ s_3 &= (Q_{11} + P_3^2) + 2Q_{12}P_1^2 \end{aligned} \qquad (7)$$

TABLE 2. Tilt angle and polarization components under increasing 001 E_3 field in rhombohedral PZN:95.5 PT 4.5 single crystal. Tilt is measured from the 001 axial direction.

Field kV/cm	Polarization P_3 $\mu c/cm^2$	Angle θ	Polarization P_1 $\mu c/cm^2$
5	27.8	50.1	23.47
10	29.8	46.5	22.21
15	31.4	43.4	21.04
20	33	40.34	19.82
25	34.3	37.5	18.64
30	35.6	34.6	17.42
35	36.75	31.9	16.19
40	37.85	29.1	14.87

From equation 7 and the known P_1 and P_3, components of the strains s_1, s_2, s_3 can be computed for the induced monoclinic phase in the anhysteritic range up to 35 Kv/cm E_3 field (fig. 7). Clearly the intrinsic strains in the monoclinic form are adequate to describe the induced total deformation.

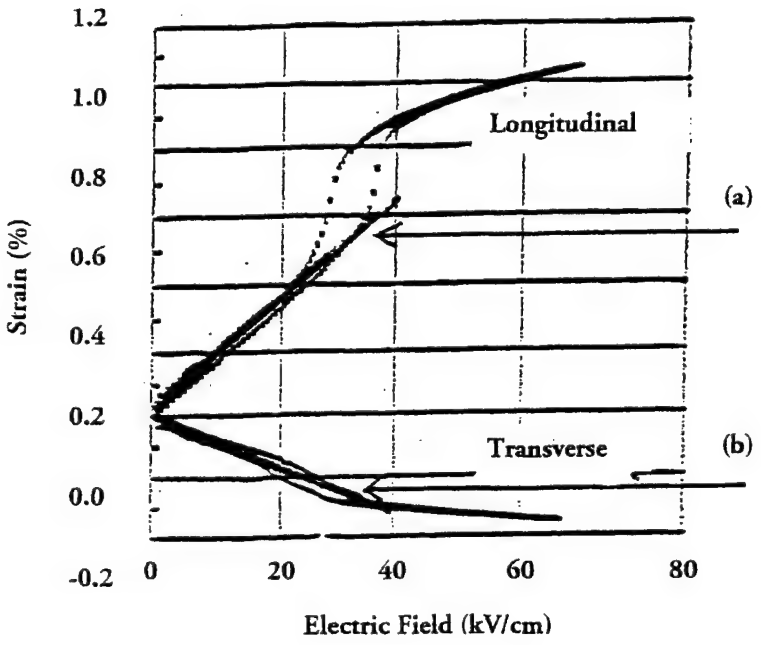

FIGURE 7. Calculated intrinsic strain in the field induced monoclinic phase (a) S_3 (b) S_1.

If this proposed explanation for high strain behavior is valid it should be expected that other peroskite structure ferroelectrics would show high intrinsic strain effects at temperatures close to phase boundaries. Strong enhancement of d_{33} at temperatures below but close to both rhombohedral/orthorhombic and orthorhomic/tetragonal phase changes in $BaTiO_3$ single crystals have been demonstrated [2]. Of particular relevance is the study by Wada et. al. [3] of the inverse transition, i.e. tetragonal to rhombohedral in 111 cut $BaTiO_3$ crystal under increasing 111 oriented electric field. The sequence of changes taken from their paper is depicted schematically in fig. 8. The 111 poling field first induces 100, 010, and 001 orientation of P_s in the tetragonal state. Under this condition for fields below 5 Kv/cm at 0.1 Hz a monoclinic phase is induced with intrinsic $d_{33} \sim 203$ pC/N (fig. 8a).

At higher fields, the system becomes hysteritic and the family of 110, 101, and 011 orthorombic domain orientations is finally induced (fig. 8b).

A new linear regimen of strain is evident for fields up to 45 Kv/cm, again exhibiting monoclinic symmetry, until the system moves by a hysteritic first order change to rhombohedral symmetry (fig. 8c). It is interesting to note that the second linear strain range has a different slope corresponding to a $d_{33} \sim 295$ pC/N.

We suggest (fig. 8) that because of the closeness to room temperature of the 4mm/mm2 change in $BaTiO_3$, the polarization vector under 111 field first moves out into the cube mirror (m_1) catalyzing the change to mm2 symmetry, but then at higher field must move in the dodecahedral mirror (m_2) to achieve the rhombohedral orientation. After achieving the rhombohedral state, it would appear the P_s chooses to stay in the dodecahedral mirror which connects directly to the tetragonal state. Since the two monoclinic phases accessible from m3m are quite distinct this would account for the different piezoelectric slopes measured in the experiment.

Since there is a very complete Gibbs Free Energy Function for $BaTiO_3$ [21] it should be a simple matter to do the full three dimensional energy plots, to calculate the lowest energy trajectories for the polarization change and thus to verify the major role of the E•P term in Energy for these "soft" ferroelectric perovskites.

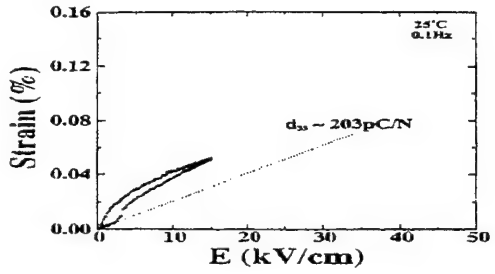

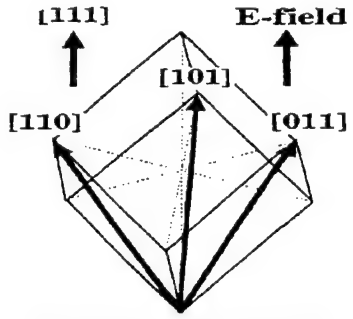

(a) Strain vs electric-field curve for [111] oriented $BaTiO_3$ crystal under unipolar electric field below 5kV/cm with 0.1 Hz at 25°C.

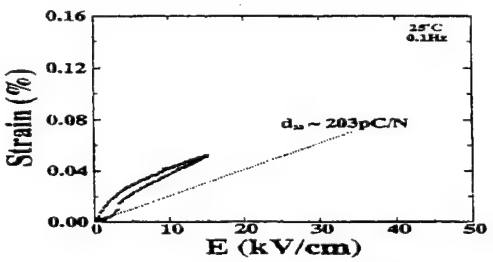

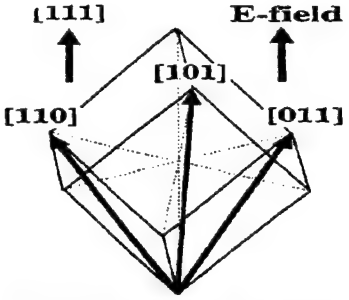

(b) Strain vs electric-field curve for [111] oriented $BaTiO_3$ crystal under unipolar electric field below 16 kV/cm with 0.1 Hz at 25°C.

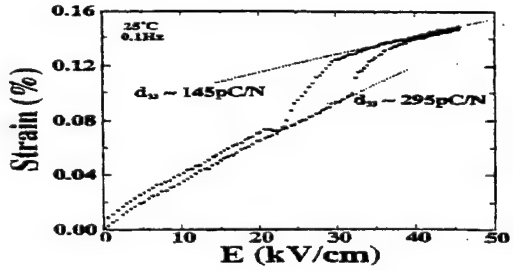

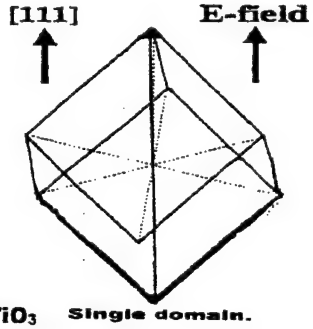

(c) Strain vs electric-field curve for [111] oriented $BaTiO_3$ crystal under unipolar electric field below 45 kV/cm with0.1 Hz at 25°C.

FIGURE 8. Sequence of domain and strain changes in 111 poled $BaTiO_3$ crystal at room temperature after Wada et. al. (2).

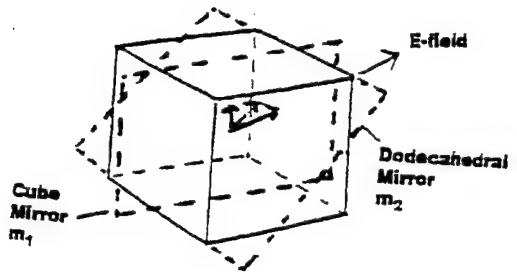

$P_3^2 \neq 0$	$P_1^2 = P_2^2 = 0$		Tetragonal
$P_3^2 \neq 0$	$P_2^2 \neq 0$ $P_3^2 \neq P_2^2$	$P_1^2 = 0$	monoclinic (cube m)
$P_3^2 = P_2^2 \neq 0$	$P_1^2 = 0$		Orthorhombic
$P_3^2 = P_2^2 \neq 0$	$P_1^2 \neq 0$	$P_1^2 \neq P_3^2$	monoclinic (Dodecahedron m)
$P_3^2 = P_2^2 = P_1^2 \neq 0$			Rhombohedral

E_{111}

FIGURE 9. Suggested model for the inverse field induced transition from 4mm ⇒ 3m in single crystal $BaTiO_3$ at 25°C.

Conclusions

In polycrystal ceramic PZT piezoelectrics the current balance of evidence still suggests a strong contribution to dielectric and piezoelectric responses from ferroelastic:ferroelectric domain wall motion. New evidence of a stable monoclinic phase just on the rhombohedral side of the MPB does however require revision of the earlier thermodynamic phenomenology to describe the intrinsic single domain responses and also contributes the possibility of previously unimagined new extrinsic contributions to response.

For the single crystal lead zinc niobate lead titanate at the 4.5% lead titanate composition the very high linear anhysteritic strain induced by 001 oriented E-field is suggested to be intrinsic and to result from the induction of a monoclinic phase in which P_S is substantially tilted from 111. In $BaTiO_3$ for the "inverse experiment" forcing tetragonal to rhombohedral symmetry at room temperature it is suggested that with increasing E-field P_S moves first in the cube mirror to orthorhombic, then in the doecahedral mirror towards rhombohedral symmetry, but at very high field may chose to accomplish complete switching in the alternative dodecahedral mirror.

References

[1] Fu, H., and Cohen, R.E., *Nature* 403, 281-283 (2000).

[2] Park, S.-E., Wada, S., Cross, L.E., and Shrout, T.R., *J. Appl. Phys.* **86** (5), 2746 (1999).

[3] Wada, S., Suzuki, S., Nomura, T., Suzuki, T., Osada, M., Kakihana, M., Park, S., Cross, L.E., and Shrout, T.R., *Jpn. J. Appl. Phys.* **38**, 5505 (1999).

[4] Carl, K., and Hardtl, K.H., *Ferroelectrics* **17**, 472 (1978).

[5] Dederichs, D., and Arlt, G., *Ferroelectrics* **68**, 281 (1986).

[6] Kugel, V.D., and Cross, L.E., *J. Appl. Phys.* **84**, 2815 (1998).

[7] Damjanovic, D., Demarlin, M., Shulman, H.S., Testorf, M., and Setter, N., *Sensors and Actuators A* **353** (1996).

[8] Tan, Q., Li, J.F., and Viehland, D., *Ferroelectrics* **206**, 275 (1998).

[9] Haun, M.J., Furman, E., Jiang, S.J., and Cross, L.E., *Ferroelectrics* **99**, 13 (1989).

[10] Haun, M.J., Furman, E., McKinstry, H.A., and Cross, L.E., *Ferroelectrics* **99**, 27 (1989).

[11] Haun, M.J., Zhuang, Z.Q., Furman, E., Jang, S.J., and Cross, L.E., *Ferroelectrics* **99**, 45 (1989).

[12] Haun, M.J., Furman, E., Halemane, T.R., and Cross, L.E., *Ferroelectrics* **99**, 55 (1989).

[13] Haun, M.J., Furman, E., Jang, S.J., and Cross, L.E., *Ferroelectrics* **99**, 63 (1989).

[14] Noheda, B., Cox, D.E., Shirane, G., Gonzalo, J.A., Cross, L.E., and Park, S.-E., *Appl. Phys. Letters* **74**, 2059 (1999).

[15] Noheda, B., Gonzalo, J.A., Guo, R., Park, S.-E., Cross, L.E., Cox, D.E., and Shirane, G., "The monoclinic phase in PZT; new light on morphotropic phase boundaries," *Proceedings Workshop on Fundamental Physics of Ferroelectrics*, Aspen, Colorado (February 2000).

[16] Kuwata, J., Uchino, K., and Nomura, S., *Jpn. J. Appl. Phys.* **21**, 1298 (1982).

[17] Park, S.-E., and Shrout, T.R., *Science* **275**, 1878 (1997).

[18] Park, S.-E., and Shrout, T.R., *Mat. Res. Innovation* **1**, 20 (1997).

[19] Park, S.E., and Shrout, T.R., *IEEE Trans. UFFC* **44**, 1140 (1997).

[20] Liu, S.-F., Park, S.-E., Shrout, T.R., and Cross, L.E., *J. Appl. Phys.* 85, 2810 (1999).

[21] Bell, A.J., and Cross, L.E., *Ferroelectrics* **59**, 197 (1984).

Appendix 6

Polarization Rotation via a Monoclinic Phase in the Piezoelectric $92\%PbZn_{1/3}Nb_{2/3}O_3$-$8\%PbTiO_3$

B. Noheda,[1,*] D. E. Cox,[1] G. Shirane,[1] S.-E. Park,[2,†] L. E. Cross,[2] and Z. Zhong[3]

[1]*Physics Department, Brookhaven National Laboratory, Upton, New York 11973*

[2]*Materials Research Laboratory, Pennsylvania State University, University Park, Pennsylvania 16802*

[3]*National Synchrotron Light Source, Brookhaven National Laboratory, Upton, New York 11973*

(Received 18 September 2000)

The origin of ultrahigh piezoelectricity in the relaxor ferroelectric $PbZn_{1/3}Nb_{2/3}O_3$-$PbTiO_3$ was studied with an electric field applied along the [001] direction. The zero-field rhombohedral R phase starts to follow the direct polarization path to tetragonal symmetry via an intermediate monoclinic M phase, but then jumps irreversibly to an alternate path involving a different type of monoclinic distortion. Details of the structure and domain configuration of this novel phase are described. This result suggests that there is a nearby R-M phase boundary as found in the $Pb(Ti,Zr)O_3$ system.

DOI: 10.1103/PhysRevLett.86.3891 PACS numbers: 77.65.–j, 61.10.Nz, 77.84.Dy

Recently, two important advances have been made in searching for the origin of high piezo response in the perovskite oxides. One is a theoretical consideration [1–3] of the polarization rotation path under an electric field, emphasized by Fu and Cohen [1]. The second is the experimental discovery of a monoclinic phase in $Pb(Ti,Zr)O_3$ [4,5] close to a "morphotropic" phase boundary (MPB), a nearly vertical line between the rhombohedral and tetragonal phases. In this paper we demonstrate that these two seemingly disparate aspects are closely connected.

Solid solutions of $Pb(Zn_{1/3}Nb_{2/3})O_3$ containing a few percent of $PbTiO_3$ (PZN-xPT) are relaxor ferroelectrics with ultrahigh piezoelectric responses an order of magnitude larger than those of conventional piezoelectric ceramics [6–8]. They have a cubic perovskite-type structure at high temperatures, but undergo a diffuse ferroelectric phase transition at lower temperatures [6]. Materials in the ferroelectric region have structures with either rhombohedral or tetragonal symmetry, separated by a morphotropic phase boundary at $x \simeq 10\%$, similar to that of the well-known piezoelectric system $PbZr_{1-x}Ti_xO_3$ (PZT) [9]. Extraordinarily high levels of electromechanical coupling and strain have been reported by Park and Shrout [8] in rhombohedral crystals that are poled along [001], despite the fact that the polar axis lies along [111] [7,10].

A typical strain-field loop for the rhombohedral composition $92\%PbZn_{1/3}Nb_{2/3}O_3$-$8\%PbTiO_3$ (PZN-8%PT) (close to the MPB) with an electric field applied along [001] is plotted in Fig. 1 (top), after Durbin *et al.* [11]. For this poling configuration, the strain behaves linearly below a certain threshold field, which is smaller for compositions closer to the MPB [8,10]. This feature, together with the high strain levels obtained, makes these materials very promising for actuator applications. Above the threshold field, the strain shows a sharp jump, nonlinear behavior, and hysteresis. X-ray diffraction experiments performed on PZN-8%PT crystals under an applied electric field [11] have shown that the lattice parameter vs field loop exactly reflects the strain behavior, confirming that the high macroscopic strain levels observed are due to the microscopic strain of the crystal lattice. The jump observed at the threshold field was attributed to a structural phase transition between the rhombohedral and the tetragonal phases. Very recently, it was also reported that the high-field tetragonal phase changes, after removal of the field, into a mixture of a dominant monoclinic phase with a remnant tetragonal phase [12].

Our current study with high-energy x rays of 67 keV gives a very different picture. We show that the rhombohedral phase in the unpoled sample transforms into a purely monoclinic phase by the application of an electric field along the [001] direction which, surprisingly, remains monoclinic after the field is removed. This monoclinic phase, in which b_m is directed along the pseudocubic [010] axis, is not the same as that observed in PZT, in which b_m lies along pseudocubic [110] [4]. The monoclinic phase in PZT represents the *a-g-f-e* path (see Fig. 1, bottom) proposed by Fu and Cohen [1] for the polarization to rotate between the rhombohedral and the tetragonal phases, while the monoclinic PZN-8%PT phase represents the rotation path along *a-c-d-e*.

Four crystals with composition PZN-8%PT, grown by the high temperature flux technique [8,13], were kindly provided by the authors of Refs. [11,12]. The crystals were oriented using a Laue backreflection camera as described previously [8], and cut into $2 \times 2 \times 2$ mm^3 cubes with their faces perpendicular to the $\langle 100 \rangle$ directions.

Synchrotron x-ray diffraction measurements were initially performed at beamline X7A, at the National Synchrotron Light Source (NSLS), with x rays of about 18 keV from a Si(111) double-crystal monochromator. Because of the high lead content, the samples are quite opaque at these energies, with a penetration depth of only about 1 μm, at the typical scattering angles used, and the measurements are therefore sensitive to inhomogeneous piezoelectric strains close to the surface (skin effect). In order to avoid this

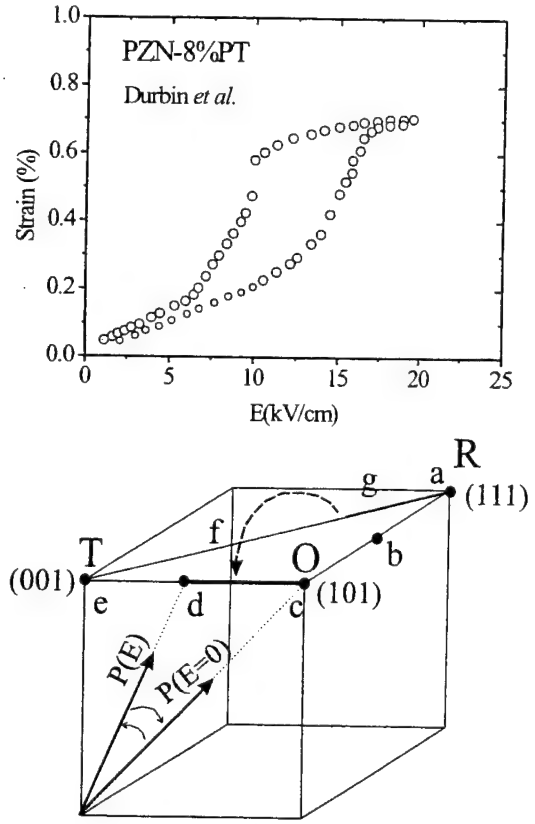

FIG. 1. Top: strain-field loop for PZN-8%PT (after Durbin *et al.* [11]). Bottom: scheme of the two possible paths (*R-T* and *R-O-T*) for the polarization direction to change from [111] in the rhombohedral (*R*) phase to [001] in the tetragonal (*T*) phase, as proposed by Fu and Cohen [1]. The thickest lines represent the path followed by the polarization in PZN-8%PT under the application of the electric field, as demonstrated by this work. The solid arrows illustrate the orientation of the polarization in a particular domain with and without an electric field.

effect, high-energy x-ray experiments were perfomed at 67 keV at the superconducting-Wiggler beamline X17B at the NSLS.

The 67-keV x rays were obtained with a Si(220) Laue-Bragg monochromator, and the measurements were made on a four-circle Huber diffractometer equipped with a Si(220) analyzer, with an electric field applied to the crystal *in situ*. For this purpose thin wires were attached to the sample electrodes using a small drop of conducting epoxy, and a silicon grease with a high dielectrical breakdown was used to prevent arcing.

As-grown crystals of the composition under study are rhombohedral [6,8] (see Table I). However, when an electric field above a certain value is applied, the crystal symmetry changes and the rhombohedral phase can only be recovered either by annealing above the Curie temperature or by crushing the crystal. The initial rhombohedral state and the phase transition(s) undergone during the first field cycle are currently under investigation by Ohwada [14].

Once the rhombohedral phase is irreversibly transformed into the monoclinic one, the monoclinic lattice

TABLE I. Lattice parameters, unit cell volume, and symmetry of PZN-8%PT as-grown, under a high field of 20 kV/cm, and after the field is removed. *S* denotes the crystal symmetry.

	a (Å)	b (Å)	c (Å)	α/β (°)	V (Å^3)	S
As-grown, $E = 0$[a]	4.053	4.053	4.053	89.90	66.58	*R*
$E = 20$ kV/cm[b]	4.047	4.029	4.086	90.16	66.62	*M*
After field, $E = 0$[a,b]	4.061	4.030	4.061	90.15	66.46	*M*

[a]From powder diffraction.
[b]From single crystal diffraction.

shows reversible changes as a function of the electric field, as shown in Fig. 2 (see also Table I). The monoclinic angle, $\beta = 90.15°$, and the monoclinic axis, b_m, are field independent in the studied range between 0 and 20 kV/cm. c_m increases with the electric field and shows a jump at about 15 kV/cm and hysteresis, in agreement with Durbin *et al.* [11], while a_m decreases as the field is increased and approaches the c_m value in the $E = 0$ limit [15].

The domain configuration observed in this experiment is illustrated in the representations of the reciprocal space shown in Fig. 3 [16]. Usually monoclinic symmetry leads to a very complicated domain configuration. However, once the field is applied, a much simpler situation prevails. The *c* axis is now fixed along the field direction. As shown in the representation of the HK0 plane in Fig. 3a, there are only two *b* domains related by a 90° rotation about the *c* axis. Each of these *b* domains contains two *a* domains in which a_m forms angles of either β or $180° - \beta$, respectively, with c_m (see Fig. 3b). The polarization vectors in each of the four domains, which rotate under the electric field within the *ac* plane, form identical angles with the [001] direction. It is evident from Fig. 3a that the domain twinning confers upon the lattice a pseudotetragonal symmetry, which might account for the previous assignment of tetragonal symmetry to this phase based on optical measurements [13].

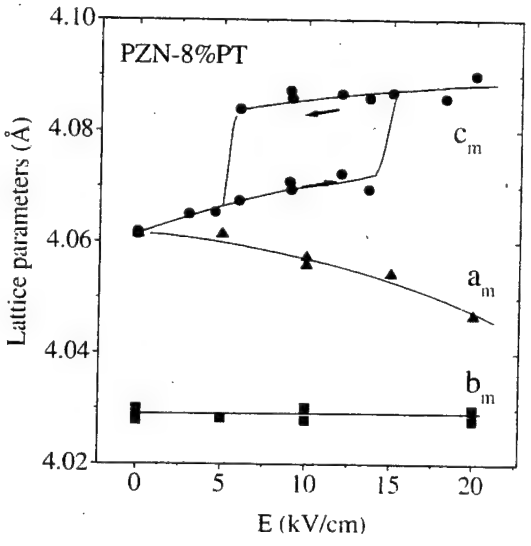

FIG. 2. Evolution of the lattice parameters. a_m, b_m, and c_m, of PZN-8%PT with electric field. No change in the monoclinic angle, β, is observed in this range of fields.

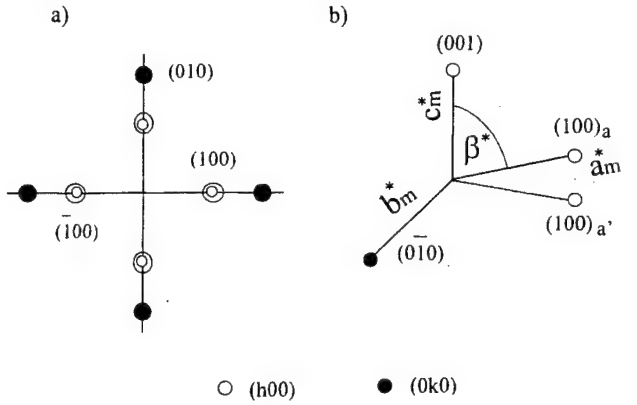

FIG. 3. (a) HK0 plane in reciprocal space for monoclinic PZN-8%PT showing the two b domains at 90°, shaded and unshaded, in which H and K are interchanged with respect to each other. The double circles represent the two a domains, illustrated in b. (b) Scheme of the reciprocal unit cell of one of the b domains showing the two a domains, a and a', respectively.

Some examples of the x-ray peak profiles are shown in Fig. 4. The longitudinal scans over the (002) reflection at 0 kV/cm and at 20 kV/cm shown in the upper left of the figure illustrate the drastic change of the c axis with the electric field ($L = 2$ corresponds to the $c_m = a_m$ value at $E = 0$). The very narrow mosaic at high fields is apparent in the upper right of the figure, which shows a transverse scan (L scan) over the (020) Bragg peak at $E =$ 20 kV/cm ($K = 2$ corresponds to the $c_m = a_m$ value at $E = 0$ so $K = 2.015$ means $b_m/a_m = 2/2.015$). The lower part of the figure is a contour map of the H0L zone around (200) after removal of the field, which shows the b domain containing the two a domains illustrated in Fig. 3a and 3b. The symmetric splitting along the transverse direction (L scan), corresponds to the twin angle between the a domains, so the L coordinate of 0.005 corresponds to a monoclinic angle $\beta = 90.16°$ that is found to be independent of the electric field. Although the (020) peak is very narrow, a small shoulder can be observed at positive L values (also present at 20 kV/cm, in the upper-right plot), which probably results from the crystal mosaic.

The low-energy experiments at 18 keV essentially reproduce the results obtained by Durbin *et al.* [11,12]. The c_m lattice parameter along the field direction [001] exhibits the same strongly nonlinear field dependence illustrated in Fig. 2. Measurements made with the scattering vector perpendicular to the field direction after the field was removed show the same characteristic diffraction features as recently reported [12], namely, a very broad peak on the low-angle side and a very sharp peak on the high-angle side, corresponding to $H = 2.000$ and $K = 2.015$, respectively. The broad peak changes with field while the sharp peak is field independent, in agreement with our high-energy x-ray results described above. The markedly different widths of these two peaks led Durbin *et al.* to postulate the coexistence of two phases (monoclinic and tetragonal) at $E = 0$ kV/cm, with very different domain sizes. However, since the broadening of the (h00) peaks was not observed with high-energy x rays, it can be attributed to a "skin" effect.

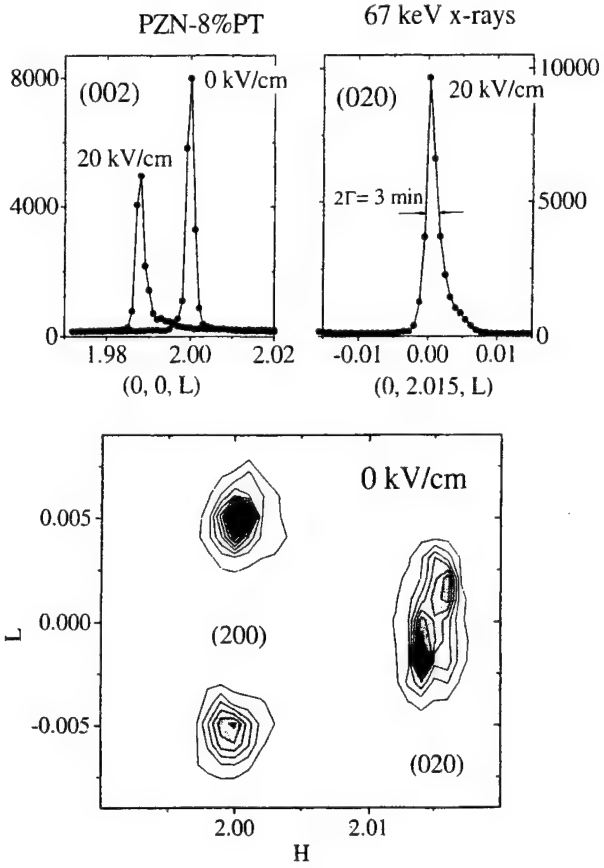

FIG. 4. Radial (L) scans over the (002) reflection at 20 kV/cm and at 0 kV/cm, after the field is removed (top left). The transverse (L) scan around (0, 2.015, 0) at 20 kV/cm is shown (top right). Bottom: an H0L mesh scan around the (200) Bragg reflection after the removal of the electric field. $H = K = L = 2.0$ have been defined to correspond to the a_m value at $E = 0$ kV/cm.

Powder diffraction data collected from a sample prepared by crushing a small crystal piece after the application and removal of an electric field have confirmed that the monoclinic indexing of our single-crystal experiments is correct. Lattice parameters $a_m = c_m = 4.061$ Å, $b_m =$ 4.030 Å, and $\beta = 90.15°$ were extracted, in complete agreement with the single-crystal data. In this case, however, the monoclinic phase was found to coexist with a rhombohedral phase with $a_r = 4.054$ Å and $\alpha = 89.9°$ (see Table I).

Comparison of our experimental results with the theoretical model of Fu and Cohen [1] brings out several interesting features. These authors calculated the free energies along the polarization rotation paths between the rhombohedral R and tetragonal T points for $BaTiO_3$ (see Fig. 1), and concluded that the R-T path (a-g-f-e) is the most energetically favorable one. PZN-8%PT starts out at the R point in Fig. 1, since the as-grown crystal is rhombohedral, but then changes irreversibly to the O-T path (c-d-e), with monoclinic symmetry. As mentioned above, this process of change between the rhombohedral and the monoclinic

phases (dashed arrow in Fig. 1) is being studied elsewhere in detail [14]. When the field is decreased, the crystal remains on the O-T path. During this process a_m and c_m gradually approach each other until they eventually reach the same value at $E = 0$ kV/cm [15]. When the field is increased, a_m approaches b_m (see Fig. 2), while following the O-T path, approaching the T point in Fig. 1. The polarization of each domain rotates within the (010) plane, and the polarization direction gets closer to the tetragonal polar axis, [001], as the field is increased, as shown by the solid arrows in Fig. 1. However, the T point is not yet reached at the maximum electric fields ($E = 20$ kV/cm) used in this study. Work is being carried out on other compositions, such as PZN-4.5%PT and PZN-9%PT, to determine the compositional range in which this behavior is observed. The major remaining questions are why and how the sudden change at 15 kV/cm is reflected only in c_m. The jump observed in c_m is very sensitive to the mechanical stress and can be completely eliminated if the sample is slightly stressed [17]. Work is in progress to address this point.

The electric field experiments reported by Guo *et al.* [5] on rhombohedral PZT showed that, by poling at high temperatures, a monoclinic phase is also induced by the electric field and retained after the field is removed. This monoclinic cell is such that b_m lies along pseudocubic [110] [4], indicating that the polarization moves along the R-T (e-g-f-e) path when the field is applied. On the other hand, unpoled PZT has a monoclinic phase region from $x = 0.46$ to $x = 0.52$ at 20 K [18]. The existence of an irreversible rhombohedral-to-monoclinic phase transition induced by the application of an electric field in PZN-8%PT suggests that, as in the PZT case [5], a rhombohedral-to-monoclinic phase boundary exists close to $x = 8\%$ in the unpoled PZN-xPT phase diagram. This would clarify some of the apparent puzzles reported, such as the optical observation of symmetry lowering in PZN-9%PT [19,20]. If the monoclinic phase is found to exist in unpoled PZN-9%PT, then the phase diagram of PZN-PT becomes almost identical to that of PZT. Our current results suggest that the near degeneracy between the two monoclinic paths (R-T and R-O-T) might be responsible for the larger piezoelectric response in PZN-xPT, compared with that of PZT, in which only rotation is allowed. We expect that first-principles calculations may well clarify some of these important questions.

After submission of this Letter, the very relevant work by Vanderbilt and Cohen [21] came to our attention. By means of an eighth-order expansion of the Devonshire theory, these authors were able to predict three different monoclinic phases. Two of these, M_A and M_C, correspond, respectively, to that previously observed in PZT and the one in PZN-8%PT described above.

We thank M. Durbin, Y. Fujii, P. Gehring, R. Guo, J. Hastings, K. Hirota, K. Ohwada, D. Vanderbilt, and T. Vogt for helpful discussions. Financial support by the U.S. DOE under Contract No. DE-AC02-98CH10886, by ONR Grant No. N00014-98-1-0527, and project MURI (N00014-96-1-1173) is also acknowledged.

*Corresponding author.
Electronic address: noheda@bnl.gov
On leave from Universidad Autonoma de Madrid.
†Present address: Fraunhofer Technology Center, Hialeah, Florida 33010.

[1] H. Fu and R. E. Cohen, Nature (London) **403**, 281 (2000).
[2] A. Garcia and D. Vanderbilt, Appl. Phys. Lett. **72**, 2981 (1998).
[3] L. Bellaiche, A. Garcia, and D. Vanderbilt, Phys. Rev. Lett. **84**, 5427 (2000).
[4] B. Noheda, J. A. Gonzalo, L. E. Cross, R. Guo, S-E. Park, D. E. Cox, and G. Shirane, Phys. Rev. B **61**, 8687 (2000).
[5] R. Guo, L. E. Cross, S-E. Park, B. Noheda, D. E. Cox, and G. Shirane, Phys. Rev. Lett. **84**, 5423 (2000).
[6] J. Kuwata, K. Uchino, and S. Nomura, Ferroelectrics **37**, 579 (1981).
[7] J. Kuwata, K. Uchino, and S. Nomura, Jpn. J. Appl. Phys. **21**, 1298 (1982).
[8] S-E. Park and T. R. Shrout, J. Appl. Phys. **82**, 1804 (1997).
[9] B. Jaffe, W. R. Cook, and H. Jaffe, *Piezoelectric Ceramics* (Academic Press, London, 1971).
[10] S-F. Liu, S-E. Park, T. R. Shrout, and L. E. Cross, J. Appl. Phys. **85**, 2810 (1999).
[11] M. K. Durbin, E. W. Jacobs, J. C. Hicks, and S.-E. Park, Appl. Phys. Lett. **74**, 2848 (1999).
[12] M. K. Durbin, J. C. Hicks, S-E. Park, and T. R. Shrout, J. Appl. Phys. **87**, 8159 (2000).
[13] D-S. Paik, S-E. Park, S. Wada, S-F. Liu, and T. R. Shrout, J. Appl. Phys. **85**, 1080 (1999).
[14] K. Ohwada (private communication).
[15] In the limit at which $a_m = c_m$ and $\beta > 90°$, the crystal symmetry becomes orthorhombic, corresponding to the O point in Fig. 1 (bottom). This orthorhombic cell is doubled in volume with respect to the monoclinic cell, with lattice parameters $a_0 = 2a_m \sin(\beta/2) = 5.751$ Å, $b_0 = b_m = 4.030$ Å, and $c_0 = 2a_m \cos(\beta/2) = 5.736$ Å. The space group is probably $Bmm2$, by analogy to the orthorhombic phase of $BaTiO_3$.
[16] The real and the reciprocal lattice parameters are related by $a_m^* = 2\pi/(a_m \sin\beta)$, $b_m^* = 2\pi/b_m$, $c_m^* = 2\pi/(c_m \sin\beta)$, and $\beta^* = 180° - \beta$.
[17] D. Viehland, J. Appl. Phys. **88**, 4794 (2000).
[18] B. Noheda, D. E. Cox, G. Shirane, R. Guo, B. Jones, and L. E. Cross, Phys. Rev. B **63**, 014103 (2001).
[19] Y. Uesu, Y. Yamada, K. Fujishiro, H. Tazawa, S. Enokido, J.-M. Kiat, and B. Dkhil, Ferroelectrics **217**, 319 (1998).
[20] K. Fujishiro, R. Vlokh, Y. Uesu, Y. Yamada, J.-M. Kiat, B. Dkhil, and Y. Yamashita, Jpn. J. Appl. Phys. **37**, 5246 (1998).
[21] D. Vanderbilt and M. H. Cohen, Phys. Rev. B **63**, 094108 (2001).

Appendix 7

Crystallographically engineered $BaTiO_3$ single crystals for high-performance piezoelectrics

Seung-Eek Park,[a] Satoshi Wada,[b] L. E. Cross, and Thomas R. Shrout
Materials Research Laboratory, The Pennsylvania State University, University Park, Pennsylvania 16802

(Received 11 March 1999; accepted for publication 27 May 1999)

Dielectric and piezoelectric properties of $BaTiO_3$ single crystals polarized along the ⟨001⟩ crystallographic axes were investigated as a function of temperature and dc bias. Electromechanical coupling (k_{33})~85% and piezoelectric coefficients (d_{33})~500 pC/N, better or comparable to those of lead-based $Pb(Zr, Ti)O_3$ (PZT), were found from ⟨001⟩-oriented orthorhombic crystals at 0 °C, as a result of crystallographic engineering. A rhombohedral $BaTiO_3$ crystal polarized along ⟨001⟩ also exhibited enhanced piezoelectric performance, i.e., k_{33}~79% and d_{33}~400 pC/N at −90 °C, superior to PZTs at the same temperature. It was found that the crystal structure determined the (in)stability of the engineered domain state in $BaTiO_3$ single crystals. Rhombohedral (3m) crystals at −100 °C exhibited a stable domain configuration, whereas depoling occurred in crystals in the adjacent orthorhombic phase upon removal of the E field. © *1999 American Institute of Physics.* [S0021-8979(99)04517-X]

I. INTRODUCTION

Recent innovations in regard to relaxor-based single-crystal piezoelectrics such as $Pb(Zn_{1/3}Nb_{2/3})O_3$, $Pb(Mg_{1/3}Nb_{2/3})O_3$, and their solid solution with $PbTiO_3$ are based on crystallographic engineering associated with an engineered domain state and crystal anisotropy, which is not achievable in polycrystalline ceramics. Longitudinal coupling coefficients (k_{33}) as high as 94%, piezoelectric coefficients (d_{33}) >2500 pC/N with strain levels exceeding 1.7% (Refs. 1–3) were recognized by electrically polarizing relaxor-based rhombohedral single crystals along their nonpolar pseudocubic ⟨001⟩ direction. In contrast, rhombohedral crystals poled along their polar direction ⟨111⟩ exhibited significantly inferior properties, i.e., k_{33}<50% and d_{33}~100 pC/N.[2,4]

In addition to ultrahigh piezoelectric performance, strain versus E-field behavior with minimal hysteresis, and low dielectric loss (<1%), was another important characteristic of the crystallographically engineered relaxor-based single crystals,[2] a consequence of four equally populated rhombohedral types of domains.[5] Although in a multidomain state, the stable domain configuration resulted in materials with enhanced reliability, i.e., no degradation detected after more than 10^7 cycles of unipolar driving at high fields (>50 kV/cm, 1 kHz).[6] From a crystallographic point of view, it was suggested[5,7,8] that the macroscopic symmetry of rhombohedral relaxor ferroelectric crystals poled, or dc biased along ⟨001⟩, should be 4 mm, describing the macrosymmetry of an entire single crystal composed of a stable engineered domain configuration.

Based on the concept of crystallographic engineering used in relaxor ferroelectric single crystals, single crystals or epitaxial forms of any known ferroelectric materials should exhibit significant enhancement in electromechanical performance at temperature or composition close to an appropriate phase transition. It was the objective of this work, therefore, to apply the concept of crystallographic engineering to normal ferroelectric crystals such as $BaTiO_3$, and to evaluate the possibility of enhanced piezoelectric performance. Low-temperature phases of $BaTiO_3$ single crystals, such as orthorhombic and rhombohedral, were poled along ⟨001⟩ to induce an engineered domain state. The obtained piezoelectric properties were compared with values predicted by axis transformation for single-domain $BaTiO_3$ crystals using the Devonshire theory.[9]

II. EXPERIMENTAL PROCEDURE

Samples for measuring dielectric and piezoelectric properties were prepared using commercially available $BaTiO_3$ single crystals (optical grade, Fujikura Ltd.) grown by the top-seeded solution growth (TSSG) technique. According to company brochures and the related report,[10] concentration of impurities such as Cr, Mn, Co, Ni, Fe, and Cu was less than 3 ppm. Individual crystals were oriented along their pseudocubic ⟨001⟩ axis using a Laue back-reflection camera.

For electrical characterization, samples were prepared by polishing with silicon carbide and alumina polishing powders to achieve flat and parallel surfaces. Gold electrodes were sputtered on both sides of the samples. Prior to electrical characterization, all samples were heat treated at 250 °C for 14 h to eliminate residual stresses induced during sample preparation. For low-field measurements using the IEEE resonance technique,[11] samples were poled either by field cooling (10 kV/cm) from 150 °C or by applying 40 kV/cm at room temperature.

Low-temperature properties under dc bias were measured using an HP4194 impedance analyzer in conjunction with a computer-controlled temperature chamber (Delta De-

[a]Electronic mail: sxp37@psu.edu
[b]Current Address: Department of Applied Chemistry, Tokyo University of Agriculture and Technology, 24-16, Nakamachi 2-chome, Koganei, Tokyo 184-8588, Japan.

TABLE I. Phase transitions of $BaTiO_3$ crystal as a function of temperature.

Temperature range	>130 °C	120 to 0 °C	0 to −90 °C	<−90 °C
Primitive cell symmetry	Cubic	Tetragonal	Pseudomonoclinic (orthorhombic[a])	Rhombohedral
Point group	m3m	4mm	mm2	3m
Macrosymmetry[b]	···	4mm	4mm	4mm

[a]Unit-cell symmetry.
[b]Under dc bias along ⟨001⟩.

sign Inc., model MK 2300) and a dc bias blocking circuit with a maximum capacity of 1000 V. For longitudinal piezoelectric coefficient (d_{33}) determination, bar-shape samples of 0.4×0.4×1.6 mm in length were prepared. High-field measurements included polarization and strain hysteresis using a modified Sawyer–Tower circuit and a linear variable differential transducer (LVDT) driven by a lock-in amplifier (Stanford Research Systems, model SR830). Plate-shape samples with thickness ranging from 0.2 to 0.5 mm were used. Electric fields as high as ~140 kV/cm were applied using an amplified unipolar wave form at 0.1 Hz, from a Trek 609C-6 high-voltage dc amplifier. During testing the samples were submerged in Fluorinert (FC-40, 3M, St. Paul, MN), an insulating liquid, to prevent arcing.

III. RESULTS AND DISCUSSION

Table I summarizes the phase transitions of $BaTiO_3$. As considered in the phenomenological theory by Devonshire,[12] the unit-cell symmetry dictates the direction of the polar shift, i.e., orthogonal (4mm), face diagonal (mm2), and body diagonal (3m), based on the primitive perovskite cell. When an E field is applied along an orthogonal direction at various temperatures, a single-domain state may be achieved only for tetragonal crystals. In contrast, in orthorhombic as well as in rhombohedral crystals, four polarization directions (⟨101⟩, ⟨011⟩, ⟨−101⟩, ⟨0−11⟩ and ⟨111⟩, ⟨−111⟩, ⟨1−11⟩, ⟨−1−11⟩, respectively) are energetically equivalent and four types of domains will be equally populated under the ⟨001⟩ E field. Using analogy with rhombohedral relaxor ferroelectric single crystals,[5,7] we propose that this configuration should result in a macroscopic symmetry 4mm, as shown in Table I. It is interesting to note that the crystal macrosymmetry retains 4mm regardless of lattice symmetry changes, under the ⟨001⟩ E field. The macroscopic symmetry of crystals at zero E field that were exposed to the ⟨001⟩ E field was determined by the stability of the engineered domain configuration. A certain magnitude of the ⟨001⟩ E field will ultimately induce the phase transition into a single-domain tetragonal phase. Details on the E-field-induced phase transition can be found elsewhere.[8,13] Details on domain (in)stability will be discussed in the following sections.

Figure 1 presents longitudinal electromechanical coupling coefficients (k_{33}) as a function of temperature for the ⟨001⟩-poled $BaTiO_3$ crystal under dc bias. At room temperature, the value of k_{33} increased from ~0.53 (0 kV/cm) to 0.65 (6 kV/cm) as a result of the domain reorientation in the crystal, which had been partially depoled due to domain instability. Regardless of the magnitude of the dc bias, the initial partially depoled state reappeared upon removal of the E field. It is important to note that k_{33}~0.53(0 kV/cm), a value from the partially depoled crystals in this work, corresponds to values reported earlier, i.e., ~0.56 (Ref. 14) and ~0.55 (Ref. 15) for tetragonal $BaTiO_3$ crystals, suggesting that they were not those of single-domain crystals.

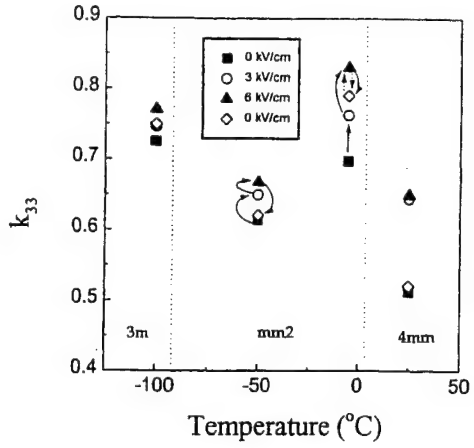

FIG. 1. k_{33} as a function of temperature for the ⟨001⟩-poled $BaTiO_3$ crystal under various dc bias. (solid arrows: first cycle, dashed arrows: second cycle).

At lower temperatures, k_{33} was also found to be dependent on the dc bias due to crystal depoling as a result of phase transitions as well as domain instability. Figure 2 shows k_{33} as a function of the E field for orthorhombic crystals (−5 °C). k_{33}~0.7 initially detected at 0 kV/cm increased with increasing bias, to a value of k_{33} as high as 0.83 at 6 kV/cm. After E-field exposure, the unbiased k_{33} value was as high as 0.79, being a starting point for the second cycle (dashed arrows in Fig. 1). The initial lower value for the first cycle (solid arrows in Fig. 1) must be a consequence of partial depoling caused by the tetragonal–orthorhombic phase transition. It is noted that when the E field was constant at 6 kV/cm, the k_{33} value increased from 0.79 to 0.83, indicating that higher k_{33}'s may be obtained under larger dc bias. Similar behavior was observed for rhombohedral crystals at −100 °C, with maximum k_{33} as high as 0.78 at 6 kV/cm.

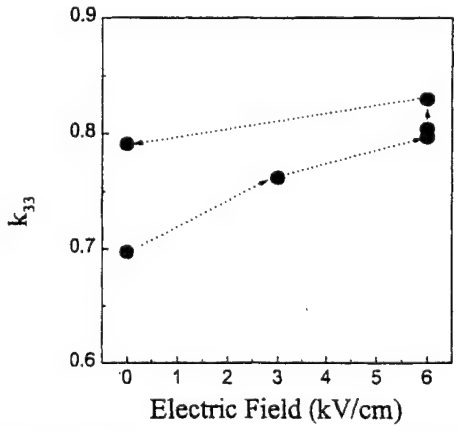

FIG. 2. k_{33} as a function of dc-bias (first cycle) for the ⟨001⟩-oriented $BaTiO_3$ crystal at −5 °C.

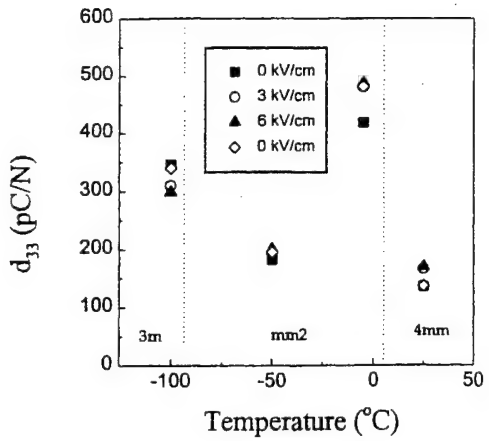

FIG. 3. d_{33} as a function of temperature for the ⟨001⟩-poled $BaTiO_3$ crystal under various dc bias, measured using the IEEE standard method.

Note that these k_{33} values of $BaTiO_3$ crystals are larger than room-temperature k_{33} values of Pb-based polycrystalline $Pb(Zr,Ti)O_3$ (PZTs) (0.5–0.75), the current piezoelectric material of choice.

Piezoelectric coefficients (d_{33}) versus dc bias at various temperatures are shown in Fig. 3. For the ⟨001⟩-poled $BaTiO_3$ crystals, change in d_{33} as a function of the ⟨001⟩ E field was not as significant as in the case of k_{33}, as evident from the equation,

$$d_{33}=k_{33}\sqrt{(\epsilon_{33}^{T}s_{33}^{E})}, \tag{1}$$

with ϵ_{33}^{T} (free-dielectric permitivity) quickly decreasing with increased E field while k_{33} increased and s_{33}^{E} (elastic compliance) remained almost constant as demonstrated in Fig. 4. It is noted that the d_{33} value of ~490 pC/N, which was measured at −5 °C is comparable to the room-temperature d_{33} values of the PZTs. Rhombohedral $BaTiO_3$ crystals at −100 °C exhibited d_{33}'s as high as 350 pC/N, also larger than that of polycrystalline PZTs at the same temperature.[16]

In regard to domain instability in single crystals, d_{33} was also determined directly from strain versus E-field curves. Figure 5 presents strain versus unipolar E-field behavior for the ⟨001⟩-poled $BaTiO_3$ crystals at various temperatures.

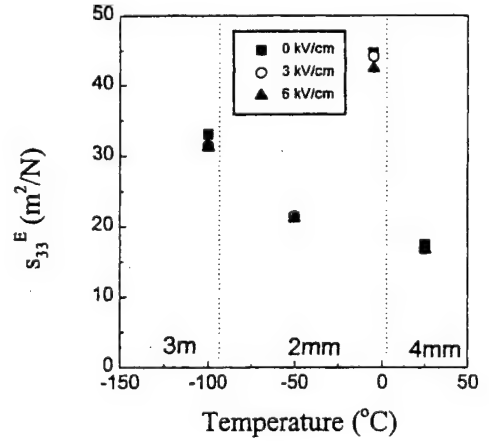

FIG. 4. s_{33}^{E} as a function of temperature for the ⟨001⟩-poled $BaTiO_3$ crystals under various dc bias.

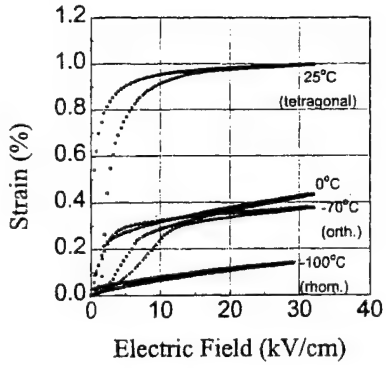

FIG. 5. Strain vs E-field behavior (unipolar) for the ⟨001⟩-oriented $BaTiO_3$ crystal.

Room-temperature strain values (unipolar) as high as 1% were quite surprising, considering that a total 1.07% strain is involved with the full spontaneous ferroelectric strain (c/a−1) of $BaTiO_3$ crystals at room temperature. This ultrahigh unipolar strain behavior, although unusable for practical actuation, indicates that crystal depoling involved almost full 90° domain switching rather than 180° switching upon the removal of the E field. Although still not completely clear, it is suspected that the very small amount of compressive force under the probe of the LVDT (see the experimental procedure) might cause this depoling behavior. The single-domain state of the tetragonal crystals, reflected by nonhysteretic strain versus E-field behavior, could be achieved at E fields >~10 kV/cm at room temperature as shown in Fig. 5, with d_{33}~128 pC/N values determined at 20 kV/cm.

The hysteresis ($E<10$ kV/cm) found in the orthorhombic crystal (0 and −70 °C in Fig. 5) was also ascribed to domain instability. In contrast, the engineered domain state of rhombohedral crystals (−100 °C) was found to be stable, as can be seen in Fig. 5, retaining macrosymmetry 4mm over the full range (unipolar) of the E field. Note that relaxor-based single crystals with a stable engineered domain state were also rhombohedral. Although further study is required to clarify the relationship between the crystal structure and the engineered domain state, it is suggested that lattice symmetry determines the (in)stability of the domain configuration. Rhombic lattice distortion might be critical to stabilize the engineered domain state in ⟨001⟩-poled ferroelectric crystals. However, depoling affected by the weak uniaxial stress described above may also be noted. Only in the ⟨001⟩-poled rhombohedral crystals is the domain configuration unaffected by uniaxial stress along ⟨001⟩.

Nonhysteretic regions of the strain versus E-field ($E>10$ kV/cm) curves are presented in Fig. 6. Apparent d_{33}'s calculated from such nonhysteretic regions of the strain versus E-field curves are plotted in Fig. 7. The d_{33} values in Fig. 7 confirm those (Fig. 3) obtained from the IEEE standard technique under bias (6 kV/cm).

According to Devonshire,[9] d_{33} values of single-domain $BaTiO_3$ crystals under weak field or stress can be calculated using the following equations:

$$d_{33}=2\epsilon_o Q_{11}\eta_{33}P_3,$$

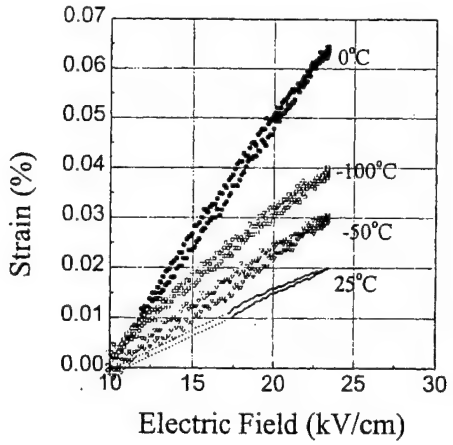

FIG. 6. Nonhysteretic portion of strain vs E-field curves (unipolar) for the ⟨001⟩-oriented $BaTiO_3$ crystal.

where $P_3 = P_s$ (spontaneous polarization),

for tetragonal crystals, (2)

$$d_{33} = 2\epsilon_o(Q_{11}\eta_{33} + Q_{12}\eta_{23})P_3,$$

where $P_3 = P_s/\sqrt{2}$, for orthorhombic crystals, (3)

$$d_{33} = 2\epsilon_o(Q_{11}\eta_{11} + 2Q_{12}\eta_{12})P_3,$$

where $P_3 = P_s/\sqrt{3}$, for rhombohedral crystals, (4)

where ϵ_0 is the permittivity of free space, Q_{ij} the electrostrictive coefficients, and η_{ij} the dielectric susceptibility. For crystallographically engineered orthorhombic and rhombohedral crystals with engineered multidomain states, however, the lattice symmetry is expected to change under higher ⟨001⟩ E field. For instance, orthorhombic and rhombohedral lattices strained by the ⟨001⟩ E field lack two-fold and three-fold symmetry, respectively. Microscopically, this results in pseudomonoclinic symmetry with $P_1^2 \neq P_3^2$, and $P_1^2 = P_2^2 \neq P_3^2$ for orthorhombic and rhombohedral crystals, respectively. For the engineered domain state under the ⟨001⟩ E field, therefore, Eqs. (3) and (4) are rewritten as

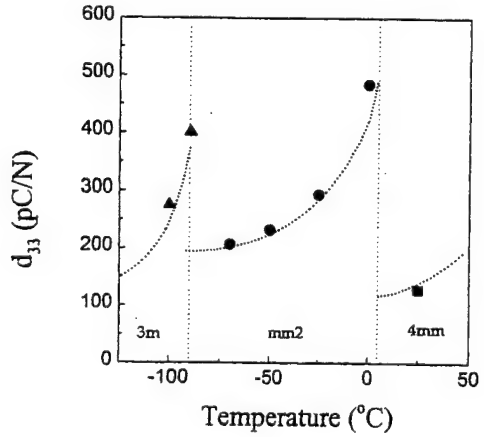

FIG. 7. d_{33} of the ⟨001⟩-oriented $BaTiO_3$ crystal, calculated from the slope of strain vs E-field curves in Fig. 6 (dashed lines: calculated values for single-domain $BaTiO_3$ crystals).

$$d_{33} = 2\epsilon_o(Q_{11}\eta_{33}P_3 + Q_{12}\eta_{23}P_1),$$

for orthorhombic crystals, (5)

$$d_{33} = 2\epsilon_o(Q_{11}\eta_{11}P_3 + 2Q_{12}\eta_{12}P_1),$$

for rhombohedral crystals. (6)

Although crystallographically engineered $BaTiO_3$ crystals consist of an engineered multidomain state, d_{33} based on Eqs. (5) and (6) could not be calculated due to the lack of experimental data. The authors' efforts to obtain experimental data for the engineered domain state are ongoing. In this work instead, the d_{33} values calculated for single-domain $BaTiO_3$ crystals under weak field are plotted on Fig. 7 (dashed line). The measured d_{33} values [see specifically the orthorhombic (mm2) range] fit well to the theoretical values for single-domain crystals derived in this way, suggesting that P_3/P_1 is not large at the field levels used in this work, and/or may be compensated by changes in η_{ij}. Although further research is required, it may be suggested that intrinsic effects are the major contribution to large piezoelectric coefficients and subsequent shape changes of $BaTiO_3$ crystals, on the basis of the curve fit in Fig. 7.

IV. CONCLUSION

$BaTiO_3$ single crystals are promising candidates for high-performance nonlead piezoelectrics at low temperatures. Crystallographic engineering, by polarizing crystals under dc bias toward the nonpolar ⟨001⟩ direction, resulted in orthorhombic and rhombohedral crystals with macroscopic symmetry 4mm. Piezoelectric properties with an electromechanical coupling coefficient (k_{33})~85% and piezoelectric coefficient (d_{33})~500 pC/N, better or comparable to those of PZTs were obtained from orthorhombic crystals at 0 °C. At −90 °C, rhombohedral $BaTiO_3$ crystals with k_{33}~79% and d_{33}~400 pC/N were found to be superior to PZTs at the same temperature. The stability of the engineered domain state in $BaTiO_3$ crystals was dependent upon the crystal structure. Although possessing the same macroscopic symmetry 4mm, rhombohedral (3m) crystals (−100 °C) exhibited a stable domain configuration whereas the adjacent orthorhombic state (−70 °C) was depoled. A possible role of weak uniaxial stress in the depoling must be further examined. The intrinsic piezoelectric response could explain most of the measured values.

Orthorhombic or rhombohedral $BaTiO_3$, stabilized by proper dopants such as zirconium, are expected to be a high-performance nonlead piezoelectric in single-crystal or epitaxial form at room temperature.

ACKNOWLEDGMENTS

This work has been supported by DARPA and the Office of Naval Research. The authors would like to thank Hua Lei for her help with sample preparation.

[1] J. Kuwata, K. Uchino, and S. Nomura, Jpn. J. Appl. Phys., Part I **21**, 1298 (1982).
[2] S.-E. Park and T. R. Shrout, IEEE Trans. Ultrason. Ferroelectr. Freq. Control **44**, 1140 (1997).

[3] S.-E. Park and T. R. Shrout, J. Appl. Phys. **82**, 1804 (1997).
[4] S.-E. Park, M. Mulvihill, G. Risch, M. Zipparo, and T. R. Shrout, Proceedings of the 10th IEEE International Symposium on the Application of Ferroelectrics **1**, 79 (1996).
[5] S. Wada, S.-E. Park, L. E. Cross, and T. R. Shrout, J. Korean Phys. Soc. **32**, 1290 (1998).
[6] S.-E. Park, V. Vedula, M.-J. Pan, W. S. Hackenberger, P. Pertsch, and T. R. Shrout, in Effect of Prestress on the Strain Behavior of Relaxor-based Single Crystals, SPIE's 5th Annual International Symmposium on Smart Structures and Materials, San Diego, CA, March 1998.
[7] S.-E. Park and T. R. Shrout, in Relaxor-based Ferroelectric Single Crystals with High Piezoelectric Performance, Proceedings of the 8th U.S.–Japan Seminar on Dielectric and Piezoelectric Ceramic Thin Films, pp. 235–241, Plymouth, MA, October 1997.
[8] S.-F. Liu, S.-E. Park, T. R. Shrout, and L. E. Cross, J. Appl. Phys. **85**, 2810 (1999).
[9] A. F. Devonshire, Philos. Mag. **42**, 1065 (1951).
[10] S. Ajumura, K. Tomomatu, O. Nakao, A. Kurosaka, H. Tominaga, and O. Fukuda, J. Opt. Soc. Am. B **9**, 1609 (1992).
[11] IEEE Standard on Piezoelectricity, American National Standards Institute, 1976.
[12] A. F. Devonshire, Philos. Mag. **40**, 1040 (1951).
[13] D.-S. Paik, S.-E. Park, S. Wada, S.-F. Liu, and T. R. Shrout, J. Appl. Phys. **85**, 1080 (1999).
[14] B. Jaffe, W. R. Cook, and H. L. Jaffe, *Piezoelectric Ceramics* (Academic, New York, 1971).
[15] M. Zgonik, P. Bernasconi, M. Duelli, R. Schlesser, and P. Gunter, Phys. Rev. B **50**, 5941 (1994).
[16] X. L. Zhang, Z. X. Chen, L. E. Cross, and W. A. Schulze, J. Mater. Sci. **18**, 968 (1983).

Appendix 8

Enhanced Piezoelectric Property of Barium Titanate Single Crystals with Engineered Domain Configurations

Satoshi WADA*, Shingo SUZUKI, Tatsuo NOMA, Takeyuki SUZUKI, Minoru OSADA[1], Masato KAKIHANA[2], Seung-Eek PARK[3], L. Eric CROSS[3] and Thomas R. SHROUT[3]

Department of Applied Chemistry, Tokyo University of Agriculture & Technology, 24-16 Nakamachi 2-chome, Koganei, Tokyo 184-8588, Japan
[1]*Institute of Physical & Chemical Research, 2-1 Hirosawa, Wako, Saitama 351-0198, Japan*
[2]*Materials & Structures Laboratory, Tokyo Institute of Technology, 4259 Nagatsuta-cho, Midori-ku, Yokohama 226-8502, Japan*
[3]*Materials Research Laboratory, Pennsylvania State University, University Park, PA 16802, U.S.A.*

(Received May 10, 1999; accepted for publication June 18, 1999)

Piezoelectric properties of barium titanate single crystals were investigated at room temperature as a function of crystallographic orientation. When a unipolar electric field was applied along [001], its strain *vs* electric-field curve showed a large hysteresis, and finally barium titanate crystal became to single-domain state with piezoelectric constant d_{33} of 125 pC/N over 20 kV/cm. On the other hand, electric-field exposure below 6 kV/cm along [111] resulted in a high d_{33} of 203 pC/N and a hysteresis-free strain *vs* electric-field behavior, which suggested the formation of an engineered domain configuration in a tetragonal barium titanate crystal. Moreover, when an electric field over 6 kV/cm was applied along [111], two discontinuous changes were observed in its strain *vs* electric-field curve. *In situ* domain observation and Raman measurement under an electric field suggested an electric-field-induced phase transition from tetragonal to monoclinic at around 10 kV/cm, and that from monoclinic to rhombohedral at around 30 kV/cm. Moreover, in a monoclinic barium titanate crystal, electric-field exposure along [111] resulted in the formation of another new engineered domain configuration with d_{33} of 295 pC/N.

KEYWORDS: engineered domain configuration, piezoelectric property, barium titanate single crystal, *in situ* domain observation, *in situ* Raman measurement, crystallographic orientation, electric-field induced phase transition

1. Introduction

Recently, in [001] oriented rhombohedral $Pb(Zn_{1/3}Nb_{2/3})O_3$–$PbTiO_3$ (PZN–PT) single crystals, ultrahigh piezoelectric activities were found by Park *et al.*[1] and Park and Shrout,[2–4] with strain over 1.7%, piezoelectric constant d_{33} over 2500pC/N, electromechanical coupling factor k_{33} over 90% and hysteresis-free strain *vs* electric-field behavior. $(1-x)$PZN–xPT single crystals with $x<0.09$ have rhombohedral **3*m*** symmetry at room temperature, and their polar directions are ⟨111⟩.[5,6] However, unipolar electric-field exposure along the [111] direction showed a large hysteretic strain *vs* electric-field behavior and a low d_{33} below 100 pC/N. On the other hand, unipolar electric-field exposure along the [001] direction exhibited non-hysteretic strain *vs* electric-field behavior and d_{33} over 2500 pC/N in 0.92PZN–0.08PT crystals. To explain the above strong anisotropy in piezoelectric properties, *in situ* domain observation was done using [111] and [001] oriented pure PZN and 0.92PZN–0.08PT single crystals.[7,8] As a result, when electric field was applied along the [001] direction, a very stable domain structure appeared under 0.2 kV/cm, and domain wall motion was undetectable under DC-bias of up to 20 kV/cm, resulting in hysteresis-minimized strain *vs* electric-field behavior.

Figure 1 shows a schematic domain configuration for [001] poled rhombohedral **3*m*** crystals. [001] poled **3*m*** crystals must have four domains with four equivalent polar vectors along [111], $[\bar{1}11]$, $[1\bar{1}1]$ and $[\bar{1}\bar{1}1]$ directions because of their polar directions of ⟨111⟩. Therefore, the component of each polar vector along the [001] direction is completely equal each other, so that each domain wall cannot move under electric-field exposure along the [001] direction owing to the equivalent domain wall energies.[2–4] This suggests the possibility of controlling domain configuration in single crystals using crystallographic orientation, and the appearance of a new technology in domain engineering field, as well as a conventional constraint of domain wall motion by acceptor dopants, i.e., "Hard" PZT. Thus, this special domain structure in single crystals (Fig. 1) using crystallographic orientation was called an engineered domain configuration.[2–4,7,8]

The engineered domain configuration is expected to possess the following three features for piezoelectric performance: (1) hysteresis-free strain *vs* electric-field behavior owing to inhibition of domain wall motion, (2) higher piezoelec-

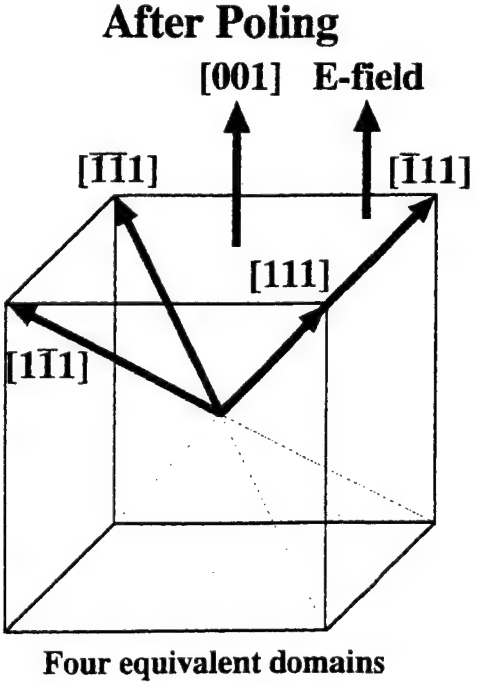

Fig. 1. Schematic domain configuration for [001] poled rhombohedral **3*m*** crystal.

*E-mail address: swada@cc.tuat.ac.jp

tric constant along the non-polar direction than that along the polar direction and (3) change of macroscopic symmetry in crystals with engineered domain configuration.[7,8] Therefore, if the concept of the engineered domain configuration can be applied to other ferroelectric single crystals, enhanced piezoelectric properties are expected. In this study, a barium titanate ($BaTiO_3$) single crystal was chosen for the first step in the application of the engineered domain configuration. This is because $BaTiO_3$ single crystal is one of the well-studied ferroelectrics, a typical non-lead ferroelectric, and a perovskite-type structure similar to PZN and PZN-PT.

In this study, the piezoelectric properties of $BaTiO_3$ single crystals were investigated at room temperature as a function of crystallographic orientation, such as [001] and [111] directions. Their domain configurations were also observed as a function of electric field and crystallographic orientation using a polarizing microscope. The behavior of domain wall motion will be discussed in relation to the observed strain *vs* electric-field behavior. Moreover, *in situ* Raman measurement was done to study changes in crystal symmetry as a function of electric field and crystallographic orientation.

2. Experimental

2.1 Sample

$BaTiO_3$ single crystals were prepared by a top-seeded solution growth (TSSG) method at Fujikura, Ltd. In TSSG-grown $BaTiO_3$ crystals, the concentration of most impurities (Cr, Mn, Fe, Co, Ni, Cu) was below 2–3 ppm.[9,10] Optically, $BaTiO_3$ crystals were transparent and light yellow. The details of preparation of $BaTiO_3$ single crystals and their characterization were described elsewhere.[9–12] These crystals were oriented along [001] and [111] directions using the back-reflection Laue method. All characterizations and treatments were done at Fujikura, Ltd.

2.2 Measurement of piezoelectric property

For electrical measurement of $BaTiO_3$ crystals, samples were prepared by polishing to achieve flat and parallel surfaces onto which gold electrodes were sputtered. Prior to piezoelectric measurements, dielectric properties were measured with a LCR meter (Hewlett- Packard 4263A) at room temperature, and it was confirmed that their dielectric loss was below 0.1% at 100 Hz. High electric field measurements included polarization and strain using a modified Sawyer-Tower circuit and a linear variable differential transducer (LVDT) driven by a lock-in amplifier (Stanford Res. Sys., model SR830). Electric fields were applied using an amplified triangular waveform at 0.1 Hz, using a Kepco BOP-1000M high-voltage DC amplifier (<1 kV) and a Trek 609C-6 high-voltage DC amplifier (≥1 kV).

2.3 In situ domain observation and in situ Raman measurement

For *in situ* domain observation and Raman measurement under DC-bias, samples were prepared by polishing to an optimum size of approximately $0.2 \times 0.5 \times 4\ mm^3$. Their top and bottom surfaces ($0.5 \times 4\ mm^2$) were mirror-polished, normal to an incident light. Gold electrodes were sputtered on both sides ($0.2 \times 4\ mm^2$), and the width between electrodes was around 0.5 mm along the [001] or [111] direction. The details were described elsewhere.[7,8,13] Domain configuration was always observed under crossed-nicols using a polarizing microscope (Olympus, BX50-31P). DC-bias exposure was done along the [001] or [111] direction, being normal to the incident polarized light, using a Trek 610D high-voltage DC amplifier. Raman spectra under DC-bias were measured in the backward scattering geometry using a Raman scattering spectrometer with a triple monochromator (Jobin-Yvon, T64000). DC-bias exposure was done in the same way as that in domain observation. The top surface ($0.5 \times 4\ mm^2$) was excited by unpolarized Ar ion laser with a wavelength of 514.5 nm and power below $20\ W/cm^2$. The details are described elsewhere.[14]

3. Results and Discussion

3.1 [001] oriented $BaTiO_3$ single crystals

Figure 2 shows a strain *vs* electric-field curve of a [001] oriented $BaTiO_3$ crystal measured using a unipolar electric field with 0.1 Hz at 25°C. It should be noted that this curve was not obtained at the 1st cycle of electric-field exposure, but after the 2nd cycle of electric-field exposure, i.e., this strain behavior means that after poling. The strain behavior in [001] oriented $BaTiO_3$ crystal exhibits a large strain of around 1% and a remarkable hysteresis. Such a large strain of around 1caused by tetragonality of $BaTiO_3$, $c/a \sim 1.011$, which suggests that domain reorientation can contribute significantly to strain behavior. Moreover, at high electric field above 20 kV/cm, the apparent d_{33} was directly estimated at 125 pC/N from Fig. 2. This value was close to d_{33}~90 pC/N in the single-domain $BaTiO_3$ crystal reported by Zgonik *et al.*,[15] which indicated that over 20 kV/cm, $BaTiO_3$ crystal might be single-domain state. Therefore, Fig. 2 suggests that domain wall motion can affect largely strain behavior in [001] oriented $BaTiO_3$ crystal.

Figure 3 shows the results of *in situ* domain observation under DC-bias below 22.1 kV/cm in a [001] oriented $BaTiO_3$ crystal. The results in Fig. 3 was also obtained after the 2nd cycle of electric-field exposure, and thus indicates that domain configuration in Fig. 3(a) was domain configuration without DC-bias after poling at 22.1 kV/cm. Figure 3(a) shows systematic domain configuration with 90° W_f domain

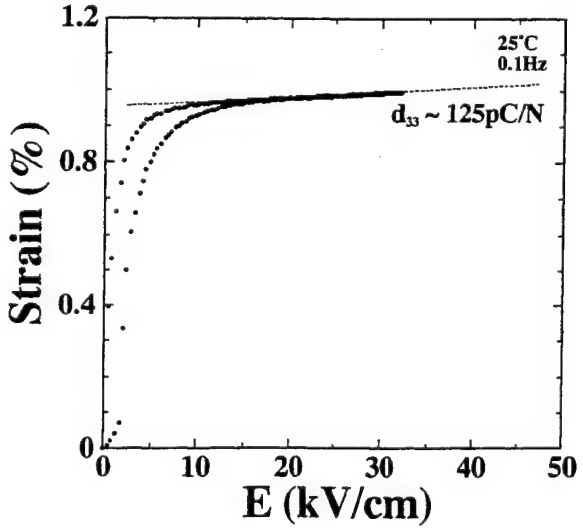

Fig. 2. Strain *vs* electric-field curve for [001] oriented $BaTiO_3$ crystal under unipolar electric field below 35 kV/cm with 0.1 Hz at 25°C.

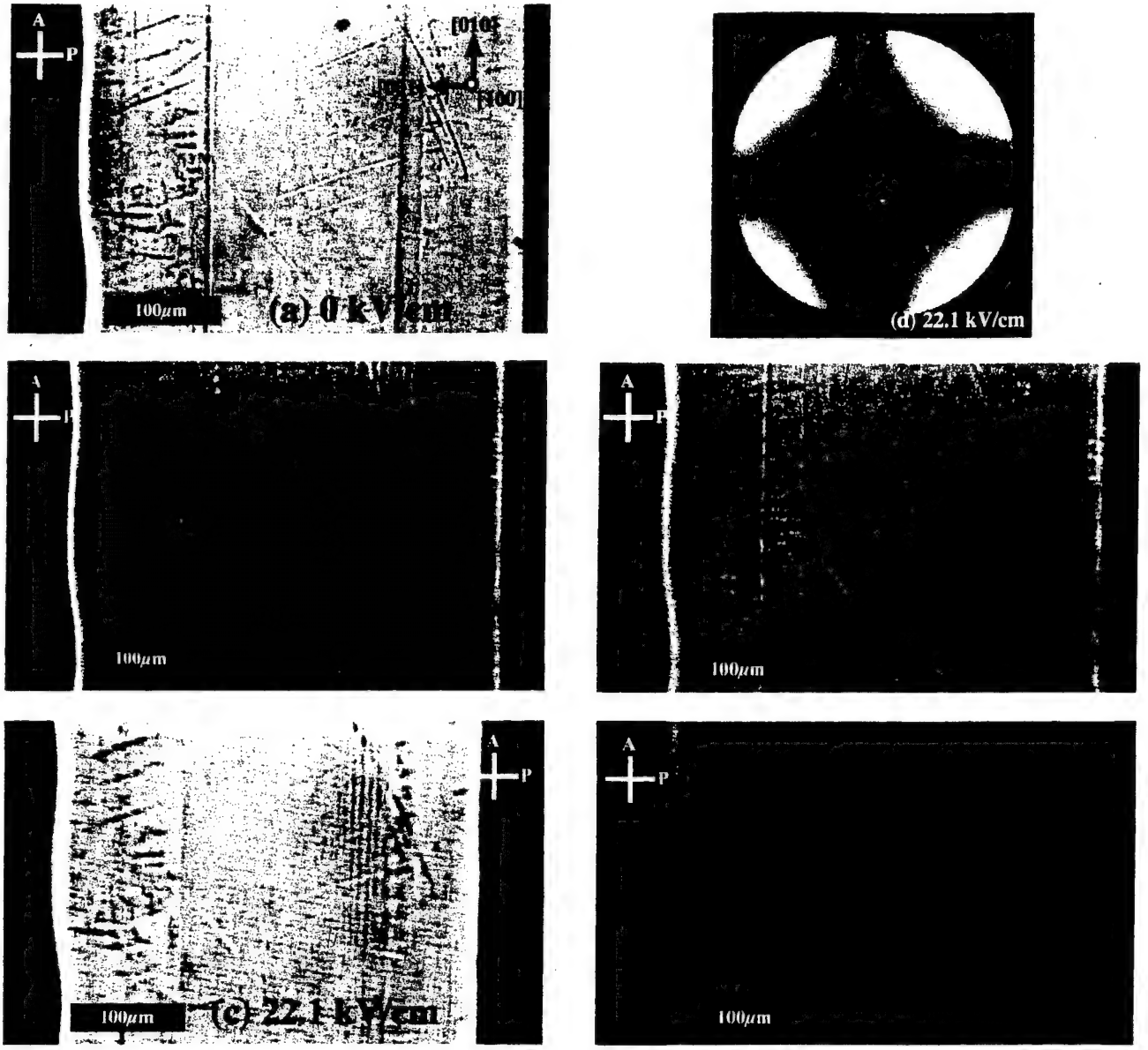

Fig. 3. *In situ* domain observation at various electric fields below 22.1 kV/cm in [001] oriented $BaTiO_3$ crystal.

walls of {101} planes.[16] With increasing electric field, domain wall motion was observed below 1 kV/cm, and finally at around 22.1 kV/cm, an almost single-domain state was achieved, except near the surface, as shown in Fig. 3(c). Moreover, a conoscopic figure (Fig. 3(d)) in the same region as that of Fig. 3(c) corresponded to a uniaxial flush interference figure, which can be given under a conoscope when the optic axis of uniaxial crystals, the [001] direction in a tetragonal $BaTiO_3$ crystal, is parallel to a microscopic stage.[17] This means that at 22.1 kV/cm, most of the crystal was transformed to the single-domain state.

On the other hand, with decreasing electric field from 22.1 kV/cm, new domains appeared and domain wall density increased (Figs. 3(e) and 3(f)). However, domain wall density at decrease of electric field was less than that at increase of electric field, even if the electric fields had the same values, *e.g.*, a comparison between Figs. 3(b) and 3(e). This revealed that a difference in the domain wall density at increasing and decreasing electric fields caused the large hysteresis in the strain *vs* electric-field curve (Fig. 2).

3.2 [111] oriented $BaTiO_3$ single crystals

Strain *vs* electric-field behaviors in [111] oriented $BaTiO_3$ single crystals were very complicated, as shown in Figs. 4–6. All these curves were also obtained after the 2nd cycle of electric-field exposure, i.e., these strain behaviors represent those after poling. To simplify the complicated phenomena, these strain *vs* electric-field behaviors were separated into four regions: (1) low electric field under 5 kV/cm, (2) middle electric field from 5 to 16 kV/cm, (3) high electric field from 16 to 26 kV/cm and (4) ultrahigh electric field above 26 kV/cm, and each behavior is discussed.

3.2.1 Low electric-field region under 5 kV/cm

In the low electric-field region as shown in Fig. 4, strain was almost proportional to electric field without hysteresis. In tetragonal $BaTiO_3$, the coercive electric field E_c was reported to be around 1 kV/cm.[18] and in this study, domain wall motion in [001] oriented $BaTiO_3$ crystals was observed below 1 kV/cm (Fig. 3). Thus, the strain behavior in Fig. 4 suggested that the engineered domain configuration shown in Fig. 7 was induced in [111] poled tetragonal $BaTiO_3$ crystals. Moreover,

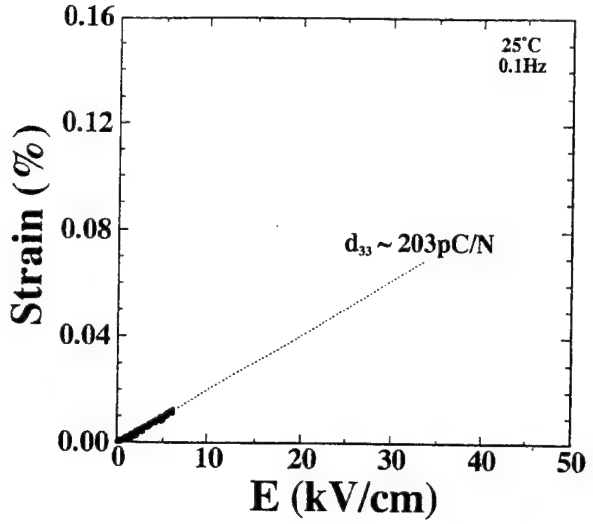

Fig. 4. Strain *vs* electric-field curve for [111] oriented $BaTiO_3$ crystal under unipolar electric field below 5 kV/cm with 0.1 Hz at 25°C.

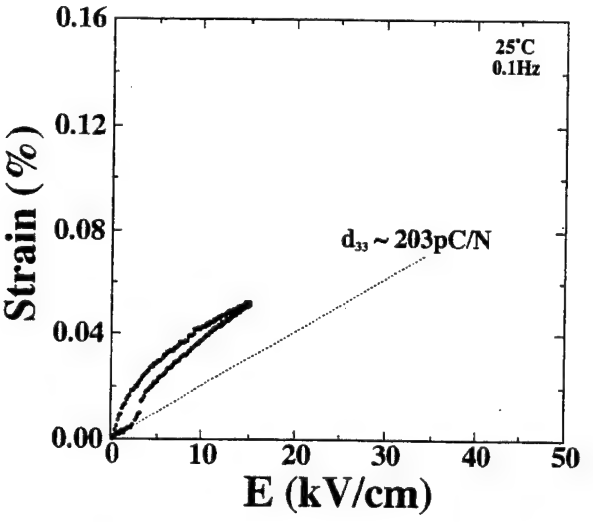

Fig. 5. Strain *vs* electric-field curve for [111] oriented $BaTiO_3$ crystal under unipolar electric field below 16 kV/cm with 0.1 Hz at 25°C.

the apparent d_{33} obtained directly from Fig. 4 was 203 pC/N, which was almost 1.6 times higher than that in a [001] poled single-domain $BaTiO_3$ crystal.

To confirm the formation of the engineered domain configuration, *in situ* domain observation in [111] oriented tetragonal $BaTiO_3$ crystals was done below 5 kV/cm. Figure 8 shows the domain configuration at various electric fields below 3.8 kV/cm. The domain structure under no DC-bias was highly systematic, and three ferroelectric domains with polar directions of [100], [010] and [001] were observed, as shown in Fig. 8(a). Although the electric field increased to 3.8 kV/cm, the domain structure did not change, except near the surface. This domain configuration was almost the same as the expected one in Fig. 7. Thus, we confirmed the formation of the engineered domain configuration in [111] poled tetragonal $BaTiO_3$ crystals.

The above results indicate that application of the engineered domain configuration to tetragonal $BaTiO_3$ crystals resulted in enhanced piezoelectric activities, *i.e.*, higher d_{33} and non-hysteretic strain *vs* electric-field behavior. Therefore, we believe that the concept of the engineered domain configuration is universal, and can apply to all perovskite-type ferroelectric crystals.

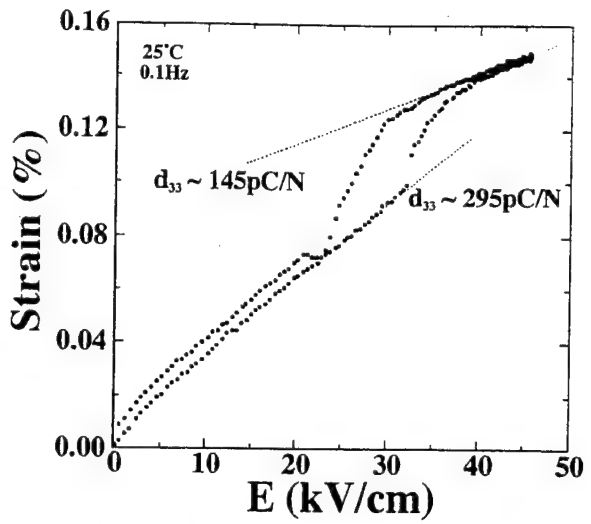

Fig. 6. Strain *vs* electric-field curve for [111] oriented $BaTiO_3$ crystal under unipolar electric field below 45 kV/cm with 0.1 Hz at 25°C.

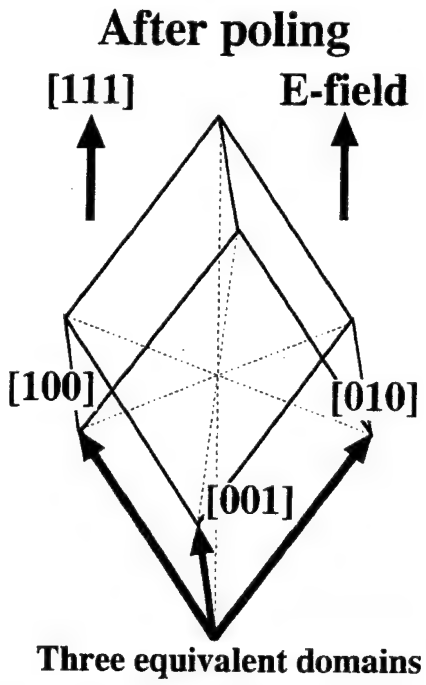

Fig. 7. Schematic engineered domain configuration for [111] poled tetragonal ***4mm*** $BaTiO_3$ crystal.

3.2.2 Middle electric-field region from 5 to 16 kV/cm

In the middle electric-field region from 5 to 16 kV/cm, a discontinuous change and a large hysteresis were observed, as shown in Fig. 5. In general, a hysteresis in the strain *vs* electric-field curve suggests the occurrence of domain wall motion or electric-field-induced phase transition. Thus, *in situ* domain observation and *in situ* Raman observation were done in the electric-field region. As a result, with increasing electric field from 6 to 10 kV/cm, domain wall density increased, while with increasing electric field from 10 to 16 kV/cm, domain wall density decreased, and partially single-domain region appeared. Measurement of the extinction position in the observed single-domain region revealed that the regions were assigned to ones with polar directions of ⟨110⟩. This sug-

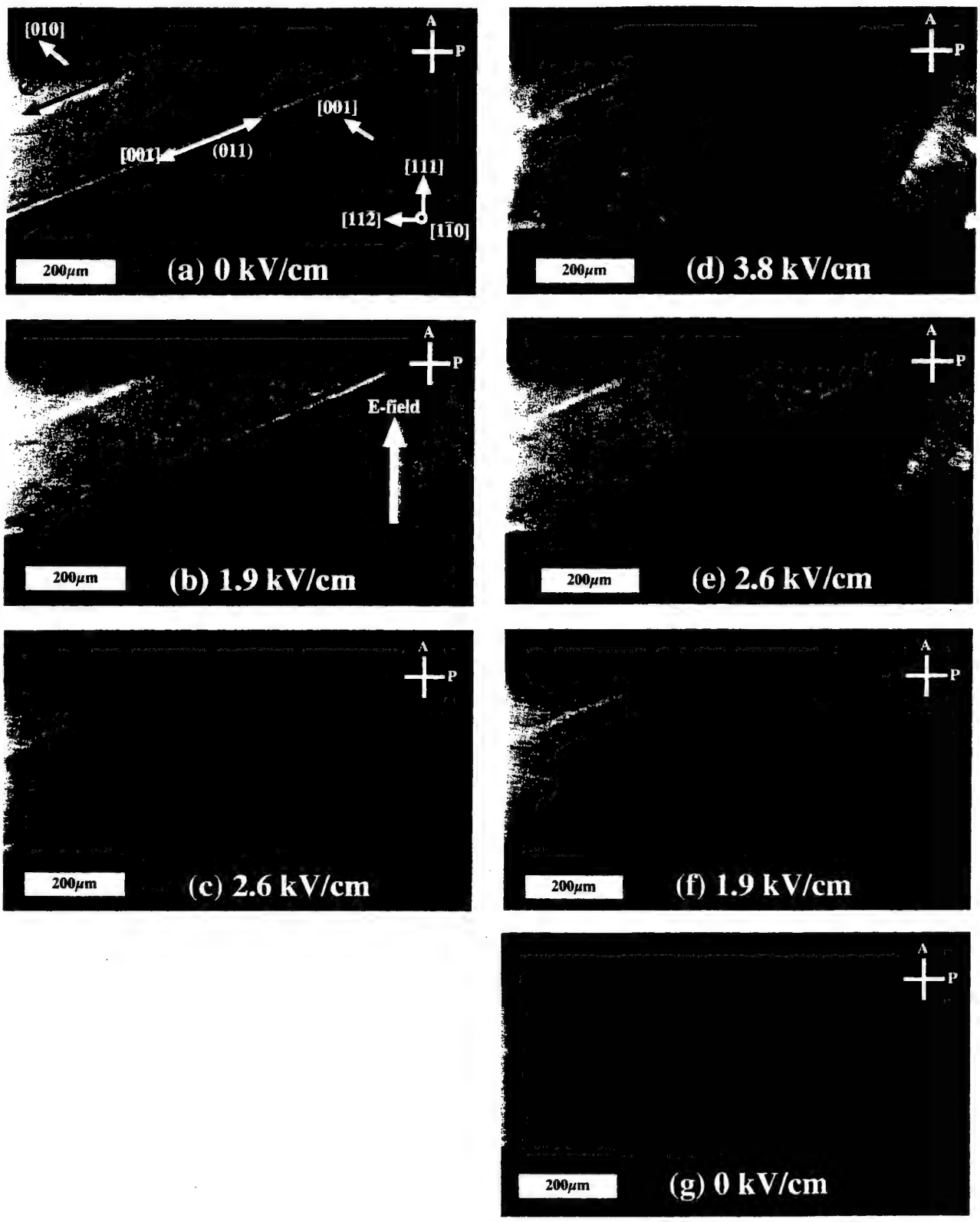

Fig. 8. *In situ* domain observation at various electric fields below 3.8 kV/cm in [111] oriented $BaTiO_3$ crystal.

gests the formation of monoclinic (=orthorhombic) ***m*** phase in tetragonal $BaTiO_3$ crystals. The details are described elsewhere.[14] Moreover, *in situ* Raman measurement was also done in the same electric-field region. As a result, it was found that in electric-field region from 6 to 16 kV/cm, two phases, tetragonal ***4mm*** and monoclinic ***m***, coexisted, and at 16 kV/cm, all regions became to monoclinic ***m*** phase. The details are also described elsewhere.[14] The above results suggested that from 6 to 16 kV/cm, an electric-field-induced phase transition occurred from tetragonal to monoclinic phase, which is accompanied by the discontinuous change and large hysteresis as shown in Fig. 5, but more work may be needed.

3.2.3 High electric-field region from 16 to 26 kV/cm

In the high electric-field from 16 to 26 kV/cm, strain was almost proportional to electric field with a non-hysteretic be-

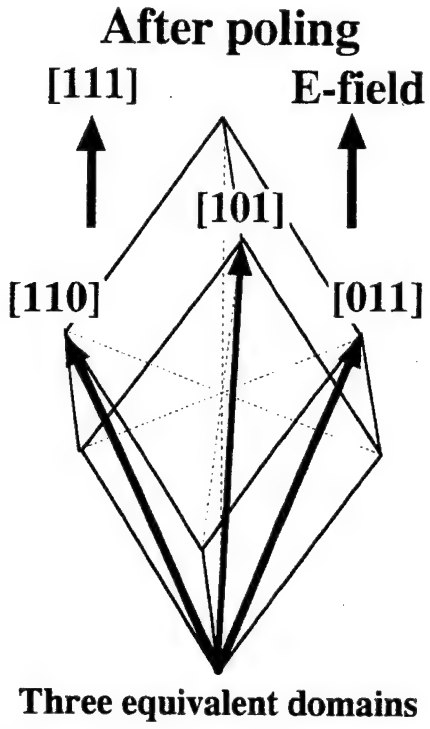

Fig. 9. Schematic engineered domain configuration for [111] poled monoclinic *m* $BaTiO_3$ crystal.

havior, as shown in Fig. 6. This strain behavior suggested that another engineered domain configuration such as that shown in Fig. 9 can be induced in [111] poled monoclinic $BaTiO_3$ crystals. Moreover, the apparent d_{33} obtained directly from Fig. 6 was 295 pC/N, which was almost 2.4 times higher than that in a [001] poled single-domain $BaTiO_3$ crystal. *In situ* Raman measurement in this region revealed that its symmetry was still monoclinic *m*. To confirm the existence of this new engineered domain configuration, *in situ* domain observation in the same electric-field was also done. Figure 10 shows domain configuration at various electric fields from 16.3 to 24.5 kV/cm. Domain walls in Fig. 10(a) appear so complicated, but all domain walls were assigned to 60° and 120° W_f domain walls of {110} and 90° W_f domain walls of {100}.[16] Even if the electric field increased from 16.3 to 24.5 kV/cm, the domain structure did not change, except near the surface. This domain configuration was almost the same as the expected one in Fig. 9. Thus, we confirmed a formation of another new engineered domain configuration in [111] poled monoclinic $BaTiO_3$ crystals and its enhanced piezoelectric property.

However, based on our expectation regarding the three effects of the engineered domain configuration on piezoelectric performance, as described in *Introduction*, we cannot explain why [111] poled monoclinic $BaTiO_3$ crystals with the engineered domain configuration (Fig. 9) have 1.5 times higher d_{33} than [111] poled tetragonal $BaTiO_3$ crystals with the engineered domain configuration (Fig. 7). This difference should be explained on the basis of crystallographic approach, as will be described elsewhere.[14]

3.2.4 Ultrahigh electric-field region above 26 kV/cm

In the ultrahigh electric-field region above 26 kV/cm, a discontinuous change and a large hysteresis were observed in

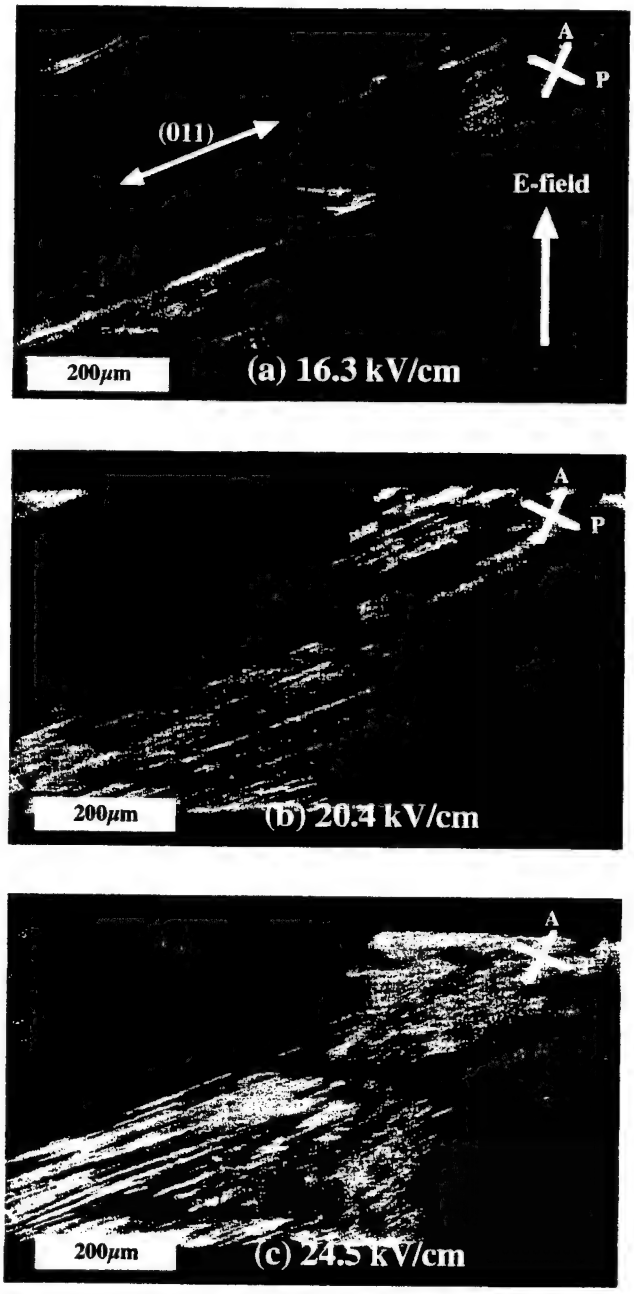

Fig. 10. *In situ* domain observation at various electric fields from 16.3 to 24.5 kV/cm in [111] oriented $BaTiO_3$ crystal.

in situ domain observation was done under electric fields from 25 to 30 kV/cm. As a result, at 29 kV/cm, small cracks occurred near the electrodes, and the cracks grew with increasing electric field. At 30 kV/cm, some regions with the extinction position along the [111] direction appeared partially, and then the crystal broke. This indicates the appearance of regions with polar direction of [111] at 30 kV/cm, *i.e.*, the formation of rhombohedral *3m* phase in monoclinic *m* $BaTiO_3$ crystals. Details on this are also described elsewhere.[14] As shown in Fig. 6, above 40 kV/cm, there is no hysteresis, which suggests the formation of single-domain state in rhombohedral $BaTiO_3$ crystals. Therefore, we consider that in the electric-field region from 30 to 40 kV/cm, two phases, monoclinic *m* and rhombohedral *3m*, coexisted, and above 40 kV/cm, all of regions became to rhombohedral

electric-field-induced phase transition occurred from monoclinic to rhombohedral phase, and thus resulted in the discontinuous change and large hysteresis as shown in Fig. 6. Moreover, in single-domain rhombohedral $BaTiO_3$ crystals over 40 kV/cm, the apparent d_{33} was around 145 pC/N, which was 1.2 times larger than that in [001] poled single-domain tetragonal $BaTiO_3$ crystals. This difference is also discussed elsewhere.[14]

4. Conclusions

In $BaTiO_3$ single crystals, piezoelectric properties were investigated at room temperature as a function of the crystal crystallographic orientation. When a unipolar electric field was applied along the [001] direction, the strain *vs* electric-field curve showed a large hysteresis, and finally $BaTiO_3$ crystal became to single-domain state with d_{33} of 125 pC/N over 20 kV/cm. *In situ* domain observation revealed that this large hysteresis is caused by a difference in domain wall density at increase and decrease of electric fields. On the other hand, the strain *vs* electric-field curve in [111] oriented $BaTiO_3$ single crystals exhibited a very complicated strain behavior. An electric-field exposure below 6 kV/cm along the [111] direction resulted in a high d_{33} of 203 pC/N and a non-hysteretic strain *vs* electric-field behavior, which suggested the formation of the engineered domain configuration in a tetragonal $BaTiO_3$ crystal. Therefore, it was confirmed that application of the engineered domain configuration to tetragonal $BaTiO_3$ crystals caused more enhanced piezoelectric activities compared with single-domain $BaTiO_3$ crystals. Moreover, when electric field over 6 kV/cm were applied along the [111] direction, two discontinuous changes at around 10 and 30 kV/cm were observed in the strain *vs* electric-field curve. *In situ* domain observation and *in situ* Raman measurement under electric fields suggested that the discontinuous change around 10 kV/cm can be assigned to the electric-field-induced phase transition from ***4mm*** to ***m*** while the discontinuous change around 30 kV/cm was assigned to the electric-field-induced phase transition from ***m*** to ***3m***. Moreover, in monoclinic $BaTiO_3$ crystal, an electric-field exposure from 16 to 26 kV/cm along the [111] direction gave a high d_{33} of 295 pC/N and a hysteresis-free strain *vs* electric-field behavior, which revealed the formation of another new engineered domain configuration in a monoclinic $BaTiO_3$ crystal. In this study, we found two engineered domain configurations in the [111] poled ***4mm*** and ***m*** $BaTiO_3$ single crystals and their enhanced piezoelectric properties. The difference in d_{33} between tetragonal and monoclinic phases with different engineered domain configurations will be discussed on the basis of crystallography elsewhere.[14] On the basis of the above results, we believe that the concept of the engineered domain configuration is universal and can be applied to all perovskite-type ferroelectric crystals, and improved piezoelectric activity can be achieved.

Acknowledgements

We would like to thank Dr. A. Kurosaka and Mr. O. Nakao of Fujikura, Ltd. for preparing TSSG-grown $BaTiO_3$ single crystals with excellent chemical quality. This study was partially supported by a Grant-in-Aid for Scientific Research (11555164) from the Ministry of Education, Science, Sports and Culture, Japan.

1) S.-E. Park, M. L. Mulvihill, P. D. Lopath, M. Zipparo and T. R. Shrout: Proc. 10th IEEE Int. Symp. Applications of Ferroelectrics (1996) Vol. 1, p. 79.
2) S.-E. Park and T. R. Shrout: IEEE Trans. Ultrason. Ferroelectr. & Freq. Control **44** (1997) 1140.
3) S.-E. Park and T. R. Shrout: Mater. Res. Innovat. **1** (1997) 20.
4) S.-E. Park and T. R. Shrout: J. Appl. Phys. **82** (1997) 1804.
5) J. Kuwata, K. Uchino and S. Nomura: Ferroelectrics **37** (1981) 579.
6) J. Kuwata, K. Uchino and S. Nomura: Jpn. J. Appl. Phys. **21** (1982) 1298.
7) S. Wada, S.-E. Park, L. E. Cross and T. R. Shrout: J. Korean Phys. Soc. **32** (1998) S1290.
8) S. Wada, S.-E. Park, L. E. Cross and T. R. Shrout: Ferroelectrics **221** (1999) 147.
9) A. Kurosaka, K. Tomomatu, O. Nakao, S. Ajimura, H. Tominaga and H. Osanai: J. Soc. Mater. Eng. Res. **5** (1992) 74 [in Japanese].
10) S. Ajimura, K. Tomomatu, O. Nakao, A. Kurosaka, H. Tominaga and O. Fukuda: J. Opt. Soc. Am. B **9** (1992) 1609.
11) O. Nakao, K. Tomomatsu, S. Ajimura, A. Kurosaka and H. Tominaga: Jpn. J. Appl. Phys. **31** (1992) 3117.
12) O. Nakao, K. Tomomatsu, S. Ajimura, A. Kurosaka and H. Tominaga: Ferroelectrics **156** (1994) 135.
13) D.-S. Paik, S.-E. Park, S. Wada, S.-F. Liu and T. R. Shrout: J. Appl. Phys. **85** (1999) 1080.
14) S. Wada, S. Suzuki, T. Noma, T. Suzuki, M. Osada, M. Kakihana, S.-E. Park, L. E. Cross and T. R. Shrout: submitted to J. Appl. Phys.
15) M. Zgonik, P. Bernasconi, M. Duelli, R. Schlesser, P. Gunter, M. H. Garrett, D. Rytz, Y. Zhu and X. Wu: Phys. Rev. B **50** (1994) 5941.
16) J. Fousek: Czech. J. Phys. **B21** (1971) 955.
17) E. E. Wahlstrom: *Optical Crystallography* (John Wiley and Sons, New York, 1979) 5th ed., Chap. 10.
18) W. Merz: Phys. Rev. **91** (1953) 513.

Appendix 9

ARTICLES

Tetragonal-to-monoclinic phase transition in a ferroelectric perovskite: The structure of $PbZr_{0.52}Ti_{0.48}O_3$

B. Noheda* and J. A. Gonzalo
Departamento de Fisica de Materiales, UAM, Cantoblanco, 28049 Madrid, Spain

L. E. Cross, R. Guo, and S.-E. Park
Materials Research Laboratory, The Pennsylvania State University, Pennsylvania 16802-4800

D. E. Cox and G. Shirane
Department of Physics, Brookhaven National Laboratory, Upton, New York 11973-5000
(Received 11 October 1999; revised manuscript received 27 December 1999)

The perovskitelike ferroelectric system $PbZr_{1-x}Ti_xO_3$ (PZT) has a nearly vertical morphotropic phase boundary (MPB) around $x=0.45$–0.50. Recent synchrotron x-ray powder diffraction measurements by Noheda *et al.* [Appl. Phys. Lett. **74**, 2059 (1999)] have revealed a monoclinic phase between the previously established tetragonal and rhombohedral regions. In the present work we describe a Rietveld analysis of the detailed structure of the tetragonal and monoclinic PZT phases on a sample with $x=0.48$ for which the lattice parameters are, respectively, $a_t=4.044$ Å, $c_t=4.138$ Å, at 325 K, and $a_m=5.721$ Å, $b_m=5.708$ Å, $c_m=4.138$ Å, $\beta=90.496°$, at 20 K. In the tetragonal phase the shifts of the atoms along the polar [001] direction are similar to those in $PbTiO_3$ but the refinement indicates that there are, in addition, local disordered shifts of the Pb atoms of ~0.2 Å perpendicular to the polar axis. The monoclinic structure can be viewed as a condensation along one of the ⟨110⟩ directions of the local displacements present in the tetragonal phase. It equally well corresponds to a freezing-out of the local displacements along one of the ⟨100⟩ directions recently reported by Corker *et al.*[J. Phys.: Condens. Matter **10**, 6251 (1998)] for rhombohedral PZT. The monoclinic structure therefore provides a microscopic picture of the MPB region in which one of the "locally" monoclinic phases in the "average" rhombohedral or tetragonal structures freezes out, and thus represents a bridge between these two phases.

I. INTRODUCTION

Perovskitelike oxides have been at the center of research on ferroelectric and piezoelectric materials for the past fifty years because of their simple cubic structure at high temperatures and the variety of high symmetry phases with polar states found at lower temperatures. Among these materials the ferroelectric $PbZr_{1-x}Ti_xO_3$ (PZT) solid solutions have attracted special attention since they exhibit an unusual phase boundary which divides regions with rhombohedral and tetragonal structures, called the morphotropic phase boundary (MPB) by Jaffe *et al.*[1] Materials in this region exhibit a very high piezoelectric response, and it has been conjectured that these two features are intrinsically related. The simplicity of the perovskite structure is in part responsible for the considerable progress made recently in the determination of the basic structural properties and stability of phases of some important perovskite oxides, based on *ab initio* calculations (see, e.g., Refs. 2–9). Recently, such calculations have also been used to investigate solid solutions and, in particular, PZT, where the effective Hamiltonian includes both structural and compositional degrees of freedom.[10–12]

The PZT phase diagram of Jaffe *et al.*,[1] which covers only temperatures above 300 K, has been accepted as the basic characterization of the PZT solid solution. The ferroelectric region of the phase diagram consists mainly of two different regions: the Zr-rich rhombohedral region, (F_R) that contains two phases with space groups $R3m$ and $R3c$, and the Ti-rich tetragonal region (F_T), with space group $P4mm$.[13] The two regions are separated by a boundary that is nearly independent of temperature, the MPB mentioned above, which lies at a composition close to $x=0.47$. Many structural studies have been reported around the MPB, since the early 1950's, when these solid solutions were first studied,[13,14] since the high piezoelectric figure of merit that makes PZT so extraordinary is closely associated with this line.[1,15] The difficulty in obtaining good single crystals in this region, and the characteristics of the boundary itself, make good compositional homogeneity essential if single phase ceramic materials are to be obtained. Because of this, the MPB is frequently reported as a region of phase coexistence whose width depends on the sample processing conditions.[16–19]

Recently, another feature of the morphotropic phase boundary has been revealed by the discovery of a ferroelectric monoclinic phase (F_M) in the $Pb(Zr_{1-x}Ti_x)O_3$ ceramic system.[20] From a synchrotron x-ray powder diffraction study of a composition with $x=0.48$, a tetragonal-to-monoclinic phase transition was discovered at ~300 K. The monoclinic

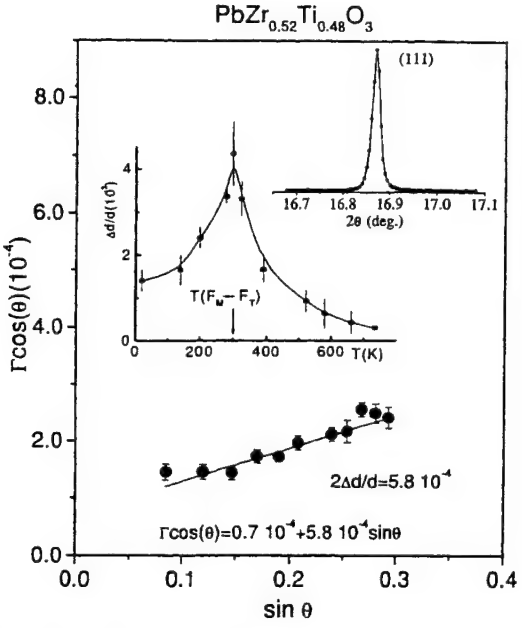

FIG. 2. The Williamson-Hall plot for PZT ($x=0.48$) derived from the measured diffraction peak widths in the cubic phase ($T=736$ K). Particle size and microstrain are estimated from a linear fit (solid line). The plot for the (111) reflection in the cubic phase demonstrates the excellent quality of the ceramic sample (peak width $\sim 0.02°$). The plot of $\Delta d/d$ vs temperature is also shown as an inset.

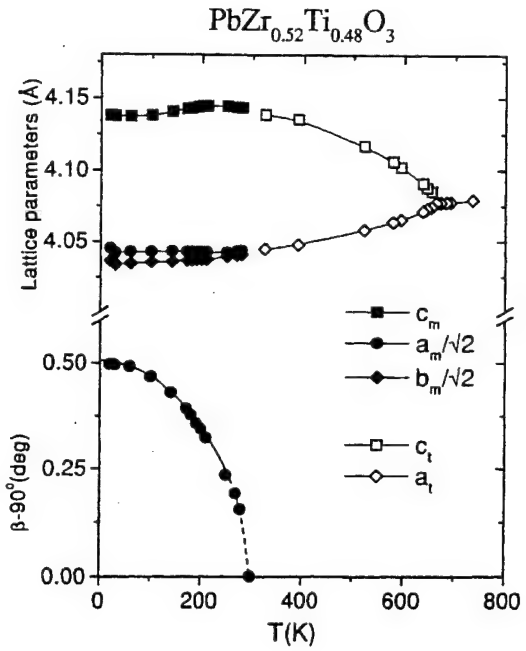

FIG. 3. Lattice parameters versus temperature for PZT ($x=0.48$) over the whole range of temperatures from 20 to 750 K showing the evolution from the monoclinic phase to the cubic phase via the tetragonal phase.

shown in Fig. 1. The measurements made on the pellet in the cubic phase at 736 K demonstrate the excellent quality of the sample, which exhibits diffraction peaks with full-widths at half-maximum (FWHM) ranging from 0.01° to 0.03° as shown for the (111) reflection plotted as the upper-right inset in Fig. 2. The FWHM's (Γ) for several peaks were determined from least-squares fits to a pseudo-Voigt function with the appropriate corrections for asymmetry effects,[25] and corrected for instrumental resolution. The corrected values are shown in Fig. 2 in the form of a Williamson-Hall plot[26]

$$\Gamma \cos\theta = \lambda/L + 2(\Delta d/d)\sin\theta, \tag{3.1}$$

where λ is the wavelength and L is the mean crystallite size. From the slope of a linear fit to the data, the distribution of d spacings, $\Delta d/d$, is estimated to be $\sim 3\times 10^{-4}$, corresponding to a compositional inhomogeneity Δx of less than ± 0.003. From the intercept of the line on the ordinate axis the mean crystallite size is estimated to be ~ 1 μm.

A tetragonal-to-monoclinic phase transition in PZT with $x=0.48$ was recently reported by Noheda *et al.*[20] Additional data have been obtained near the phase transition around 300 K which have allowed a better determination of the phase transition to be made, as shown by the evolution of the lattice parameters as a function of temperature in Fig. 3. The tetragonal strain c_t/a_t increases as the temperature decreases from the Curie point ($T\approx 660$ K), to a value of 1.0247 at 300 K, below which peak splittings characteristic of a monoclinic phase with $a_m \approx b_m \approx a_t\sqrt{2}, \beta \neq 90°$, are observed (Fig. 3). As the temperature continues to decrease down to 20 K, a_m (which is defined to lie along the $[\bar{1}\bar{1}0]$ tetragonal direction) increases very slightly, and b_m (which lies along the $[1\bar{1}0]$ tetragonal direction) decreases. The c_m lattice parameter reaches a broad maximum value of 4.144 Å between 240–210 K and then reaches a shallow minimum value of 4.137 Å at 60 K. Over the same temperature region there is a striking variation of $\Delta d/d$ determined from Williamson-Hall plots at various temperatures, as shown in the upper-left inset in Fig. 2. $\Delta d/d$ increases rapidly as the temperature approaches the F_T-F_M transition at 300 K, in a similar fashion to the tetragonal strain, and then decreases rapidly below this temperature in the monoclinic region. Thus the microstrain responsible for the large increase in $\Delta d/d$ is an important feature of the phase transition, which may be associated with the development of local monoclinic order, and is very likely responsible for the large electromechanical response of PZT close to the MPB.[1]

The deviation of the monoclinic angle β from 90° is an order parameter of the F_T-F_M transition, and its evolution with temperature is also depicted in Fig. 3. This phase transition presents a special problem due to the steepness of the phase boundary (the MPB in Fig. 1). As shown in the previous section, the compositional fluctuations are quite small in these ceramic samples ($\Delta x \approx \pm 0.003$) but, even in this case, the nature of the MPB implies an associated temperature uncertainty of $\Delta T \approx 100$ K. There is, therefore, a rather wide range of transition temperatures instead of a single well-defined transition, so that the order parameter is smeared out as a function of temperature around the phase change, thereby concealing the nature of the transition.

Scans over the $(220)_c$ region for several different temperatures are plotted in Fig. 4, which shows the evolution of phases from the cubic phase at 687 K (upper-left plot) to the monoclinic phase at 20 K (lower-right plot), passing through the tetragonal phase at intermediate temperatures. With decreasing temperature, the tetragonal phase appears at ~ 660 K and the development of the tetragonal distortion can be observed on the left side of the figure from the splitting of

TABLE I. Structure refinement results for tetragonal $PbZr_{0.52}Ti_{0.48}O_3$ at 325 K, space group $P4mm$, lattice parameters $a_t=4.0460(1)$ Å, $c_t=4.1394(1)$ Å. Fractional occupancies N for all atoms taken as unity except for Pb in model II, where $N=0.25$. Agreement factors, R_{wp}, R_{F^2}, and χ^2 are defined in Ref. 33.

	Model I anisotropic lead temperature factors				Model II local ⟨110⟩ lead shifts			
	x	y	z	U(Å^2)	x	y	z	U_{iso} (Å^2)
Pb	0	0	0	$U_{11}=0.0319(4)$ $U_{33}=0.0127(4)$	0.0328(5)	0.0328(5)	0	0.0127(4)
Zr/Ti	0.5	0.5	0.4517(7)	$U_{iso}=0.0052(6)$	0.5	0.5	0.4509(7)	0.0041(6)
O(1)	0.5	0.5	−0.1027(28)	$U_{iso}=0.0061(34)$	0.5	0.5	−0.1027(28)	0.0072(35)
O(2)	0.5	0	0.3785(24)	$U_{iso}=0.0198(30)$	0.5	0	0.3786(24)	0.0197(30)
R_{wp}			4.00%				3.99%	
R_{F^2}			6.11%				6.04%	
χ^2			11.4				11.3	

as Corker *et al.* were able to do,[23] were likewise unsuccessful, presumably because the scattering contrast for x rays is much less than for neutrons.

From the values of the atomic coordinates listed in Table I, it can be inferred that the oxygen octahedra are somewhat more distorted than in $PbTiO_3$, the O(1) atoms being displaced 0.08 Å towards the O(2) plane above. The cation displacements are slightly larger than those recently reported by Wilkinson *et al.*[37] for samples close to the MPB containing a mixture of rhombohedral and tetragonal phases, and in excellent agreement with the theoretical values obtained by Bellaiche and Vanderbilt[38] for PZT with $x=0.50$ from first principles calculations. As far as we are aware no other structural analysis of PZT compositions in the tetragonal region has been reported in the literature.

Selected bond distances for the two models are shown in Table II. For model I, Zr/Ti has short and long bonds with O(1) of 1.85 and 2.29 Å, respectively, and four intermediate-length O(2) bonds of 2.05 Å. There are four intermediate-length Pb-O(1) bonds of 2.89 Å , four short Pb-O(2) bonds of 2.56 Å and four much larger Pb-O(2) distances of 3.27 Å. For model II, the Zr/Ti-O distances are the same, but the Pb-O distances change significantly. A Pb atom in one of the four equivalent $(x,x,0)$ sites in Table I now has a highly distorted coordination, consisting of two short and two intermediate Pb-O(2) bonds of 2.46 and 2.67 Å, and one slightly longer Pb-O(1) bond of 2.71 Å (Table II). The tendency of Pb^{+2}, which has a lone sp electron pair, to form short covalent bonds with a few neighboring oxygens is well documented in the literature.[23,39–41]

The observed and calculated diffraction profiles and the difference plot are shown in Fig. 6 for a selected 2θ range between 7° and 34° (upper figure). The short vertical markers represent the calculated peak positions. The upper and lower sets of markers correspond to the cubic and tetragonal phases, respectively. We note that although agreement between the observed and the calculated profiles is considerably better when the diffuse scattering is modeled with a cubic phase, the refined values of the atomic coordinates are not significantly affected by the inclusion of this phase. The anisotropic peak broadening was found to be satisfactorily

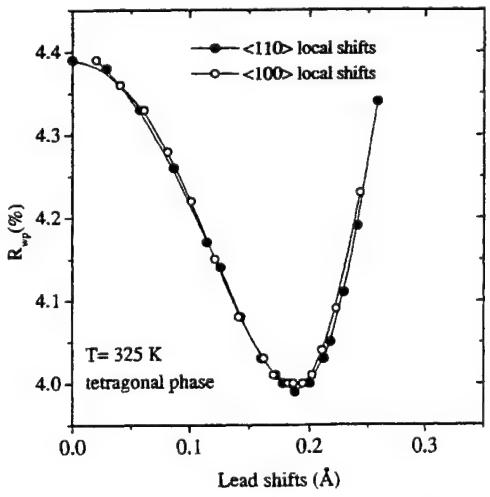

FIG. 5. Agreement factor R_{wp} as a function of Pb displacements for refinements with fixed values of x along tetragonal ⟨110⟩ and ⟨100⟩ directions as described in text. The well-defined minimum at $x\sim0.19$ Å confirms the result listed in Table I for model II.

TABLE II. Selected Zr/Ti-O and Pb-O bond lengths in the tetragonal and monoclinic structures. Models I and II refer to the refinements with anisotropic temperature factors and local ⟨110⟩ displacements for Pb, respectively (see Table I). The standard errors in the bond lengths are ~0.01 Å .

	Bond lengths (Å)		
	tetragonal		monoclinic
	model I	model II	
Zr/Ti-O(1)	1.85×1	1.85×1	1.87×1
	2.29×1	2.29×1	2.28×1
Zr/Ti-O(2)	2.05×4	2.05×4	2.13×2
			1.96×2
Pb-O(1)	2.89×4	2.90×2	2.90×2
		2.71×1	2.60×1
Pb-O(2)	2.56×4	2.67×2	2.64×2
		2.46×2	2.46×2

TABLE IV. Comparison of refined values of atomic coordinates in the monoclinic phase with the corresponding values in the tetragonal and rhombohedral phases for both the "ideal" structures and those with local shifts, as discussed in text.

	tetragonal $x=0.48$, 325 K		monoclinic $x=0.48$, 20 K	rhombohedral (Ref. 43) $x=0.40$, 295 K	
	ideal	local shifts [a]	as refined	local shifts [b]	ideal
$x_{Zr/Ti}$	0.500	0.530	0.523	0.520	0.540
$z_{Zr/Ti}$	0.451	0.451	0.449	0.420	0.460
$x_{O(1)}$	0.500	0.530	0.551	0.547	0.567
$z_{O(1)}$	−0.103	−0.103	−0.099	0.093	−0.053
$x_{O(2)}$	0.250	0.280	0.288	0.290	0.310
$y_{O(2)}$	0.250	0.250	0.243	0.257	0.257
$z_{O(2)}$	0.379	0.379	0.373	0.393	0.433
a_m(Å)	5.722		5.722	5.787	
b_m(Å)	5.722		5.710	5.755	
c_m(Å)	4.139		4.137	4.081	
β(°)	90.0		90.50	90.45	

[a]Tetragonal local shifts of (0.03,0.03,0).
[b]Hexagonal local shifts of (−0.02,0.02,0).

We now consider the refined values of the Pb atom positions with local displacements for rhombohedral PZT listed in Table IV of Ref. 23. With the use of the appropriate transformation matrices, it is straightforward to show that these shifts correspond to displacements of 0.2–0.25 Å along the direction of the monoclinic [100] axis, similar to what is actually observed for $x=0.48$. It thus seems equally plausible that the monoclinic phase can also result from the condensation of local displacements perpendicular to the [111] axis.

The monoclinic structure can thus be pictured as providing a "bridge" between the rhombohedral and tetragonal structures in the region of the MPB. This is illustrated in Table IV, which compares the results for PZT with $x=0.48$ obtained in the present study with earlier results[43] for rhombohedral PZT with $x=0.40$ expressed in terms of the monoclinic cell.[44] For $x=0.48$, the atomic coordinates for Zr/Ti, O(1) and O(2) are listed for the "ideal" tetragonal structure (model I) and for a similar structure with local shifts of (0.03,0.03,0) in the first two columns, and for the monoclinic structure in the third column. The last two columns describe the rhombohedral structure for $x=0.40$ assuming local shifts of (−0.02,0.02,0) along the hexagonal axes and the as-refined "ideal" structure, respectively. It is clear that the condensation of these local shifts gives a very plausible description of the monoclinic structure in both cases. It is also interesting to note the behavior of the corresponding lattice parameters; metrically the monoclinic cell is very similar to the tetragonal cell except for the monoclinic angle, which is close to that of the rhombohedral cell.

Evidence for a tetragonal-to-monoclinic transition in the ferroelectric material $PbFe_{0.5}Nb_{0.5}O_3$ has also been reported by Bonny *et al.*[45] from single crystal and synchrotron x-ray powder diffraction measurements. The latter data show a cubic-tetragonal transition at ~376 K, and a second transition at ~355 K. Although the resolution was not sufficient to reveal any systematic splitting of the peaks, it was concluded that the data were consistent with a very weak monoclinic distortion of the pseudorhombohedral unit cell. In a recent neutron and x-ray powder study, Lampis *et al.*[46] have shown that Rietveld refinement gives better agreement for the monoclinic structure at 80 and 250 K than for the rhombohedral one. The resulting monoclinic distortion is very weak, and the large thermal factor obtained for Pb is indicative of a high degree of disorder.

The relationships between the PZT rhombohedral, tetragonal and monoclinic structures are also shown schematically in Fig. 7, in which the displacements of the Pb atom are shown projected on the pseudocubic (110) mirror plane. The four locally disordered ⟨110⟩ shifts postulated in the present paper for the tetragonal phase are shown superimposed on the [001] shift at the left [Fig. 7(a)] and the three locally disordered ⟨100⟩ shifts proposed by Corker *et al.*[23] for the rhombohedral phase are shown superimposed on the [111]

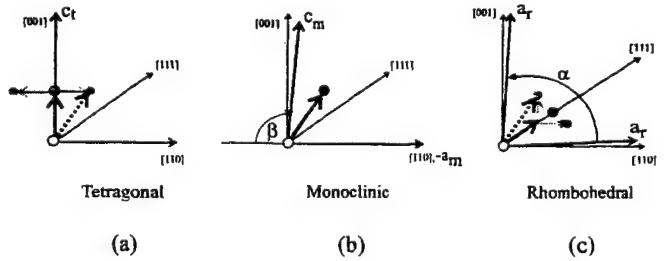

FIG. 7. Schematic illustration of the tetragonal (a), monoclinic (b), and rhombohedral (c) distortions of the perovskite unit cell projected on the pseudocubic (110) plane. The solid circles represent the observed shifts with respect to the ideal cubic structure. The light grey circles represent the four locally disordered ⟨100⟩ shifts in the tetragonal structure (a) and the three locally disordered shifts in the rhombohedral structure (c) described by Corker *et al.* (Ref. 23). The heavy dashed arrows represent the freezing-out of one of these shifts to give the monoclinic observed structure. Note that the resultant shifts in the rhombohedral structure can be viewed as a combination of a [111] shift with local ⟨100⟩ shifts, as indicated by the light grey arrows.

[17] J.C. Fernandes, D.A. Hall, M.R. Cockburn, and G.N. Greaves, Nucl. Instrum. Methods Phys. Res. B **97**, 137 (1995).
[18] M. Hammer, C. Monty, A. Endriss, and M.J. Hoffmann, J. Am. Ceram. Soc. **81**, 721 (1998).
[19] W. Cao and L.E. Cross, Phys. Rev. B **47**, 4825 (1993).
[20] B. Noheda, D.E. Cox, G. Shirane, J.A. Gonzalo, L.E. Cross, and S-E. Park, Appl. Phys. Lett. **74**, 2059 (1999).
[21] The $[\bar{1}\bar{1}0]$ and $[1\bar{1}0]$ directions are chosen so that the monoclinic angle $\beta > 90°$ to conform with usual crystallographic convention.
[22] B. Noheda, J.A. Gonzalo, A.C. Caballero, C. Moure, D.E. Cox, and G. Shirane, cond-mat/9907286, Ferroelectrics (to be published).
[23] D.L. Corker, A.M. Glazer, R.W. Whatmore, A. Stallard, and F. Fauth, J. Phys.: Condens. Matter **10**, 6251 (1998).
[24] C.W. Dwiggins Jr., Acta Crystallogr., Sect. A: Cryst. Phys., Diffr., Theor. Gen. Crystallogr. **31**, 146 (1975).
[25] L.W. Finger, D.E. Cox, and A.P. Jephcoat, J. Appl. Crystallogr. **27**, 892 (1994).
[26] G.K. Williamson and W.H. Hall, Acta Metall. **1**, 22 (1953).
[27] A.C. Larson and R.B. Von Dreele (unpublished).
[28] P.W. Stephens, J. Appl. Crystallogr. **32**, 281 (1999).
[29] C. Muller, J.-L. Baudour, V. Madigou, F. Bouree, J.-M. Kiat, C. Favotto, and M. Roubin, Acta Crystallogr., Sect. B: Struct. Sci. **55**, 8 (1999).
[30] A.M. Glazer and S.A. Mabud, Acta Crystallogr., Sect. B: Struct. Crystallogr. Cryst. Chem. **34**, 1065 (1978).
[31] R.J. Nelmes and W.F. Kuhs, Solid State Commun. **54**, 721 (1985).
[32] The structure factor correction is defined in terms of the anisotropic u_{ij} thermal factors as $\exp\{-[2\pi^2(\Sigma i, j u_{ij} a_i^* a_j^*)]\}$, a_i^* being the lattice vectors of the reciprocal unit cell.
[33] L.B. McCusker, R.B. von Dreele, D.E. Cox, D. Louër, and P. Scardi, J. Appl. Crystallogr. **32**, 36 (1999).
[34] K. Itoh, L.Z. Zeng, E. Nakamura, and N. Mishima, Ferroelectrics **63**, 29 (1985).
[35] C. Malibert, B. Dkhil, J.M. Kiat, D. Durand, J.F. Berar, and A. Spasojevic-de Bire, J. Phys.: Condens. Matter **9**, 7485 (1997).
[36] G. Shirane, R. Pepinski, and B.C. Frazer, Acta Crystallogr. **9**, 131 (1956).
[37] A.P. Wilkinson, J. Xu, S. Pattanaik, and J.L. Billinge, Chem. Mater. **10**, 3611 (1998).
[38] L. Bellaiche and D. Vanderbilt, Phys. Rev. Lett. **83**, 1347 (1999).
[39] S. Teslic, T. Egami, and D. Viehland, J. Phys. Chem. Solids **57**, 1537 (1996); Ferroelectrics **194**, 271 (1997).
[40] D.L. Corker, A.M. Glazer, W. Kaminsky, R.W. Whatmore, J. Dec, and K. Roleder, Acta Crystallogr., Sect. B: Struct. Sci. **54**, 18 (1998).
[41] S. Teslic and T. Egami, Acta Crystallogr., Sect. B: Struct. Sci. **54**, 750 (1998).
[42] A.M. Glazer, S.A. Mabud, and R. Clarke, Acta Crystallogr., Sect. B: Struct. Crystallogr. Cryst. Chem. **34**, 1060 (1978).
[43] A. Amin, R.E. Newnham, L.E. Cross, and D.E. Cox, J. Solid State Chem. **37**, 248 (1981).
[44] The rhombohedral unit cell can be expressed in terms of a monoclinic one by $a_m = 2a_r\cos(\alpha/2)$, $b_m = 2a_r\sin(\alpha/2)$, $c_m = a_r$, $\beta = 180° - \phi$, where $\cos\phi = 1 - 2\sin^2(\alpha/2)/\cos(\alpha/2)$ and a_r and α are the $R3m$ cell parameters. Note that a_r in Ref. 43 refers to the doubled cell.
[45] V. Bonny, M. Bonin, P. Sciau, K.J. Schenk, and G. Chapuis, Solid State Commun. **102**, 347 (1997).
[46] N. Lampis, P. Sciau, and A.G. Lehmann, J. Phys.: Condens. Matter **11**, 3489 (1999).
[47] L.A. Shuvalov, J. Phys. Soc. Jpn. **28**, 38 (1970).
[48] S.C. Abrahams and E.T. Keve, Ferroelectrics **2**, 129 (1971).
[49] X-h Du, J. Zheng, U. Belegundu, and K. Uchino, Appl. Phys. Lett. **72**, 2421 (1998).
[50] K. Fujishiro, R. Vlokh, Y. Uesu, Y. Yamada, J-M. Kiat, B. Dkhil, and Y. Yamashita, Ferroelectrics (to be published).

Appendix 10

Stability of the monoclinic phase in the ferroelectric perovskite $PbZr_{1-x}Ti_xO_3$

B. Noheda,* D. E. Cox, and G. Shirane
Physics Department, Brookhaven National Laboratory, Upton, New York 11973

R. Guo, B. Jones, and L. E. Cross
Materials Research Laboratory, The Pennsylvania State University, University Park, Pennsylvania 16802
(Received 9 June 2000; published 12 December 2000)

Recent structural studies of ferroelectric $PbZr_{1-x}Ti_xO_3$ (PZT) with $x=0.48$, have revealed a monoclinic phase in the vicinity of the morphotropic phase boundary (MPB), previously regarded as the boundary separating the rhombohedral and tetragonal regions of the PZT phase diagram. In the present paper, the stability region of all three phases has been established from high-resolution synchrotron x-ray powder-diffraction measurements on a series of highly homogeneous samples with $0.42 \leqslant x \leqslant 0.52$. At 20 K, the monoclinic phase is stable in the range $0.46 \leqslant x \leqslant 0.51$, and this range narrows as the temperature is increased. A first-order phase transition from tetragonal to rhombohedral symmetry is observed only for $x=0.45$. The MPB, therefore, corresponds not to the tetragonal-rhombohedral phase boundary, but instead to the boundary between the tetragonal and *monoclinic* phases for $0.46 \leqslant x \leqslant 0.51$. This result provides important insight into the close relationship between the monoclinic phase and the striking piezoelectric properties of PZT; in particular, investigations of poled samples have shown that the monoclinic distortion is the origin of the unusually high piezoelectric response of PZT.

DOI: 10.1103/PhysRevB.63.014103 PACS number(s): 77.84.Dy, 61.10.−i

I. INTRODUCTION

Exceptionally striking dielectric and piezoelectric properties are found in $PbZr_{1-x}Ti_xO_3$ (PZT), the perovskite-type oxide system that is the basis of practically all transducers and other piezoelectric devices. This solid solution is cubic at high temperatures but becomes slightly distorted at lower temperatures, where it is ferroelectric. Except for a narrow region close to $PbZrO_3$, the ferroelectric phase is divided in two regions of different symmetry, rhombohedral for Zr-rich compositions and tetragonal for Ti-rich compositions. The highest piezoelectric response in this system is found at the boundary between these two phases, at $x \simeq 0.47$; the so-called morphotropic phase boundary (MPB). The term "morphotropic" was coined by Jaffe *et al.*[1] and means literally "the boundary between two forms." However, it is usually assumed to mean nearly vertical, i.e., composition independent. The PZT phase diagram for compositions around the MPB is shown in Fig. 1, where the open circles represent the data of Jaffe *et al.*,[1] which define the MPB above room temperature. The sharpness of this line is such that a composition fluctuation of $\Delta x=0.01$ corresponds to a temperature uncertainty of $\Delta T \simeq 90$ K. Recently, high-resolution x-ray diffraction measurements on extremely homogenous samples by Noheda *et al.* showed that an intermediate monoclinic phase exists between the rhombohedral and tetragonal PZT phases.[2–4] The observation of this monoclinic phase in two different compositions, $x=0.48$[2,4] and $x=0.50$,[3] has allowed a preliminary modification of the phase diagram, as shown in Fig. 1. Furthermore, the discovery of this phase around the MPB in PZT answers many of the questions raised by previous investigators[5–10] about the nature of the MPB and the underlying basis for the special physical properties of PZT in this region of the phase diagram, especially in the context of the coexistence of rhombohedral and tetragonal phases.

The monoclinic unit cell is doubled with respect to the tetragonal one and has b as the unique axis. a_m and b_m are directed along the pseudocubic $[\bar{1}\bar{1}0]$ and $[1\bar{1}0]$ directions, respectively, while c_m is close to the tetragonal c axis, along [001], but tilted away from it such that the angle β between a_m and c_m is slightly larger than 90°. This monoclinic phase has unique characteristics in comparison to all other ferroelectric perovskite phases. The polar axis is not determined by symmetry and can be directed anywhere within the monoclinic ac plane; that is, the polar axis is allowed to rotate within this plane. In the case of PZT, the pseudocubic [111] and [001] directions are contained within the monoclinic plane and the monoclinic polar axis is tilted away from the polar axis of the tetragonal phase [001] towards that of the rhombohedral phase [111].[4] As has already been pointed out by other authors,[11–13] the diffraction data show clearly that the local structure of PZT differs from that of the average one. A structure analysis of rhombohedral PZT by Corker *et al.*[13] indicated that the Pb and Zr/Ti cations in the Zr-rich compositions are distributed among three locally disordered sites with monoclinic symmetry (see the gray circles in the top left plot of Fig. 1), resulting in average rhombohedral symmetry (black circle in the top left plot of Fig. 1).[4] In a similar structure analysis of tetragonal PZT close to the MPB,[4] the diffraction data were shown to be consistent with Pb and Zr/Ti cations distributed among four locally disordered cation sites with monoclinic symmetry, resulting in average tetragonal symmetry.[4]

In recent years, the development of first-principles calculations applied to the study of ferroelectric perovskites has contributed greatly to the understanding of the physical properties of these materials (see, e.g., Refs. 14–19). The incorporation of a compositional degree of freedom to allow for the study of solid solutions has been an important advance, which has opened up the possibility of investigating more

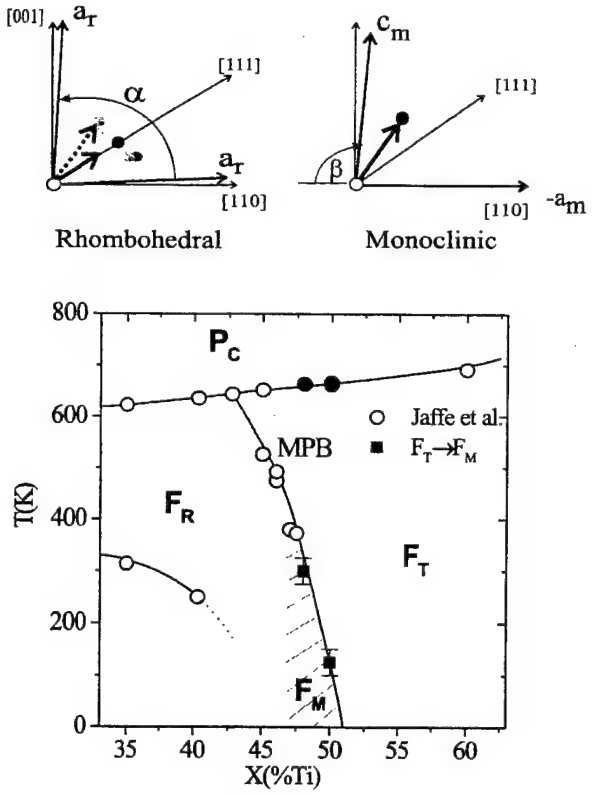

FIG. 1. The lower part of the figure shows the PZT phase diagram close to the MPB reported by Jaffe *et al.* (Ref. 1) (open symbols), and the preliminary modification proposed in Ref. 3, including the monoclinic phase. The solid symbols represent the observed phase transitions for $x=0.48$ (Ref. 4) and $x=0.50$ (Ref. 3). The upper part of the figure depicts the microscopic model proposed for the rhombohedral and the monoclinic phases in Ref. 4 (see text).

complex ferroelectric materials such as PZT and related systems.[20–26] Very recently, Bellaiche *et al.*[27] have succeeded in deriving the monoclinic phase of PZT from first-principles calculations. These authors also show that the value of the piezoelectric coefficient calculated, taking into account rotation of the polarization vector in the monoclinic plane, is in good agreement with the high values observed in PZT.

In the present paper, the stability region of the monoclinic phase in PZT is characterized by means of synchrotron x-ray powder-diffraction measurements made on PZT compositions at closely spaced intervals in the range $x=0.42-0.52$. The monoclinic phase is observed at 20 K for $0.46 \leqslant x \leqslant 0.51$, and this composition range narrows as the temperature increases. The transition temperature between the tetragonal and monoclinic phases is very steep as a function of composition and coincides with the previously mentioned MPB of Jaffe *et al.*[1] above ambient temperature.

II. EXPERIMENT

PZT samples with $x=0.42$, 0.45, 0.46, 0.47, 0.50, 0.51, and 0.52 were prepared by conventional solid-state reaction techniques similar to those used previously for PZT with $x=0.48$.[4] During the calcination, two steps were used. First, the desired solid solution was formed at 900 °C using the appropriate amounts of reagent-grade powders of lead carbonate, zirconium oxide, and titanium oxide with chemical purity better than 99.9%. Second, the formed product was pulverized and allowed to reach homogeneity by heating for 6 h at 850 °C (lower than the temperature at which PbO evaporates). Pellets were then pressed using an organic binder and, after burnout of the binder, heated to 1250 °C at a ramp rate of 10 °C/min, held at this temperature in a covered crucible for 2 h, and cooled to room temperature. During sintering, $PbZrO_3$ was used as a lead source to maintain a PbO-rich atmosphere.

Several sets of high-resolution synchrotron x-ray powder-diffraction measurements were made on different occasions at beam line X7A at the Brookhaven National Synchrotron Light Source. Data were collected from the ceramic disks in symmetric flat-plate reflection geometry using θ-2θ scans over selected angular regions in the temperature range 20–750 K. The sample was rocked 1°−2° during data collection to improve powder averaging. In all these experiments a Ge(111) double-crystal monochromator was used to provide an incident beam with a wavelength close to 0.7 Å . A Ge(220) crystal analyzer and scintillation detector were mounted in the diffracted beam, giving an instrumental resolution of about 0.01° on the 2θ scale. As described in Ref. 4, measurements above room temperature were performed with the disk mounted inside a wire-wound BN tube furnace. The accuracy of the temperature in the furnace is estimated to be about 10 K. For low-temperature measurements, the pellet was loaded in a closed-cycle He cryostat, which has an estimated temperature accuracy of 2 K. With this type of diffraction geometry, it is not always possible to eliminate preferred orientation and texture effects, but the peak positions, on which the present results are based, are not affected.

In many cases the peak profiles were quite complex, necessitating a very detailed and careful peak-fitting analysis. The peak positions were determined from least-squares fits to the profile recorded for each of the selected regions. A pseudo-Voigt peak shape function with an asymmetry correction was used,[28] and factors such as anisotropic peak widths, coexisting phases, and diffuse scattering between peaks were taken into account. The lattice parameters of individual phases were obtained from fits to the observed peak positions for several reflections. Because of the complicated peak shapes, we found that the above procedure gave more consistent results than standard profile-fitting programs.

Examples of selected regions of the diffraction patterns for the three PZT phases, tetragonal (top), monoclinic (center), and rhombohedral (bottom), around the morphotropic phase boundary are shown in Fig. 2. The narrow width of the peaks demonstrates the excellent quality of the ceramic samples and allows the specific characteristics of each phase to be clearly distinguished. In particular, the monoclinic phase exhibits unique features that cannot be accounted for by either of the other phases or a mixture of them. In the monoclinic phase, the unit cell is doubled in volume with respect to the tetragonal one, with a_m and b_m lying along the tetragonal $[\bar{1}\bar{1}0]$ and $[1\bar{1}0]$ directions, and c_m tilted slightly

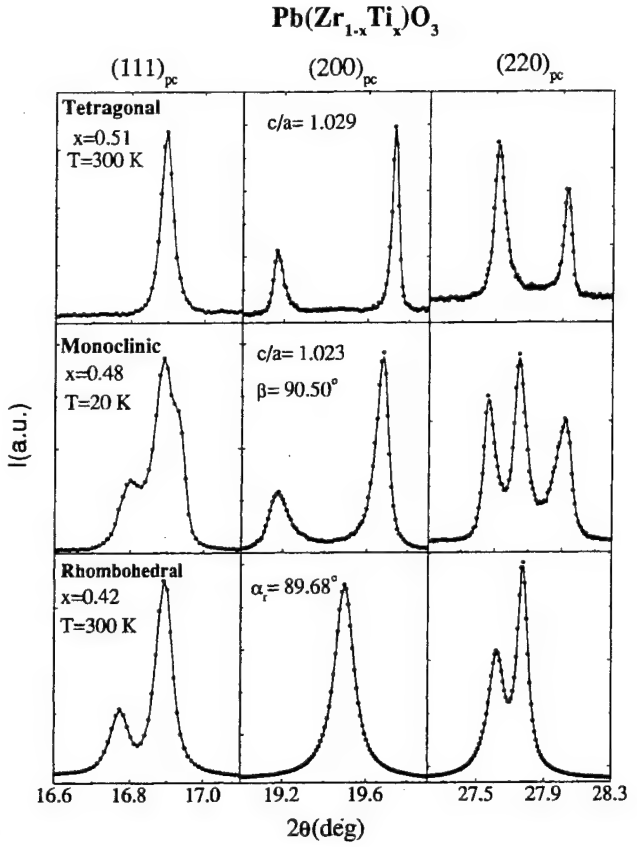

FIG. 2. Pseudocubic (111), (200), and (220) reflections for PZT with $x=0.51$ at 300 K (top), $x=0.48$ at 20 K (center), and $x=0.42$ at 300 K (bottom), showing the distinctive features of the tetragonal, monoclinic, and rhombohedral PZT phases, respectively.

away from the [001] direction. The monoclinic phase illustrated in this figure corresponds to the composition $x=0.48$ at 20 K, described in detail in Ref. 4, with $a_m=5.721$ Å, $b_m=5.708$ Å, $c_m=4.138$ Å, and $\beta=90.50°$. The c/a value in Fig. 2 (center) is defined as $2\sqrt{2}c_m/(a_m+b_m)$, in order to correspond to the c_t/a_t ratio in the tetragonal case (top).

III. PHASE TRANSITIONS

The evolution of the different structures as a function of temperature has been determined for all the PZT samples in the present study ($x=0.42$, 0.45, 0.46, 0.47, 0.51, and 0.52) and combined with previous data obtained for $x=0.48$ and $x=0.50$.[2–4] These results give a complete picture of the phase transitions occurring around the morphotropic phase boundary from 20 to 700 K. Three different low-temperature phases, with rhombohedral, monoclinic, and tetragonal symmetry, are observed. An important result is that the MPB defined by Jaffe *et al.*[1] is shown to correspond to the limit of the *monoclinic* phase rather than that of the rhombohedral phase and is a very robust line that is reproduced for all the samples under investigation. Both the tetragonal-monoclinic and the tetragonal-rhombohedral phase transitions will be described in this section, as well as the rhombohedral-rhombohedral phase transitions observed for $x=0.42$ at lower temperatures.

A. Tetragonal-monoclinic phase transition

The tetragonal phase in PZT is very similar to that of pure $PbTiO_3$.[29–31] The effects of Zr substitution on the structure of the tetragonal phase are basically two: first, as the Zr content increases, the tetragonal strain c_t/a_t decreases, and, second, the cubic-to-tetragonal phase transition evolves from first order to second-order. Figure 3 (top) shows the lattice parameters of PZT with $x=0.51$ as a function of temperature. The paraelectric-ferroelectric phase transition at $T\simeq 660$ K is of second order, as expected,[32] and the ferroelectric phase is purely tetragonal down to 100 K. Below this temperature, structural changes can be noticed; in particular, the tetragonal $(h0h)_t$ and $(hhh)_t$ reflections broaden markedly. This is apparent in the lower part of Fig. 3, where the pseudocubic $(220)_{pc}$ reflections are shown at high temperature (right), at an intermediate temperature (center), and at low temperature (left). Based on a careful peak-fitting analysis, the broadening at low temperatures of these reflections can be attributed to two separated peaks, consistent with the monoclinic symmetry observed in PZT with $x=0.48$,[4] also illustrated in Fig. 2. However, the monoclinic distortion is quite small, with $a_m\simeq b_m$ and $\beta\simeq 90.2°$. Similar behavior was observed for a sample of PZT with $x=0.50$ (Ref. 3) prepared under slightly different conditions, to be discussed later. As seen from Fig. 3, the monoclinic angle β is small, and the tetragonal-to-monoclinic transition temperature can only be approximately defined at $T_{T\text{-}M}\simeq 50$ K. On the other hand, data collected from PZT with $x=0.52$ show a well-defined tetragonal phase down to 20 K.

The evolution of the lattice parameters with temperature for PZT with $x=0.46$ is shown in Fig. 4 (top). The features displayed by this composition are similar to those of PZT with $x=0.48$.[4] A comparison with the latter data at low temperatures shows that the monoclinic angle β is larger for $x=0.46$ than for $x=0.48$. With decreasing x (Ti content), the differences between a_m and b_m also increase, while the difference between a_m and c_m decreases, corresponding to the evolution to a rhombohedral phase in which "$a_m=b_m=c_m$"[4]. The monoclinic phase is very well defined at low temperatures, as shown by the pseudocubic $(110)_{pc}$ reflections plotted at the bottom left of Fig. 4. The evolution of $\beta-90°$ shows a transition to a tetragonal phase at $T_{T-M}\simeq 450$ K, in agreement with the MPB of Jaffe *et al.* However, the characteristic features of the tetragonal phase also appear well below this temperature, and there is a wide region of phase coexistence between the tetragonal and monoclinic phases, as shown in the central plot at the bottom of the figure. In this plot, the peak positions for the pseudocubic $(110)_{pc}$ reflections corresponding to the monoclinic and tetragonal phases are shown together with the experimental data. From the observed data, a reliable peak-fitting analysis can be carried out and the lattice parameters determined for both phases in this region, as plotted as a function of temperature at the top of Fig. 4. The measurements on PZT with $x=0.47$ show similar behavior, but with a narrower coexistence region (300 K $<T<$ 400 K). For this composition the evolution of the order parameter, $(\beta-90°)$, suggests a tetragonal-to-monoclinic phase transition at $T_{T\text{-}M}\simeq$ 310 K,

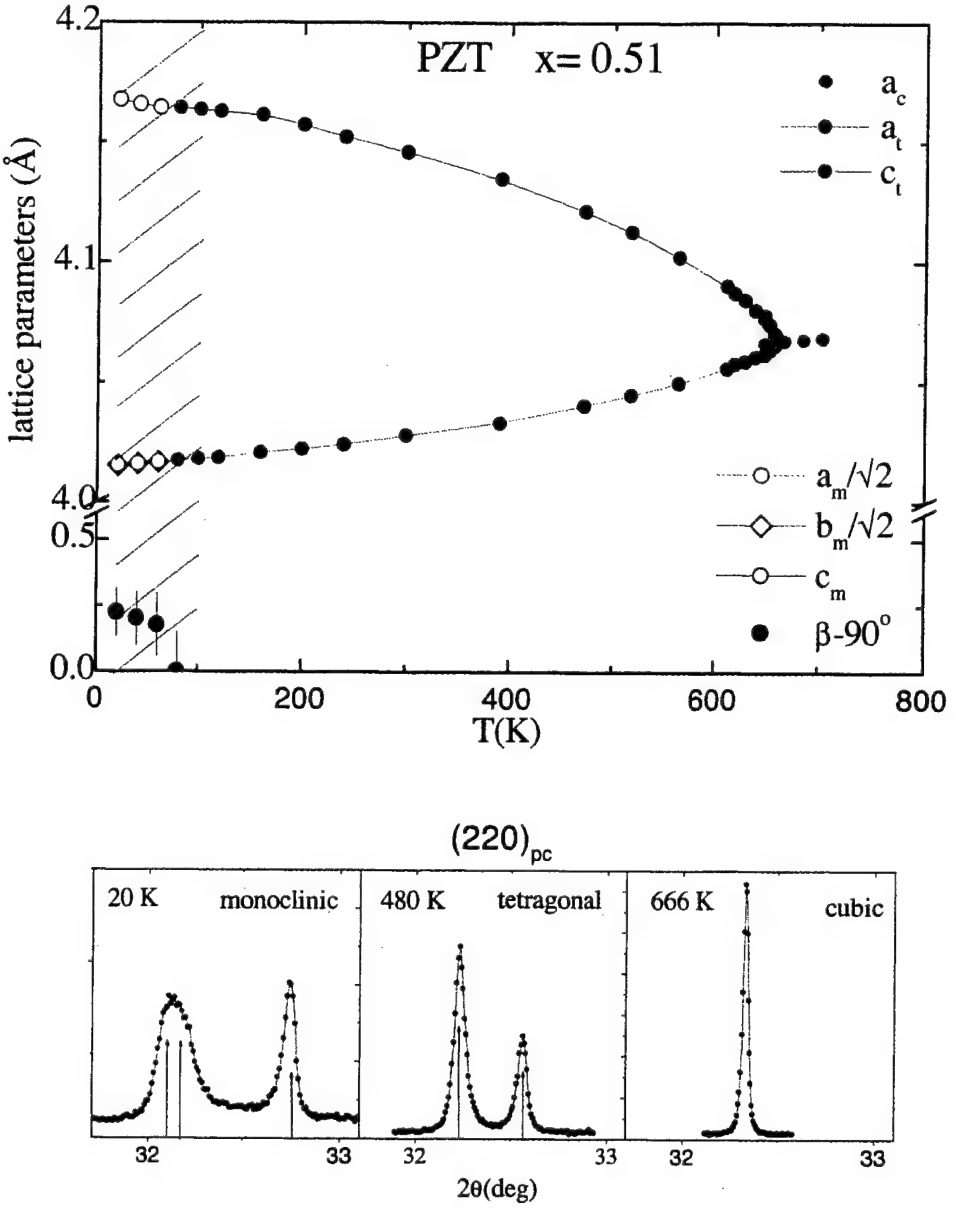

FIG. 3. (Color) Temperature evolution of the lattice parameters of PZT with $x=0.51$ from 20 K to 700 K, for the monoclinic, a_m, b_m, c_m, and β; tetragonal, a_t and c_t; and cubic, a_c, phases. The dashed region in the figure represents the uncertainty in the tetragonal-monoclinic phase transition. At the bottom of the figure, the pseudocubic (220) reflection is plotted at 20 K (monoclinic), 480 K (tetragonal), and 666 K (cubic) to illustrate the differences between the three phases.

very close to that observed for $x=0.48$, but the sample is not fully tetragonal until the temperature is greater than 400 K, corresponding to the MPB of Jaffe *el al.* for this composition.

B. Tetragonal-rhombohedral phase transition

A similar analysis for PZT with $x=0.45$ yields completely different results, as shown by the evolution of the $(200)_{pc}$ reflection in the lower part of Fig. 5. At low temperature the sample is rhombohedral (left) and remains rhombohedral up to $T\simeq 500$ K, while for $T>550$ K, this composition is tetragonal. Some diffuse scattering is observed between the tetragonal peaks, as shown in the bottom right of Fig. 5. This feature is present in all compositions in the study, as previously noted in Ref. 4, and is associated with the existence of twin boundaries in the tetragonal ferroelectric phase.[33] From the evolution of the order parameter $(90°-\alpha_r)$, it is possible to determine that the tetragonal-rhombohedral phase transition is complete at $T_{T\text{-}R}\simeq 580$ K. A coexistence region is observed in the interval 500 K $<T<$ 580 K. In the central plot at the bottom of the figure, the $(200)_{pc}$ reflection in this region is depicted together with the calculated peak positions for both phases.

C. Low-temperature rhombohedral phase

The data obtained for the PZT sample with $x=0.42$ show that this composition has rhombohedral symmetry all the

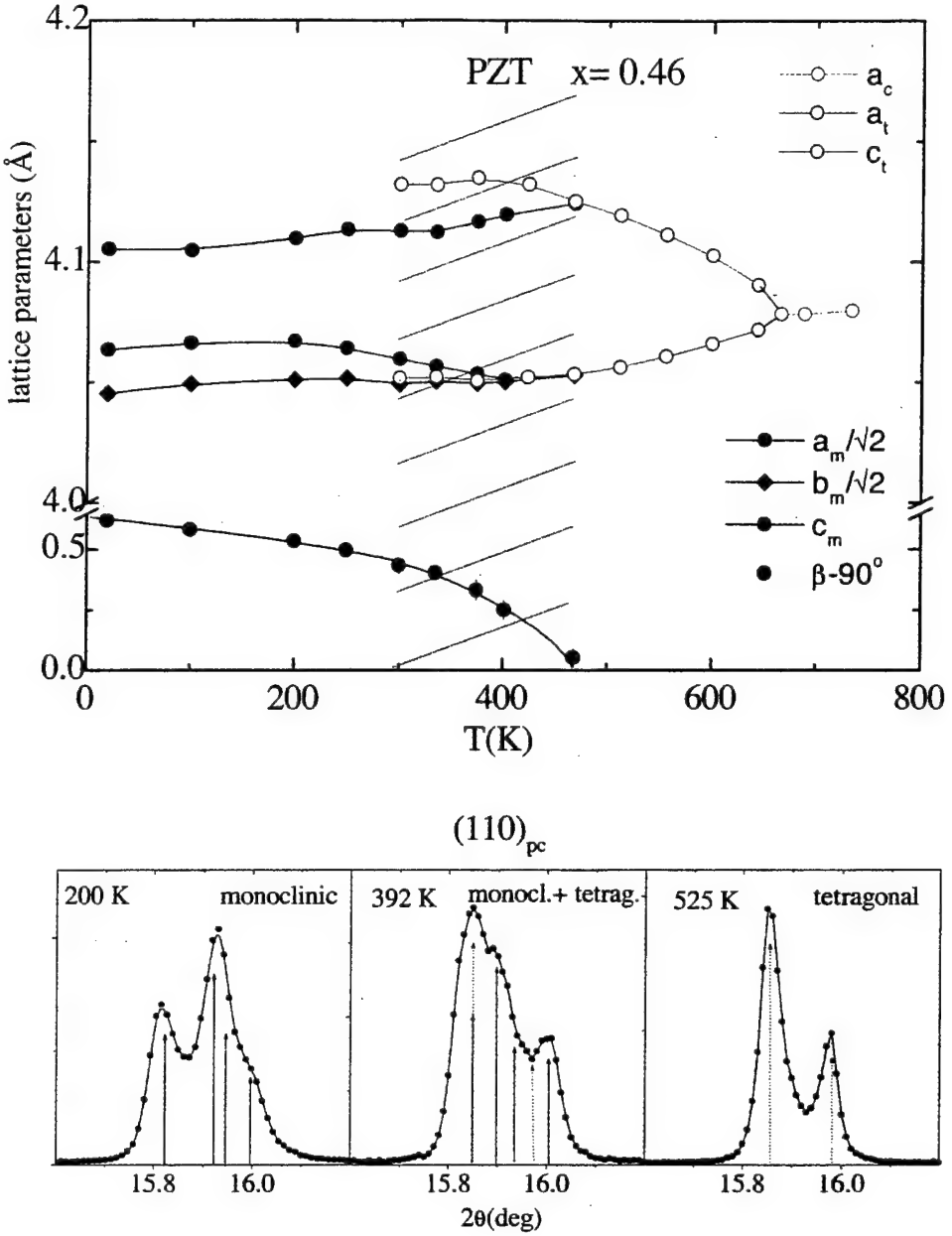

FIG. 4. (Color) Temperature evolution of the lattice parameters of PZT with $x=0.46$ from 20 K to 710 K, for the monoclinic, a_m, b_m, c_m, and β; tetragonal, a_t and c_t; and cubic, a_c, phases. The dashed area in the figure represents the region of tetragonal and monoclinic phase coexistence. At the bottom of the figure, the pseudocubic (110) reflection is plotted at 200 K (monoclinic phase), 392 K (tetragonal-monoclinic phase coexistence), and 525 K (tetragonal phase), where the calculated peak positions are indicated by solid arrows in the monoclinic phase and dashed arrows in the tetragonal phase.

way down to 20 K from the Curie point at $T_c \simeq 650$ K. At 20 K, the rhombohedral lattice parameters are $a=4.0921$ Å and $\alpha_r=89.61°$. With increasing temperature, the rhombohedral angle α_r increases gradually until the cubic phase is reached, while a remains practically constant.

Two different rhombohedral phases have been observed in PZT: a high-temperature phase ($F_{R(HT)}$) and a low-temperature rhombohedral phase ($F_{R(LT)}$)[34], which have space groups $R3m$ and $R3c$, respectively. In the latter phase, adjacent oxygen octahedra along the [111] polar axis are rotated about this axis in opposite directions, so that the unit cell is doubled with respect to the high-temperature phase.[35,36] The corresponding phase boundary was also determined by Jaffe *et al.*[1] in the region of the phase diagram above room temperature. An extension of this boundary below room temperature was reported in a neutron powder-diffraction study by Amin *et al.*,[37] who investigated the superlattice peaks from a sample with $x=0.40$ and found the transition temperature to occur at about 250 K. In the present work, we were also able to observe very weak superlattice peaks from a composition with $x=0.42$ below room temperature in the synchrotron x-ray patterns. The phase boundary in this case was found to lie at approximately 175 K (see Fig. 6).

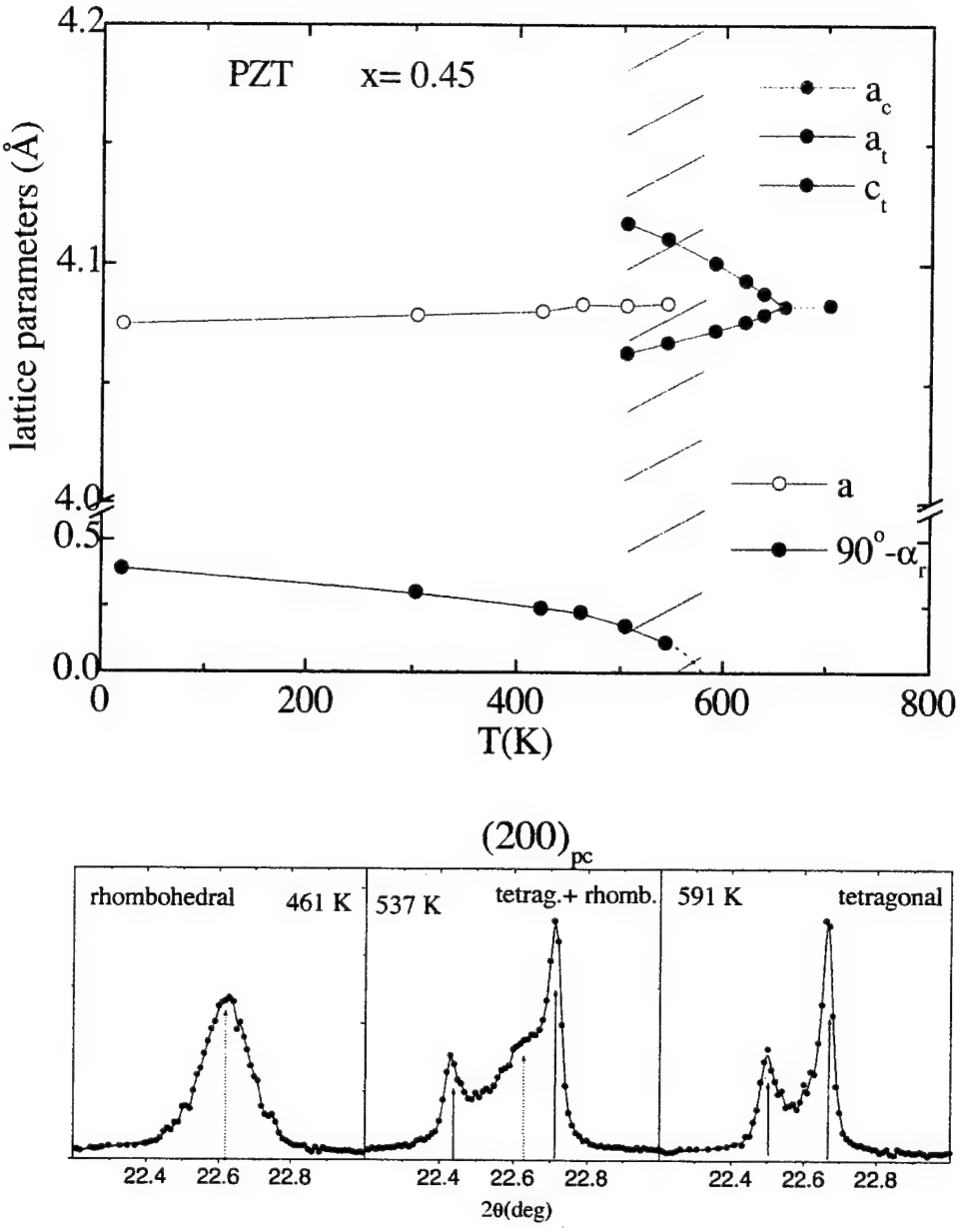

FIG. 5. (Color) Temperature evolution of the lattice parameters of PZT with $x=0.45$ from 20 K to 710 K, for the rhombohedral, a and α_r; tetragonal, a_t and c_t; and cubic, a_c, phases. The dashed area in the figure represents the region of tetragonal and rhombohedral phase coexistence. At the bottom of the figure, the pseudocubic (200) reflection is plotted at 461 K (rhombohedral phase), 537 K (tetragonal-rhombohedral phase coexistence), and 591 K (tetragonal phase), where the calculated peak positions are indicated by dashed arrows in the rhombohedral phase and solid arrows in the tetragonal phase.

We have also observed one very weak superlattice peak in a recent neutron diffraction study of a sample with $x=0.48$ at 20 K. This peak can be indexed in terms of a monoclinic cell with a doubled c axis, but the nature of the distortion and any possible relationship with that in the low-temperature rhombohedral phase has not yet been determined.

IV. DISCUSSION

The results presented above are summarized and compared with previous data from $x=0.48$ and $x=0.50$ in Fig. 6, which represents the new PZT phase diagram around the MPB. The data obtained for the tetragonal-(monoclinic/rhombohedral) transition temperatures for $0.45<x<0.51$ are very consistent and lie on a well-defined line, which reproduces the MPB of Jaffe *et al.*[1] above ambient temperature. The boundary between the rhombohedral and monoclinic regions is shown as a vertical line between $0.45<x<0.46$, since no evidence of a monoclinic-rhombohedral phase transition has been observed. The lattice parameters at 20 and 300 K for the compositions under study are listed in Table I, which also shows clearly the widening of the monoclinic region at lower temperatures. Figure 7 shows the evolution of the lattice parameters of the different phases as a function of composition at 300 K, from the rhombohedral to the tetragonal PZT phases via the monoclinic phase. At the top of

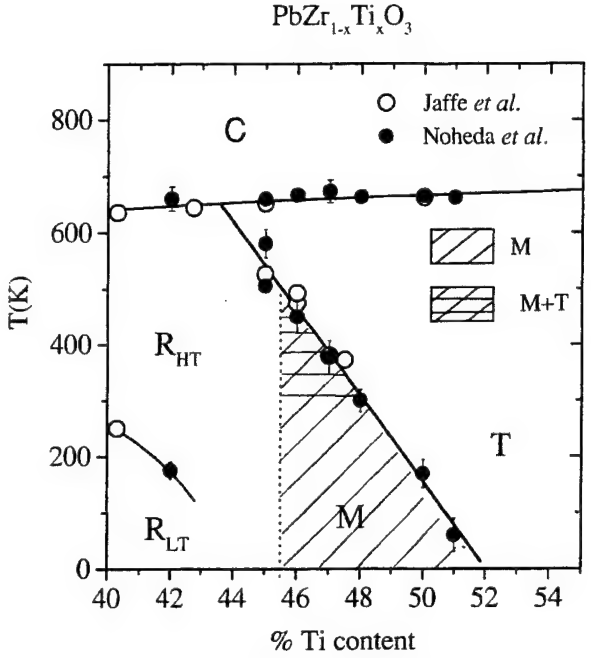

FIG. 6. New PZT phase diagram around the MPB. The solid symbols are the results from the current work, together with those in Ref. 3 ($x=0.50$) and Ref. 4 ($x=0.48$). Data from Jaffe *et al.* (Ref. 1) and Amin *et al.* (Ref. 37) are represented by open circles. The monoclinic region is shaded with diagonal lines. Horizontal lines are superimposed in the region of tetragonal-monoclinic phase coexistence. For $x=0.45$, the solid symbols represent the limits of the tetragonal-rhombohedral coexistence region.

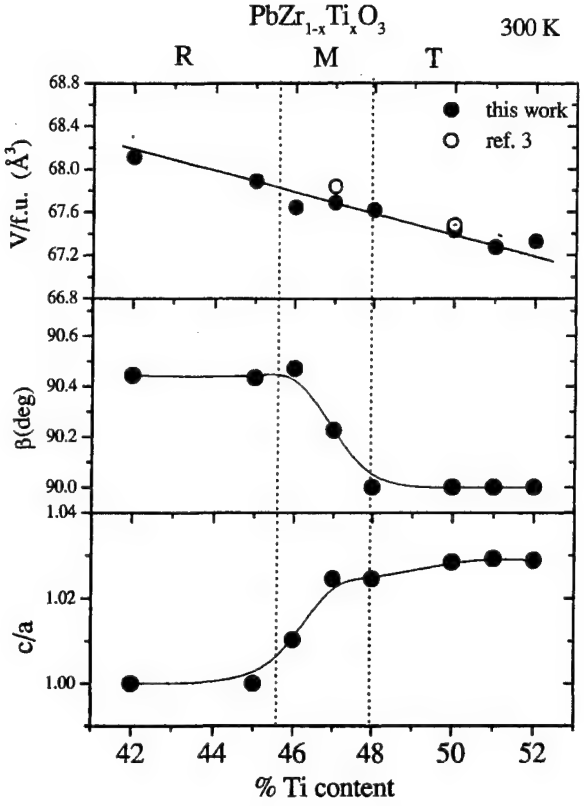

FIG. 7. The structural evolution with composition from the rhombohedral to the tetragonal PZT phases, through the monoclinic phase, as illustrated by the cell volume per formula unit, V (top), the monoclinic angle β (center) (Ref. 38), and the lattice strain c/a (bottom) for PZT with $0.42 \leqslant x \leqslant 0.52$ at 300 K. The cell volumes of the samples in Ref. 3 are also plotted as open circles at the top of the figure.

the figure, the unit-cell volume shows an essentially linear behavior with composition in the range studied. The monoclinic angle β and lattice strain c/a at 300 K are also plotted as a function of composition in Fig. 7, where the rhombohedral cell with lattice parameters a and α_r (see Table I) has been expressed in terms of the monoclinic cell.[38] c/a corresponds to c_t/a_t, $2\sqrt{2}c_m/(a_m+b_m)$, and 1, in the tetragonal, monoclinic, and rhombohedral cases, respectively. β is 90° for a tetragonal cell and is the monoclinic angle for the monoclinic cell. The role of the monoclinic phase as a "bridge" between the tetragonal and rhombohedral phases in PZT is clearly demonstrated in these plots. The monoclinic phase has also been observed by Raman scattering in a very recent paper by Souza Filho *et al.*[39]

The structural studies reported here, together with those in Refs. 2–4, comprise data from ten samples from two different origins spanning the composition range $0.42 \leqslant x \leqslant 0.52$. Only one of these samples was inconsistent with the picture

TABLE I. Lattice parameters at 20 and 300 K for PZT, with x in the range 0.42–0.52. The symmetry S of the unit cell, rhombohedral (R), monoclinic (M), or tetragonal (T) is indicated in each case. For rhombohedral symmetry $a=b=c$, and α_r is the rhombohedral angle. In the monoclinic case, β is the monoclinic angle. In the tetragonal case $a=b=a_t$, and $\beta=90°$.

	20 K						300 K					
%Ti	S	a (Å)	b (Å)	c (Å)	α_r(°)	β (°)	S	a (Å)	b (Å)	c (Å)	α_r(°)	β (°)
42	R	4.078			89.61		R	4.084			89.68	
45	R	4.075			89.61		R	4.079			89.69	
46	M	5.747	5.721	4.104		90.62	M	5.754	5.731	4.103		90.47
47	M	5.731	5.713	4.123		90.58	M	5.720	5.715	4.142		90.22
48	M	5.717	5.703	4.143		90.53	T	4.041		4.140		
50	M	5.693	5.690	4.159		90.35	T	4.032		4.147		
51	M	5.681	5.680	4.169		90.22	T	4.028		4.146		
52	T	4.009		4.158			T	4.030		4.145		

shown in Fig. 6, namely, PZT with $x=0.47$ described in Ref. 3. For this composition, it was found that the tetragonal phase transformed to a rhombohedral phase at low temperatures, while at intermediate temperatures, a poorly defined region of coexisting phases was observed. On the other hand, the data for the $x=0.47$ sample studied in the present work shows, as described above, characteristics similar to those of $x=0.46$ or $x=0.48$; in particular, the existence of a monoclinic phase at low temperatures and no traces of a rhombohedral phase. It is noteworthy that an analysis of the peak widths in the cubic phase shows clear differences in the microstructure of the two sets of samples. The microstrain $\Delta d/d$, and crystallite size of the samples used in the present study are estimated to be about 3×10^{-4} and 1 μm, respectively.[4] A similar analysis for the $x=0.47$ sample described in Ref. 3 yields values of 5×10^{-4} and 0.2 μm, respectively. One possible explanation is that because of the smaller crystallite size in the ceramic samples in Ref. 3, the inhomogeneous internal stress "prematurely" induces the tetragonal-rhombohedral phase transitions and inhibits the formation of the intermediate monoclinic phase. With a larger crystallite size, the internal strain is more easily relieved,[40,41] presumably through the formation of non-180° domains,[42] and the monoclinic phase is stabilized.

It is interesting to address the question of why the monoclinic phase was not observed in any of the previous studies. One important factor is the very superior resolution of synchrotron powder-diffraction equipment compared to that of laboratory equipment. A second is the presence of wide regions of rhombohedral-tetragonal phase coexistence in many of these studies, due to compositional fluctuations and/or small grain sizes,[8,43–46] which would obscure the evidence for monoclinic symmetry. For samples prepared by conventional "dry" solid-state techniques, a much narrower range of compositional fluctuations and large grain size can be achieved by the use of a final heat treatment at 1250 °C, as in the present case, or by the use of "semiwet" methods of synthesis and lower firing temperatures.[47–50] However, perhaps the key element for clarifying the phase diagram is to carry out the structural studies at low temperatures, as clearly demonstrated in Fig. 6.

Very recently, experiments on poled samples by Guo *et al.*[51] have further underlined the crucial role of the monoclinic phase in PZT. These experiments have revealed that poling induces the monoclinic distortion. The application of an electric field causes the rotation of the polar axis and an associated monoclinic distortion, which is retained after the field is removed. These features are shown to be the origin of the high piezoelectric response in PZT. It is observed that for rhombohedral PZT close to the MPB, the region of stability of the monoclinic phase increases after an electric field is applied. The field-induced monoclinic phase is found to be considerably wider on the Zr side of the phase diagram, at room temperature, extending at least to a Ti content of $x=0.42$. These experiments[51] validate the microscopic model for the MPB proposed in Ref. 4; i.e., the application of a field would favor one of the local sites, which corresponds exactly to the observed monoclinic distortion (see the dashed arrow in the top left plot of Fig. 1), and induces the monoclinic phase (see the top right plot in Fig. 1). Further studies of the poled samples are in progress, and will be reported in a subsequent publication.

ACKNOWLEDGMENTS

The authors are especially grateful to J. A. Gonzalo and S-E. Park, who were collaborators in the initial stages of this investigation, for their advice and encouragement. We also wish to thank L. Bellaiche, T. Egami, E. Salje, B. A. Tuttle, D. Vanderbilt, and T. Vogt for very helpful discussions. Financial support by the U.S. Department of Energy, Division of Materials Sciences (Contract No. DE-AC02-98CH10886) and ONR (MURI Project No. N00014-96-1-1173) is also acknowledged.

*Corresponding author. On leave from U. Autonoma de Madrid, Spain. Email address: noheda@bnl.gov

[1] B. Jaffe, W.R. Cook, and H. Jaffe, *Piezoelectric Ceramics* (Academic Press, London, 1971).
[2] B. Noheda, D.E. Cox, G. Shirane, J.A. Gonzalo, L.E. Cross, and S-E. Park, Appl. Phys. Lett. **74**, 2059 (1999).
[3] B. Noheda, J.A. Gonzalo, A.C. Caballero, C. Moure, D.E. Cox, and G. Shirane, Ferroelectrics **237**, 237 (2000).
[4] B. Noheda, J.A. Gonzalo, L.E. Cross, R. Guo, S-E. Park, D.E. Cox, and G. Shirane, Phys. Rev. B **61**, 8687 (2000).
[5] G. Shirane and K. Suzuki, J. Phys. Soc. Jpn. **7**, 333 (1952).
[6] E. Sawaguchi, J. Phys. Soc. Jpn. **8**, 615 (1953).
[7] L. Hanh, K. Uchino, and S. Nomura, Jpn. J. Appl. Phys. **17**, 637 (1978).
[8] W. Cao and L.E. Cross, Phys. Rev. B **47**, 4825 (1993).
[9] S.K. Mishra, D. Pandey, and A. Singh, Appl. Phys. Lett. **69**, 1707 (1996).
[10] X-h Du, J. Zheng, U. Belegundu, and K. Uchino, Appl. Phys. Lett. **72**, 2421 (1998).
[11] S. Teslic, T. Egami, and D. Viehland, J. Phys. Chem. Solids **57**, 1537 (1996); Ferroelectrics **194**, 271 (1997).
[12] J. Ricote, D.L. Corker, R.W. Whatmore, S.A. Impey, A.M. Glazer, J. Dec, and K. Roleder, J. Phys.: Condens. Matter **10**, 1767 (1998).
[13] D.L. Corker, A.M. Glazer, R.W. Whatmore, A. Stallard, and F. Fauth, J. Phys.: Condens. Matter **10**, 6251 (1998).
[14] R.E. Cohen, Nature (London) **358**, 136 (1992).
[15] R.D. King-Smith and D. Vanderbilt, Phys. Rev. B **49**, 5828 (1994).
[16] W. Zhong, D. Vanderbilt, and K.M. Rabe, Phys. Rev. Lett. **73**, 1861 (1994); Phys. Rev. B **52**, 6301 (1995).
[17] A. Garcia and D. Vanderbilt, Phys. Rev. B **54**, 3817 (1996).
[18] A. Garcia and D. Vanderbilt, Appl. Phys. Lett. **72**, 2981 (1998).
[19] U.V. Waghmare and K.M. Rabe, Phys. Rev. B **55**, 6161 (1997).
[20] K.M. Rabe and E. Cockayne, in *First-Principles Calculations for Ferroelectics*, edited by Ronald E. Cohen, AIP Conf. Proc. No. 436 (AIP, Woodbury, NY, 1998), p. 61.
[21] Ph. Ghosez, E. Cockayne, U.V. Waghmare, and K.M. Rabe, Phys. Rev. B **60**, 836 (1999).
[22] L. Bellaiche, J. Padilla, and D. Vanderbilt, Phys. Rev. B **59**, 1834 (1999).

[23] G. Saghi-Szabo, R.E. Cohen, and H. Krakauer, Phys. Rev. B **59**, 12 771 (1999).
[24] B.P. Burton and E. Cockayne, Phys. Rev. B **60**, R12 542 (1999).
[25] H. Fu and R. Cohen, Nature (London) **403**, 281 (2000).
[26] L. Bellaiche and D. Vanderbilt, Phys. Rev. Lett. **83**, 1347 (1999).
[27] L. Bellaiche, A. Garcia, and D. Vanderbilt, Phys. Rev. Lett. **84**, 5427 (2000).
[28] L.W. Finger, D.E. Cox, and A.P. Jephcoat, J. Appl. Crystallogr. **27**, 892 (1994).
[29] A.M. Glazer and S.A. Mabud, Acta Crystallogr., Sect. B: Struct. Crystallogr. Cryst. Chem. **34**, 1065 (1978).
[30] R.J. Nelmes and W.F. Kuhs, Solid State Commun. **54**, 721 (1985).
[31] G. Shirane, R. Pepinski, and B.C. Frazer, Acta Crystallogr. **9**, 131 (1956).
[32] G.A. Rosetti, Jr. and A. Navrotsky, J. Solid State Chem. **144**, 188 (1999).
[33] A.I. Ustinov, J.-C. Niepce, C. Valot, L.A. Olikhovska, and F. Bernard, Mater. Sci. Forum **321-324**, 109 (2000).
[34] H.M. Barnett, J. Appl. Phys. **33**, 1606 (1962).
[35] C. Michel, J-M. Moreau, G.D. Achenbach, R. Gerson, and W.J. James, Solid State Commun. **7**, 865 (1969).
[36] A.M. Glazer, S.A. Mabud, and R. Clarke, Acta Crystallogr., Sect. B: Struct. Crystallogr. Cryst. Chem. **34**, 1060 (1978).
[37] A. Amin, R.E. Newnham, L.E. Cross, and D.E. Cox, J. Solid State Chem. **37**, 248 (1981).
[38] The rhombohedral unit cell with lattice parameters a and α_r can be expressed in terms of a monoclinic unit cell as follows: $a_m = 2a\cos(\alpha_r/2)$, $b_m = 2a\sin(\alpha_r/2)$, $c_m = a$ and $\beta = 180° - \arccos[\{1-2\sin^2(\alpha_r/2)\}/\cos(\alpha_r/2)]$.
[39] A.G. Souza Filho, K.C.V. Lima, A.P. Ayala, I. Guedes, P.T.C. Freire, J. Mendes Filho, E.B. Araujo, and J.A. Eiras, Phys. Rev. B **61**, 14 283 (2000).
[40] W.R. Buessem, L.E. Cross, and A.K. Goswami, J. Am. Ceram. Soc. **49**, 33 (1966).
[41] B. Tuttle and D.A. Payne, Ferroelectrics **37**, 603 (1981).
[42] R.W. Cahn, Adv. Phys. **3**, 363 (1954).
[43] P. Ari-Gur and L. Benguigui, J. Phys. D **8**, 1856 (1975).
[44] J.C. Fernandes, D.A. Hall, M.R. Cockburn, and G.N. Greaves, Nucl. Instrum. Methods Phys. Res. B **97**, 137 (1995).
[45] A.P. Wilkinson, J. Xu, S. Pattanaik, and S.J.L. Billinge, Chem. Mater. **10**, 3611 (1998).
[46] E.R. Leite, M. Cerqueira, L.A. Perazoli, R.S. Nasar, and E. Longo, J. Am. Ceram. Soc. **79**, 1563 (1996).
[47] K. Kakegawa, J. Mohri, T. Takahashi, H. Yamamura, and S. Shirasaki, Solid State Commun. **24**, 769 (1977).
[48] K. Kakegawa, J. Mohri, S. Shirasaki, and K. Takahashi, J. Am. Ceram. Soc. **65**, 515 (1982).
[49] A.P. Singh, S.K. Mishra, D. Pandey, Ch.D. Prasad, and R. Lal, J. Mater. Sci. **28**, 5050 (1993).
[50] A. Cüneyt Taş, J. Am. Ceram. Soc. **82**, 1582 (1999).
[51] R. Guo, L.E. Cross, S-E. Park, B. Noheda, D.E. Cox, and G. Shirane, Phys. Rev. Lett. **84**, 5423 (2000).

Appendix 11

The monoclinic phase in PZT: new light on morphotropic phase boundaries

B. Noheda[1], J. A. Gonzalo
Universidad Autonoma de Madrid, Cantoblanco 28049, Spain

R. Guo, S.-E. Park, L.E. Cross
Materials Reasearch Lab., Penn. State University, PA 16802

D.E. Cox, and G. Shirane
Physics department, Brookhaven National Lab., Upton, NY 11973

A summary of the work recently carried out on the morphotropic phase boundary (MPB) of PZT is presented. By means of x-ray powder diffraction on ceramic samples of excellent quality, the MPB has been successfully characterized by changing temperature in a series of closely spaced compositions. As a result, an unexpected monoclinic phase has been found to exist in between the well-known tetragonal and rhombohedral PZT phases. A detailed structural analysis, together with the investigation of the field effect in this region of compositions, have led to an important advance in understanding the mechanisms responsible for the physical properties of PZT as well as other piezoelectric materials with similar morphotropic phase boundaries.

INTRODUCTION

"The morphotropic phase boundary (MPB) of $PbZr_{1-x}Ti_xO_3$ (PZT) has been finally characterized on extremely homogeneous ceramic samples by high resolution x-ray measurements. The boundary has been found to define the limit between the tetragonal phase and a new PZT phase with monoclinic symmetry. The recent work on this finding is reviewed [1,2,3,4].

The remarkable physical properties of the ferroelectric system $PbZr_{1-x}Ti_xO_3$ (PZT) for compositions close to x= 0.47 have been known for many years. In particular, its high piezoelectric response has made PZT one of the most widely used materials for electromechanical applications. PZT was first studied five decades ago [5,6] and the main structural characteristics of the system were investigated at that time. At high temperatures PZT is cubic with the perovskite structure. When lowering the temperature the material becomes ferroelectric, with the symmetry of the ferroelectric phase being tetragonal (F_T) for Ti-rich compositions and rhombohedral (F_R) for Zr-rich compositions. Subsequent studies led to the generally accepted phase diagram after Jaffe et al. [7], which covers temperatures above 300 K. Jaffe's phase diagram is represented by open circles in Fig. 1 for $0.33 \leq x \leq 0.63$. A complete phenomenological theory was developed for this system that is able to calculate thermal, elastic, dielectric and piezoelectric parameters of ferroelectric single crystal states [8].

The boundary between the tetragonal and the rhombohedral phases, at compositions close to x= 0.47, the so-called morphotropic phase boundary (MPB) [7], is nearly vertical in temperature scale. It has been experimentally observed that the maximum values of the dielectric permittivity, as well as the electromechanical coupling factors and piezoelectric coefficients of PZT at room temperature occur on this phase boundary. However, the maximum value of the remanent polarization is shifted to smaller Ti contents [7].

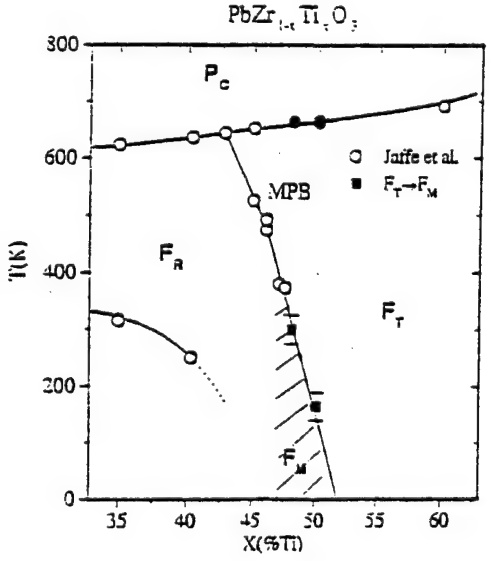

FIG. 1. Preliminary modification of the PZT phase diagram after Noheda et al. [3]. The open symbols represent the PZT phase diagram after Jaffe et al. [7].

The space groups of the tetragonal and rhombohedral phases (P4mm and R3m, respectively) are not symmetry-

"To appear in the proceedings of the Workshop on *Fundamental Physics of Ferroelectrics* held in Aspen, Feb. 2000.

[1]Present address: Physics department, Brookhaven National Lab., Upton, NY 11973.

related, so a first order phase transition is expected at the MPB. However, this has never been observed and, as far as we know, only composition dependence studies are available in the literature. One of the main difficulties in the experimental approach to this problem is the lack of single crystals of PZT. Because of the steepness of the phase boundary, any small compositional inhomogeneity leads to a region of phase coexistence (see e.g. [9,10,11,12]) that conceals the tetragonal-to-rhombohedral phase transition. The width of the coexistence region has been also connected to the particle size [13] and depends on the processing conditions, so a meaningful comparison of available data in this region is often not possible.

On the other hand, the richness of phases in PZT and the simplicity of its unit cell have encouraged important theoretical efforts in recent years. So far, the first-principles studies have been successful in reproducing many of the physical properties of PZT [14,15]. But, in spite of the proven validity, these calculations had not yet accounted for the remarkable increment of the piezoelectric response observed when the material approaches its MPB.

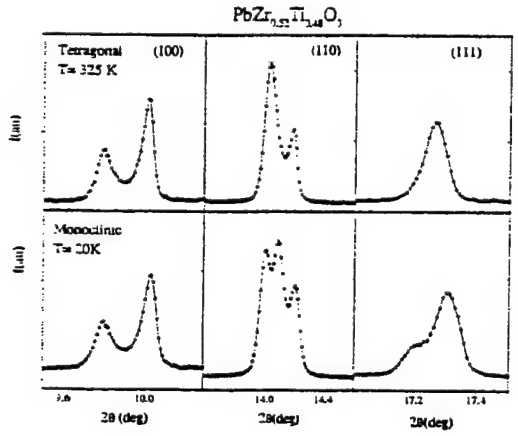

FIG. 2. Three selected peaks. (100), (110) and (111), from the diffraction profiles in the tetragonal (top) and monoclinic (bottom) PZT (x= 0.48) phases. The diffraction profiles are shown in Noheda et al. [3], Fig.6.

It was accordingly clear that there was something missing in the understanding of PZT, mainly due to experimental difficulties, and we addressed our efforts in this direction. The slight deviation from verticality of the MPB encouraged us to attempt the investigation of a temperature driven $F_T - F_R$ phase transition knowing that only samples of exceptional quality would allow us to succeed. With this purpose such ceramics were prepared by the Penn. State group. Our collaboration has resulted in the discovery of a new monoclinic phase (F_M) in this ferroelectric system [1,2]. The detailed structural analysis of tetragonal [3] and rhombohedral [16] phases of PZT seemed to indicate that the local structure is different from the average one and that, in both phases, such local structure has monoclinic symmetry. This local structure would be the precursor of the observed monoclinic phase. Diffraction measurements of the effect of the electric field on ceramic samples have confirmed this model [4]. Measurements on PZT samples with x= 0.48 and x= 0.50 allowed for a modification of the PZT phase diagram as shown in Fig. 1. It should be noted that the MPB defined by Jaffe et al. is still a perfectly valid line that corresponds to the F_T-F_M phase transition.

EXPERIMENTAL

PZT samples were prepared by conventional solid-state reaction techniques as described in refs. [1,3] at the MRL, Penn. State University, and samples with x= 0.50 were prepared at ICG, CSIC, Spain, as described in ref. [2]. High-resolution synchrotron x-ray powder diffraction measurements were carried out at the X7A diffractometer, at the Brookhaven National Synchrotron Light Source. Two types of experiments were done, as explained in ref. [3]. In the first one, data were collected from a disk in a symmetric flat-plate reflection geometry over selected angular regions as a function of temperature. These measurements demonstrated the high quality of the ceramic samples, whose diffraction peaks in the cubic phase have full-widths at half-maximum of 0.02° for x= 0.48. By means of a Williamson-Hall analysis in the cubic phase, a compositional error of less than $\Delta x = \pm 0.003$ was estimated [3] for this composition. To perform a detailed structure determination, additional measurements were made for PZT with x= 0.48, at 20 and 325 K, in the monoclinic and tetragonal phases, respectively. In this case, the sample was loaded in a rotating capillary of 0.2 mm diameter to avoid texture and preferred orientation effects [3].

THE MONOCLINIC PHASE

According to the PZT phase diagram [7], a sample with x= 0.48 is tetragonal just below the Curie point and rhombohedral below room temperature. The measurements on the pellets for selected diffraction peaks, with decreasing temperature from the cubic phase, showed the expected tetragonal phase down to ~300 K. Below this temperature however new features appeared in the diffractograms, but they were not compatible with either a rhombohedral phase or with a mixture of both phases (tetragonal and rhombohedral), and they clearly corresponded to a monoclinic phase with b as a unique axis [1]. This can be observed in Figure 2 where selected parts of the diffraction profile are plotted for the monoclinic (20 K) and the tetragonal (325 K) phases.

The cell parameters of PZT (x=0.48) are represented in Fig. 3 as a function of temperature. In the tetragonal phase (below T_c= 660 K), the tetragonal strain c_t/a_t, increases as the temperature decreases. At T$\simeq$ 300K the tetragonal-to-monoclinic ($F_T - F_M$) phase transition takes place and the c_t/a_t ratio starts decreasing slightly. The microstrain present in the sample during the evolution of the tetragonal phase seems to play a crucial role in the phase transition. $\Delta d/d$ is obtained from a Williamson-Hall analysis of the diffraction line widths [3] and is shown as a function of temperature at the bottom of the plot. At high temperatures, $\Delta d/d$ increases as the temperature decreases. At first, the increment is slow and no anomaly is observed at the cubic-to-tetragonal transition. At lower temperatures $\Delta d/d$ shows a rapid increase that reaches a sharp maximum just at the $F_T - F_M$ phase transition. For this amount of Zr substituted, the tetragonal phase cannot support the stress in the structure, which is to a large extent released by the onset of the monoclinic phase. Further analysis is being done in order to compare the microstrain exhibited by different compositions with that observed in pure $PbTiO_3$, where the tetragonal phase is stable at very low temperatures.

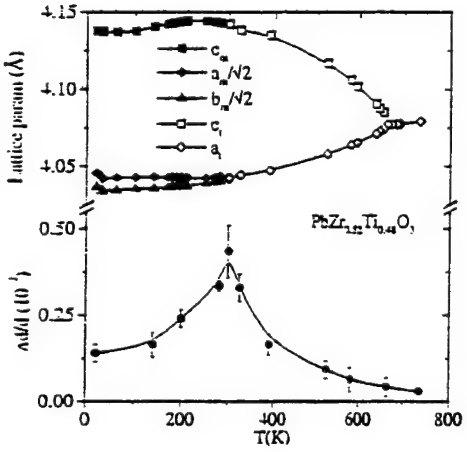

FIG. 3. Cell parameters as a function of temperature in the cubic, tetragonal and monoclinic phases for PZT x= 0.48. The evolution with temperature of $\Delta d/d$ is shown is the bottom plot. After Noheda et al. [3]

The monoclinic unit cell is doubled with respect to the tetragonal one: a_m and b_m are aligned along the $[\bar{1}10]$ and $[1\bar{1}0]$ directions, respectively, and c_m remains approximately equal to the tetragonal c_t but it is tilted with respect to it in the monoclinic plane, as illustrated in the inset in Fig. 4. Such a unit cell is chosen in order to have a monoclinic angle, β, larger than 90° (according to the usual convention) and $\beta - 90°$ is then defined as the order parameter of the $F_T - F_M$ transition. Its temperature evolution is depicted in Fig. 4. The transition seems to be of second order which is allowed in this case, since Cm is a subgroup of P4mm. PZT samples with x= 0.50, prepared in a slightly different way [2], showed also a monoclinic phase for temperatures below 200 K. In this case a_m is approximately equal to b_m and the monoclinic angle, β was found to be smaller than that observed for x= 0.48. Its evolution with temperature is also plotted in Fig.4 [2]. A direct comparison of these data for samples from different origins must be regarded with caution. Further work is being carried out in which samples with compositions in the range x= 0.42-0.51 processed under the same conditions are studied. However, with the data obtained so far it is already possible to represent a modification of the PZT phase diagram as the one shown in figure 1. It can be observed that the MPB established by Jaffe et al. [7] above room temperature seems to lie exactly along the F_T-F_M phase boundary.

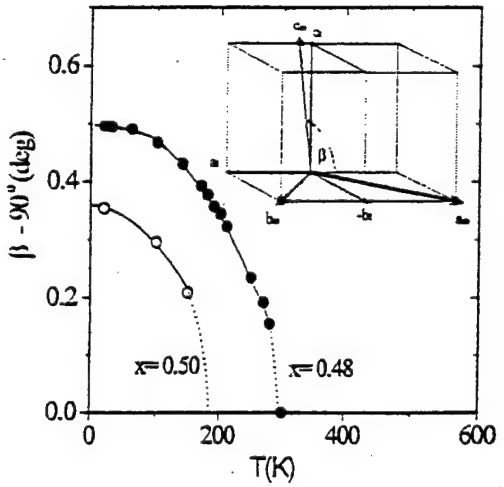

FIG. 4. Temperature evolution of the order parameter of the $F_T - F_M$ transition for PZT with x= 0.48 and x= 0.50. A representation of the monoclinic unit cell is included as an inset. After Noheda et al. [1,2,3].

Contrary to what occurs in the tetragonal and rhombohedral phases, in the monoclinic phase the polar axis is not determined by symmetry and could be along any direction within the monoclinic plane. To determine this direction the atom positions need to be known. A detailed structure investigation by means of a Rietveld profile analysis of the tetragonal and monoclinic phases of PZT (x= 0.48) has produced interesting results [3]. In the tetragonal phase at 325 K the unit cell has $a_t = 4.044\text{Å}$ and $c_t = 4.138\text{Å}$ and the atoms were found to be displaced in the same way as in pure $PbTiO_3$: Pb and Zr/Ti were shifted 0.48 Å and 0.27 Å, respectively, along the polar [001] axis. Anisotropic temperature factors gave a much better refinement but the resultant thermal ellipsoids were unphysically flattened perpendicularly to the polar direction. This is not a new problem in PZT: Rietveld refinement of the rhombohedral PZT

[17] structure also produced thermal disk-shaped ellipsoids flattened perpendicular to the rhombohedral polar axis [111]. This observed behavior has been previously associated with the existence of certain local ordering different from the long-range order.

The local order has been studied in rhombohedral PZT by means of the Pair Distribution Function [18] and, more recently, by modelling local disordered cation shifts by means of a Rietveld profile refinement [16]. The authors found that by considering three equivalent disordered displacements along the ⟨001⟩ directions, superimposed on the rhombohedral cation displacement along [111] (see figure 5) the refinement produced much more reasonable temperature factors.

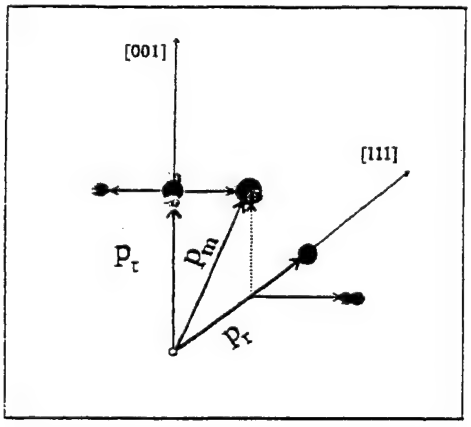

FIG. 5. Schematic view of the cation shifts in the tetragonal (p_t), monoclinic (p_m) and rhombohedral (p_r) unit cells. The solid circles and the arrows represent the cation positions in each one of the three structures. In the tetragonal and rhombohedral cases, the long-range structure is an average of the short-range or local structures (three in the rhombohedral one and four in the tetragonal one) represented by smaller grey circles [3]

In the same way, for tetragonal PZT(x= 0.48) at 325 K. we can model local disordered sites for the lead atoms perpendicular to the polar axis, that is, we allow Pb to move towards the four sites allowed by symmetry, i.e. at the ⟨xxz⟩ positions [3], which give an average tetragonal ⟨00z⟩ cation shift (see figure 5). Similar results are obtained if the refinement is carried out modelling local disorder shifts along the ⟨x0z⟩ directions. The refinement gives local shifts of 0.2 Å perpendicular to the polar axis in adition to the common shift of 0.48 Å along the polar axis, which is similar to that of $PbTiO_3$, and gives also physically reasonable isotropic temperature factors.

The structure of the monoclinic phase at 20 K does not present this kind of problems. The refinement is very good considering isotropic temperature factors for all atoms except lead, and the resulting anisotropy for lead is not unreasonable [3]. The refined unit cell was $a_m = 5.721$ Å, $b_m = 5.708$ Å, $c_m = 4.138$ Å with $\beta = 90.496°$. The results os the refinement [3] have defined the monoclinic polar axis. This lies within the monoclinic plane along a direction between the polar axes of the tetragonal and the rhombohedral phases, 24° away from the former (see figure 5). This value could become slightly different after the oxygen positions are more accurately determined by a neutron study that is underway. This is the first example of a ferroelectric material with $P_x^2 = P_y^2 \neq P_z^2$, where P_x,P_y and P_z are the Cartesian components of the spontaneous polarization.

Although this result is interesting, the striking fact about it is that the monoclinic shifts exactly corresponds to one of the four locally disordered shifts proposed for the tetragonal phase, as it can be observed in fig.5. The monoclinic phase appears, as the temperature is lowered, by the condensation of one of the local shifts existing in the tetragonal phase. Most interesting is the fact that the monoclinic displacement also corresponds to one of the three locally disordered shifts proposed by Corker et al. [16] for the rhombohedral phase (see fig. 5), so the condensation of this particular site would also give rise to the observed monoclinic phase.

FIELD EFFECT

Diffraction experiments with poled ceramics as well as with PZT ceramics under electric field applied *in-situ* were carried out. This measurement were taken on the flat plate on symmetric reflection. which means that only scattering vectors perpendicular to the surfaces are measured [4]. A plot of selected diffraction peaks of poled and unpoled samples (Fig. 6) shows the expected intensity differences which are attributed to differences in domain populations after poling. in both the tetragonal (x= 0.48) and a rhombohedral (x= 0.42) compositions. The behavior of the peak positions after poling was, however, unexpected. As shown in the same figure for the rhombohedral composition. the (hhh) diffraction peaks, corresponding to the polar direction, were not shifted after poling. A large shift of the (h00) peak position was observed, however, which means that the piezoelectric elongation of the unit cell is not along the polar direction, but along [001]. In a similar way, for the tetragonal composition (x= 0.48), no shift was observed along the polar [001] direction, while clear poling effects were evident in the (hhh) peaks. The explanation of this striking behavior lies in the monoclinic phase. The piezoelectric strain occurs, for compositions close to the MPB not along the polar axes but along the directions that induce the monoclinic distortion.

All these observations lead us to propose that the so-called morphotropic phase boundary is not a boundary but rather a phase with monoclinic symmetry. This new phase is intermediate between the tetragonal and rhombohedral PZT phases. Its symmetry relates both phases

(Cm being a subgroup of both P4mm and R3m) through the only common symmetry element, the mirror plane. Both, the tetragonal and rhombohedral phases (at least in the proximity of the MPB) have a local structure different from the long-range one and at low temperatures a monoclinic long range order is established by the freezing-out of one of the "local monoclinic structures" in both the rhombohedral and the tetragonal phases. Under the application of an electric field, one of the locally disordered sites becomes preferred, inducing the monoclinic distortion. This induced monoclinic phase is stable and remains after the field is removed.

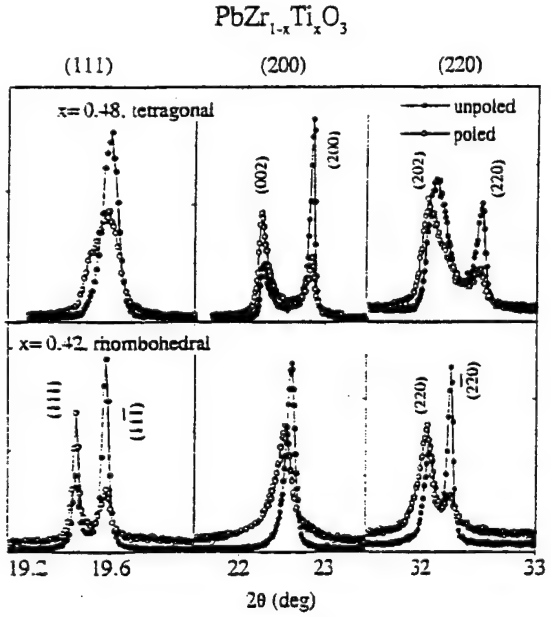

FIG. 6. (111), (200) and (220) pseudo-cubic reflections for the x= 0.48 (tetragonal) and x= 0.42 (rhombohedral) PZT compositions, before and after poling. After Guo et al. [4]

These results can explain some of the puzzles in PZT, such as the larger piezoelectric coefficient found in rhombohedral PZT along the tetragonal direction [19]. Taking into account the monoclinic phase, very recent *ab initio* calculations have been able to explain the high piezoelectric response of these materials by considering rotations of the polar axis in the monoclinic plane (d_{15}) [20]. Indications of a phase of lower symmetry than tetragonal have been found by optical measurement on single crystals of PZN-PT close to the MPB [21]. Something similar could be true in other ferroelectric systems with similar MPBs as PMN-PT or some Tungsten-Bronzes.

We thank L. Bellaiche, T. Egami, A.M. Glazer and C. Moure for helpful discussions, B. Jones for the excellent samples, and A. Langhorn for his technical support during the field experiments. Financial support by the U.S. Department of Energy under contract No. DE-AC02-98CH10886 and ONR under project MURI (N00014- 96-1-1173) is also acknowledged.

[1] B. Noheda, D.E. Cox, G. Shirane, J.A. Gonzalo, L.E. Cross, and S-E. Park, Appl. Phys. Lett. **74**, 2059 (1999).

[2] B. Noheda, J.A. Gonzalo, A.C. Caballero, C. Moure, D.E. Cox, and G. Shirane, presented at the *9th European Meeting on Ferroelectricity*, Prague, July1999 (to be published in Ferroelectrics, March 2000). e-print:cond-mat/9907286.

[3] B. Noheda, J.A. Gonzalo, L.E. Cross, R. Guo, S-E. Park, D.E. Cox, and G. Shirane, Phys. Rev. B **61** (in press), 1 April (2000). e-print:cond-mat/9910066

[4] R. Guo, L.E. Cross, S-E. Park, B. Noheda, D.E. Cox, and G. Shirane, e-print:cond-mat/9912118 (to be published).

[5] G. Shirane and K. Suzuki, J. Phys. Soc. Japan **7**, 333 (1952).

[6] E. Sawaguchi, J. Phys. Soc. Japan **8**, 615 (1953).

[7] B. Jaffe, W.R. Cook, and H. Jaffe, *Piezoelectric Ceramics* (Academic Press, London, 1971). We are unable to locate the original publication that describes how the MPB was determined.

[8] M. J. Haun, E. Furman, S.J. Jang, and L.E. Cross, Ferroelectrics **99**,13 (1989).

[9] K. Kakewaga, O. Matsunaga, T. Kato, and Y. Sasaki, J. Amer. Ceram. Soc. **78**, 1071 (1995).

[10] S. K. Mishra, D. Pandey, Appl. Phys. Lett. 69, 1707 (1996)

[11] S. Zhang, X. Dong, S. Kojima, Jpn. J. Appl. Phys. 36, 2994(1997).

[12] A.P. Wilkinson, J. Xu, S. Pattanaik and J.L. Billinge, Chem. Mat. **10**, 3611 (1998).

[13] W. Cao and L.E. Cross, Phys. Rev. B **47**, 4825 (1993).

[14] G. Saghi-Szabo, R. Cohen, and H. Krakauer, Phys. Rev. B **59**, 12771 (1999).

[15] L. Bellaiche and D. Vanderbilt, Phys. Rev. Lett. **83**, 1347 (1999).

[16] D.L. Corker, A.M. Glazer, R.W. Whatmore, A. Stallard, and F. Fauth, J. Phys.:Condens. Matter **10**, 6251 (1998).

[17] A.M. Glazer and S.A. mabud, Asta Cryst. **B34**, 1060 (1978).

[18] S. Teslic, T. Egami, and D. Viehland, J. Phys. Chem. Solids **57**, 1537 (1996); Ferroelectrics **194**, 271 (1997).

[19] X-h Du, J. Zheng, U. Belegundu, and K. Uchino, Appl. Phys. Lett **72**, 2421 (1998).

[20] L. Bellaiche, A. Garcia, and D. Vanderbilt (to be published).

[21] K. Fujishiro, R. Vlokh, Y. Uesu, Y. Yamada, J-M. Kiat, B. Dkhil, and Y. Yamashita, presented at the *9th European Meeting on Ferroelectricity*, Prague, July 1999 (to be published in Ferroelectrics, March 2000).

Appendix 12

Origin of the high piezoelectric response in $PbZr_{1-x}Ti_xO_3$

R. Guo[1], L.E. Cross[1], S-E. Park[1], B. Noheda[2,3], D.E. Cox[3], and G. Shirane[3]
[1] *Mat. Res. Lab., Pennsylvania State University, PA 16802-4800*
[2] *Universidad Autonoma de Madrid. 28049-Madrid, Spain*
[3] *Brookhaven National Laboratory, Upton, NY 11973-5000*
(December 7, 1999)

High resolution x-ray powder diffraction measurements on poled $PbZr_{1-x}Ti_xO_3$ (PZT) ceramic samples close to the rhombohedral-tetragonal phase boundary (the so-called morphotropic phase boundary, MPB) have shown that for both rhombohedral and tetragonal compositions, the piezoelectric elongation of the unit cell does not occur along the polar directions but along those directions associated with the monoclinic distortion. This work provides the first direct evidence for the origin of the very high piezoelectricity in PZT.

Scheduled for 5 June 2000, *Physical Review Letters*, Volume **84**, Number 23

The ferroelectric $PbZr_{1-x}Ti_xO_3$ (PZT) system has been extensively studied because of its interesting physical properties close to the morphotropic phase boundary (MPB), the nearly vertical phase boundary between the tetragonal and rhombohedral regions of the phase diagram close to x= 0.50, where the material exhibits outstanding electromechanical properties [1]. The existence of directional behavior for the dielectric and piezoelectric response functions in the PZT system has been predicted by Du *et al.* [2], [3] from a phenomenological approach [4]. These authors showed that for rhombohedral compositions the piezoelectric response should be larger for crystals oriented along the [001] direction than for those oriented along the [111] direction. Experimental confirmation of this prediction was obtained [5,6,7] for the related ferroelectric relaxor system $PbZn_{1/3}Nb_{2/3}$-$PbTiO_3$ (PZN-PT), which has a rhombohedral-to-tetragonal MPB similar to that of PZT, but it has not been possible to verify similar behavior in PZT due to the lack of single crystals. Furthermore, *ab initio* calculations based on the assumption of tetragonal symmetry, that have been successful for calculating the piezoelectric properties of pure $PbTiO_3$ [8,9,10,11], were unable to account for the much larger piezoelectric response in PZT compositions close to the MPB. Thus, it is clear that the current theoretical models lack some ingredient which is crucial to understanding the striking piezoelectric behavior of PZT.

The stable monoclinic phase recently discovered in the ferroelectric $PbZr_{1-x}Ti_xO_3$ system (PZT) close to the MPB [12], provides a new perspective to view the rhombohedral-to-tetragonal phase transformation in PZT and in other systems with similar phase boundaries [13]. We believe that, very likely, it plays a key role in explaining some of the unsolved puzzles of PZT. The polar axis of this monoclinic phase is contained in the (110) plane along a direction between that of the tetragonal and rhombohedral polar axes [12]. An investigation of several compositions around the MPB has suggested a modification of the PZT phase diagram [1] as shown in Fig. 1(top right) [13].

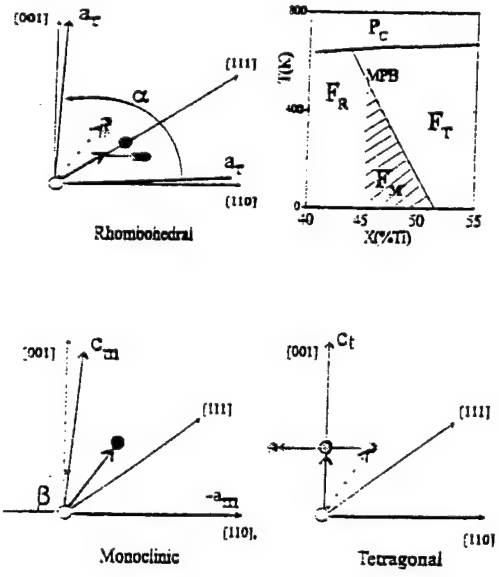

FIG. 1. Schematic view of the PZT phase diagram in the vicinity of the MPB showing the monoclinic region (top right). A projection of the rhombohedral (top left), monoclinic (bottom left) and tetragonal (bottom right) unit cells on the pseudo-cubic (110) plane is sketched. The solid circles represent the observed lead shifts with respect to the ideal cubic structure and the grey circles the locally-disordered shifts, four in the tetragonal phase and three in the rhombohedral phase. The heavy dashed arrows represent the freezing-out of one of these shifts to give the observed long-range monoclinic structure [13].

A local order different from the long-range order in the rhombohedral and tetragonal phases has been proposed from a detailed structural data analysis. Based on this, a model has been constructed in which the monoclinic distortion (Fig. 1, bottom-left) can be viewed as either a condensation along one of the ⟨110⟩ directions of the local displacements present in the tetragonal phase [13] (Fig. 1 bottom-right), or as a condensation of the local displacements along one of the ⟨100⟩ directions present in

the rhombohedral phase [14] (Fig. 1 top-left). The monoclinic structure, therefore, represents a bridge between these two phases and provides a microscopic picture of the MPB region [13].

In the present work experimental evidence of an enhanced elongation along [001] for rhombohedral PZT and along [101] for tetragonal PZT ceramic disks revealed by high-resolution x-ray diffraction measurements during and after the application of an electric field is presented. This experiment was originally designed to address the question whether poling in the MPB region would simply change the domain population in the ferroelectric material, or whether it would induce a permanent change in the unit cell. As shown below, from measurements of selected peaks in the diffraction patterns, a series of changes in the peak profiles from the differently oriented grains are revealed which provide key information about the PZT problem.

$PbZr_{1-x}Ti_xO_3$ ceramic samples with x= 0.42, 0.45 and 0.48 were prepared by conventional solid-state reaction techniques using high purity (better than 99.9%) lead carbonate, zirconium oxide and titanium oxide as starting compounds. Powders were calcined at 900°C for six hours and recalcined as appropriate. After milling, sieving, and the addition of the binder, the pellets were formed by uniaxial cold pressing. After burnout of the binder, the pellets were sintered at 1250°C in a covered crucible for 2 hours, and furnace-cooled. During sintering, $PbZrO_3$ was used as a lead source in the crucible to minimize volatilization of lead. The sintered ceramic samples of about 1 cm diameter were ground to give parallel plates of 1 mm thickness, and polished with 1 μm diamond paste to a smooth surface finish. To eliminate strains caused by grinding and polishing, samples were annealed in air at 550°C for five hours and then slow-cooled. Silver electrodes were applied to both surfaces of the annealed ceramic samples and air-dried. Disks of all compositions were poled under a DC field of 20 kV/cm at 125°C for 10 minutes and then field-cooled to near room temperature. The electrodes were then removed chemically from the x= 0.42 and 0.48 samples. For the x= 0.45 sample (which had been ground to a smaller thickness, about 0.3 mm), the electrodes were retained, so that diffraction measurements could be carried out under an electric field.

Several sets of high-resolution synchrotron x-ray powder diffraction measurements were made at beam line X7A at the Brookhaven National Synchrotron Light Source. A Ge(111) double-crystal monochromator was used in combination with a Ge(220) analyser, with a wavelength of about 0.8 Å in each case. In this configuration, the instrumental resolution, $\Delta 2\theta$, is an order-of-magnitude better than that of a conventional laboratory instrument (better than 0.01° in the 2θ region 0-30°). The poled and unpoled pellets were mounted in symmetric reflection geometry and scans made over selected peaks in the low-angle region of the pattern. It should be noted that since lead is strongly absorbing, the penetration depth below the surface of the pellet at $2\theta = 20°$ is only about 2 μm. In the case of the x= 0.45 sample, the diffraction measurements were carried out with an electric field applied in-situ via the silver electrodes.

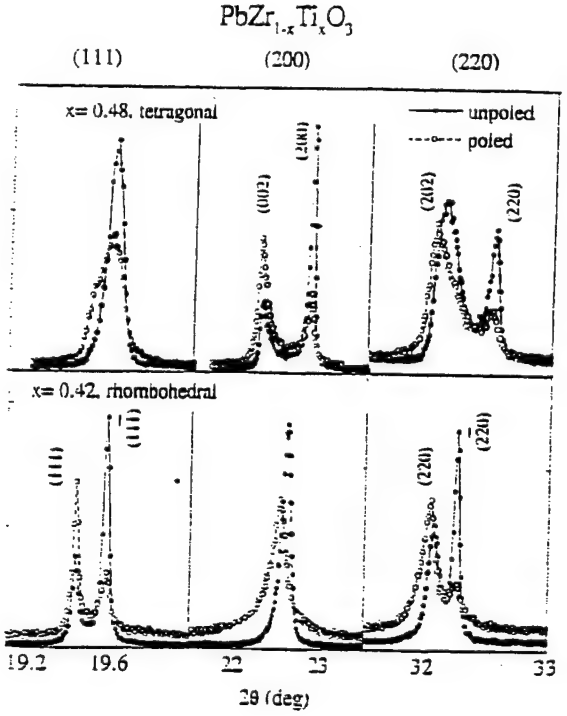

FIG. 2. Comparison of (111), (200) and (220) pseudo-cubic reflections for the x= 0.48 (tetragonal), and x= 0.42 (rhombohedral) PZT compositions before and after poling

Powder diffraction measurements on a flat plate in symmetric reflection, in which both the incident and the diffracted wave vectors are at the same angle, θ, with the sample plate, ensures that the scattering vectors are perpendicular to the sample surface. Thus only crystallites with their scattering vector parallel to the applied electric field are sampled. Scans over selected regions of the diffractogram, containing the (111), (200) and (220) pseudo-cubic reflections, are plotted in Fig.2 for poled and unpoled PZT samples with the compositions x= 0.48 (top) and x= 0.42 (bottom), which are in the tetragonal and rhombohedral region of the phase diagram, respectively. The diffraction profiles of the poled and unpoled samples show very distinctive features. For the tetragonal composition (top), the (200) pseudo-cubic reflection (center) shows a large increase in the tetragonal (002)/(200) intensity ratio after poling due to the change in the domain population, which is also reflected in the increased (202)/(220) intensity ratio in the right

side of the figure. In the rhombohedral composition with x= 0.42 (bottom of Fig.2), the expected change in the domain population can be observed from the change of the intensity ratios of the rhombohedral (111) and $(11\bar{1})$ reflections (left side) and the (220) and $(2\bar{2}0)$ reflections (right side).

In addition to the intensity changes, the diffraction patterns of the poled samples show explicit changes in the peak positions with respect to the unpoled samples, corresponding to specific alterations in the unit cell dimensions. In the rhombohedral case (x= 0.42), the electric field produces no shift in the (111) peak position (see bottom-left plot in Fig.2), indicating the absence of any elongation along the polar directions after the application of the field. In contrast, the poling does produce a notable shift of the (001) reflections (center plot), which corresponds to a very significant change of d-spacing, with $\Delta d/d = 0.32\%$, $\Delta d/d$ being defined as $(d_p \quad d_u)/d_u$, where d_p and d_u are the d-spacings of the poled and unpoled samples, respectively. This provides experimental confirmation of the behavior predicted by Du *et al.* [3] for rhombohedral PZT, as mentioned above. The induced change in the dimensions of the unit cell is also reflected as a smaller shift in the (202) reflection (right side plot), corresponding to a $\Delta d/d$ along [101] of 0.12%.

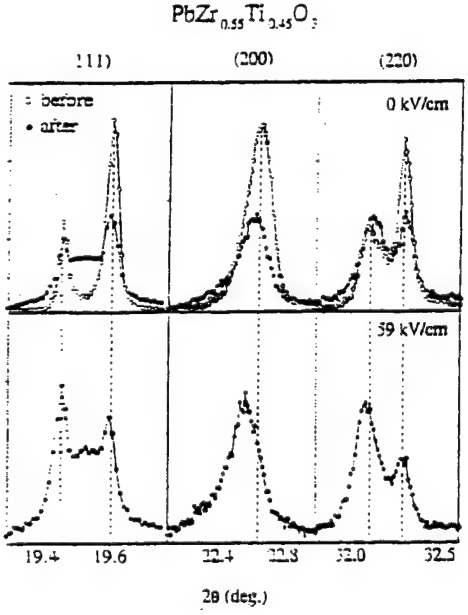

FIG. 3. (111), (200) and (220) pseudocubic reflections for PZT with x= 0.45 measured on an unpoled sample (open circles) and on a similar sample after the application and removal of a field of 59 kV/cm at room temperature (solid circles) are plotted in the upper part of the figure. The scattered intensity at $2\theta = 19.52°$ from the second sample corresponds to the (111) reflection from the silver electrode. Measurements on the latter sample under an electric field of 59 kV/cm applied *in situ* are plotted in the lower part of the figure.

In the tetragonal case for x= 0.48 (top of Fig.2), there is no peak shift observed along the polar [001] direction (center plot), but the (202) and the (111) reflections exhibit striking shifts (right and left sides, respectively). Furthermore, this composition, which at room temperature is just at the monoclinic-tetragonal phase boundary, shows, after poling, a clear tendency towards monoclinic symmetry, in that the (111) and (202) reflections, already noticeably broadened in the unpoled sample and indicative of an incipient monoclinicity, are split after poling. These data clearly demonstrate, therefore, that whereas the changes induced in the unit cell after the application of an electric field do not increase either the rhombohedral or the tetragonal strains, a definite elongation is induced along those directions associated with the monoclinic distortion.

In addition to the measurements on the poled and unpoled samples, diffraction measurements were performed *in situ* on the rhombohedral PZT sample with x= 0.45 as a function of applied electric field at room temperature. The results are shown in Fig.3 where the (111), (200) and (220) pseudo-cubic reflections are plotted with no field applied (top) and with an applied field of 59 kV/cm field (bottom). The top part of the figure also shows data taken after removal of the field. As can be seen, measurements with the field applied show no shift along the polar [111] direction but, in contrast, there is a substantial shift along the [001] direction similar to that for the poled sample with x= 0.42 shown in Fig. 2, proving that the unit cell elongation induced by the application of a field during the poling process corresponds to the piezoelectric effect induced by the in-situ application of a field. Comparison of the two sets of data for x= 0.45 before and after the application of the field shows that the poling effect of the electric field at room temperature is partially retained after the field is removed, although the poling is not as pronounced as for the x= 0.42 sample in Fig. 2.

A quantification of the induced microstrain along the different directions has been made by measuring the peak shifts under fields of 31 and 59 kV/cm. In Fig. 4, $\Delta d/d$ is plotted *versus* the applied field, E, for the (200) and (111) reflections. These data show an approximately linear increase in $\Delta d/d$ for (200) with field, with $\Delta d/d = 0.30\%$ at 59 kV/cm, corresponding to a piezoelectric coefficient $d_{33} \approx 500$ pm/V, but essentially no change in the d-spacing for (111).

It is interesting to compare in Fig.4 the results of dilatometric measurements of the macroscopic linear elongation ($\Delta l/l$) on the same pellet, which must also reflect the effects of domain reorientation. At higher fields, this contribution diminishes and one could expect the $\Delta l/l$ vs. E curve to fall off between those for the [100] and [111] oriented grains, typical of the strain behaviour of polycrystalline ceramics [15]. Although such a trend is seen above 30 kV/cm, it is intriguing to note that be-

low this value, the macroscopic behavior is essentially the same as the microscopic behavior for the (200) reflection.

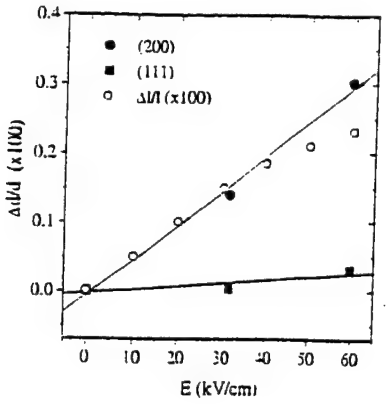

FIG. 4. Fractional change of d-spacing, $\Delta d/d$ for PZT with x= 0.45 from the rhombohedral (200) and (111) reflections as a function of electric field (closed symbols). Dilatometric measurements of the macroscopic $\Delta l/l$ for the same pellet are also shown (open circles)

We therefore conclude that the piezoelectric strain in PZT close to the morphotropic phase boundary, which produces such striking electromechanical properties, is not along the polar directions associated with the monoclinic distortion. This supports a model based of the existence of local monoclinic shifts superimposed on the rhombohedral and tetragonal displacements in PZT which has been proposed from a detailed structural analysis of tetragonal [13] and rhombohedral [14] PZT samples.

As demonstrated above, these high resolution powder data provide key information to understanding the piezoelectric effect in PZT. In particular, they allow an accurate determination of the elongation of the unit cell along the direction of the electric field, although they give no information about the dimensional changes occurring along the perpendicular directions, which would give a more complete characterization of the new structure induced by the electric field. It is interesting to note that in the case of the related ferroelectric system PZN-PT, the availability of single crystals has allowed Durbin *et al.* [7] to carry out diffraction experiments along similar lines at a laboratory x-ray source. Synchrotron x-ray experiments by the present authors are currently being undertaken on PZN-PT single crystals with Ti content of 4.5 and 8% under an electric field, and also on other ceramic PZT samples. Preliminary results on samples with x= 0.46 and 0.47, which are monoclinic at room temperature, have already been obtained. In these cases, the changes of the powder profiles induced by poling are so drastic that further work is needed in order to achieve a proper interpretation.

We thank A. M. Glazer, J.A. Gonzalo and K. Uchino for their stimulating dicussions, B. Jones and E. Alberta for assisting in the sample preparation, and A. L. Langhorn for his invaluable technical support. Financial support by the U.S. Department of Energy under contract No. DE-AC02-98CH10886, and by ONR under project MURI (N00014-96-1-1173) is also acknowledged.

[1] B. Jaffe, W.R. Cook, and H. Jaffe, Piezoelectric Ceramics, Academic Press, London (1971).
[2] X-h Du, U. Belegundu, and K. Uchino, Jpn. J. Appl. Phys. **36**, 5580 (1997).
[3] X-h Du, J. Zheng, U. Belegundu, and K. Uchino, Appl. Phys. Lett **72**, 2421 (1998).
[4] M. J. Haun, E. Furman, S-J. Jang, and L.E. Cross, Ferroelectrics **72**, 13(1989).
[5] J. Kuwata, K. Uchino, and S. Nomura, Jpn. J. Appl. Phys. **21**, 1298(1982).
[6] S-E. Park and T. R. Shrout, J. Appl. Phys. **82**, 1804 (1997).
[7] M. K. Durbin, E.W. Jacobs, J.C. Hicks, and S.-E. Parks, Appl. Phys. Lett. **74**, 2848 (1999).
[8] K.M. Rabe and E. Cockayne, in *First-Principles Calculations for Ferroelectrics: Fifth Williamsburg Workshop*, edited by R.E. Cohen (AIP, Woodbury,1998), p. 61.
[9] G. Saghi-Szabo, R.E. Cohen, and H. Krakauer, Phys. Rev. Lett. **80**, 4321 (1998).
[10] G. Saghi-Szabo, R.E. Cohen, and H. Krakauer, Phys. Rev. B **59**, 12771 (1999).
[11] L. Bellaiche and D. Vanderbilt, Phys. Rev. Lett. **83**, 1347 (1999).
[12] B. Noheda, D.E. Cox, G. Shirane, J.A. Gonzalo, L.E. Cross, and S-E. Park, Appl. Phys. Lett. **74**, 2059 (1999).
[13] B. Noheda, J. A. Gonzalo, L.E. Cross, R. Guo, S-E. Park, D.E. Cox, and G. Shirane,(to be published), e-print: cond-mat/9910066 .
[14] D.L. Corker, A.M. Glazer, R.W. Whatmore, A. Stallard, and F. Fauth, J. Phys.:Condens. Matter **10**, 6251 (1998).
[15] S.-E. Park, T.R. Shrout, P. Bridenbaugh, J. Rottenberg, and G. Loiacono, Ferroelectrics **207**, 519 (1998).

Appendix 13

Importance of random fields on the properties and ferroelectric phase stability of ⟨001⟩ oriented 0.7 $Pb(Mg_{1/3}Nb_{2/3})O_3$–0.3 $PbTiO_3$ crystals

D. Viehland[a] and J. Powers
Naval Sea Systems Command, Newport, Rhode Island 02841

L. E. Cross
Materials Research Laboratory, Penn. State University, State College, Pennsylvania 16802

J. F. Li
Department of Physics, University of Rhode Island, South Kingston, Rhode Island 02845

(Received 15 January 2001; accepted for publication 2 March 2001)

Temperature dependent dielectric constant measurements have been performed on ⟨001⟩ oriented 0.7 $Pb(Mg_{1/3}Nb_{2/3})O_3$–0.3 $PbTiO_3$ crystals. These investigations have revealed an irreversible secondary transformation between a normal ferroelectric state and a relaxor ferroelectric state with increasing temperature. The results demonstrate that the anisotropy of the high performance piezocrystal state is only metastably locked in under application of field. Clearly, local random fields play a crucial role upon the ferroelectric phase stability and properties of ⟨001⟩ oriented piezocrystals. © *2001 American Institute of Physics.* [DOI: 10.1063/1.1368371]

Single crystals of $Pb(Mg_{1/3}Nb_{2/3})O_3$–$PbTiO_3$ (PMN–PT) and $Pb(Zn_{1/3}Nb_{2/3})O_3$–$PbTiO_3$ (PZN–PT) are currently under investigation as high performance piezoelectric actuator and transducer materials. Efforts have focused on compositions close to the morphotropic phase boundary (MPB) between rhombohedral (FE_r) and tetragonal (FE_t) ferroelectric phases. In ⟨001⟩ oriented crystals of FE_r close to the MPB, electrically induced strains and electromechanical coupling coefficients of up to 1.2×10^{-2} and 0.94 have been reported, respectively.[1–4]

The origins of the high electromechanical performance have been attributed to an electrically induced phase transformation between the FE_r and FE_t states.[3,4] Recently, a metastable orthorhombic ferroelectric (FE_o) state has been shown to exist close to the MPB.[5] Furthermore, other recent investigations have shown that this FE_o state transforms to a monoclinc ferroelectric state (FE_m) under electrical field directed along the ⟨001⟩.[6] Removal of the field results in the re-stabilization of the FE_o state. The c lattice parameter of the FE_m state is ~4.09 A, which is close to that of the FE_t phase. Clearly, the phase transformational sequence in ⟨001⟩ oriented piezocrystals is complicated.

The purpose of this letter is to demonstrate that ⟨001⟩ oriented crystals of MPB compositions of PMN–PT undergo an irreversible transition at temperatures significantly below T_{max}, from a poled condition (which is the high electromechanical performance condition) to a relaxor ferroelectric state with pseudocubic symmetry. The results demonstrate the importance of random fields, and support a concept in which the unique properties of PMN–PT and PZN–PT piezocrystals are due to meso level contributions.

⟨001⟩ oriented 0.7 $Pb(Mg_{1/3}Nb_{2/3})O_3$–0.3 $PbTiO_3$ grown by a flux method have been obtained from Rockwell International Science Center (Thousand Oaks, CA). The crystals were of dimensions $0.05\times0.5\times0.5$ mm. The specimens were electroded with gold and poled. The dielectric response was measured as a function of frequency and temperature. The frequencies used were between 20 and 10^6 Hz. Measurements under zero dc electrical bias were made in the temperature range of 30–230 °C on heating and subsequent recooling at a rate of 4 °C/min using a Delta Design oven. Measurements were made using an automated HP 4284 LCR meter.

Figure 1(a) shows the dielectric constant as a function of temperature. Data are shown for both increasing and subsequently decreasing temperature sweeps. Initially, measurements were started from the poled condition. On heating, two peaks can clearly be seen at ~90 °C (T_m) and ~125 °C (T_{max}). In the temperature range $25\,°C<T<T_m$, the dielectric constant can be seen to be frequency independent, and to increase significantly from ~6000 to ~35000 with increasing temperature. For $T_m<T<T_{max}$, frequency dependence became evident. Also, the value of T_{max} can clearly be seen to be frequency dependent, typical of a ferroelectric relaxor.[7] On subsequent recooling, strong ferroelectric relaxor characteristics were observed, with no secondary transformation at lower temperatures. Figure 1(b) shows the temperature dependent dielectric constant on a secondary heating and subsequent recooling measurement. These data reveal only a single peak near T_{max}. Clearly, the additional dielectric peak in Fig. 1(a) at T_m is irreversible.

The results in Fig. 1(a) demonstrate a "macro to micro domain" transition, similar to that previously reported for La modified PZT (PLZT) polycrystalline ceramics.[8] A macrodomain state is metastably locked in under electric field, however, upon thermal cycling this state is not recovered. Figure 2 shows T_{max} as a function of measurement frequency. Analysis of these data with the Vogel–Fulcher relationship yielded a freezing temperature (T_f) of ~90 °C.[9] Comparisons will reveal that T_f is close to the temperature of the secondary phase transformation on heating in Fig. 1(a).

First principles derived approaches have recently been

[a]Electronic mail: viehlandd@npt.nuwc.navy.mil

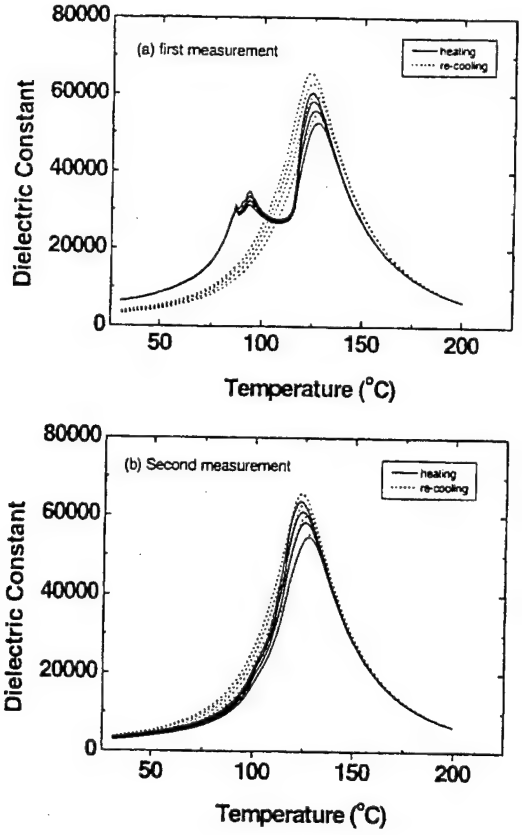

FIG. 1. Temperature dependent dielectric response for a ⟨001⟩-oriented PMN–PT crystal. (a) First measurement taken on heating and subsequent recooling, and (b) second measurement taken right after the first on heating and subsequent recooling. Data are shown for measurement frequencies of 10^2, 10^3, 10^4, and 10^5 Hz.

used to predict the phase stability and properties of MPB piezocrystals.[10] In a compositionally homogeneous approximation, only FE_r and FE_t phases were predicted to be stable at the MPB, as conventionally believed. However, upon including an on-site alloying self energy term (up to 4th power), a FE_m state was predicted to exist that effectively bridged the FE_r and FE_t states. It is important to realize that this alloying self energy term is a random field approximation, and that it is only possible to stabilize the FE_m state by randomly quenched disorder. A phenomenological extension of this concept was then used to thermodynamically model MPB systems.[11] It was found that 6th power expansions of the polarization were insufficient to stabilize a FE_m state, rather 8th power terms were required. It was conjectured that

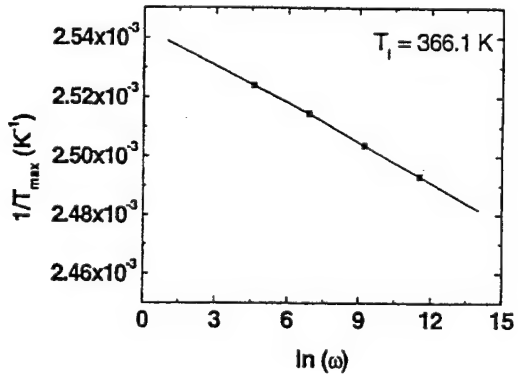

FIG. 2. Vogel–Fulcher fit of T_{max} as function of measurement frequency ω for the dielectric peak near 90 °C in Fig. 1(a).

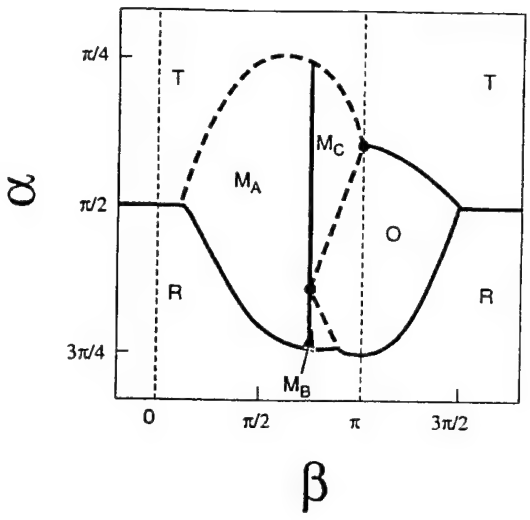

FIG. 3. Calculated phase diagram using 8th order thermodynamic approach. Taken from Ref. 11. The variables α and β refer to phase angles through which the polarization was rotated in the thermodynamic calculations.

random fields (RFs) could be the origins of the importance of the higher anharmonicity. The phase diagram predicted by this model is shown in Fig. 3 where M_A, M_B, and M_C refer to ferroelectric phases in which the polarization is confined to the ⟨*hhk*⟩ (i.e., $h>k$), ⟨*hhk*⟩ (i.e., $h<k$), and ⟨$0k1$⟩ planes, respectively.[11]

The assumption underlying both the first principles derived and the phenomenological approaches is that ferroelectric order is homogeneous, and remains so under applied field. This may be the case for MPB compositions of $Pb(Zr, Ti)O_3$. However, in the case of PMN–PT piezocrystals, a ferroelectric relaxor state exists in the unpoled condition characterized by polar clusters and strong frequency relaxation. In this case, the random field contributions to the total energy no longer simply provide a corrective factor, but rather induce a random or spherical bond state (i.e., a glassy condition).[9,12] Accordingly, anisotropy is only metastably locked in under applied field.

We believe that random fields are the key elements in understanding poled oriented piezocrystals. Recently, a symmetrically adaptive ferroelectric mesostate model was proposed for ⟨001⟩ oriented piezocrystals.[5,13] Random fields were a crucial part of this model, in addition to meso level symmetry adaptations to achieve strain accomodation.[14] Accordingly, metastable FE_o and FE_m states were shown to exist, as a consequence of the FE_r–FE_t transformation.[5,13] "Polarization rotation" can occur within these meso states from ⟨111⟩ to ⟨110⟩, and subsequently to ⟨001⟩, via the ⟨$0k1$⟩ plane. This would be consistent with experimental neutron diffraction observations[6] of the FE_m state being M_c in PZN–PT (and presumably PMN–PT), and inconsistent with first principles and phenomelogical predictions[10,11] where polarization would be confined to the ⟨*hhk*⟩ plane (i.e., M_a or M_b)[11] near a MPB, such as for the M_a state of MPB PZT.[15]

In summary, the results illustrate the key role of quenched random fields upon the ferroelectric phase stability and properties of ⟨001⟩ oriented crystals. These systems are intrinsically poised near a ferroelectric relaxor state, in addition to a MPB. The high performance characteristics of pi-

ezocrystals result from symmetry adaptations on the meso scale in the vicinity of quenched disorder, which occurs within normal micron sized domains.

This work was supported by the Office of Naval Research.

[1] J. Kuwata, K. Uchino, and S. Nomura, Ferroelectrics **37**, 579 (1981).
[2] J. Kuwata, K. Uchino, and S. Nomura, Jpn. J. Appl. Phys., Part 1 **21**, 1298 (1982).
[3] S. Park and T. R. Shrout, J. Appl. Phys. **82**, 1804 (1997).
[4] S. Park and T. R. Shrout, IEEE Trans. Ultrason. Ferroelectr. Freq. Control **44**, 1140 (1997).
[5] D. Viehland, J. Appl. Phys. **88**, 4794 (2000).
[6] B. Nohea, D. Cox, G. Shirane, S. Park, L. E. Cross, and Z. Zhong, Phys. Rev. Lett. (submitted) (See www.arXiv.cond-mat/0009227).
[7] L. E. Cross, Ferroelectrics **76**, 249 (1987).
[8] Y. Xi, C. Zhilli, and L. Cross, Ferroelectrics **54**, 163 (1983).
[9] D. Viehland, M. Wuttig, and L. E. Cross, J. Appl. Phys. **68**, 2916 (1990).
[10] L. Bellaiche, A. Garcia, and D. Vanderbilt, Phys. Rev. Lett. **84**, 5427 (2000).
[11] D. Vanderbilt and M. Cohen, Phys. Rev. Lett. (submitted) (See www.arXiv.cond-mat/009337).
[12] R. Blinc, Proceedings of the IXth International Workshop on the Fundamentals of Ferroelectrics, Williamsburg, VA, 1999.
[13] D. Viehland, J. Powers, L. Ewart, and J. Li, J. Appl. Phys. **88**, 4907 (2000).
[14] D. Viehland and Y. Chen, J. Appl. Phys. **88**, 6696 (2000).
[15] B. Noheda, J. Gonzalo, L. E. Cross, R. Guo, S. Park, D. Cox, and G. Shirane, Phys. Rev. B **61**, 8687 (1999).

Appendix 14

INSTITUTE OF PHYSICS PUBLISHING JOURNAL OF PHYSICS: CONDENSED MATTER

J. Phys.: Condens. Matter 13 (2001) L33–L38 www.iop.org/Journals/cm PII: S0953-8984(01)17769-6

LETTER TO THE EDITOR

Domain geometry engineering and domain average engineering of ferroics

J Fousek[1,2], D B Litvin[3] and L E Cross[2]

[1] Department of Physics and International Centre for Piezoelectric Research, Liberec University of Technology, Liberec, CZ 46117, Czech Republic
[2] Materials Research Laboratory, The Pennsylvania State University, University Park, PA 16802, USA
[3] Department of Physics, The Pennsylvania State University, Berks Campus, Reading, PA 19610, USA

Received 5 October 2000

Abstract

Multidomain samples of ferroics (ferroelectrics, ferroelastics, and related materials) with *fixed* geometrical distribution of domains can offer new macroscopic properties required for particular applications. Two extreme cases of such applications are defined. In *domain-geometry-engineered* samples of ferroic crystals, the spatial distribution of domains and thus the spatial distribution of tensorial properties is tuned to correspond to the k-vectors of applied electric, optical or acoustic fields. For a given wavelength, the size, geometry, and distribution of domains give rise to a qualitatively new kind of response specified by the symmetry of the multidomain system. In *domain-average-engineered* samples of ferroic crystals, the specimen is subdivided into a very large number of domains, representing μ domain states where μ is smaller than the theoretically allowed maximum number, and forming a regular or irregular pattern. Its response to external fields is roughly described by tensorial properties averaged over all of the domain states involved. The effective symmetry of the domain-average-engineered system is given by a point group H and we show how it can be determined. As an example, all groups H are specified for domain-average-engineered samples which can arise in a material undergoing the phase transition with symmetry change from $m\bar{3}m$ to $3m$.

Ferroic materials (and here we concentrate on non-magnetic materials, i.e. on ferroelectrics, ferroelastics, and higher-order ferroics) play an essential role in a number of technical applications. In some of them, dynamic domain processes are essential (e.g. thin-film memories, electron emitters) while in others the static distribution domains in the sample play the crucial role. In this contribution we concentrate on the latter case and wish to specify a clear distinction between two kinds of such static multidomain system.

We have in mind materials undergoing a structural phase transition from the parent phase of point group G into the ferroic phase of symmetry $F \subset G$ (such a material is referred to

0953-8984/01/010033+06$30.00

as belonging to the species $G - F$). This leads necessarily to the possibility of a coexistence of ν domain states [1]; $\nu = |G|/|F|$ where $|A|$ is the order of the group A. Assuming that domain walls are of negligible thickness compared with the size of the domains, there are two different ways of specifying—and utilizing—properties of a multidomain sample with a *fixed* distribution of domains; we propose to refer to them as *domain geometry engineering* and *domain average engineering*, respectively. It is the purpose of this contribution to give their definitions and in particular to specify symmetry properties of domain-average-engineered multidomain samples.

First, we consider *domain geometry engineering*. Consider a multidomain sample for which the geometry of the spatial distribution of domains and therefore that of the tensorial material coefficients is specified. Macroscopic responses of such samples to external fields (forces) of defined frequency are determined by this distribution. If the applied fields are static, the response of a multidomain sample is primarily determined by the spatial distribution of tensorial properties (domains) and of the applied field, and codetermined by the boundary conditions along domain walls. (Only in cases of the simplest geometry of domains, namely a single system of parallel domain walls in the case of ferroelastic species, can the latter be eliminated.) As an example, consider a multidomain piezoelectrically active sample. The spatial distribution of strain is

$$\varepsilon_{jk}(\boldsymbol{r}) = d_{ijk}(\boldsymbol{r})E_i(\boldsymbol{r}) \tag{1a}$$

$$d_{ijk}(\boldsymbol{r}) = d_{ijk}^{(\alpha)} f^{(\alpha)}(\boldsymbol{r}) \tag{1b}$$

where d_{ijk} stands for the piezoelectric tensor, the factor $f^{(\alpha)}(\boldsymbol{r}) = 0$ or 1, and α denotes the domain state: $\alpha = 1, 2, \ldots, \mu$ with $\mu \leqslant \nu$. Domain geometry engineering related to *dynamic external fields* is of particular interest. The k-vector of the applied fields defines the wavelength whose magnitude is chosen to be appropriately related to the size of domains and whose direction is correlated with the domain geometry. For a given wavelength, the size, geometry, and distribution of domains give rise to a qualitatively new kind of response specified by the symmetry of the multidomain system. In the example specified above, we expect the presence of new piezoelectric resonance frequencies. It was this case which was suggested by Newnham *et al* [2], offering new resonance modes of a two-domain sample. Recently, more involved multidomain piezoelectric systems were suggested and realized [3] in crystals of $LiNbO_3$ and $LiTaO_3$. Referred to as acoustic superlattices, they can be used to generate and detect ultrasonic waves with frequencies in the range up to several hundreds of MHz. Another example, which has received unusual attention, is quasi-phase-matched optical multipliers. When the conventional phase-matching condition ($n_{2\omega} = n_{\omega}$) cannot be realized in a particular material because of unsuitable dispersion of refractive indices, often a quasi-phase-matched system can be constructed which offers a high integrated non-linear optical response leading to frequency doubling [4]. This requires that a periodic domain pattern be fabricated with a period twice the coherence length l_c. Such domain-shape-engineered systems are now widely used. An even more intricate geometry-engineered domain pattern has been designed [5] in which two geometrically different building blocks A, B, each containing two domains with antiparallel spontaneous polarizations, are arranged to form a Fibonacci sequence. This leads to the possibility of second-harmonic light generation simultaneously for several optical frequencies.

While domain-geometry-engineered systems have been repeatedly realized and theoretically analysed, the alternative approach to studying and utilizing multidomain ferroic samples with static chaotic distribution of domains has only recently become extremely attractive. By the term *domain average engineering* we mean a situation in which the ferroic sample is subdivided into a very large number of domains, representing μ domain states where

$\mu < \nu$, and forming a regular or irregular pattern. Ideally, the domain size is expected to be much smaller than the wavelength of externally applied fields. Here, in contrast to the case for domain shape engineering, the spatial distribution of tensorial material coefficients is not defined or is irrelevant. The response of the sample can be to some approximation described by tensorial properties averaged over all domain states involved. Considering, as an example, again a sample consisting of piezoelectrically active domains, we expect for the multidomain sample

$$\bar{\varepsilon}_{jk} = \bar{d}_{ijk}\bar{E}_i \tag{2a}$$

$$\bar{d}_{ijk} = \frac{1}{V}\sum_{\alpha=1}^{\mu} d_{ijk}^{(\alpha)} V^{(\alpha)} \qquad \mu < \nu. \tag{2b}$$

Both equations (1), (2) can be easily generalized for tensors of higher order.

Recently, a case of this character was considered [6–8] to allow discussion of piezoelectric properties of PZN-PT single crystals poled along one of the {001} directions. Assuming that the material went through the phase transition from $G = m\bar{3}m$ to $F = 3m$, poling along [100] supports the coexistence of four domain states with spontaneous polarization along the directions [111], [1$\bar{1}$1], [11$\bar{1}$], and [1$\bar{1}\bar{1}$], with equal probability. In this statement, it is assumed that the domain wall orientation (i.e. mechanical compatibility) aspects can be neglected. In fact, in samples of ferroelastic crystals, strictly speaking, only one set of mechanically permissible parallel domain walls is allowed [9] while in real samples walls of various orientations coexist connected with additional elastic strains, paid for by increased elastic energy [10].

We now discuss the symmetry of *domain-average-engineered* samples in which the volumes of the domain states represented are identical, i.e. $V(\alpha) = V/\mu$. Such situations can be achieved by cooling samples through their phase transition temperatures under properly oriented stresses, electric fields or combinations of these. We introduce a classification of domain-average-engineered ferroic samples and determine their average point symmetries. This average symmetry is taken to be the symmetry of the subset of domain states contained in the multidomain ferroic sample.

Consider the phase transition from G to F. The symmetry analysis is based on the coset decomposition of the point group G with respect to its subgroup F, i.e.

$$G = F + g_2F + g_3F + \cdots + g_\nu F$$

where the elements g_i are the coset representatives of the decomposition and $g_1 = 1$. We denote the ν domain states which may arise at the transition as $S_1, S_2, \ldots, S_\nu$. The symmetry groups F_i of the domain states and the relative orientations of the domain states and their polarizations P_i are all determined by the coset representatives, i.e. $F_1 = F$, $F_i = g_iF_1g_i^{-1}$, $S_i = g_iS_1$, and $P_i = g_iP_1$, $i = 2, 3, \ldots, \nu$. The closure of the group G under multiplication implies a permutation of the cosets of the coset decomposition and in turn a permutation of the domain states S_i under elements g of G. The action of an element g of G on S_i is defined as $gS_i = gg_iS_1 = g_jfS_1 = g_jS_1 = S_j$, where f is an element of F, and the domain state S_i is transformed by the element g into the domain state S_j. The action of an element g of G on a subset of domains is denoted by $g\{S_1, S_2, \ldots, S_\mu\} = \{gS_1, gS_2, \ldots, gS_\mu\}$.

Two subsets of domains $\{S_1, S_2, \ldots, S_\mu\}$ and $\{S'_1, S'_2, \ldots, S'_\mu\}$ are said to belong to the same class of subsets of domains if there exists an element g of G such that $g\{S_1, S_2, \ldots, S_\mu\} = \{gS_1, gS_2, \ldots, gS_\mu\} = \{S'_1, S'_2, \ldots, S'_\mu\}$. The symmetry group H of a subset of domains $\{S_1, S_2, \ldots, S_\mu\}$ is defined as the group of all elements g of G which leave the set invariant, i.e. $g\{S_1, S_2, \ldots, S_\mu\} = \{S_1, S_2, \ldots, S_\mu\}$. The group H represents the effective symmetry of the domain-average-engineered system consisting of the subset of domains $\{S_1, S_2, \ldots, S_\mu\}$.

As an example, we consider the phase transition from $G = m\bar{3}m$ to $F = 3_{xyz}m_{\bar{x}y}$. Here $\nu = 8$. The indexing of the domain states, the corresponding coset representatives of the coset decomposition of G with respect to F, the symmetry groups, and the corresponding polarizations in each domain state are given in table 1.

Table 1. Domain state index, coset representative, symmetry group, and polarization.

Index i	Coset representative g_i	$F_i = g_i F_1 g_i^{-1}$	$P_i = g_i P_1$
1	1	$3_{xyz}m_{\bar{x}y}$	(A, A, A)
2	2_x	$3_{\bar{x}yz}m_{\bar{y}z}$	$(A, -A, -A)$
3	2_z	$3_{xy\bar{z}}m_{\bar{x}y}$	$(-A, -A, A)$
4	2_y	$3_{x\bar{y}z}m_{\bar{x}z}$	$(-A, A, -A)$
5	$\bar{1}$	$3_{xyz}m_{\bar{x}y}$	$(-A, -A, -A)$
6	m_x	$3_{\bar{x}yz}m_{\bar{y}z}$	$(-A, A, A)$
7	m_z	$3_{xy\bar{z}}m_{\bar{x}y}$	$(A, A, -A)$
8	m_y	$3_{x\bar{y}z}m_{\bar{x}z}$	$(A, -A, A)$

All subsets of these domain states have been classified into classes as defined above. In table 2 we list one subset of domain states from each class. Each subset is denoted by listing, between square brackets, the indices of the domain states contained in that subset, the indices having been given in table 1, e.g. the subset $\{S_1, S_3, S_5\}$ is denoted by [135]. In the right-hand column is the subgroup H of elements of G which leave the corresponding subset invariant. This table, in fact, represents the list of domain-average-engineered systems which can arise in a material undergoing a phase transition from $m\bar{3}m$ to $3m$.

Table 2. Representative subsets of domain states for the species $m\bar{3}m - 3m$ and the subgroups of $m\bar{3}m$ which leave them invariant.

Representative subset	Symmetry H of the subset
[1] or [2345678]	$3_{xyz}m_{\bar{x}y}$
[13] or [245678]	$m_{xy}m_{\bar{x}y}2_z$
[15] or [234678]	$\bar{3}_{xyz}m_{\bar{x}y}$
[16] or [234578]	$m_x m_{\bar{y}z}2_{yz}$
[123] or [45678]	$3_{xyz}m_{xz}$
[135] or [24678]	$m_{\bar{x}y}$
[136] or [24578]	m_{xy}
[1234]	$\bar{4}3m$
[1235]	$m_{\bar{x}z}$
[1238]	$3_{x\bar{y}z}m_{\bar{x}z}$
[1356]	$2_{\bar{x}z}$
[1357]	$m_{xy}m_{\bar{x}y}m_z$
[1368]	$4_z m_x m_{xy}$

In figure 1, for each subset listed in table 2, we schematically represent the array of domain states and their polarizations associated with the domain states of each subset. Each domain state is denoted by a heavy dot at a corner of the cube. This represents a polarization from the centre of the cube to that corner—that polarization given in table 1 associated with the corresponding domain state. Subfigure [1] denotes the single-domain state with polarization

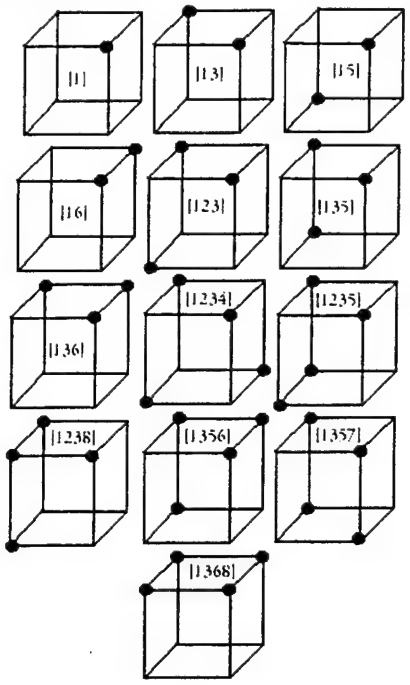

Figure 1. Graphical representation of the subsets of domain states whose symmetries are specified in table 1. Points at the cube vertices represent spontaneous polarization vectors; the origin is in the centre of the cube. The numbering is that of the indices of the domains and polarizations given in table 1.

in the [111] direction. The figure denoted by [1368], e.g., denotes a multidomain sample in which the following polarization vector directions are equally represented: [111], $[\bar{1}\bar{1}1]$, $[1\bar{1}1]$, and $[\bar{1}11]$. The corresponding symmetry groups of all these multidomain systems are listed, as already pointed out, in the right-hand-side column of table 2.

Taking into account the distribution of polarization vectors and corresponding strain tensors, one can determine which external forces should be applied in order to obtain any of the domain-average-engineered systems listed in table 1. The trivial example is the system [1] produced by the electric field $\boldsymbol{E}$ along [111]. The system [1368], discussed above (see references [6–8]) will be produced by the field along [001] while the system [16] requires the application of the field along [011]. The combination [15] requires the application of a uniaxial stress along [111] while the system [13] calls for the application of both an electric field along [001] and a uniaxial stress along $[\bar{1}10]$.

It is understood that in this symmetry approach we leave behind problems of coercive fields and stresses as well as, as already mentioned, problems of domain coexistence connected with their mechanical compatibility. It seems obvious that domain average engineering can successfully lead to the formation of crystalline systems with new desired properties, in particular in crystals where the domain size is small.

Each of the methods of domain engineering specified above can open a new vista of materials research possibilities in the area of ferroic materials and lead to multidomain assemblies with new desired properties.

JF appreciates the support of the Ministry of Education of the Czech Republic (Project No VS96006) and the assistance of the Materials Research Laboratory, The Pennsylvania State University; DBL acknowledges the hospitality of Dr V Kopsky and the Institute of Physics of the Czech Academy of Sciences, and the support of the Czech Ministry of Education under Grant ME336(1999) and of the National Science Foundation under Grants No DMR-9722799 and No DMR 0074550.

References

[1] Aizu K 1970 *Phys. Rev.* B **2** 754–72
[2] Newnham R E, Miller C S, Cross L E and Cline T W 1975 *Phys. Status Solidi* a **32** 69–78
[3] Chen Y F, Zhu A N, Zhu Y Y, Ming N B, Jin B B and Wu R F 1997 *Appl. Phys. Lett.* **70** 592–4
[4] Duan F, Ming N B, Hong J F, Yang Y S, Zhu J S, Yang Z and Wang Y N 1980 *Appl. Phys. Lett.* **37** 607–9
[5] Zhu S N, Zhu Y Y, Qin Y Q, Wang H F, Ge C Z and Ming N B 1997 *Phys. Rev. Lett.* **78** 2752–5
[6] Park S E and Shrout T R 1997 *J. Appl. Phys.* **82** 1804–11
[7] Wada S, Park S E, Cross L E and Shrout T R 1999 *Ferroelectrics* **221** 147–55
[8] Yin J and Cao W 2000 *J. Appl. Phys.* **87** 7438–41
[9] Fousek J and Janovec V 1969 *J. Appl. Phys.* **40** 135–42
[10] Salje E K H and Ishibashi Y 1996 *J. Phys.: Condens. Matter* **8** 8477–95

Appendix 15

Ferroelectrics, 2001, Vol. 252, pp. 171-180
Reprints available directly from the publisher
Photocopying permitted by license only

Engineering Multidomain Ferroic Samples

J. FOUSEK[ab] and L. E. CROSS[b]

[a]*Dept. of Physics and International Center for Piezoelectric Research, University of Technology, Liberec, 46117 Czech Republic and* [b]*Materials Research Laboratory, The Pennsylvania State University, University Park, PA 16802, U.S.A.*

(Received June 2, 2000)

The existence of domains is essential in many practical applications of ferroics. Here we discuss devices in which a *fixed* spatial distribution of domains plays the significant role. Depending on the prevailing attributes of multidomain single crystals, three different possibilities can be distinguished. In *domain-geometry-engineered* samples the spatial distribution of domains is tuned to correspond to the *k*-vectors of fields propagating through the material. In *domain-average-engineered* samples the crystal is subdivided into a very large number of domains, representing a *limited* number of domain states. In *domain-wall-engineered* samples the characteristics of static walls can play an essential role in the averaged macroscopic properties. Examples illustrating these approaches are given.

Keywords: domain engineering; domain-geometry engineering; domain-average-engineering; domain-wall-engineering; multidomain ferroics; static domain pattern

1. INTRODUCTION

Practical applications of ferroics (undergoing a phase transition from the point group G to F) are of two basically different characters: those which rely on properties of single domain samples and those in which the presence of domains is essential. The latter can be categorized into

devices based on dynamical domain processes or those in which a static distribution of domains plays a significant role. Here we discuss the last mentioned case: general characteristics of multidomain samples with fixed spatial distribution of domains.

Depending on the prevailing attributes of multidomain single crystal samples, several possibilities can be distinguished. Those discussed in the following sections 2 to 4 differ in general features of the geometry of domains and it is assumed that domain walls are of negligible thickness. In the last considered case, the thickness of domain walls is finite and specimens exhibit large wall density. Aspects of preparation and properties of such samples are discussed in the section 5.

2. DOMAIN-GEOMETRY-ENGINEERED FERROIC SAMPLES

As early as in 1964, Miller[1] showed that a regular pattern consisting of 180^0 domains in $BaTiO_3$ with a period corresponding to the coherence length could substantially increase the effectiveness of optical second harmonic generation. The idea is based on two factors: a) domain states differ in the sign of nonlinear optical coefficient, b) the width of domains is tuned to the coherence length. It was Feng Duan et al. [2] who succeeded in manufacturing a periodic domain pattern in $LiNbO_3$ and proved its efficiency in nonlinear optics. More recently, S. N. Zhu et al.[3] initiated an essential progress in this field by producing a domain pattern whose geometry corresponds to a Fibonacci superlattice and which makes it possible to realize second harmonic generation for multiple wavelengths. But the significance of domain patterns with engineered geometry was proved also in acoustics. Meeks at el.[4] produced tunable acoustic systems based on spatial modulation of elastic coefficients in a periodic domain pattern in NdP_5O_{14} while Y. Y. Zhu et al.[5] succeeded in producing transducers up to 800 MHz based on spatial modulation of piezoelectric coefficients in multidomain $LiNbO_3$.

In all these applications the periodicity of domain patterns corresponds to $\boldsymbol{k}$-vectors of propagating waves and the multidomain domain systems represent just two domain states. Up to now less than 10 ferroics have been utilized in this area, and in any of these materials the total number of domain states $\nu = |G| / |F| = 2$ (here $|G|$ and $|F|$ stand for the order of the parent and ferroic phase point groups, resp.). This is understandable since to produce a regular pattern in ferroics with $\nu > 2$ in which only two domain states are involved is not trivial.

To solve this task in particular cases experimentally is, however, possible. In fact the nature itself shows that patterns with a regular geometry of a limited number $\mu < \nu$ of domain states can be materialized. Several observations have been made of domain patterns with regular geometry, fulfilling this requirement. As an example, we refer to the Forsbergh's square-net pattern[6] shown in Fig.1, which has been repeatedly observed in $BaTiO_3$ single crystals as well as ceramic grains. It might be inspiring to examine its macroscopic properties for external fields with both $k = 0$ and $k \neq 0$, based on its symmetry characteristics.

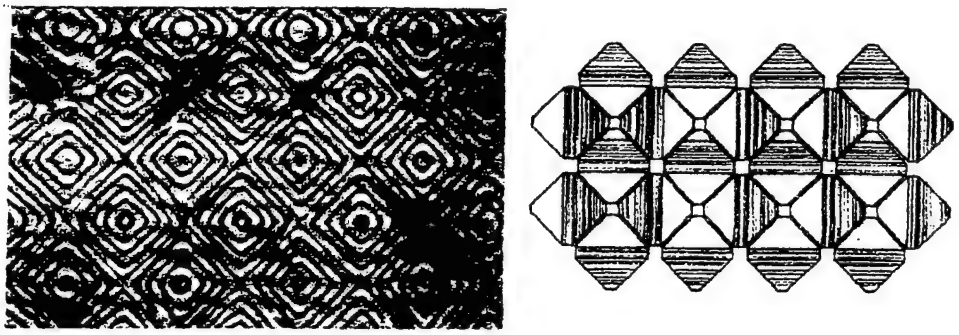

FIGURE 1 Example of a "natural" multiaxial domain-geometry engineered system: the Forsbergh's square-net pattern in tetragonal $BaTiO_3$. Left: microscopic picture; right: arrangement of tetrahedral building blocks. From Ref. [6].

Several other multiaxial threedimensional and reproducible patterns have been observed under natural conditions and there is little doubt that they could be produced artificially. To mention just one more example, we refer to the Arlt's[7] patterns α and β; till now they have been observed only in ceramic grains but very probably they could be created in crystals under properly designed external forces. Again, in order to deliberate about their properties, the symmetry analysis would be the first step to take.

Indeed, regular domain systems can offer unexpected symmetry properties. Thus, for instance, the well known Hallbach array of magnets with asymmetric distribution of magnetic field can have a simple analogy in thin ferroelectric plates containing a regular system of 90^0 domain pairs. While in the latter case, because of the existence of free charges, we do not expect pronounced external depolarizing field

effects, macroscopic properties of the array could offer new applicable aspects.

3. DOMAIN-AVERAGE-ENGINEERED FERROIC SAMPLES

In contrast to the previous cases, in *domain-average-engineered* samples of ferroic crystals the specimen is subdivided into a very large number of domains, representing just $\mu < \nu$ domain states. Such situations can be achieved by cooling samples through their phase transition temperatures under properly oriented stresses, electric fields or their combinations. The geometry of domains is irregular. The sample's response to external fields is roughly described by tensorial properties averaged over all involved domain states. Thus, e.g. for the piezoelectric response we can write in the zeroth approximation

$$\bar{\varepsilon}_{jk} = \bar{d}_{ijk}\bar{E}_i, \quad \bar{d}_{ijk} = \frac{1}{V}\sum_{\alpha=1}^{\mu} d_{ijk}^{(\alpha)} V^{(\alpha)}.$$

Here $V(\alpha)$ denotes the volume occupied by the domain state α.

In recent years, Park et al.[8,9], Yin and Cao[10] and other authors considered a case of this character to discuss piezoelectric properties of PZN-PT single crystals poled along one of the {001} directions. Assuming that the material went through the phase transition from G = $m\bar{3}m$ to F = $3m$, the poling along [100] supports the coexistence of four domain states with spontaneous polarization along the directions [111], [$1\bar{1}1$], [$11\bar{1}$] and [$1\bar{1}\bar{1}$], with equal probability. In this statement, it is assumed that the domain wall orientation aspects (e.g. mechanical compatibility) can be neglected. In fact, in samples of ferroelastic crystals strictly speaking, only one set of mechanically permissible parallel domain walls is allowed[11] while in real samples walls of various orientations coexist connected with additional elastic strains, paid by increased elastic energy.

The symmetry aspects of domain–average–engineered samples can be discussed in a general way. The task is to determine the average point symmetry H, i.e. the symmetry of the subset of domain states contained in the multidomain sample. This was addressed by Fousek et al.[12] and the procedure can be facilitated by the use of the computer programme of Schlesmann and Litvin.[13]

As an example, in Fig.2 we reproduce[12] the average symmetry groups H of six selected subsets of domain states (out of 13 leading to

different symmetries F) which arise in the phase transition specified above (here $\mu = 8$). States are represented by self-explanatory numbers and dots indicating the directions of $\mathbf{P}_S$ vectors.

Representative subset	Subset symmetry H
[1] 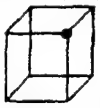	$3_{xyz}\, m_{\bar{x}y}$
[13] 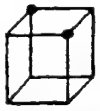	$m_{xy}\, m_{\bar{x}y}\, 2_z$
[15] 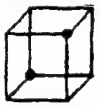	$\bar{3}_{xyz}\, m_{\bar{x}y}$
[136] 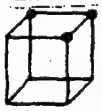	m_{xy}
[1356] 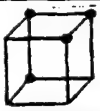	$2_{\bar{x}z}$
[1368] 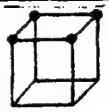	$4_z m_x m_{xy}$

FIGURE 2 Examples of subsets of domain states corresponding to the transition $m\bar{3}m - 3m$ and their symmetries.

Taking into account the distribution of polar vectors and corresponding strain tensors, one can determine which external forces should be applied in order to obtain any of the domain-average-engineered systems. The trivial example is the subset [1] produced by the electric field **E** along [111]. The subset [1368], discussed[8-10] before, will be produced by the field along [001] while the combination [15] requires the application of a uniaxial stress along [111]. The subset [13] calls for the application of both electric field along [001] and uniaxial stress along [$\bar{1}$10].

In addition to the applied fields, electrical or mechanical, there are other approaches which can eliminate particular domain states in a

given ferroic material. The stimulating example is based on chiral dopants. Keve et al.[14] showed that doping TGS with *L*-α-alanine prefers just one of the two domain states with antiparallel $\mathbf{P}_S$. Zikmund and Fousek[15,16] generalized this approach and showed that chiral substitients can reduce the number of domain states by a factor of two in a number of ferroic species.

It is understood that in the mentioned approaches we leave behind the problems of domain coexistence connected with their mechanical compatibility. It seems obvious that domain average engineering can succesfully lead to formation of crystalline systems with new desired properties in particular in crystals where the domain size is small. Crystalline systems exhibiting tweed microstructures similar to those observed in La-modified lead titanate[17] or PLZT[18] might serve as candidates for this approach.

4. PHASE- AND- DOMAIN-AVERAGE ENGINEERED FERROICS

The domain-average-engng concept can be generalized to systems in which the prescribed domain states represent two or more ferroic species. Such multiphase situations occur in PZT ceramics near the morphotropic boundary and originate[19] in concentration gradients as well as in the independent nucleations of the ferroic phases since the transition is of the 1st order. It appears that PZN-PT single crystals with a pronounced piezoelectric response contain blocks of both tetragonal and rhombohedral symmetry[20]. In the basic approximation, the piezoelectric coefficient of a properly poled sample is then described by

$$\bar{d}_{ijk} = \frac{1}{V_1}\left[\sum_{\alpha=1}^{\mu 1} d_{ijk}^{(\alpha)} V^{(\alpha)}\right] + \frac{1}{V_2}\left[\sum_{\beta=1}^{\mu 2} d_{ijk}^{(\beta)} V^{(\beta)}\right] + \\ + \Delta d_{ijk}(walls) + \Delta d_{ijk}(phase\ bndrs)$$

where μ1 and μ2 are numbers of domain states represented in the phase 1 and 2, resp., after poling. The high piezoelectric response of PZN-PT single crystals originates in the combination of intrinsic coefficients $d_{ijk}^{(\alpha)}$, $d_{ijk}^{(\beta)}$ as well as in the extrinsic contributions due to the motion of domain walls and phase boundaries. The question what role is played by any of these contributions is still to be solved.

assisted nucleation energies to produce domains in real time) looks also promissing.

6. CONCLUSIONS

Till now, the field of domain geometry engineering has been succesfully developed and applied to ferroics representing five species of ferroelectrics and one species of ferroelastics, all with two domain states. Such specimens proved to be competitive in the field of nonlinear optics and promissing in the field of ultrasonic generation and detection. But much more complex domain systems are obtainable and have not yet been considered and investigated.

Two new areas of research appear to be very promissing. Domain- and phase-average engineered systems offer increased values of macroscopic properties, probably strengthened by domain wall and/or phase boundary induced motions. We still miss detailed data about the real structure of existing compounds like PZN-PT as well as theoretical analysis of multiple domain states compatibility, the more so for multiple phase systems. Domain-wall engineered samples with high density of walls also promise a new interesting research and application area. At present, particular systems useful in selected applications could be specified and methods to produce high density domain patterns investigated experimentally.

Acknowledgments

J.F. appreciates the support of the Ministry of Education of the Czech Republic (Project VS 96006) and the assistance of the Materials Research Laboratory, The Pennsylvania State University.

References

[1] R. C. Miller. *Phys. Rev.* **134,** A1313 (1964).
[2] D. Feng, N. B. Ming, J. F. Hong, Y. S. Yang, J. S. Zhu, Z. Yang and Y. N. Wang, *Appl. Phys. Lett.* **37,** 607 (1980).
[3] S. N. Zhu, Y. Y. Zhu, Y. Q. Qin, H. F. Wang, C. Z. Ge and N. B. Ming, *Phys. Rev. Lett.* **78,** 2752 (1997).
[4] S. W. Meeks, L. Clarke and B. A. Auld, IEEE Ultrasonics Symposium, San Francisco, CA (1985).
[5] Y. Y. Zhu, N. B. Ming, W. H. Jiang and Y. A. Shui, *Appl. Phys. Lett.* **53,** 1381 (1988).
[6] P. W. Forsbergh, Jr., *Phys. Rev.* **76,** 1187 (1949).
[7] G. Arlt and P. Sasko, *J. Appl. Phys.* **51,** 4956 (1980).
[8] Seung-Eek Park and T. R. Shrout, *J. Appl. Phys.* **82,** 1804 (1997).
[9] Seung-Eek Park, S. Wada, P. W. Rehrig, Shi-Fang Liu, L. E. Cross and T. R. Shrout, "Crystallographic Engineering in High-performance Piezoelectric Crys tals." Paper presented at SPie Smart tructures and Materials (New Port Beach, 1999).

[10] Jianhua Yin and W. Cao, *J. Appl. Phys.* **87,** 7438 (2000).
[11] J. Fousek and V. Janovec, *J. Appl. Phys.* **40,** 135 (1969).
[12] J. Fousek, D. B. Litvin and L. E. Cross, submitted.
[13] J. Schlessman and D. B. Litvin, *Acta Cryst.* **A51,** 947 (1995).
[14] E. T. Keve, K. L. Bye, P. W. Whipps and A. D. Annis, *Ferroelectrics* **3,** 39 (1971).
[15] Z. Zikmund and J. Fousek, *Ferroelectrics* **79,** 73 (1988).
[16] Z. Zikmund and J. Fousek, *phys. stat. sol. (a)* **112,** 625 (1989) and **118,** 539 (1990).
[17] G. A. Rossetti, Jr., W. Cao and C. A. Randall, *Ferroelectrics* **158,**343 (1994).
[18] C. A. Randall, G. A. Rossetti, Jr. and W. Cao, *Ferroelectrics* **150,**163 (1993).
[19] V. A. Isupov, *Ferroelectrics* **46,** 217 (1983).
[20] K. Fujishiro, R. Vlokh, Y. Uesu, Y. Yamada, J.-M. Kiat, B. Dkhil and Y. Yamashita, *Jpn. J. Appl. Phys.* **37,** 5246 (1998).
[21] J. Fousek, D. B. Litvin and L. E. Cross, to be published.
[22] M. B. Walker and R. J. Gooding, *Phys. Rev. B* **32,** 7408 (1985).
[23] E. Snoeck, P. Saint-Gregoire, V. Janovec and C. Roucau, *Ferroelectrics* **155,** 371 (1994).
[24] J. Přívratská and V. Janovec, *Ferroelectrics* **191,** 17 (1997).
[25] L. M. Eng, M. Bammerlin, Ch. Loppacher, M. Guggisberg, R. Bennewitz, R. Lüthi, E. Meyer, Th. Huser, H. Heinzelman and H.-J. Güntherodt, *Ferroelectrics* **222,** 153 (1998).
[26] A. M. Bratkovsky, E. K. H. Salje and V. Heine, *Phase Transitions* **52,** 77 (1994).
[27] V. Novotna, H. Kabelka, J. Fousek, M. Havrankova and H. Warhanek, *Phys. Rev. B* **47,** 11019 (1993).
[28] J. Fousek, M. Marvan and R. S. Cudney, *Appl. Phys. Letters* **72,** 430 (1998).

When addressing the problem of average symmetries of phase-and-domain-average-engineered samples one can follow[21] a similar approach as mentioned above. Consider that two species coexist, namely $m\bar{3}m$–$3m$ and $m\bar{3}m$–$4mm$. It can be shown that when poling along principal directions, i.e. **E** ∥ [001] or **E** ∥ [011] or **E** ∥ [111], regions of the two species differ in the systems of $\mathbf{P}_S$ vectors but are of the same averaged symmetries $4mm$, $mm2$ or $3m$, resp.

It has to be stressed that in both domain-average enginnered and phase-and-domain-average engineered systems, electrical and mechanical compatibility conditions play, in the energy evaluations, a significant role. It is beyond the scope of this presentation to discuss these problems in detail and the subject will be addressed in another paper.

5. DOMAIN-WALL-ENGINEERING

In the last considered case, the thickness of domain walls is finite and the specimens exhibit large wall density. As before, the representation of specific walls can be influenced by external forces. In such *domain-wall-engineered* samples the characteristics of static walls can play an essential role in the averaged macroscopic properties.

It was predicted by Walker and Gooding[22] that Dauphiné domain walls in nonpolar quartz can carry a dipole moment and this was later demonstrated experimentally by Snoeck et al.[23], in the incommensurate phase of SiO_2. In fact it is easy to demonstrate this possibility for ferroelastic walls. If in the free energy function the invariant $\mu_{ijkl}(\partial\varepsilon_{ij}/\partial x_k)E_l$ is allowed by symmetry, a ferroelastic wall will carry polarization

$$P_l = \mu_{ijkl}\frac{\partial\varepsilon_{ij}}{\partial x_k}.$$

Here the μ-tensor describes the flexoelectric effect. As an example, consider the species $m\bar{3}m$ – $4/mmm$ represented by crystals of $SrTiO_3$, or $CsPbCl_3$ and the species $m\bar{3}m$ – $4mm$ describing the properties of $BaTiO_3$. In both cases, ferroelastic walls (90^0 wall in the latter case) are, by symmetry, allowed to carry polarization

$$P_x = P_z = (\mu_{1111} - \mu_{3311})\frac{\partial\varepsilon_{xx}}{\partial x};$$

this is demonstrated in Fig. 3. Symmetries of nonferroelastic domain walls from which their possible macroscopic properties can be envisaged have been discussed by Přívratská and Janovec[24].

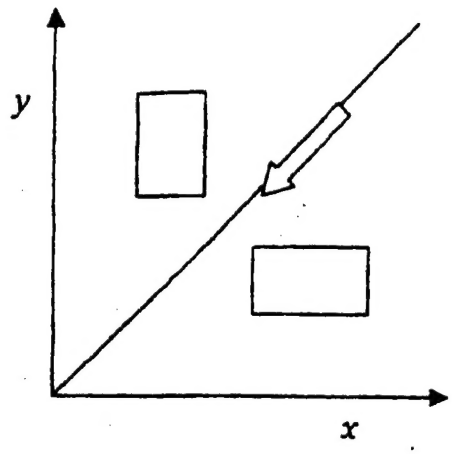

FIGURE 3 Due to flexoelectricity, domain wall separating two ferroelastic domains of species $m\bar{3}m - 4/mmm$ or $m\bar{3}m - 4mm$ can carry polarization represented by the arrow.

Should macroscopic properties of domain walls play a non-negligible role in the properties of a ferroic sample, they have to occupy a sizable volume. Realistic values of domain width and domain wall thickness are d_{domain} = 1 to 10 μm and t_w = 3 nm, resp. Suppose that the required relative volume occupied by domain walls is 10% and that there so no way how to increase the wall thickness. Then we look for methods how to reduce the average domain width to about 30 nm, i.e. how to increase the wall density 30 times or more.

It appears that there is a significant number of experimental methods which could address this problem. Here we mention in passing only some of those which might be considered. The density of defect-induced order parameter gradients could be increased at crystal growth[2]. The size of AFM-written domains[25] could be further reduced, their density increased. Attempts to freeze-in high density tweed structures[26] in some ferroelastics close above T_C or high density pattern of discommensurations in modulated phases close above the lock-in temperatures[27] appear attractive. Fixing photorefractive gratings by domains[28] in ferroelectrics with small P_S (small defect-